Institut für Chemie

Arbeitskreis Angewandte Polymerchemie
bei
Prof. Dr. André Laschewsky

New Zwitterionic Polymers for Antifouling Applications

DISSERTATION
zur Erlangung des akademischen Grades
"doctor rerum naturalium" (Dr. rer. nat.)
in der Wissenschaftsdisziplin Polymerchemie

eingereicht an der
Mathematisch-Naturwissenschaftlichen Fakultät
der Universität Potsdam

von
M.Sc. Alejandro Martínez Guajardo

Supervisor:	Prof. Dr. André Laschewsky
Second reviewer:	Prof. Dr. Andreas Taubert
Date:	January 30, 2024

Published online on the
Publication Server of the University of Potsdam:
https://doi.org/10.25932/publishup-62682
https://nbn-resolving.org/urn:nbn:de:kobv:517-opus4-626820

Get me out of here
Get me out of here man
Get me out of here

Shannon Hoon

Acknowledgements

First and foremost, I would like to thank Prof. Dr. André Laschewsky for giving me the opportunity to work in his research group. His love for science and his everlasting enthusiasm to share his knowledge were always of great inspiration during my PhD.

I would also like to express my deepest gratitude to my colleagues from the research group, Cristiane Henschel, Michelle Hechenbichler, Jasper Hansen, and René Steinbrecher who were always willing to help and ready to engage in thought-provoking dicussions and debates.

My most sincere gratitude goes to all the colleagues from the Fraunhofer IAP for their team work and support, specially to Prof. Dr. Alexander Böker, Dr. Antje Lieske, and Dr. Erik Wischerhoff for trusting me with their laboratories and instruments to conduct my research. I would also like to extend my gratitute to Dr. Kathrin Geßner, Dr. Dirk Schanzenbach, and Angela Krtitschka for their help with the various measurements that were needed for the characterization of my samples.

A special mention goes to my cooperation partners from the Ruhr University Bochum, Lisa Schardt, Jana Karthäuser, Dr. Julian Koc-Richter, and Prof. Dr. Axel Rosenhahn for the fruitful discussions and all their time and work invested in the anti-fouling assessments of my polymers.

Special thanks go to Dr. Benjamín Rodríguez and Pınar Akarsu for their unwavering friendship and understanding. Our lunches loaded with laughter and joy made the time at the institute all the more memorable.

My deepest appretiation also goes to my wife Lala Habibova, her unconditional love and support were always my biggest motor to keep pushing forward.

I would also like to thank all my family and friends, that despite the distance it always felt as if they were just by my side. Their support throughout my whole life and endeavours has always made this journey easier.

Last but not least, I would like to thank me, for always keep going, for never giving up, and for my discipline and perseverance towards this goal.

Scientific Publications

Parts of the results in this thesis were already published:

Scientific journals

- Lisa Schardt, **Alejandro Martínez Guajardo**, Julian Koc, Jessica L. Clarke, John A. Finlay, Anthony S. Clare, Harrison Gardner, Geoffrey W. Swain, Kelli Hunsucker, André Laschewsky, Axel Rosenhahn, "Low Fouling Polysulfobetaines with Variable Hydrophobic Content," *Macromolecular Rapid Communications*, vol. 43, no. 12 **2022**.
- Alice Eickenscheidt, Valentine Lavaux, Stefan Paschke, **Alejandro Martínez Guajardo**, Eric Schönemann, André Laschewsky, Karen Lienkamp, Ori Staszewski, "Effect of Poly(Oxanorbonene)- and Poly(Methacrylate)-Based Polyzwitterionic Surface Coatings on Cell Adhesion and Gene Expression of Human Keratinocytes," *Macromolecular Bioscience*, vol. 22, no. 11, **2022**.
- Jana Karthäuser, Regina Kopecz, Eric Schönemann, **Alejandro Martínez Guajardo**, André Laschewsky, Axel Rosenhahn, "Spacer Effects in Sulfo- and Sulfabetaine Polymers on Their Resistance Against Proteins and Pathogenic Bacteria," *Advanced Materials Interfaces*, vol. 11, no. 5, **2024**.

Poster presentations

- **Alejandro Martínez Guajardo**, Eric Schönemann, André Laschewsky, Axel Rosenhahn, "Long-Term Stability of Zwitterionic Polymers against Hydrolysis," *4^{th} International Congress of Bioinspired and Zwitterionic Materials – Kerkrade, NL*, **2019**
- **Alejandro Martínez Guajardo**, Eric Schönemann, André Laschewsky, Axel Rosenhahn, "Long-Term Stability of Zwitterionic Polymers against Hydrolysis," *Polydays 2019 – Berlin, DE*, **2019**
- **Alejandro Martínez Guajardo**, Eric Schönemann, André Laschewsky, Axel Rosenhahn, "Long-Term Stability of Zwitterionic Polymers against Hydrolysis," *31^{st} Tag der Chemie des Verbandes der Chemie VCI Nordost – Potsdam, DE*, **2019**
- **Alejandro Martínez Guajardo**, Eric Schönemann, André Laschewsky, Axel Rosenhahn, "Long-Term Stability of Zwitterionic Polymers against Hydrolysis," *15^{th} European Detergents Conference (EDC) – Berlin, DE*, **2019**
- Jasper Hansen, André Laschewsky, **Alejandro Martínez Guajardo**, Eric Schönemann, Jana Karthäuser, Axel Rosenhahn, Lisa Schardt, "Performance Parameters of Ultra-Low Fouling Hydrophilic Surfaces," *GDCh MAKRO 2022 – Aachen, DE*, **2022**

- Jasper Hansen, André Laschewsky, **Alejandro Martínez Guajardo**, Eric Schönemann, Jana Karthäuser, Axel Rosenhahn, Lisa Schardt, "Strategies to Reconcile Fouling-Resistance and Mechanical Stability of Zwitterionic Hydrogel Coatings," *18^{th} European Detergents Conference (EDC) – Berlin, DE*, **2022**
- Jasper Hansen, André Laschewsky, **Alejandro Martínez Guajardo**, Eric Schönemann, Jana Karthäuser, Axel Rosenhahn, Lisa Schardt, "Performance Parameters of Ultra-Low Fouling Hydrophilic Surfaces," *33^{rd} Tag der Chemie des Verbandes der Chemie VCI Nordost – Berlin, DE*, **2023**

Abstract

The remarkable antifouling properties of zwitterionic polymers in controlled environments are often counteracted by their delicate mechanical stability. In order to improve the mechanical stabilities of zwitterionic hydrogels, the effect of increased crosslinker densities was thus explored. In a first approach, terpolymers of zwitterionic monomer 3-[*N*-2(methacryloyloxy)ethyl-*N*,*N*-dimethyl]ammonio propane-1-sulfonate (SPE), hydrophobic monomer butyl methacrylate (BMA), and photo-crosslinker 2-(4-benzoylphenoxy)ethyl methacrylate (BPEMA) were synthesized. Thin hydrogel coatings of the copolymers were then produced and photo-crosslinked. Studies of the swollen hydrogel films showed that not only the mechanical stability but also, unexpectedly, the antifouling properties were improved by the presence of hydrophobic BMA units in the terpolymers.

Based on the positive results shown by the amphiphilic terpolymers and in order to further test the impact that hydrophobicity has on both the antifouling properties of zwitterionic hydrogels and on their mechanical stability, a new amphiphilic zwitterionic methacrylic monomer, 3-((2-(methacryloyloxy)-hexyl)dimethylammonio)propane-1-sulfonate (**M1**), was synthesized in good yields in a multistep synthesis. Homopolymers of **M1** were obtained by free-radical polymerization. Similarly, terpolymers of **M1**, zwitterionic monomer SPE, and photo-crosslinker BPEMA were synthesized by free-radical copolymerization and thoroughly characterized, including its solubilities in selected solvents.

Also, a new family of vinyl amide zwitterionic monomomers, namely 3-(dimethyl(2-(*N*-vinylacetamido)ethyl)ammonio)propane-1-sulfonate (**M2**), 4-(dimethyl(2-(*N*-vinylacetamido)ethyl)ammonio)butane-1-sulfonate (**M3**), and 3-(dimethyl(2-(*N*-vinylacetamido)ethyl)ammonio)propyl sulfate (**M4**), together with the new photo-crosslinker 4-benzoyl-*N*-vinylbenzamide (**M5**) that is well-suited for copolymerization with vinylamides, are introduced within the scope of the present work. The monomers are synthesized with good yields developing a multistep synthesis. Homopolymers of the new vinyl amide zwitterionic monomers are obtained by free-radical polymerization and thoroughly characterized. From the solubility tests, it is remarkable that the homopolymers produced are fully soluble in water, evidence of their high hydrophilicity. Copolymerization of the vinyl amide zwitterionic monomers, **M2**, **M3**, and **M4** with the vinyl amide photo-crosslinker **M5** proved to require very specific polymerization conditions. Nevertheless, copolymers were successfully obtained by free-radical copolymerization under appropriate conditions.

Moreover, in an attempt to mitigate the intrinsic hydrophobicity introduced in the copolymers by the photo-crosslinkers, and based on the proven affinity of quaternized diallylamines to copolymerize with vinyl amides, a new quaternized diallylamine sulfobetaine photo-crosslinker 3-(diallyl(2-(4-benzoylphenoxy)ethyl)ammonio)propane-1-sulfonate (**M6**) is synthesized. However, despite *a priori* promising copolymerization suitability, copolymerization with the vinyl amide zwitterionic monomers could not be achieved.

Zusammenfassung

Die hervorragenden Antifouling-Eigenschaften zwitterionischer Polymere in kontrollierten Bedingungen werden häufig durch ihre geringe mechanische Stabilität beeinträchtigt. Um die mechanische Eigenschaften zwitterionischer Hydrogele zu verbessern, wurde daher der Effekt einer erhöhten Vernetzungsdichte untersucht. In einem ersten Ansatz wurden Terpolymere aus dem zwitterionischen Monomer 3-[*N*-2(Methacryloyloxy)ethyl-*N*,*N*-dimethyl]ammonio propan-1-sulfonat (SPE), dem hydrophoben Monomer Butylmethacrylat (BMA) und dem Photovernetzer 2-(4-Benzoylphenoxy)ethylmethacrylat (BPEMA) synthetisiert. Daraufhin wurden dünne Beschichtungen der Copolymere hergestellt und photovernetzt. Die Untersuchung der gequollenen Hydrogelfilme zeigte, dass nicht nur die mechanischen Eigenschaften, sondern überraschenderweise auch die Antifouling-Eigenschaften der Hydrogele durch den Einbau von hydrophoben BMA-Einheiten in die Terpolymere verbessert wurden.

Aufgrund der positiven Ergebnisse der amphiphilen Terpolymere und um die Auswirkungen der Hydrophobie sowohl auf die Antifouling- als auch auf die mechanische Eigenschaften der zwitterionischen Hydrogele zu testen, wurde ein neues amphiphiles zwitterionisches Methacrylat, nämlich 3-((2-(Methacryloyloxy)hexyl)dimethylammonio)propan-1-sulfonat (**M1**), in guter Ausbeute synthetisiert. Homopolymere von **M1** wurden durch radikalische Polymerisation erhalten. In ähnlicher Weise wurden Terpolymere aus **M1**, dem zwitterionischen Monomer SPE und dem Photovernetzer BPEMA durch radikalische Copolymerisation synthetisiert und gründlich charakterisiert, einschließlich ihrer Löslichkeiten in ausgewählten Lösungsmitteln.

Außerdem wurde im Rahmen der vorliegenden Arbeit eine neue Familie von zwitterionischen Vinylamidmonomeren, nämlich 3-(Dimethyl(2-(*N*-vinylacetamido)ethyl)ammonio)propan-1-sulfonat (**M2**), 4-(Dimethyl(2-(*N*-vinylacetamido)ethyl)ammonio)butan-1-sulfonat (**M3**) und 3-(Dimethyl(2-(*N*-vinylacetamido)ethyl)ammonio)propylsulfat (**M4**), zusammen mit einem geeigneten Vinylamid-Photovernetzer, nämlich 4-Benzoyl-*N*-vinylbenzamide (**M5**) entwickelt. Die Monomere wurden in einer Mehrstufen-Synthese mit guten Ausbeuten synthetisiert. Homopolymere der neuen zwitterionischen Vinylamidmonomere wurden durch radikalische Polymerisation erhalten und eingehend charakterisiert. Die Löslichkeitstests zeigen, dass die hergestellten Homopolymere bemerkenswerterweise vollständig in reinem Wasser löslich sind, was ihre hohe Hydrophilie beweist. Die Copolymerisation der zwitterionischen Vinylamidmonomere **M2**, **M3** und **M4** mit dem Vinylamid-Photovernetzer **M5** erwies sich als schwierig. Die Copolymere lassen sich dennoch unter sehr spezifische Bedingungen durch radikalische Copolymerisation herstellen.

Des Weiteren, um die durch die Photovernetzer in die Copolymere eingebrachte inhärente Hydrophobie zu mindern und aufgrund ihrer nachgewiesenen Affinität zur Copolymerisation mit Vinylamiden, wurde ein neuer quaternisierter Diallylaminsulfobetain-Photovernetzer 3-(Diallyl(2-(4-benzoylphenoxy)-ethyl)ammonio)propan-1-sulfonat (**M6**) synthetisiert. Trotz *a priori* vielversprechender Copolymerisationseignung konnte jedoch keine Copolymerisation mit den zwitterionischen Vinylamidmonomeren erreicht werden.

Abbreviations and Variables

λ_{max}	maximum absorbance wavelength
ε	molar extinction coefficient
Đ	dispersity
$E_T(30)$	Dimroth-Reichardt empirical polarity parameter
t-BuOH	*tert*-butanol
t-BuOK	potassium *tert*-butoxide
AIBN	2,2'-azobisisobutyronitrile
ATR	attenuated total reflection
BMA	butyl methacrylate
BPEMA	2-(4-benzoylphenoxy)ethyl methacrylate
CBMA	3-[[2-(methacryloyloxy)ethyl]dimethyl-ammonio]propionate
CRU	constitutional repeat unit
DCM	dichloromethane
DMAP	4-dimethylamino-pyridine
DMF	dimethyl formamide
DMSO	dimethyl sulfoxide
DSC	differential scanning calorimetry
EA	elemental analysis
FT-IR	Fourier transform infrared
GPC	gel permeation chromatography
HFIP	hexafluoroisopropanol
ISC	intersystem crossing
M_n	number average molar mass
M_w	weight average molar mass
MeCN	acetonitrile
MeOH	methanol
MMA	methyl methacrylate
MPC	2-methacryloyloxyethyl phosphorylcholine
MTBE	methyl *tert*-butyl ether
MWCO	nominal molecular weight cutoff
P(BMA)	poly(butyl methacrylate)
P(MMA)	poly(methyl methacrylate)

P(SPE)	poly(3-[*N*-2(methacryloyloxy)ethyl-*N*,*N*-dimethyl]ammonio propane-1-sulfonate)
PEG	poly(ethylene glycol)
RT	room temperature
SPE	3-[*N*-2(methacryloyloxy)ethyl-*N*,*N*-dimethyl]-ammonio propane-1-sulfonate
SPR	surface plasmon spectroscopy
TBT-SPC	tributyltin self-polishing copolymer
TBTM	tributyltin methacrylate
TFE	trifluoroethanol
TGA	thermogravimetric analysis
THF	tetrahydrofuran
UV-Vis	ultraviolet-visible
V-086	2,2'-azobis[2-methyl-*N*-(2-hydroxyethyl)-propionamide]
V-50	2,2'-azobis(2-methylpropionamidine)dihydro-chloride
V-501	4,4'-azobis(4-cyanovaleric acid)
X_n	number average degree of polymerization

Contents

List of Tables

List of Figures

List of Schemes

Chapter 1

Objectives of the Thesis

Zwitterionic polymers have proven to have remarkable antifouling properties due to their extreme hydrophilicity [1, 2]. Most of them have been derived from methacrylate monomers, due to their good polymerizability, and the decent stability of their polymers against hydrolysis [3, 4]. However, the outstanding performance of such zwitterionic hydrogel films in controlled environments and lab assays, is counteracted in field tests by their delicate mechanical stability [5].

Enhancing the mechanical stability of the thin hydrogel films was expected to be achieved by decreasing the swelling of the hydrogel network. Increasing the hydrophobicity of the hydrogel films can limit their swelling by the formation of physical crosslinks between the polymer chains. However, a decrease in the achieved hydration can also have a negative impact on the antifouling properties of the hydrogel films. With this in mind, in an initial step, terpolymers of the widely used zwitterionic monomer 3-[*N*-2(methacryloyloxy)ethyl-*N*,*N*-dimethyl]ammonio propane-1-sulfonate (SPE), hydrophobic monomer butyl methacrylate (BMA), and 2-(4-benzoylphenoxy)ethyl methacrylate (BPEMA) acting as photo-crosslinker of the thin hydrogel films, were addressed in the scope of the present work. In order to further test the impact that increased hydrophobicity has on both the antifouling properties of zwitterionic hydrogels and the mechanical stability of the produced hydrogel films, 3-((2-(methacryloyloxy)-hexyl)dimethylammonio)propane-1-sulfonate (**M1**), a new amphiphilic zwitterionic methacrylate, which combines zwitterionic and hydrophobic moieties into one monomer, was envisaged during this work (See Figure 1.1).

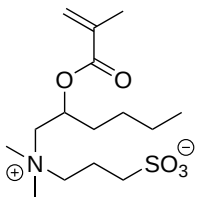

M1

Figure 1.1: New amphiphilic zwitterionic methacrylate (**M1**) to be synthesized during this work.

The use of vinyl amides in contrast to the commercially available methacrylic zwitterionic monomers is expected to have a positive impact on the hydrolytic stability of the resulting hydrogels, as amide bonds are known to be even more hydrolytically stable when compared to the ester bonds present in methacrylic polymers. Furthermore, specific properties of polyvinylamides, such as their hydrophilicity and more flexible backbone makes this type of polymers of special interest for the intended antifouling applications. Therefore, a new family of zwitterionic monomers with vinyl amide as the polymerizable group, namely 3-(dimethyl(2-(*N*-vinylacetamido)ethyl)ammonio)propane-1-sulfonate (**M2**), 4-(dimethyl(2-(*N*-vinylacetamido)ethyl)ammonio)butane-1-sulfonate (**M3**), and 3-(dimethyl(2-(*N*-vinylacetamido)ethyl)ammonio)propyl sulfate (**M4**), was explored in the present work (See Figure 1.2). However, because of their different polymerizable units, such monomers are not expected to copolymerize well with methacrylic monomers such as the photo-crosslinker BPEMA. A new vinyl amide photo-crosslinker, 4-benzoyl-*N*-vinylbenzamide (**M5**), suitable for the copolymerization with the newly synthesized vinyl amide zwitterionic monomers, was thus envisaged. A schematic representation of the new vinyl amide monomers and the new photo-crosslinker introduced in the present work is shown in Figure 1.2.

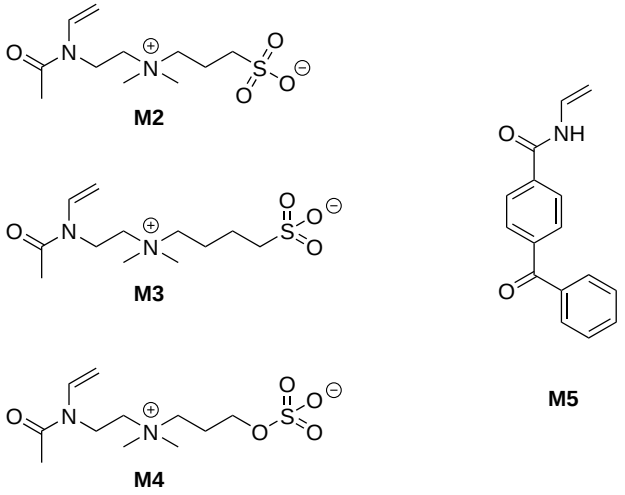

Figure 1.2: New vinyl amide zwitterionic monomers (**M2**, **M3**, and **M4**), and vinyl amide photo-crosslinker (**M5**) explored.

Another approach to reduce the swelling ratio of a hydrogel network and thus, improve its mechanical properties, is by increasing the crosslink density of the network. However, an increase in the crosslink density of hydrogels decreases the achieved hydration as the polymer chains are more restricted to swell, which can have a negative impact on the antifouling properties of said hydrogel. Moreover, an increasing proportion of the inherently hydrophobic photo-crosslinkers reduces the overall hydrophilicity of the obtained hydrogels. In order to mitigate the hydrophobicity introduced when increasing the crosslink density of zwitterionic hydrogels and thus, to maintain to the best extent its antifouling properties, a new zwitterionic photo-crosslinker, 3-(diallyl(2-(4-

benzoylphenoxy)ethyl)ammonio)propane-1-sulfonate (**M6**), was envisaged (See Figure 1.3). This newly devised zwitterionic photo-crosslinker includes a quaternized diallylammonium as its polymerizable unit, rendering it highly resistant to hydrolysis. Additionally, quaternized diallylammonium monomers are known to undergo copolymerization with vinyl amides exceptionally well, in what is known as ideal azeotropic copolymerization [6, 7]. This would allow to control not only the amount but also the intramolecular distribution of crosslinker introduced into the polymer chains.

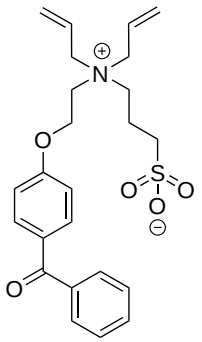

M6

Figure 1.3: New quaternized diallylamine zwitterionic photo-crosslinker (**M6**) targeted.

Chapter 2

Theoretical Background

2.1 Fouling Resistance

2.1.1 Marine Biofouling

Biofouling is understood as the colonization of surfaces by unwanted biomolecules and organisms, usually having detrimental effects on the functions of that surface [8,9]. This settlement and accumulation of organisms can have large penalties for engineered structures such as heat exchangers, shipping and leisure vessels, and structures used in aquaculture, among others [9, 10].

Marine biofouling has a wide impact, having consequences for everything from ship maintenance to ecosystem safety [8]. Specifically for marine vessels, biofouling increases the required shaft power at cruising speeds up to 76 % [9,11]. This penalty in shaft power due to marine biofouling increases fuel consumption and, furthermore, greenhouse gas emissions, to which the world's shipping fleets contribute significantly [12, 13]. Moreover, fouled ships can act as vectors for invasive species, endangering the safety of local ecosystems [8, 14, 15].

Biofouling in marine environments alone involves a vast diversity of fouling organisms, with reports identifying more than 5000 species on fouled structures worldwide, including diatoms, barnacles, mussels, and algae [16–19]. However, this number represents a very small proportion of the known marine species, as only species that have adapted to tolerate wide environmental fluctuations in parameters such as temperature, salinity, and water flow can prevail [17, 20, 21].

The fouling of surfaces starts immediately after a surface enters a marine environment, with the adsorption of dissolved organic matter, such as proteins, carbohydrates, and proteoglycans, occurring in under a minute, making the surface more hospitable for fouling organisms [8, 22, 23]. This modified surface is colonized by rapidly developing bacteria and diatoms, which form biofilms, and by other macrofoulers such as algae and barnacles [8, 17, 24]. Although biofouling is often seen as a successional process, in reality it follows a much more complex model as many foulers, like motile zoospores of the algae *Ulva linza* and cyprids of several species of barnacles, are capable of settling on pristine surfaces [8, 9, 25, 26].

2.1.2 Antifouling

Throughout the centuries, different methods against marine biofouling have been used [27]. The ancient Phoenicians and Carthaginians presumably used pitch on their ships, the Greeks and Romans reportedly then employed tar and lead sheathing [27–29]. Afterwards, copper sheathing received general recognition as the first successful antifouling surface around the 18^{th} century, and lastly, biocidal-based paints were the most successful antifouling technique in the 20^{th} century [8, 27].

From the biocidal-based paints, the most successful were tributyltin self-polishing copolymer (TBT-SPC) paints, which were estimated to have covered up to 70 % of the world's fleet by the end of the 20^{th} century [8, 17]. Tributyltin self-polishing copolymer paints were produced by the copolymerization of tributyltin methacrylate (TBTM) with a hydrophobic methacrylate, usually methyl methacrylate (MMA) (See Figure 2.1) [30]. The hydrophobicity of the TBTM-MMA copolymer prevents seawater from penetrating the paint film. However, the dissolution of water-soluble pigments such as Cu_2O and ZnO contained within the paint matrix allows water to fill the pores created after the dissolution of these pigments [17, 30]. With pH values between 8.0–8.3 the seawater is alkaline enough to cleave the carboxyl–tributyltin bond, which is hydrolytically unstable under slightly alkaline conditions. The introduction of hydrophilic free carboxylate groups in the outer layer of the polymer makes the polymer more brittle and moving seawater is able to erode it, exposing a less reacted layer of organotin acrylate polymer (self-polishing effect) [17, 30, 31]. This mechanism allows the gradual release of tributyltin, maximizing the lifetime of the coating and thus delaying dry-docking for periods of up to 5 years [17].

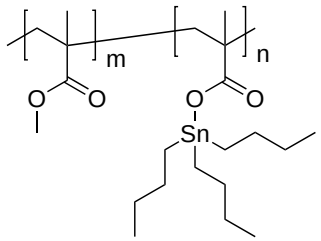

Figure 2.1: Chemical formula of a copolymer of MMA and TBTM.

Despite its unprecedented efficacy in antifouling coatings and the important economic benefits that these coatings brought, tributyltin was found to have many adverse environmental effects [17, 32, 33]. It has been linked to abnormal shell growth in oysters and identified as an endocrine disruptor in mollusks, causing the growth of male genitalia in female mussels [8, 17, 34, 35]. Because of its negative environmental impact, tributyltin paints were first banned on vessels <25 m in length, and ultimately, a worldwide ban was issued against them on January 1^{st}, 2008, by a convention set by the International Maritime Organization [10, 11, 16, 17, 36].

With the international ban issued against TBT-SPC paints, there has been increased attention towards alternative biocides [37]. These initiatives led to the development of formulations containing alternatives to tributyltin based on metals such as copper and zinc combined with organic "booster" biocides [8, 37, 38].

However, these metal-based biocides are scrutinized as well for their toxic side-effects and buildup in harbors and marinas [8, 37, 39–42]. This has brought especial interest to the development of environmentally friendly and durable antifouling coatings. These efforts have directed research both towards functional coatings with low surface energy, such as silicone and fluorocarbon polymers, as well as towards hydrogels, whose antifouling mechanisms are attributed to their highly hydrated surfaces [43].

More specifically, hydrophilic materials show antifouling potential, as water molecules bind firmly to the surface of the material, and the high enthalpy of hydration interferes physically and energetically with the absorption of maritime organisms [44, 45]. Among these hydrophilic materials, poly(ethylene glycol) (PEG) has been one of the most successful approaches, as it is inherently neutrally charged, minimizing its contributions to electrostatic adsorption of proteins, well-hydrated, and has proven to effectively prevent protein adsorption in biomedical applications [45–49]. However, despite the favorable results of PEG during short time uses, it is susceptible to oxidation in seawater, which causes a considerable deterioration of its antifouling properties [45, 50]. Therefore, interest in polyzwitterions, a new group of bioinert polymers, has increased over the last decade as a more robust solution to PEG-derived materials, mainly due to their stronger hydrophilicity and lower interaction with proteins [44, 45, 51, 52].

2.2 Zwitterionic Polymers

Zwitterions are molecules that carry an equal number of negative and positive charges linked through covalent bonds; this renders the overall charge of these molecules zero [53]. Zwitterionic polymers contain the same number of positive and negative charges within each of their constitutional repeat units, which in turn makes the overall charge already zero at the local level [3, 54].

This unique characteristic differentiates polyzwitterions from other ionic polymers such as polyampholytes, polymers that, although they also carry positive and negative charges, both charges may not be within each of their constitutional repeat units. This normally results in polymers where one charged species outnumbers the other one, making polyampholytes typically bear an overall net charge, be it positive or negative [55, 56]. This overall net charge commonly observed in polyampholytes causes their solution behavior to be similar to that of polyelectrolytes, which are polymers that contain either exclusively anionic or exclusively cationic groups within their constitutional repeat units [3, 56]. A schematic representation of these different ionic polymer classes is shown in Figure 2.2.

Because of their neutral overall net charge, polyzwitterions exhibit properties of both ionic and nonionic polymers. For instance, the high density of ionic pairs allows for strong electrostatic interactions, which in consequence renders most known zwitterionic polymers highly hydrophilic; however, their ion conductivity is practically nonexistent as no low-molar-mass counterions are present [55, 57].

This set of exceptional properties and the ample appearance of low-molar-mass zwitterions in nature in the form of phospholipids and certain amino acids at their isoelectric point have attracted great interest towards polyzwitterions in the last 40 years [3,55,58]. Although polyzwitterions are not naturally occurring, their similarities to naturally occurring compounds have incited their use in the

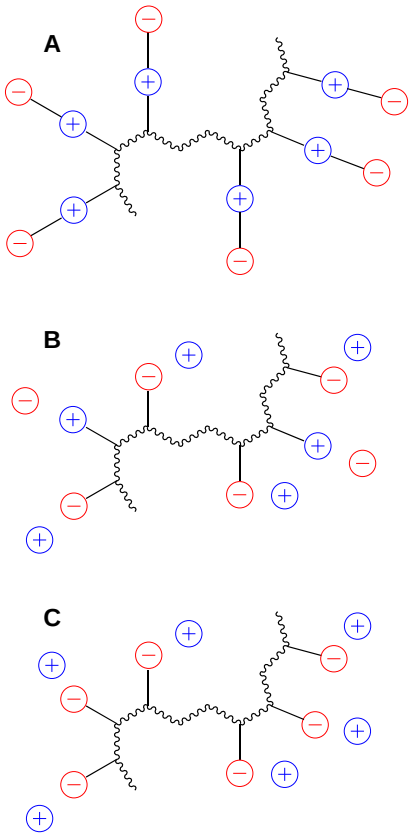

Figure 2.2: Schematic representation of polyzwitterions (**A**), polyampholytes (**B**), and polyanion as example of polyelectrolytes (**C**).

development of bioinspired materials and fueled the general perception of their biocompatibility [55, 59, 60]. Among the diverse applications in which the use of zwitterionic polymers has shown great potential are biocompatibilization, lubrication, self-assembly, and low-fouling surfaces [58, 61–64].

Particularly for their biofouling resistance and high biocompatibility, polyzwitterions have demonstrated great performance in both technical and biomedical applications [65–68]. As previously mentioned, these properties are assumed to be related to the strong electrostatic interactions that zwitterionic polymers have with water molecules, forming a stable hydration layer and therefore making the binding of proteins and biofoulers less energetically attractive, thus inhibiting the bond formation between foulants and the surface [51, 65, 69–71]. However, the strong hydration layer formed by zwitterionic polymers is not the only parameter beneficial for the low-fouling of polyzwitterions; other parameters such as the pair of anionic and cationic groups, the anchoring geometry, and the nature of the backbone, among others, have also been shown to have an impact on the antifouling properties of zwitterionic polymers [55]. This makes the design and architecture of polyzwitterions decisive for their performance as anti-fouling agents [55, 58, 67]. Figure 2.3 shows a nonextensive schematic representation of possible architectures of zwitterionic polymers.

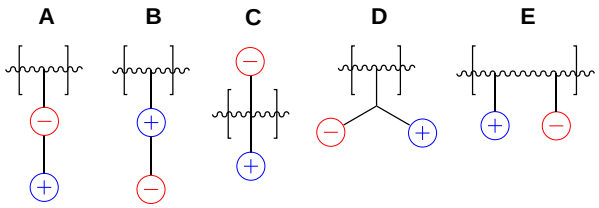

Figure 2.3: Selected examples of possible polyzwitterions architectures.

The effect that different architectures of zwitterionic polymers have on their antifouling properties has been addressed in the literature, especially for architecture types A, B, and D in Figure 2.3 [66, 67, 72–75]. Although a wide variety of combinations have been done, the combinations of a phosphate group, a carboxylate group, or a sulfonate group as anionic groups with a quaternary ammonium group as a cation (ammoniophosphates, carboxybetaines, and sulfobetaines, respectively) still predominate in the structure of polyzwitterions [3,56,70,72]. Extensive research has been conducted with polymers based on the commercially available methacrylic zwitterionic monomers SPE, 3-[[2-(methacryloyloxy)ethyl]dimethylammonio]propionate (CBMA), and 2-methacryloyloxyethyl phosphorylcholine (MPC) (see Figure 2.4) [3, 64, 72, 76].

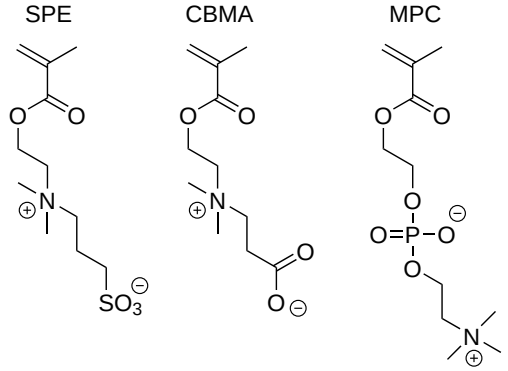

Figure 2.4: Commercially available zwitterionic monomers SPE, CBMA, and MPC.

2.3 Free-Radical Polymerization

Free-radical polymerization is a type of chain growth polymerization in which constitutional repeat units of a monomer are sequentially added to a growing polymer chain by radical addition reactions to carbon-carbon double bonds to produce long polymer molecules [77]. One of the main advantages of free-radical polymerization is that it can be carried out in relatively undemanding conditions, unlike ionic or coordination polymerizations. Free-radical polymerization exhibits a certain tolerance to trace impurities, and high-molar-mass polymers can be synthesized without the removal of the stabilizers present in commercial monomers, in the presence of trace amounts of oxygen, or in solvents that have

not undergone thorough drying or purification, as free-radical polymerization can be conducted in aqueous media [78]. These advantages over other polymerization techniques have made free-radical polymerization of special interest to the industry, and as of 2009, 45 % of the worldwide production of plastic materials and 40 % of the manufactured synthetic rubber were obtained by free-radical polymerization [79].

Extensive research performed during the first half of the 20^{th} century boosted the development of free-radical polymerization, and the basic mechanism as it is understood today was established during the 1940s and 1950s. The free-radical polymerization mechanism includes three main steps [80–82]:

1) Initiation

   i) Decomposition of initiator

   $$\mathrm{R_2} \xrightarrow{k_d} 2\,\mathrm{R^\bullet}$$

   ii) Radical attack on monomer

   $$\mathrm{R^\bullet + M} \xrightarrow{k_i} \mathrm{RM^\bullet}$$

2) Propagation

   $$\mathrm{RM^\bullet + M} \xrightarrow{k_p} \mathrm{RM_2^\bullet} \xrightarrow{k_p} \mathrm{RM_n^\bullet}$$

3) Termination

   i) Combination

   $$\mathrm{RM_n^\bullet + RM_m^\bullet} \xrightarrow{k_{t1}} \mathrm{RM_{n+m}}$$

   ii) Disproportionation

   $$\mathrm{RM_n^\bullet + RM_m^\bullet} \xrightarrow{k_{t2}} \mathrm{RM_n + RM_m}$$

The initiation step is defined as a process that starts with the generation of *primary* radicals from an initiating species (initiator) and ends with their addition to the carbon-carbon double bond of a monomer in order to produce *initiating* radicals [80]. These reactions, however, can produce a set of different *initiating* radicals as different reactions such as tail addition, head addition, H-abstraction, or aromatic substitution often compete with each other. The outcome of these reactions strongly depends on the structure of both the radical and the monomer; for this reason, the proper selection of the initiator according to its suitability for use with a given monomer is crucial to achieving the desired functionality of the polymer [80, 83, 84]. Among the most important initiator classes for free-radical polymerization reactions are peroxy compounds, azo compounds, and photochemical initiators [78, 79].

To produce polymers, the propagation step in free-radical polymerization requires the successive addition of radicals to carbon-carbon double bonds. The propagating radicals need to favor as much as possible the addition of carbon-carbon double bonds over any other reaction that can stop the polymer chain formation [80]. This is non-trivial for radical polymerizations, as unlike anionic

polymerizations, radicals have a greater potential for indiscriminate reactivity. One main distinction is that, contrary to two anions that repel one another, two radicals destroy one another in either a radical-radical coupling reaction or a disproportionation reaction, which renders the two chains inert and further expansion of the polymer is no longer possible [77, 85].

Although free-radical polymerization has its intrinsic limitations, homopolymers still have ample space for structural variety. Moreover, backbiting, cyclopolymerization, and intermolecular chain transfer reactions result in branches or rings within the polymer chain [80, 86–88].

During the termination step, three processes can be responsible for the cessation of growth of a polymer chain: the reaction of two propagating radicals with each other by combination or disproportionation; the reaction of a propagating radical with a *primary* radical by similar combination or disproportionation processes; or the inhibition of a propagating radical with relatively stable radicals such as nitroxides or oxygen to produce a dead polymer chain [80, 85].

Although these are the three inherent steps in the formation of polymers by free-radical polymerization, a broad array of additional side reactions that take place during the polymerization may have an impact on the final properties of the polymer. Chain transfer to solvents and additives, reactions with oxygen, and intramolecular atom transfer are common examples of these side reactions [80, 89–91]. Nevertheless, C-centered radicals are mostly less reactive towards functional groups than C-centered ions or transition metal complexes, so that free-radical polymerization is relatively tolerant to the presence of ionic groups, nucleophiles or electrophiles as water, conditions that are needed for the synthesis of polyzwitterions.

2.3.1 Free-Radical Copolymerization

Copolymerizations are processes that result in polymer chains containing two or more different types of monomer units. This is achieved when the starting materials for the polymerization are mixtures of two or more discrete types of monomers [78, 92]. Industrially, copolymerization has been of extreme importance as the properties of the produced copolymers combine those of the parent homopolymers [92, 93]. Furthermore, depending on how the distinct monomers are incorporated into the copolymer chain, the different sequence distributions and architectures of the produced copolymers have a determining influence on their final properties; this gives unprecedented versatility to the properties of the materials that can be achieved through these processes [78, 92, 93]. A nonextensive representation of said sequence distributions is shown in Figure 2.5.

In order to better describe the rate and course of propagation in copolymerizations, various models have appeared [94–98]. However, in the simplest case of the copolymerization of two different monomers, each monomer's propagating active species ($P_i^{\bullet}$), react irreversebly with each monomer (M_i) so that four different propagation steps occur [92, 94]:

$$P_A^{\bullet} + M_A \xrightarrow{k_{AA}} P_A{-}M_A^{\bullet}$$

$$P_A^{\bullet} + M_B \xrightarrow{k_{AB}} P_A{-}M_B^{\bullet}$$

$$P_B^{\bullet} + M_A \xrightarrow{k_{BA}} P_B{-}M_A^{\bullet}$$

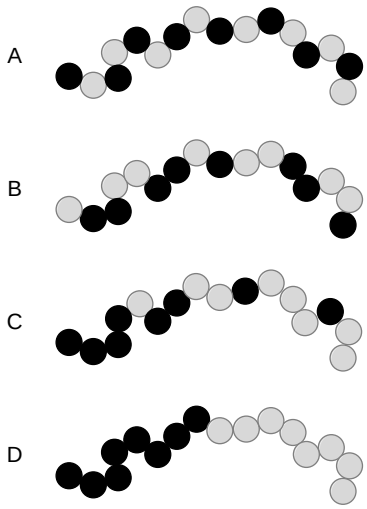

Figure 2.5: Schematic representation of alternating copolymers (**A**), statistical copolymers (**B**), gradient copolymers (**C**), and block copolymers (**D**).

$$\mathrm{P_B^{\bullet}} + \mathrm{M_B} \xrightarrow{k_{BB}} \mathrm{P_B{-}M_B^{\bullet}}$$

If the influence of the initiation and termination are neglected under the assumption that the produced polymer chains are long, the relative monomer consumption is then Equation (2.1) [78, 92, 94].

$$\frac{d\,[\mathrm{M_A}]}{d\,[\mathrm{M_B}]} = \frac{k_{\mathrm{AA}}\,[\mathrm{P_A^{\bullet}}]\,[\mathrm{M_A}] + k_{\mathrm{BA}}\,[\mathrm{P_B^{\bullet}}]\,[\mathrm{M_A}]}{k_{\mathrm{AB}}\,[\mathrm{P_A^{\bullet}}]\,[\mathrm{M_B}] + k_{\mathrm{BB}}\,[\mathrm{P_B^{\bullet}}]\,[\mathrm{M_B}]} \tag{2.1}$$

Assuming that the two propagating species $\mathrm{P_A^{\bullet}}$ and $\mathrm{P_B^{\bullet}}$ achieve a steady state ($k_{\mathrm{AB}}\,[\mathrm{P_A^{\bullet}}]\,[\mathrm{M_B}] = k_{\mathrm{BA}}\,[\mathrm{P_B^{\bullet}}]\,[\mathrm{M_A}]$) allows the elimination of the radical concentrations, resulting in the Mayo-Lewis equation [78, 92, 94].

$$\frac{d\,[\mathrm{M_A}]}{d\,[\mathrm{M_B}]} = \frac{[\mathrm{M_A}]}{[\mathrm{M_B}]}\left(\frac{\left(\frac{k_{\mathrm{AA}}}{k_{\mathrm{AB}}}\right)[\mathrm{M_A}] + [\mathrm{M_B}]}{\left(\frac{k_{\mathrm{BB}}}{k_{\mathrm{BA}}}\right)[\mathrm{M_B}] + [\mathrm{M_A}]}\right) \tag{2.2}$$

From Equation (2.2) the monomer reactivity ratios (r_{A} and r_{B}) are defined as the ratio of homoreaction to cross-reaction rate constants:

$$r_{\mathrm{A}} \equiv \frac{k_{\mathrm{AA}}}{k_{\mathrm{AB}}}, \quad r_{\mathrm{B}} \equiv \frac{k_{\mathrm{BB}}}{k_{\mathrm{BA}}} \tag{2.3}$$

Further simplifying Equation (2.2).

$$\frac{d\,[\mathrm{M_A}]}{d\,[\mathrm{M_B}]} = \frac{[\mathrm{M_A}]}{[\mathrm{M_B}]}\left(\frac{r_{\mathrm{A}}\,[\mathrm{M_A}] + [\mathrm{M_B}]}{r_{\mathrm{B}}\,[\mathrm{M_B}] + [\mathrm{M_A}]}\right) \tag{2.4}$$

With this model, the copolymer composition for a given monomer feed can be predicted if the reactivity ratios are determined. Furthermore, the values of r_{A} and r_{B} can give a quick estimation of the sequence distributions of the produced copolymers, in particular for the following cases [78, 92]:

(a) For reactivity ratios $r = 0$ the homopolymerization will not be preferred, unlike monomer will always be added to the growing end.

(b) For reactivity ratios below unity ($r < 1$) unlike monomer is preferred, but homopolymerization can still happen to a lower extent.

(c) Monomer reactivity ratios equal to unity ($r = 1$) favour both homopolymerization and cross-propagation equally.

(d) Reactivity ratios greater than one ($r > 1$) prefer homopolymerization, but not exclusively.

Additionally, as both active species compete for monomer at any given time, the differences of both copolymerization parameters also have to be considered while classifying copolymerizations [78, 92]:

(e) For copolymerizations where r_A and r_B are both smaller than 1 ($r_A < 1$, $r_B < 1$), there will always be a tendency for alternation. In the extreme case where both copolymerization parameters are equal to zero ($r_A = r_B = 0$) cross-propagation always occurs, and an alternating copolymer will be produced.

(f) For copolymerizations where r_A and r_B are both greater than 1 ($r_A > 1$, $r_B > 1$), homopropagation will always be preferred, and the produced copolymer will have a certain degree of blockiness.

In both previous cases (e) and (f), where r_A and r_B are both either smaller or greater than unity ($r_A < 1$, $r_B < 1$ or $r_A > 1$, $r_B > 1$), there will be an "azeotropic composition" where the copolymer composition will be the same as the monomer feed composition [78, 92].

Lastly, three more special cases are of particular importance for understanding how the relative magnitudes of the reactivity ratios affect the copolymerization of two monomers [78]:

(g) Copolymerizations where the product of the copolymerization parameters is unity ($r_A \cdot r_B = 1$) are called ideal because the probabilities of a monomer adding to either one of the two propagating species are identical, resulting in a common sequence within the macromolecules that follows "ideal", i.e., Bernouilli statistics, so that random copolymers are formed.

(h) When one of the monomers' copolymerization parameter is greater than unity and the other one is smaller than unity ($r_A < 1$, $r_B > 1$ or $r_A > 1$, $r_B < 1$) the copolymer will always be richer in one monomer than the other, and these copolymerizations have no "azeotropic composition".

(i) For copolymerizations where both r_A and r_B equal unity ($r_A = r_B = 1$), both monomers are consumed at random according to the monomer feed composition, which makes the relative concentration of the comonomers to remain stable throughout the polymerization, so that no compositional drift is observed throughout the copolymerization. Moreover, the product is a random copolymer.

Importantly, the relative concentrations of the comonomers during the copolymerization remain stable only in the case (i), or at the precise azeotropic composition in the case of (e) and (f). Otherwise, a compositional drift over the ongoing conversion occurs if not special countermeasures are taken, resulting in a broad, conversion-dependent mixture of the composition of the copolymers formed.

Since the composition and sequence distribution of copolymers impact the final physical and chemical properties of the copolymers considerably, it is important to control them to the best extent possible [93]. Copolymerization models, although approximative, allow the prediction of the outcome of the copolymerization. A selection of the previous cases is depicted in Figure 2.6.

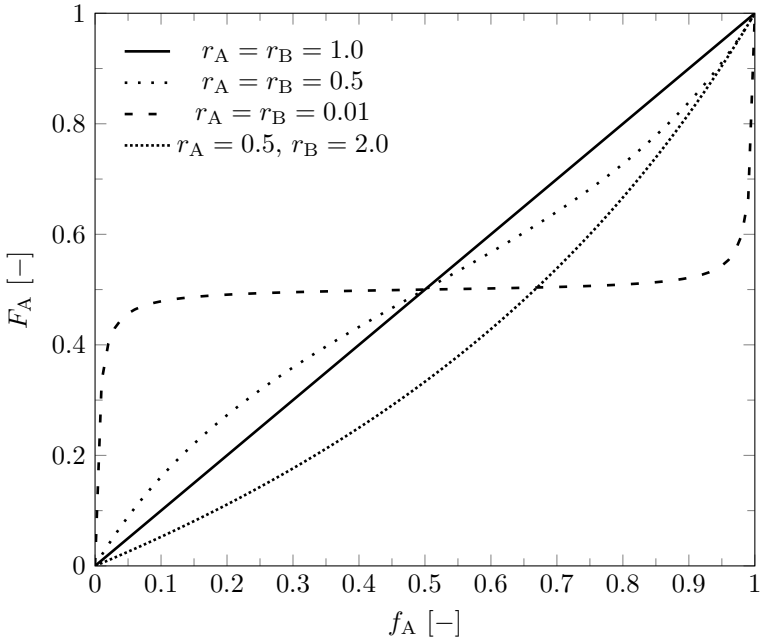

Figure 2.6: Plot of the instantaneous copolymer composition (F_A) *vs.* monomer feed composition (f_A) for different scenarios.

2.4 Hydrogels

Hydrogels are three-dimensional crosslinked networks of hydrophilic polymers that are able, often under physiological conditions, to swell and retain a significant fraction of water (>20 wt.%) [99–101]. In nature, hydrogels are widespread, as muscles and cartilages in animal tissues, and xylems and phloems in plants; this makes them interesting for their use in biomimetic applications, which are of importance in both scientific and industrial fields [43,99,102,103]. Specifically because of their high water content, flexibility, and biocompatibility, hydrogels have been of special interest for more than half a century in the development of materials with biomedical applications such as wound dressing, drug delivery, and contact lenses, among many others [43, 104–107].

The categorization of hydrogels can be done by taking into account many of their different attributes; physical properties, ionic charges, degradability, and the nature of their crosslinking are some examples. Regarding the nature of their crosslinking, there are two main classes into which hydrogels can be categorized: physical and chemical crosslinking. Physical crosslinking comprises all the physical processes through which crosslinking can be achieved, such as hydrogen bonding, hydrophobic association, chain aggregation, and crystallization, to name a few. Chemical crosslinking refers to crosslinking through a chemical process, e.g., a chemical covalent bond. The properties of this type of hydrogel can be of great relevance for certain applications, as chemical bonds are normally permanent and irreversible [100].

The type and the degree of crosslinking present in a hydrogel are decisive on the amount of water that a network polymer can adsorb. As the crosslinking density increases, the polymer chains become more restricted which impacts their ability to swell and adsorb water [99, 108]. Moreover, these parameters also play a decisive role in the mechanical properties of the hydrogel and their stability when immobilized onto a substrate [58, 66].

2.4.1 Benzophenone as Photo-crosslinker

Due to its exceptional photochemical characteristics and the commercial availability of the reagents, benzophenone has become one of the most widely used photophores in organic chemistry, bioorganic chemistry, and material science in the last couple of decades [109]. Since nearly half a century ago, when biochemists first became interested in its photochemistry, especially as an agent to identify the binding sites on target proteins, benzophenone has played a significant role in a variety of fields, from material science and technology to biology and pharmacology [109–112].

Because of its ability to effectively absorb ultraviolet light, benzophenone has been used as a probe to clarify peptide-peptide interactions, as a photoinitiator in 3D printing applications, and more importantly for the current work, as a photo-crosslinker for the creation of gel networks and immobilization of polymers onto surfaces [43, 66, 110, 112–114].

The distinct photochemical characteristic of benzophenone is the formation of a biradical by the absorption of an ultraviolet photon with a wavelength of 250–365 nm by the benzophenone chromophore; this promotes a nonbonding electron from the oxygen into the carbonyl π^* orbital. From this singlet state, a triplet can be produced via intersystem crossing (ISC), as direct $S_0 - T_1$ transition is spin forbidden (See Figure 2.7) [109, 115, 116].

The formed $n-\pi^*$ triplet can be represented as a biradical where, in addition to the ketyl radical, an aliphatic carbon-centered radical is also yielded (See Scheme 2.1) [109,113,115]. The lifetime of the formed triplet is highly dependent both on the substitution pattern of the aryl ring and on the reactivity of the medium, varying from 5 ns in isopropanol to 300 ns in cyclohexane and to 3 µs in benzene [109,117]. Furthermore, the fact that this process is known to continue effectively even when oxygen is present makes benzophenone a reliable and widely applicable photochemically reactive species [113, 118, 119].

The most important photochemical reactions that the formed biradical is capable of are the addition to carbon-carbon double bonds, and more important to the current work, the abstraction of aliphatic hydrogens, especially if these are

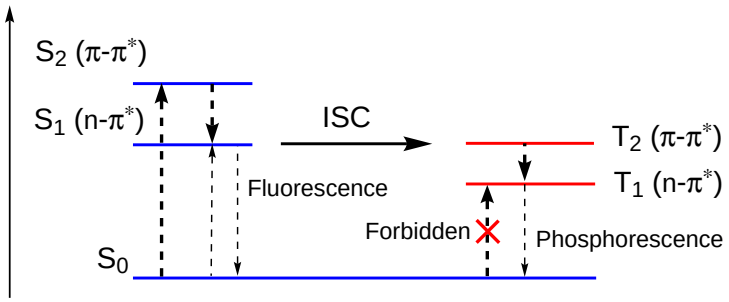

Figure 2.7: Simplified Jablonski diagram for the benzophenone excited states.

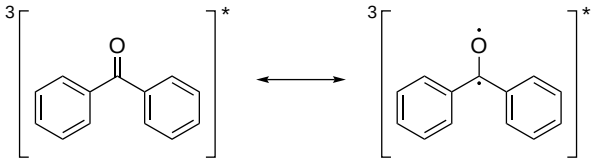

Scheme 2.1: Triplet states of benzophenone with resonance structure.

at the α-position to an electron-donating atom such as oxygen or nitrogen (See **I** in Scheme 2.2) [109,110,113]. The radical formed by the H-abstraction can then react with the remaining carbon-centered radical from the benzophenone moiety (**IIa** in Scheme 2.2), or with another radical produced by the H-abstraction in a different polymer chain (**IIb** in Scheme 2.2).

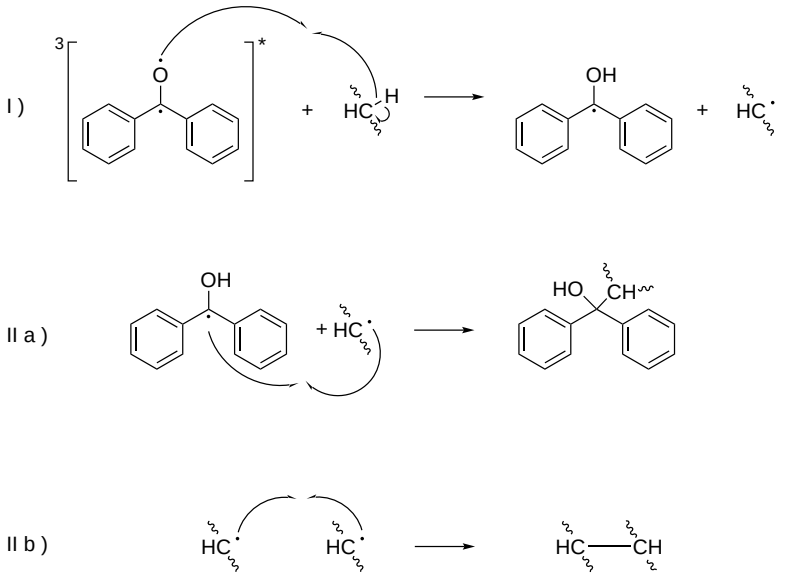

Scheme 2.2: Mechanism of H-abstraction and crosslinking by benzophenone biradical.

Chapter 3

Amphiphilic Sulfobetaine Copolymers

3.1 Synthesis and Characterization of Amphiphilic Sulfobetaine Copolymers

Ternary copolymers of SPE, BMA, and BPEMA, namely poly(SPE$_{90}$-*co*-BMA$_{10}$-*co*-BPEMA$_1$) (**P(SPE$_{90}$-BMA$_{10}$)**), poly(SPE$_{70}$-*co*-BMA$_{30}$-*co*-BPEMA$_1$) (**P(SPE$_{70}$-BMA$_{30}$)**), and poly(SPE$_{50}$-*co*-BMA$_{50}$-*co*-BPEMA$_1$) (**P(SPE$_{50}$-BMA$_{50}$)**), were synthesized by free-radical solution copolymerization in trifluoroethanol (TFE) using 2,2'-azobisisobutyronitrile (AIBN) as initiator. After dialysis against ultra pure water using a membrane with nominal molecular weight cutoff (MWCO) of 3500 g mol^{-1} and further lyophilization for the removal of H_2O, pure copolymers were obtained.

The quantitative determination of the composition of the ternary statistical copolymers is non-trivial. Due to the broad and poorly resolved signals, the ^{1}H NMR spectra do not enable a precise compositional analysis. The evaluation of the data from the elemental analysis (EA) for determining the composition of the ternary copolymers is complicated by the marked hygroscopy of all samples and the resulting residual water content. As the H contents of all four components SPE, BMA, BPEMA, and H_2O are similar, the determined H contents of the copolymers are not suitable for a meaningful compositional analysis, while the elements N and S occur only in the SPE units. Therefore, compositions could only be calculated from the analytical data using the C/N or C/S ratios (in this way eliminating the effect of the residual water in the samples), assuming that the molar ratios of the hydrophobic monomers BMA/BPEMA in the copolymers were the same as in the feed. Due to the low content of BPEMA (1 mol%) in the reaction mixtures and the high yields (> 60%), this approximation seems justified concerning the contents of the majority components, SPE and BMA. The possible error for the calculated ratio SPE/BMA in the copolymers would be rather small even if no BPEMA was incorporated. Under the previous asumptions the composition calculated for the copolymers are summarized in Table 3.1. Still, the precision of the calculated ratios SPE/BMA is inevitably limited and the values are only reliable ± 10 rel.%.

Table 3.1: Molar composition of amphiphilic copolymers calculated from the data obtained by elemental analysis

Copolymer	SPE [mol%]	BMA [mol%]	BPEMA [mol%]
P(SPE$_{90}$-BMA$_{10}$)	90	10	1
P(SPE$_{70}$-BMA$_{30}$)	70	30	1
P(SPE$_{50}$-BMA$_{50}$)	50	50	1

In contrast, elemental analysis does not enable a meaningful estimation of the low BPEMA contents. Still the ^{1}H NMR spectra of the copolymers clearly indicate the incorporation of non-negligible amounts of BPEMA. A rough estimation according to the integrals of the characteristic ^{1}H NMR signals of BMA and of BPEMA support the view of their approximately equivalent incorporation into the copolymers, i.e., the BPEMA content is the order of 1 mol% with an estimated error margin of ±50 rel.% (See Figures 3.1, 3.2, and 3.3).

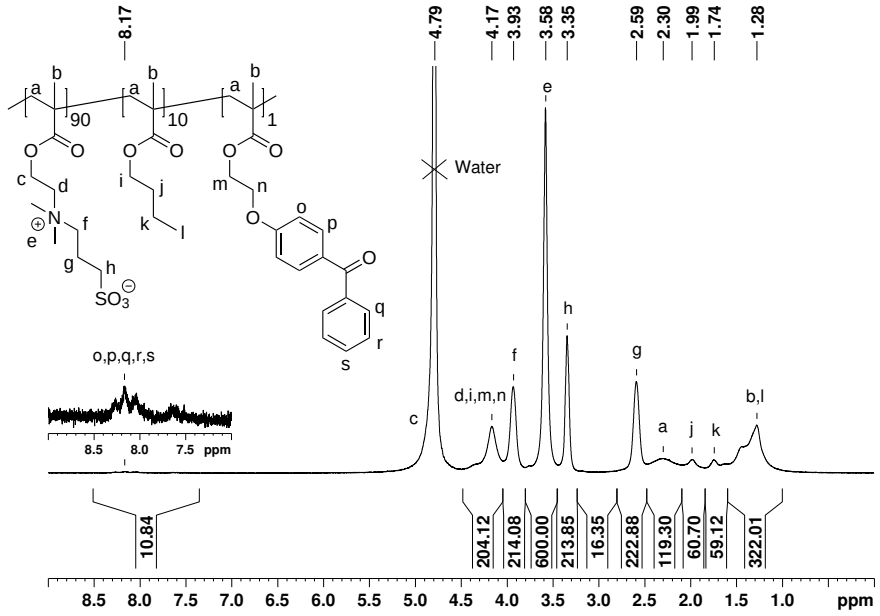

Figure 3.1: ^{1}H NMR spectrum of copolymer **P(SPE$_{90}$-BMA$_{10}$)** in a saturated solution of NaCl in D_2O.

Alternatively, the content of photoreactive BPEMA units in the copolymers was quantified by ultraviolet-visible (UV-Vis) spectroscopy. The maximum absorbance wavelength (λ_{max}) of the methacrylic photo-crosslinker BPEMA was determined at 292 nm in TFE (See Figure 3.4), which is in accordance to previous reports in the literature [58]. Additionally, its molar extinction coefficient

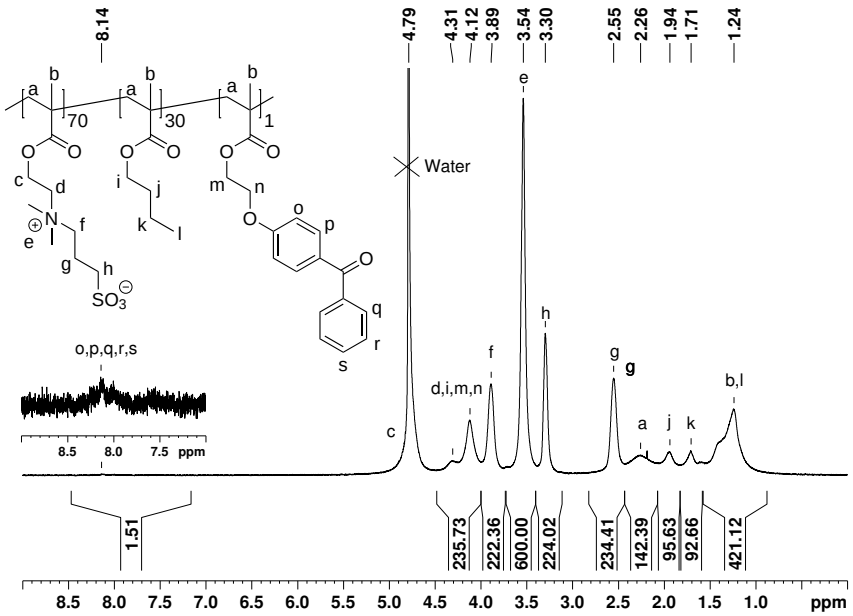

Figure 3.2: ^{1}H NMR spectrum of copolymer **P(SPE$_{70}$-BMA$_{30}$)** in a saturated solution of NaCl in D_2O.

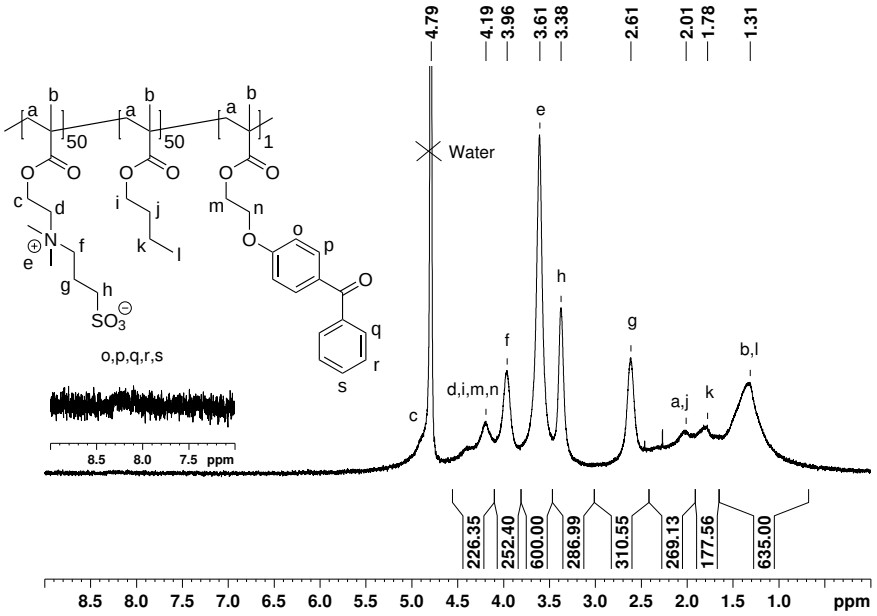

Figure 3.3: ^{1}H NMR spectrum of copolymer **P(SPE$_{50}$-BMA$_{50}$)** in a saturated solution of NaCl in D_2O.

(ε) was calculated by measuring the UV-Vis absorption of samples at different concentrations in TFE. The absorption measurements at different molar concentrations were then fitted to a linear regression that intersects at $(0, 0)$, a value of ε of $20\,449\,\mathrm{L\,mol^{-1}\,cm^{-1}}$ with an estimated error margin of ± 5 rel.% was determined by Equation 3.1 (See Figure 3.5).

$$A = \varepsilon d C \tag{3.1}$$

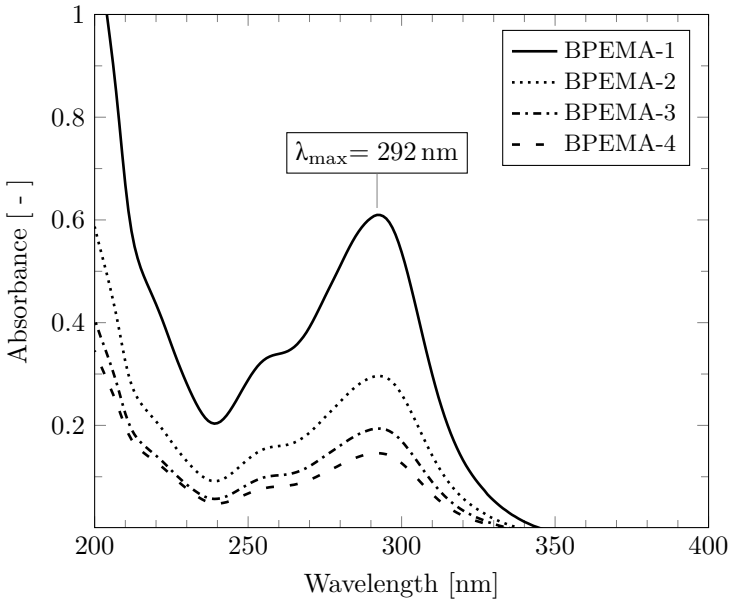

Figure 3.4: UV-Vis spectra of monomer BPEMA at different concentrations in TFE.

The absorbances at 292 nm for weighed-in masses of the copolymers in TFE were determined. Under the assumption that the value of ε does not change after incorporation into the copolymers, the measured absorptions of the amphiphilic copolymers were 0.453, 0.509, and 0.436 for copolymers **P(SPE$_{90}$-BMA$_{10}$)**, **P(SPE$_{70}$-BMA$_{30}$)**, and **P(SPE$_{50}$-BMA$_{50}$)**, respectively (See Figure 3.6). When compared to the weighed-in mass of the sample, these values represent a 0.79 mol% of photo-crosslinker BPEMA in copolymer **P(SPE$_{90}$-BMA$_{10}$)**, 0.75 mol% in copolymer **P(SPE$_{70}$-BMA$_{30}$)**, and 0.73 mol% in copolymer **P(SPE$_{50}$-BMA$_{50}$)**. Given the experimental errors, these results further support a BPEMA content of 1 mol% in the final copolymers.

As the amphiphilic copolymers have different amounts of hydrophilic sulfobetaine moieties in their compositions, their hydrophilicity is expected to decrease with the hydrophobic content of each copolymer. The thermogravimetric analysis (TGA) of the copolymers show a non-negligible mass loss at temperatures at which no thermal decomposition of the samples is expected i.e., <150 °C. This mass loss could be attributed to the evaporation of water molecules bound to the hydrophilic moieties of the amphiphilic copolymers. From the TGA a mass loss of 8.9, 6.2, and 5.1 % for copolymers **P(SPE$_{90}$-BMA$_{10}$)**, **P(SPE$_{70}$-BMA$_{30}$)**,

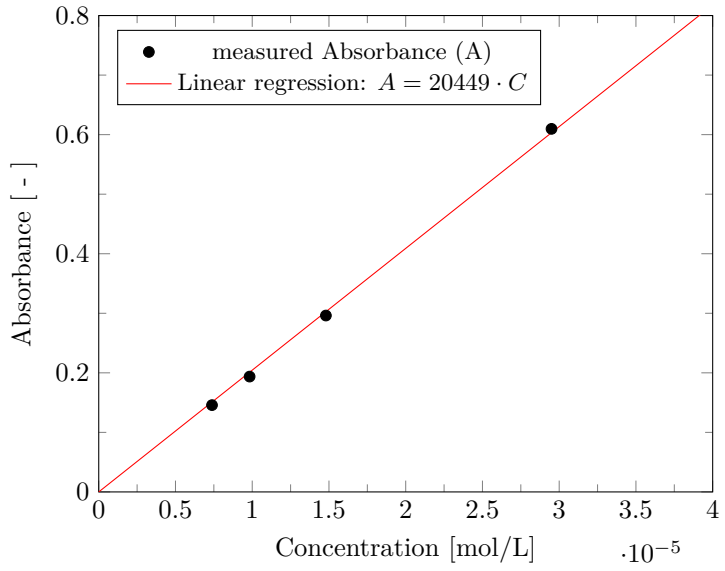

Figure 3.5: Determination of the extinction coefficient of monomer BPEMA in TFE.

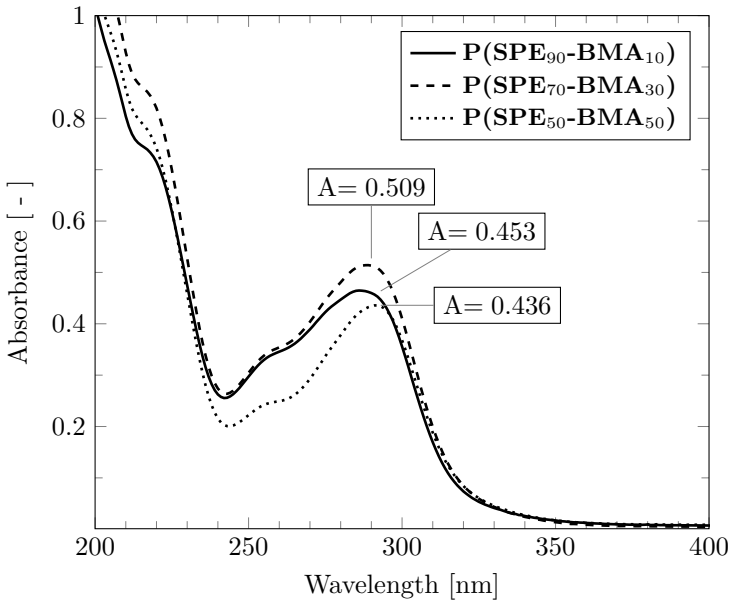

Figure 3.6: UV-Vis spectra of the BPEMA-derived absorption maxima of dilute solutions of amphiphilic copolymers **P(SPE$_{90}$-BMA$_{10}$)**, **P(SPE$_{70}$-BMA$_{30}$)**, and **P(SPE$_{50}$-BMA$_{50}$)** in TFE with concentrations of 724, 826, and 627 mg L^{-1}, respectively.

and **P(SPE$_{50}$-BMA$_{50}$)**, respectively, was observed at temperatures <150 °C (See Figures 3.7, 3.8, and 3.9). These results would represent 1.7, 1.4, and 1.6 molecules of H_2O per zwitterionic repeat unit in the copolymers **P(SPE$_{90}$-BMA$_{10}$)**, **P(SPE$_{70}$-BMA$_{30}$)**, and **P(SPE$_{50}$-BMA$_{50}$)**, respectively, which is in accordance with the information obtained from the elemental analysis of the copolymers.

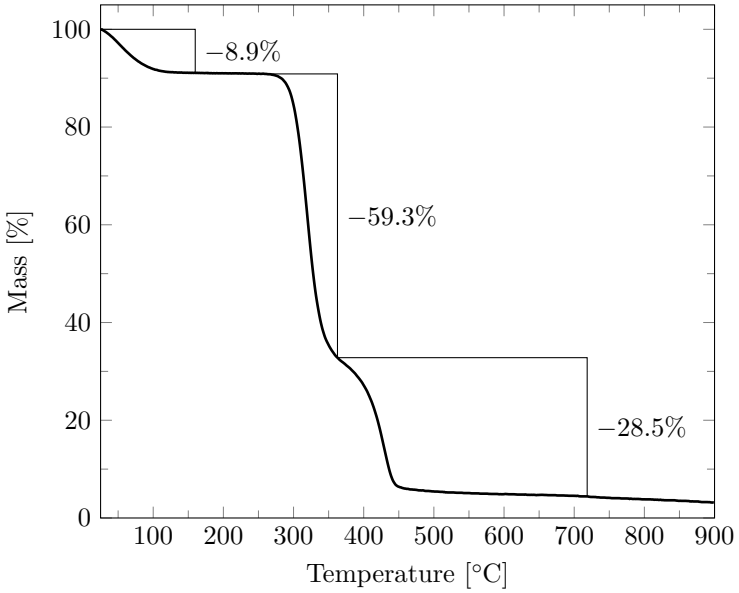

Figure 3.7: TGA of amphiphilic copolymer **P(SPE$_{90}$-BMA$_{10}$)** under N_2 atmosphere with a heating rate of 10 K min^{-1}.

In order to estimate the number of crosslinking sites per polymer chain, molar mass distributions of the amphiphilic copolymers were measured by gel permeation chromatography (GPC) using hexafluoroisopropanol (HFIP) with 50 mM of sodium trifluoroacetate as eluent and a calibration by narrowly distributed poly(methyl methacrylate) (P(MMA)) standards (See Figure 3.10). From the GPC data, values for number average molar mass (M_n), weight average molar mass (M_w), and dispersity (Đ) of each amphiphilic copolymer were determined, these are summarized in Table 3.2.

It is important to mention that a decrease in the M_w of the copolymers is observed as the proportion of hydrophobic monomer BMA increases. This can be explained by the difference of the polarities of the two monomers and the reduction of polarity introduced by the hydrophobic monomer during the copolymerization (See Table 3.2) [93]. Another important observation is the apparent shoulder in the regions above 1×10^6 g mol^{-1} (See Figure 3.10). However, this is most likely an artifact, as the exclusion limit of the chromatography column is reportedly within this range of molar masses, which renders all molecules above this limit to elute at the same elution volume and no effective separation of the polymer chains can be expected.

With the values of M_n and a weighted average molecular weight of the monomers, number average degree of polymerization (X_n) values in the range of

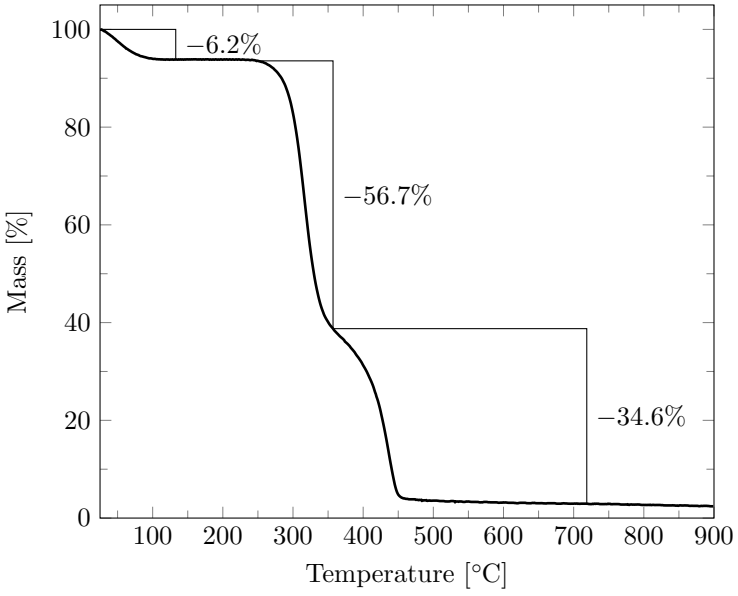

Figure 3.8: TGA of amphiphilic copolymer **P(SPE$_{70}$-BMA$_{30}$)** under N_2 atmosphere with a heating rate of $10\,\mathrm{K\,min^{-1}}$.

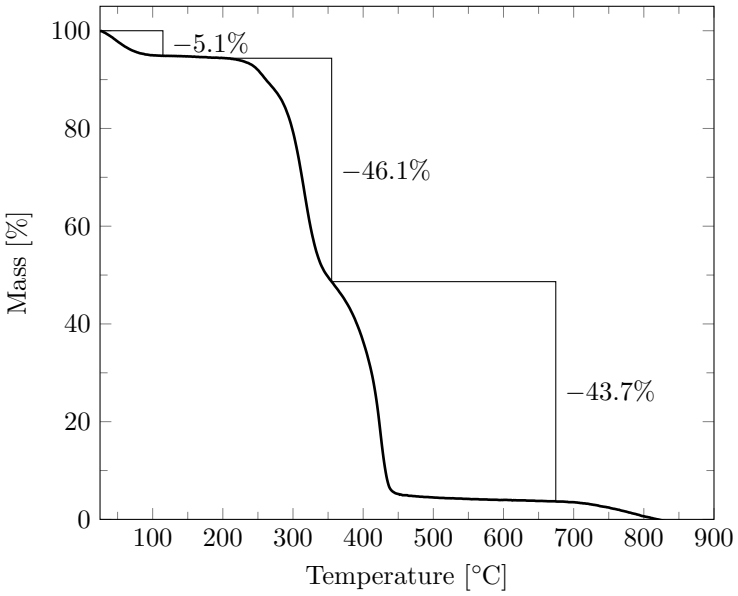

Figure 3.9: TGA of amphiphilic copolymer **P(SPE$_{50}$-BMA$_{50}$)** under N_2 atmosphere with a heating rate of $10\,\mathrm{K\,min^{-1}}$.

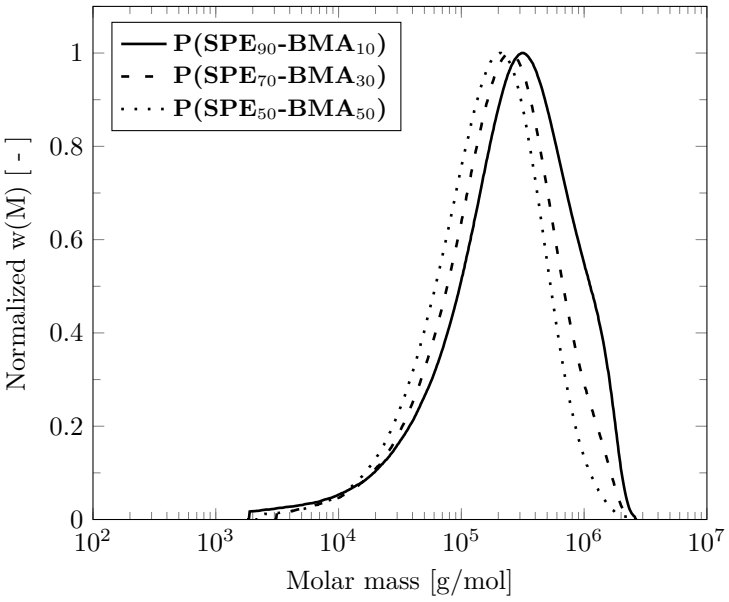

Figure 3.10: Molar mass distributions of amphiphilic copolymers **P(SPE$_{90}$-BMA$_{10}$)**, **P(SPE$_{70}$-BMA$_{30}$)**, and **P(SPE$_{50}$-BMA$_{50}$)** according to GPC-analysis (eluent HFIP with 50 mM of sodium trifluoroacetate, calibration by narrowly distributed P(MMA) standards).

Table 3.2: Apparent molar masses of amphiphilic copolymers according to GPC analysis (See Figure 3.10).

Copolymer	M_n [kg/mol]	M_w [kg/mol]	Đ [−]
P(SPE$_{90}$-BMA$_{10}$)	90	420	4.7
P(SPE$_{70}$-BMA$_{30}$)	100	320	3.3
P(SPE$_{50}$-BMA$_{50}$)	80	240	3.1

350–400 were calculated. As determined by UV-Vis and other characterization techniques, the synthesized amphiphilic copolymers contain, within the experimental error, 1 mol% BPEMA. With this information, on average, the number of potential crosslinking sites per copolymer chain is expected to be in the range of 3–4. This value is of importance for the formation of hydrogel networks, as at least >1 crosslinking sites per polymer chain on average are needed in order to form a stable hydrogel network.

3.2 Properties of Thin Hydrogel Films of Amphiphilic Copolymers

Thin hydrogel films were produced by spin coating of the amphiphilic copolymers dissolved in TFE onto silicon and glass substrates modified with a (3-aminopropyl)dimethylethoxysilane monolayer. The produced thin films were subsequently photo-crosslinked by UV irradiation for 30 min. A detailed description of the procedure is found in Section 8.2.9 on page 88 of this thesis.

The stability of the produced hydrogels was tested by measuring the thickness of the thin films by ellipsometry before crosslinking, after crosslinking, and after washing three times with ultra pure water baths while agitating. The hydrogel thin films showed good stability as their thickness showed no substantial decrease after washing with ultra pure water under agitation (See Figure 3.11).

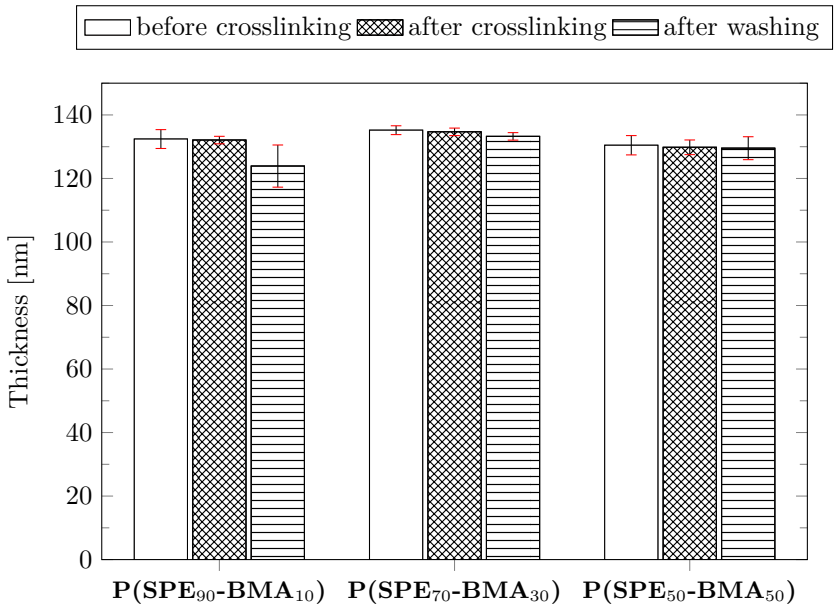

Figure 3.11: Stability of immobilized thin hydrogel films of **P(SPE-BMA)** amphiphilic copolymers.

The resistance against non-specific protein adsorption of the **P(SPE-BMA)** amphiphilic copolymers was evaluated by surface plasmon spectroscopy (SPR) by cooperation partners at the Ruhr University Bochum, namely the results

of these evaluations have already been published [65]. In the assessment, the resistance of the amphiphilic copolymers against non-specific adsorption of two proteins was evaluated. For these experiments, two model proteins were used: fibrinogen, which is a slightly negatively charged protein at pH 7.4 (pI 5.5, molar mass 340 kDa), and lysozyme, which has a distinct positive charge (pI 10.9, molar mass 14 kDa). In their evaluations, it was found that the adsorption of fibrinogen to **P(SPE$_{50}$-BMA$_{50}$)** showed a more than 200-fold lower protein adsorption when compared to the hydrophobic reference poly(butyl methacrylate) (P(BMA)). Whereas protein adsorption on the copolymers **P(SPE$_{70}$-BMA$_{30}$)**, **P(SPE$_{90}$-BMA$_{10}$)**, and poly(3-[*N*-2(methacryloyloxy)ethyl-*N*,*N*-dimethyl]ammonio propane-1-sulfonate) (P(SPE)) was already negligible and too low to discriminate between them at a level of significance of 5 % (See Figure 3.12) [65].

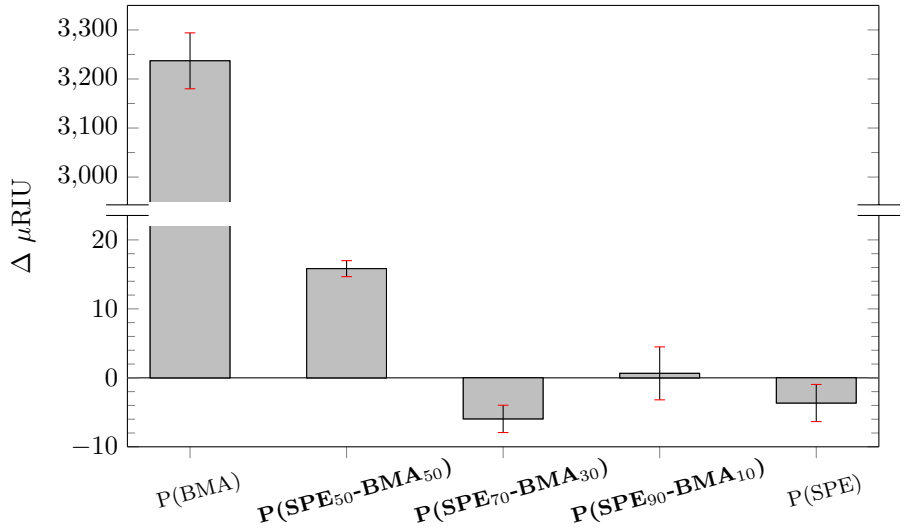

Figure 3.12: Irreversible adsorption of fibrinogen on the **P(SPE-BMA)** copolymers determined by SPR at a flow rate of 10 µL min^{-1} in refractive index units (RIU). Error bars indicate the standard error ($n = 3$) [65].

The adsorption of lysozyme, however, showed slightly different results. Here the amphiphilic copolymers showed the highest resistance against the protein adsorption. The coating with copolymer **P(SPE$_{70}$-BMA$_{30}$)** had no detectable protein adsorption, while the protein adsorption on copolymers **P(SPE$_{90}$-BMA$_{10}$)** and **P(SPE$_{50}$-BMA$_{50}$)** was already very small. The hydrophobic reference P(BMA) showed against the highest contamination, and P(SPE) exhibited a significantly higher protein adsorption ($p< 0.05$, post-hoc Tukey test) when compared to the amphiphilic copolymers (See Figure 3.13) [65].

Additional to the protein adsorption assessments, the settlement and removal of the green algae *U. linza* were also evaluated by our cooperation partners at the Ruhr University Bochum, within the scope of the previously mentioned publication [65]. The studies showed that all amphiphilic polymers had significantly lower settlement ($p< 0.05$, post-hoc Tukey test) of the green algae

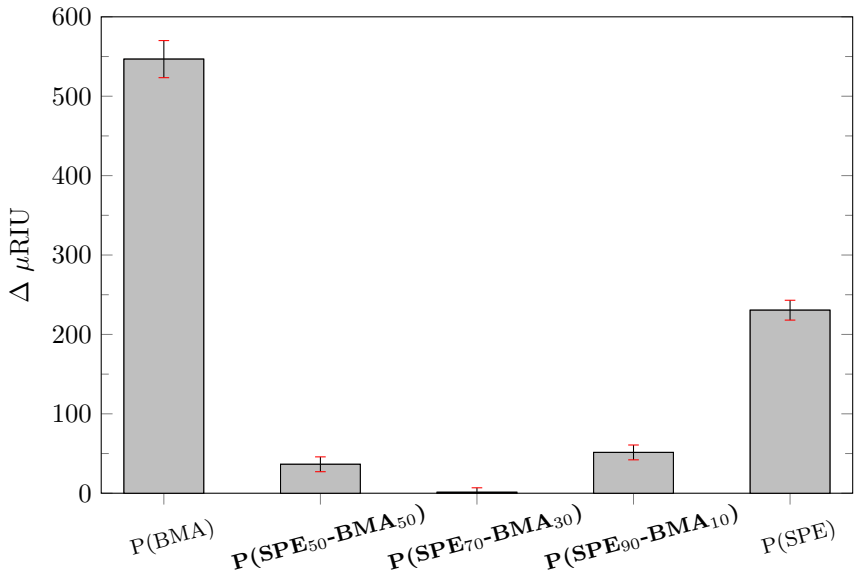

Figure 3.13: Irreversible adsorption of lysozyme on the **P(SPE-BMA)** amphiphilic copolymers determined by SPR at a flow rate of $10\,\mu L\,min^{-1}$ in refractive index units (RIU). Error bars indicate the standard error ($n = 3$) [65].

U. linza when compared to both the hydrophobic reference P(BMA) and the hydrophilic P(SPE) (See Figure 3.14) [65]. Moreover, after application of a turbulent flow, the removal of the spores from the amphiphilic coatings **P(SPE$_{90}$-BMA$_{10}$)**, **P(SPE$_{70}$-BMA$_{30}$)**, and **P(SPE$_{50}$-BMA$_{50}$)** was greater than those of the parent homopolymers P(SPE) and P(BMA), indicating a lower attachment strength of the spores on the amphiphilic surfaces (See Figure 3.14) [65].

Finally, our cooperation partners at the Ruhr University Bochum, tested the mechanical stability of the samples by challenging the coatings by incubation in an autoclaved sediment suspension for 2 h, the amount of incorporated sediment particles was then determined photometrically. The results of the evaluation showed a decrease in the sediment incorporation as the content of BMA in the copolymers increased (See Figure 3.15) [65].

In general, within the assessments done by our cooperation partners at the Ruhr University Bochum, it was found that the presence of hydrophobic BMA units in the copolymers significantly improved the anti-fouling properties of the coatings. Furthermore, the incorporation of increasing amounts of BMA also decreased the sediment uptake.

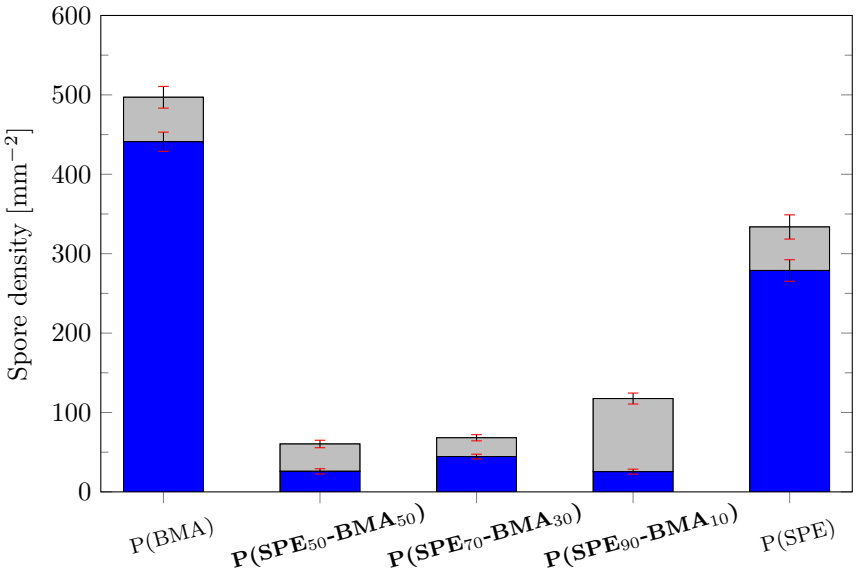

Figure 3.14: Density of settled *U. linza* zoospores on the **P(SPE-BMA)** copolymers after a 45 min settlement period (grey) and after exposure to a turbulent water flow exerting a wall shear stress of 52 Pa (blue). Error bars indicate the standard error ($n = 90$) [65].

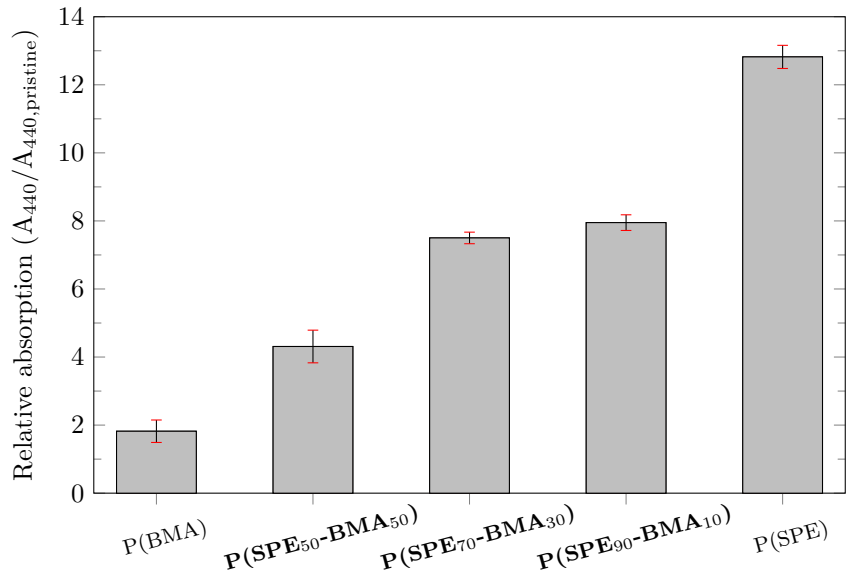

Figure 3.15: Silt uptake of the **P(SPE-BMA)** copolymer coatings after 2 h sediment immersion. Error bars indicate the standard error after six measurements on two replicate slides [65].

Chapter 4

New Amphiphilic Sulfobetaines

4.1 Synthesis and Characterization of New Amphiphilic Sulfobetaine Monomers

As mentioned in Chapter 1, an amphiphilic sulfobetaine monomer was synthesized in order to further test the impact that hydrophilicity has on both the antifouling properties of zwitterionic hydrogels and their mechanical stability. The synthesis of this amphiphilic sulfobetaine monomer was done by the ring opening of 1,2-epoxyhexane with dimethylamine, followed by the acylation of the produced alkanolamine with methacryloyl chloride. The resulting methacrylic amine 1-(dimethylamino)hexan-2-yl methacrylate (**I-2**) was then quaternized with 1,3-propane sultone, amphiphilic sulfobetaine methacrylate **M1** was obtained as a precipitate from the reaction mixture as a colorless solid (See Scheme 4.1).

The chemical structure of **M1** was characterized by ^{1}H NMR spectroscopy. Relevant signals in the ^{1}H NMR-spectrum are the vinylidene protons (signals "j" and "i") found at 6.24 and 5.83 ppm, respectively, the lone proton at the chiral carbon in the α-position from the ester bond (signal "e") found at 5.53 ppm, and the 6 protons from the methyl groups at the quaternized amine (signal "g") found at 3.17 ppm. A full characterization and description of the peaks are shown in Figure 4.1.

The structural characterization of **M1** was further analyzed by ^{1}H-^{1}H-COSY NMR. With this characterization method the signals of the methylene protons on the carbons at the α and β-positions from the methyl group at the end of the aliphatic side chain (signals "b" and "c") were better described, as coupling with the protons at the directly neighbouring carbons was observed (signals "b/a" and "d/c"). Similar couplings from the methylene protons on the carbons between the quaternized amine and the sulfonate moiety (signals "k", "l", and "m") were also utilized to get a more detailed structural characterization of **M1**. An interesting feature of the ^{1}H-^{1}H-COSY NMR spectra of **M1** is the coupling of the lone proton at the chiral carbon in the α-position from the ester bond (signal "e"), as coupling was only observed with one of the two methylene

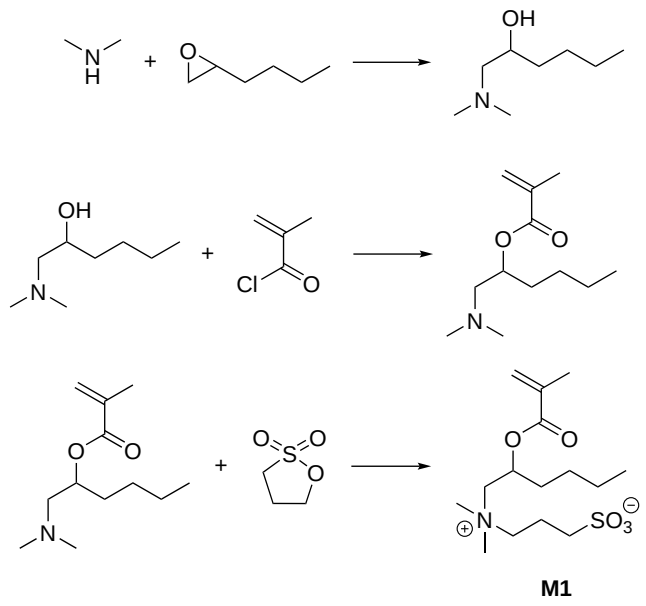

Scheme 4.1: Synthetic path to amphiphilic sulfobetaine **M1**.

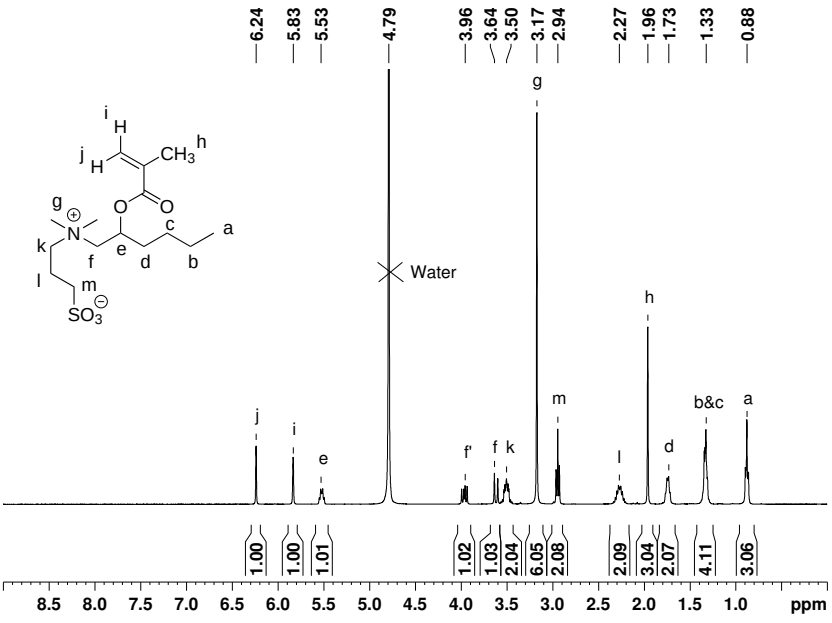

Figure 4.1: ^{1}H NMR spectrum of monomer **M1** in D_2O.

protons on the carbon in the α-position from the quaternized amine (signal "e/f′"). A full ^{1}H-^{1}H-COSY NMR-spectra characterization with descriptive annotations is shown in Figure 4.2.

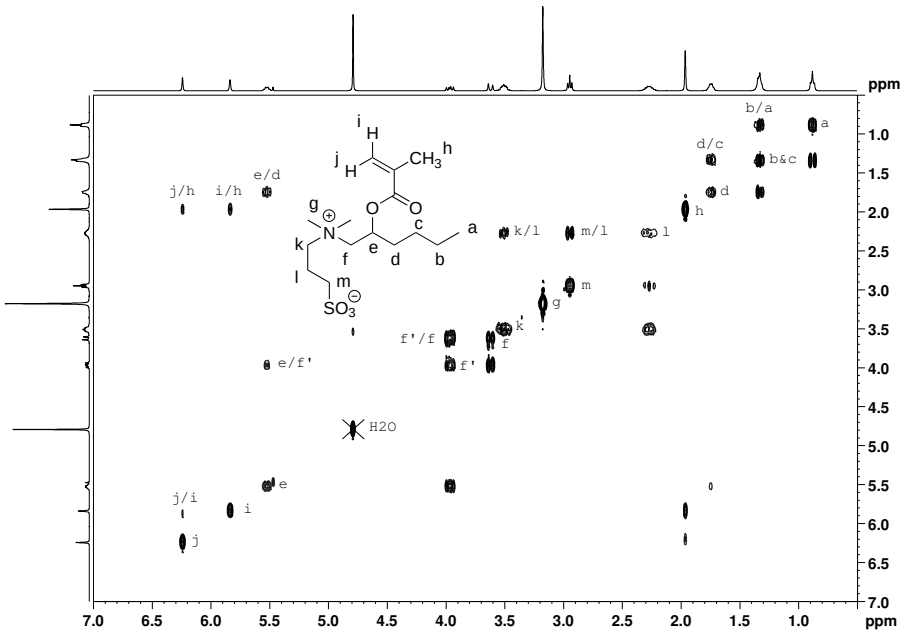

Figure 4.2: ^{1}H-^{1}H-COSY NMR spectrum of **M1** in D_2O.

By ^{13}C (APT) NMR, a more detailed characterization of **M1** was done, as this characterization method provides information not only on the chemical shift of the carbons found in the molecule, but also on the amount of hydrogen atoms bonded to each carbon, showing positive signals for carbons with an odd number of hydrogen atoms bonded (1 or 3), and negative signals for carbons with an even amount of hydrogen atoms bonded (0 or 2). With this information, only the carbons of the methyl groups (signals "A", "H", and "G") and the carbon at the α-position from the ester bond (signal "E") were expected to render positive signals in the ^{13}C (APT) NMR-spectrum, giving further confirmation of the structural composition of the desired monomer **M1**. Complete ^{13}C (APT) NMR-spectrum and characterization are shown in Figure 4.3.

Further confirmation of the previously assigned signals was achieved with ^{1}H-^{13}C-HSQC NMR characterization. It was specially important to confirm that both methylene protons assigned with signals "f" and "f′" were bonded to the same carbon (signals "f/F" and "f′/F"). Another feature of the molecule that was better described with this characterization method was the methylene protons on the carbons at the α and β-positions from the methyl group at the end of the aliphatic side chain (signals "b" and "c" in Figure 4.1), as both signals were overlapping in the ^{1}H NMR-spectrum. However, the ^{1}H-^{13}C-HSQC NMR-spectrum further confirms that two independent sets of protons are attached to two different carbons (signals "b/B" and "c/C"). Full ^{1}H-^{13}C-HSQC NMR characterization is shown in Figure 4.4.

For the full characterization of **M1**, its thermal properties were investigated

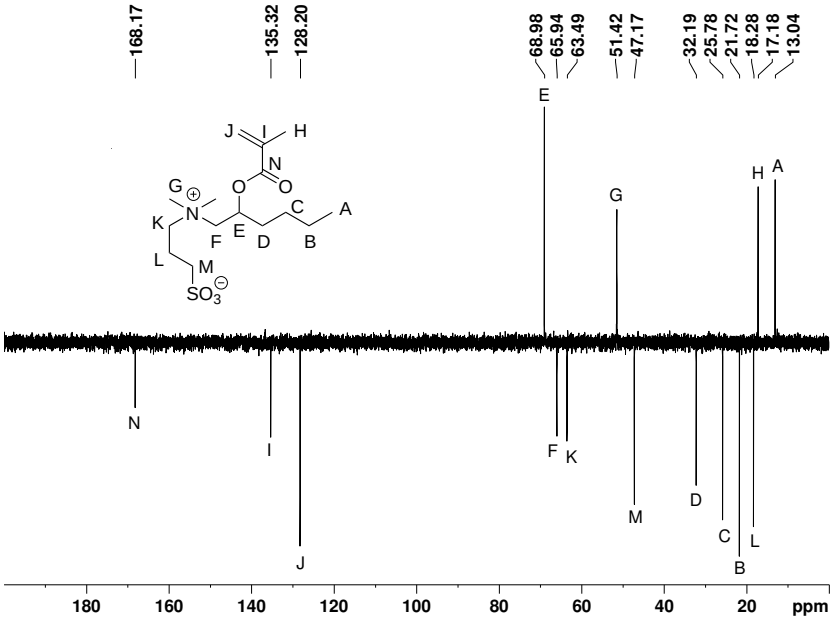

Figure 4.3: ^{13}C (APT) NMR spectrum of **M1** in D_2O.

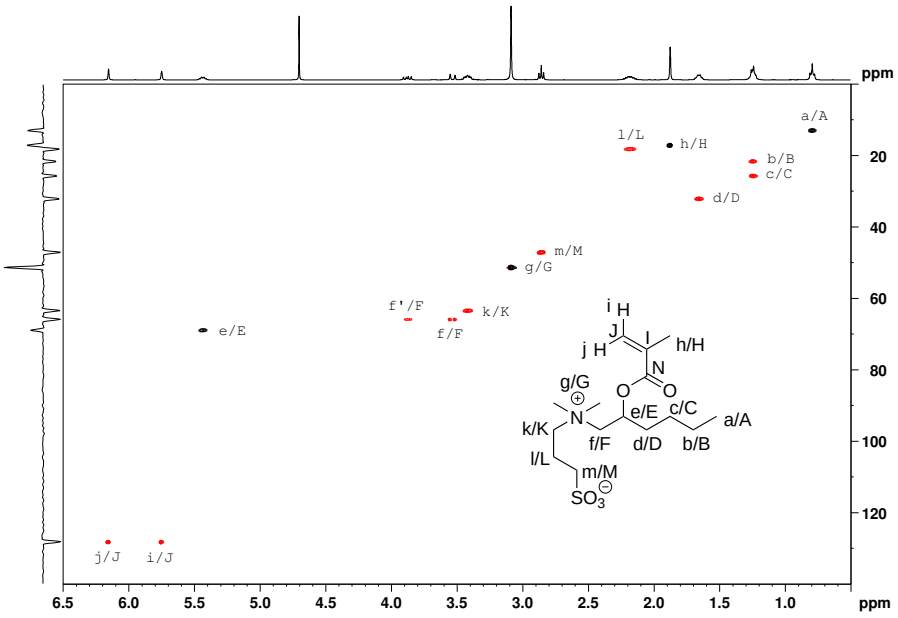

Figure 4.4: ^{1}H-^{13}C-HSQC NMR spectrum of **M1** in D_2O.

by differential scanning calorimetry (DSC) (See Figure 4.5). The thermogram showed an endothermic peak with onset at 167 °C and a normalized enthalpy of 110 J g^{-1}, the peak was reached at 172 °C. This endothermic peak is evidence of a phase transition ocurring within the sample, i.e., melting. The melting point of the monomer **M1** was thus determined at the onset of the endothermic peak (167 °C). However, with the 2nd cycle of the DSC, it was also observed that degradation of the sample took place, as its thermal properties were significantly altered after the 1st heating cycle.

Further information obtained from the DSC thermogram was that no presence of water bound to the amphiphilic monomer **M1** was found. For a monomer containing a zwitterionic moiety, certain degree of hygroscopy would be expected, however, the observed endothermic peak happens at a considerably higher temperature than the one expected due to water elimination at around 100 °C.

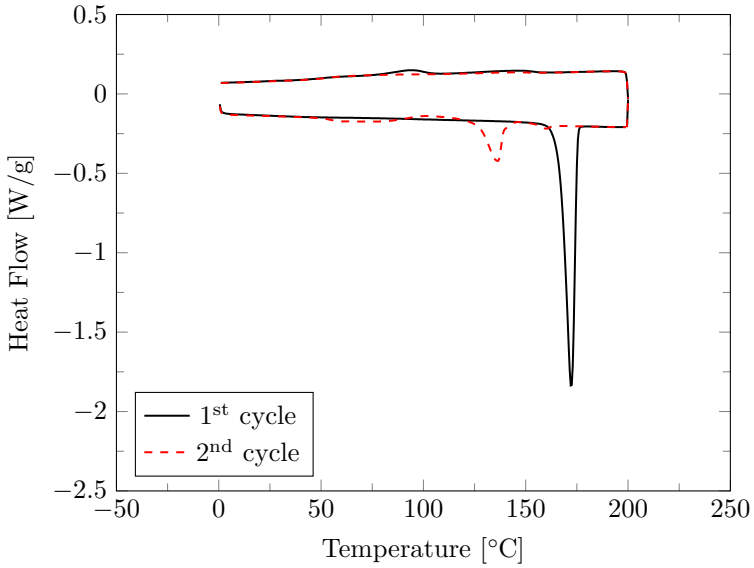

Figure 4.5: DSC thermogram of amphiphilic methacrylate **M1**, two cycles 0–200 °C at 5 K min^{-1}.

4.2 Synthesis and Characterization of Homopolymers of Amphiphilic Sulfobetaine

Homopolymers of the amphiphilic sulfobetaine methacrylate **M1** were obtained by solution polymerization in TFE using AIBN as initiator. The polymers were then purified by dialysis against ultra pure water using a membrane with MWCO of 3500 g mol^{-1}, and isolated by lyophilization.

The obtained polymer poly(3-((2-(methacryloyloxy)hexyl)dimethylammonio)-propane-1-sulfonate) (**P(M1)**) was characterized by ^{1}H NMR spectroscopy in a saturated solution of NaCl in D_2O. An important difference found when com-

paring the ^{1}H NMR-spectra of amphiphilic monomer **M1** (Figure 4.1) and of its homopolymer **P(M1)** was the abscence of the signals of the vinylidene protons characteristic of methacrylate monomers (signals "j" and "i" in Figure 4.1). Nevertheless, evidence of the aliphatic protons of the polymer backbone product from the polymerization of **M1** (signals "j" and "h" in Figure 4.6) is observed when analysing the area under the signals between 2.58–0.68 ppm. According to the most prominent signals (signals "a", "b,c", "d", and "l") a total of 11 protons is expected to be found within this range of the spectrum, however, the integral accounts for 16 protons, indicating that the methylene and methyl protons from the backbone (signals "j" and "h") are indeed within this range of the spectrum. Moreover, the general broadening of the signals, characteristic of high molecular weight molecules, i.e., polymers, is also an indication of the successful polymerization of **M1**. A full characterization and description of the peaks is shown in Figure 4.6.

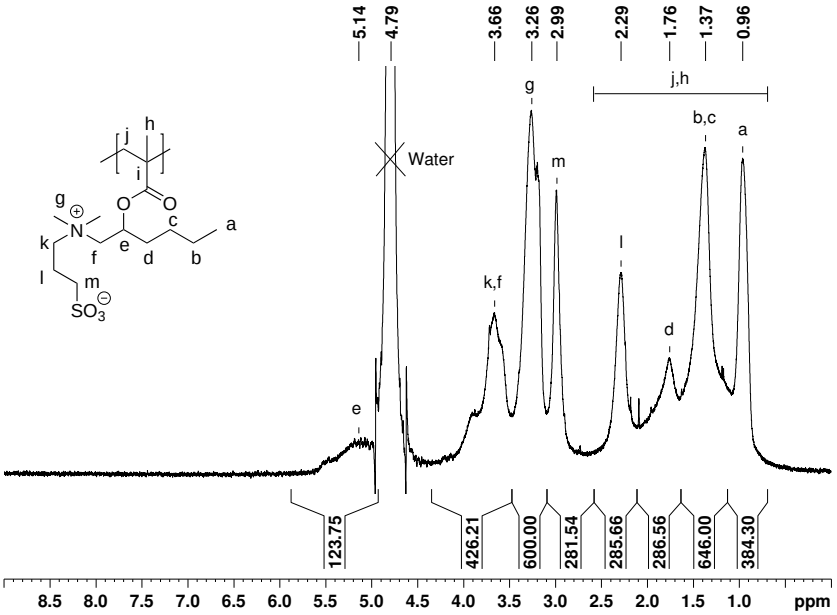

Figure 4.6: ^{1}H NMR spectrum of homopolymer **P(M1)** in a saturated solution of NaCl in D_2O.

The molar mass distributions of the produced homopolymers of the amphiphilic sulfobetaine **M1** were measured by GPC using HFIP with 50 mM of sodium trifluoroacetate as eluent and a calibration by narrowly distributed P(MMA) standards (See Figure 4.7). From the GPC data, values for M_n, M_w, and Đ were determined, these are summarized in Table 4.1. Values of 150 and 900 kg mol^{-1} were calculated for M_n and M_w, respectively. However, these values are most likely underrepresented as the exclusion limit of the column at around 1×10^6 g mol^{-1} was reached so all polymer chains above this limit elute at the same elution volume and no effective separation of the polymer chains can be expected. This is also evident from Figure 4.7 as the intensity of the peak in this range of molar masses (1×10^6 g mol^{-1}) does not correspond to

a normal distribution and hints to an unsuccessful separation of the polymer chains.

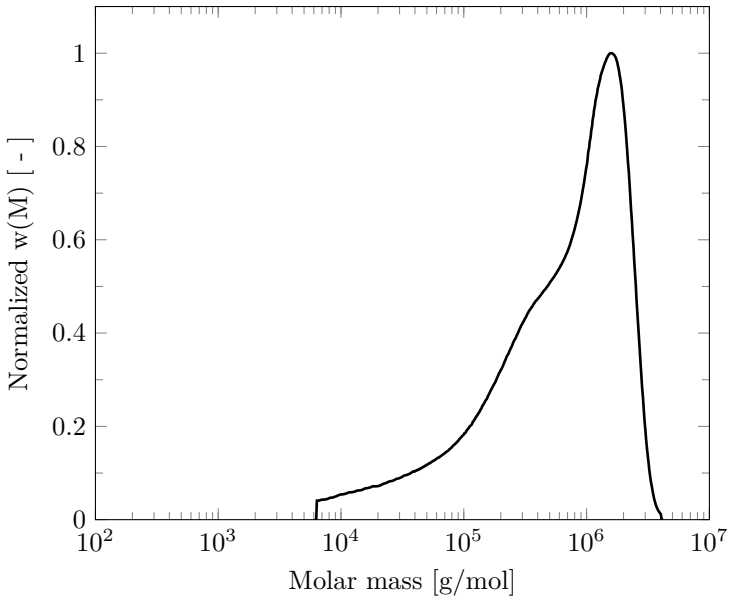

Figure 4.7: Molar mass distribution of amphiphilic homopolymer **P(M1)** according to GPC-analysis (eluent HFIP with 50 mM of sodium trifluoroacetate, calibration by narrowly distributed P(MMA) standards).

Table 4.1: Apparent molar masses of amphiphilic homopolymer **P(M1)** according to GPC analysis (See Figure 4.7).

Copolymer	M_n [kg/mol]	M_w [kg/mol]	Đ [–]
P(M1)	150	900	6.0

By TGA characterization, the upper thermal stability of homopolymer **P(M1)** was studied. Additionally, the amount of water bound to the homopolymer **P(M1)** was determined. The TGA thermogram shows a loss of mass of 13.9 % at temperatures up to 150 °C (See Figure 4.8). As this mass loss happens mostly at temperatures below 150 °C, it is attributed to the evaporation of water molecules bound to the zwitterionic moieties of the homopolymers. By calculation, this mass loss would represent about 2.5 molecules of H_2O per constitutional repeat unit (CRU) of the polymer. Further thermolysis of the homopolymers is then observed from 250 °C and up.

The solubility of homopolymer **P(M1)** in some standard solvents, together with the Dimroth-Reichardt empirical polarity parameter ($E_T(30)$), which combines polarity effects and hydrogen-bond donating capabilities of the solvents [120–122], is listed in Table 4.2.

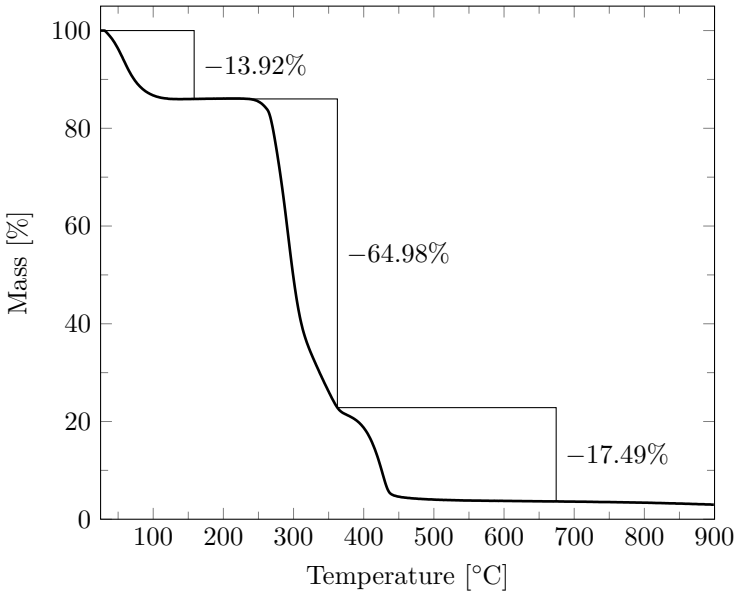

Figure 4.8: TGA thermogram of amphiphilic homopolymer **P(M1)** under N_2 atmosphere with a heating rate of $10\,\mathrm{K\,min^{-1}}$.

As it is characteristic for polysulfobetaines, **P(M1)** was insoluble in aprotic solvents, such as dioxane, tetrahydrofuran (THF), chloroform, acetone, dimethyl formamide (DMF) or dimethyl sulfoxide (DMSO) [3, 123, 124]. Also in accordance to the general trend for polyzwitterions, the solubility of **P(M1)** was restricted to protic solvents with high $E_T(30)$ values ($E_T(30) \gtrapprox 55\,\mathrm{kcal\,mol^{-1}}$) [124], such as formamide, and the fluorinated alcohols TFE and HFIP (See Table 4.2).

Although the dissolution of **P(M1)** in water was partial and only swelling was observed, similar to common polyzwitterionic behaviour, full dissolution was achieved upon addition of NaCl (See Table 4.2).

Table 4.2: Solubility of amphiphilic homopolymer **P(M1)** in selected solvents.

Solvent	$E_T(30)$[a] [kcal/mol]	**P(M1)**
dioxane	36.0	–
tetrahydrofuran	37.5	–
ethyl acetate	38.0	–
chloroform	39.1	–
dichloromethane	40.7	–
acetone	42.3	–
dimethyl formamide	43.2	–
dimethyl sulfoxide	45.1	–
acetic acid	51.7[b]	–
ethanol	51.8	–
formic acid	54.3[b]	+
methanol	55.4	–
formamide	55.9	+
trifluoroacetic acid	−−	∼
trifluoroethanol	59.8	+
hexafluoroisopropanol	65.3	+
water	63.1	∼
saturated NaCl	−−	+

[a] Unless otherwise stated, obtained from [120]
[b] Values calculated from Kosower's Z values, see references [121, 122]
+ = soluble
– = not soluble
∼ = slightly soluble (swollen)

4.3 Synthesis and Characterization of Copolymers of Amphiphilic Sulfobetaines

In order to further test the impact that enhanced hydrophilicity has on both the antifouling properties of zwitterionic hydrogels and their mechanical stability, ternary copolymers of **M1**, SPE, and BPEMA, namely poly(SPE$_{90}$-*co*-M1$_{10}$-*co*-BPEMA$_1$) (**P(SPE$_{90}$-M1$_{10}$)**), poly(SPE$_{70}$-*co*-M1$_{30}$-*co*-BPEMA$_1$) (**P(SPE$_{70}$-M1$_{30}$)**), and poly(SPE$_{50}$-*co*-M1$_{50}$-*co*-BPEMA$_1$) (**P(SPE$_{50}$-M1$_{50}$)**), were synthesized by free-radical solution copolymerization in TFE using AIBN as initiator. After dialysis against a H_2O:methanol (MeOH) [1:1] (v:v) solution using a membrane with MWCO of 3500 g mol^{-1} and further lyophilization for the removal of the solvents, pure copolymers were obtained.

Similar to the ternary copolymers of SPE, BMA, and BPEMA discussed in Chapter 3, the quantitative determination of the composition of the ternary statistical copolymers is non-trivial. Due to the broad and poorly resolved signals, the ^{1}H NMR-spectra do not enable a precise compositional analysis. However, the content of photoreactive BPEMA units in the copolymers was quantified by UV-Vis spectroscopy, as the absorbance band and absorption coefficient of the BPEMA chromofore had already been determined. Under the assumption that the absorption coefficient does not change after incorporation to the copolymers, the absorbances at 292 nm for weighed-in masses of the copolymers in TFE were determined. The measured absorptions of the amphiphilic copolymers were 0.445, 0.421, and 0.410 for copolymers **P(SPE$_{90}$-M1$_{10}$)**, **P(SPE$_{70}$-M1$_{30}$)**, and **P(SPE$_{50}$-M1$_{50}$)**, respectively (See Figure 3.6). When compared to the weighed-in mass of the sample, and under the assumption that the molar ratios of the zwitterionic monomers SPE/**M1** in the copolymers were the same as in the feed, these values represent a 0.77 mol% of photo-crosslinker BPEMA in copolymer **P(SPE$_{90}$-M1$_{10}$)**, 0.74 mol% in copolymer **P(SPE$_{70}$-M1$_{30}$)**, and 0.70 mol% in copolymer **P(SPE$_{50}$-M1$_{50}$)**. Given the experimental errors, these results support a BPEMA content of about 1 mol% in the final copolymers.

Once the amount of photo-crosslinker BPEMA was determined by UV-Vis spectroscopy, the evaluation of the data from the elemental analysis data enabled the calculation of the compositions of the SPE and **M1**. As the elements N and S occur only in the zwitterionic units, and the amount of non-zwitterionic units (BPEMA) had already been determined, systems of linear equations with two variables were set to calculate the ratios of [SPE:**M1**] of the copolymers. Under these assumptions and according to the information obtained from the elemental analysis, an [SPE:**M1**] ratio of [88:12] was calculated for copolymer **P(SPE$_{90}$-M1$_{10}$)**, [69:31] for copolymer **P(SPE$_{70}$-M1$_{30}$)**, and [53:47] for copolymer **P(SPE$_{50}$-M1$_{50}$)**. A rough estimation according to the integrals of the characteristic ^{1}H NMR signals of the aliphatic protons (signals "i", "j", "k", and "l") also support the view of their approximately equivalent incorporation into the copolymers, as the integrals consistently increased as the amount of amphiphilic sulfobetaine in the copolymers increased. However, due to the low resolution of the signals, an error margin of ± 50 rel.% is estimated (See Figures 4.10, 4.11, and 4.12).

The molar mass distributions of the copolymers were measured by GPC using HFIP with 50 mM of sodium trifluoroacetate as eluent and a calibration by narrowly distributed P(MMA) standards (See Figure 4.13). From the GPC

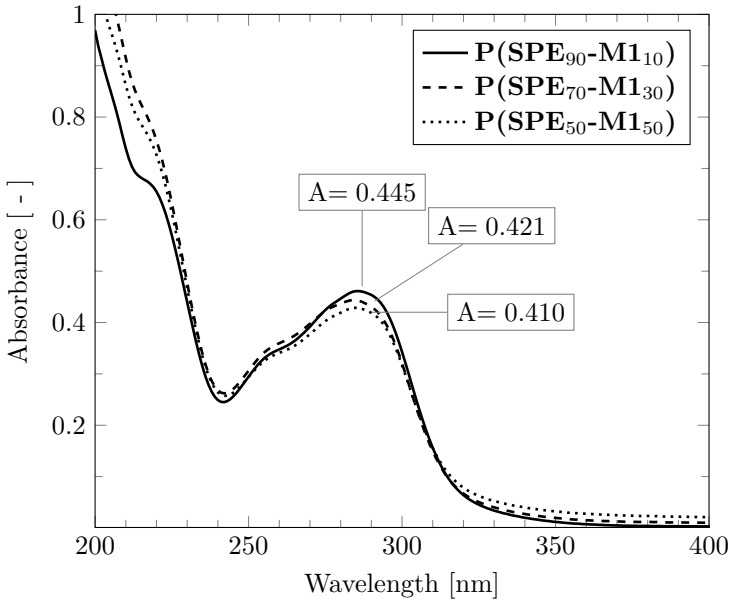

Figure 4.9: UV-Vis spectra of the BPEMA-derived absorption maxima of dilute solutions of amphiphilic copolymers **P(SPE$_{90}$-M1$_{10}$)**, **P(SPE$_{70}$-M1$_{30}$)**, and **P(SPE$_{50}$-M1$_{50}$)** in TFE with concentrations of 812, 827, and 882 mg L^{-1}, respectively.

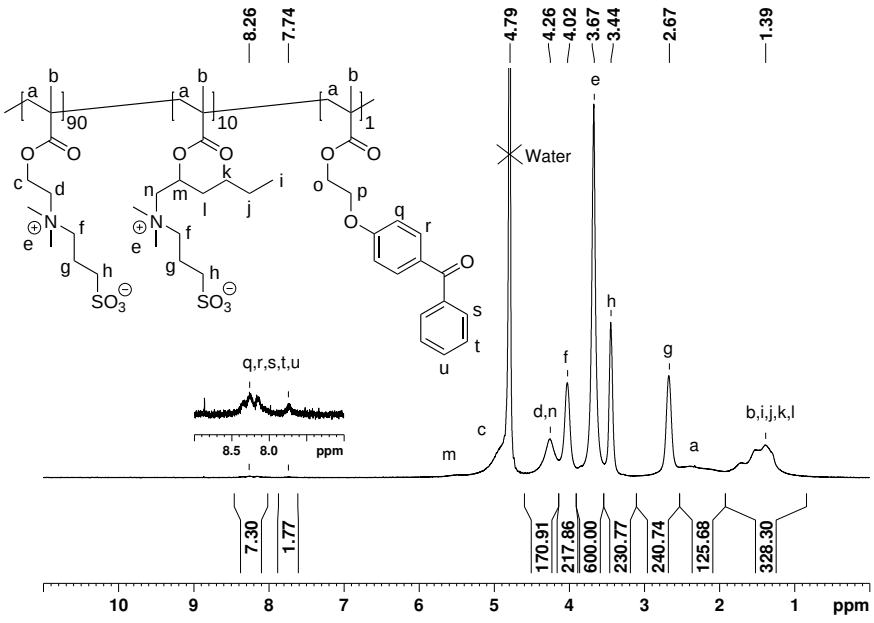

Figure 4.10: ^{1}H NMR spectrum of copolymer **P(SPE$_{90}$-M1$_{10}$)** in a saturated solution of NaCl in D_2O.

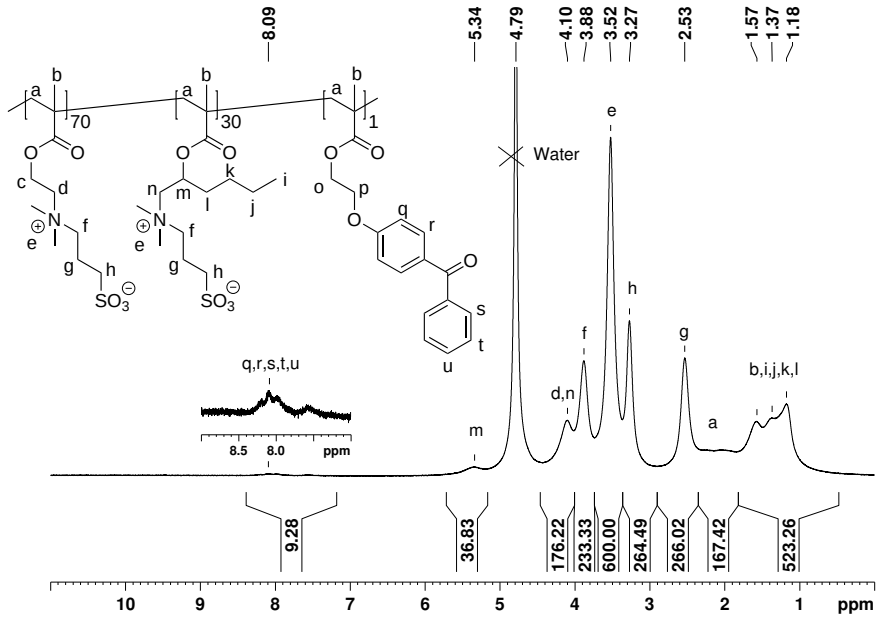

Figure 4.11: ^{1}H NMR spectrum of copolymer **P(SPE$_{70}$-M1$_{30}$)** in a saturated solution of NaCl in D_2O.

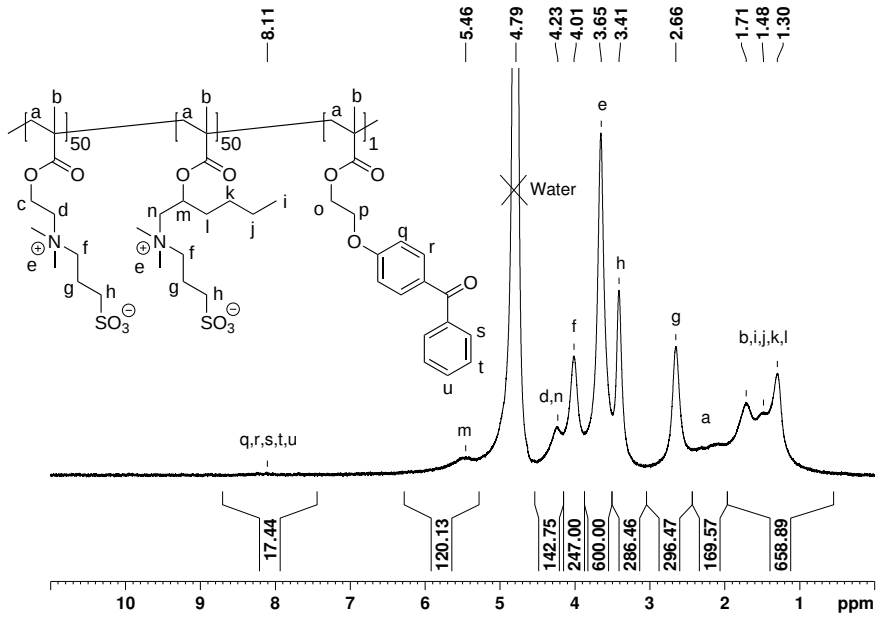

Figure 4.12: ^{1}H NMR spectrum of copolymer **P(SPE$_{50}$-M1$_{50}$)** in a saturated solution of NaCl in D_2O.

data, values for M_n, M_w, and Đ of each amphiphilic copolymer were determined, these are summarized in Table 4.3.

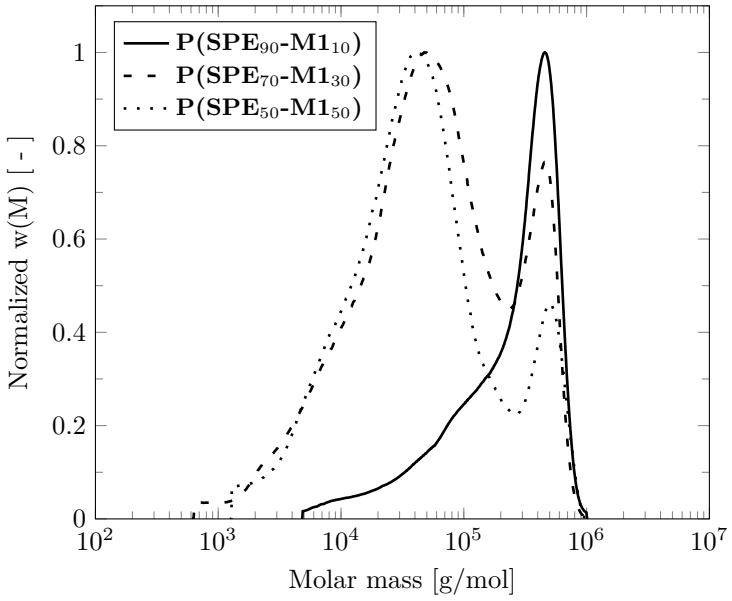

Figure 4.13: Molar mass distributions of amphiphilic copolymers **P(SPE$_{90}$-M1$_{10}$)**, **P(SPE$_{70}$-M1$_{30}$)**, and **P(SPE$_{50}$-M1$_{50}$)** according to GPC-analysis (eluent HFIP with 50 mM of sodium trifluoroacetate, calibration by narrowly distributed P(MMA) standards).

From the M_n and M_w values obtained for the different copolymers, it was noticed that the apparent molar mass of the copolymers was strongly reduced as the proportion of **M1** increased in the composition of the copolymers. It is possible that these findings could be caused by a decreasing solvent quality of the eluent due to the difference of polarity between the two comonomers [93], or by the relatively bulky side chain of monomer **M1**. Similar to the GPC measurements of the homopolymer **P(M1)**, the exclusion limit of the column was reached and an effective separation of the polymer chains was not possible (See Figure 4.13).

With the values of M_n and a weighted average molecular weight of the monomers, apparent X_n values of 350 were calculated for **P(SPE$_{90}$-M1$_{10}$)**, and of 70 for both **P(SPE$_{70}$-M1$_{30}$)** and **P(SPE$_{50}$-M1$_{50}$)**. As determined by UV-Vis and other characterization techniques, the synthesized amphiphilic copolymers contain, within the experimental error, 1 mol% BPEMA. With this information, on average, the number of potential crosslinking sites per copolymer chain can be estimated to be in the range of 3–4 for **P(SPE$_{90}$-M1$_{10}$)**, however, a much lower value is calculated for both **P(SPE$_{70}$-M1$_{30}$)** and **P(SPE$_{50}$-M1$_{50}$)**, as values <1 are calculated. This is of importance for the formation of hydrogel networks, as at least >1 crosslinking sites per polymer chain, on average, are needed in order to form a stable hydrogel network. According to this estimation, the immobilization of thin hydrogel films could be challenging.

Table 4.3: Apparent molar masses of amphiphilic copolymers **P(SPE-M1)** according to GPC analysis (See Figure 4.13).

Copolymer	M_n [kg/mol]	M_w [kg/mol]	Đ [−]
P(SPE$_{90}$-M1$_{10}$)	100	300	3.0
P(SPE$_{70}$-M1$_{30}$)	20	130	5.9
P(SPE$_{50}$-M1$_{50}$)	20	110	5.1

Analogous to the solubility tests done for homopolymer **P(M1)** discussed in the previous Section 4.2, the solubilities of the terpolymers **P(SPE$_{90}$-M1$_{10}$)**, **P(SPE$_{70}$-M1$_{30}$)**, and **P(SPE$_{50}$-M1$_{50}$)** in selected solvents are shown in Table 4.4.

From the results, interesting effects are observed with the solubilities of terpolymers **P(SPE$_{90}$-M1$_{10}$)**, **P(SPE$_{70}$-M1$_{30}$)**, and **P(SPE$_{50}$-M1$_{50}$)** in protic solvents with relatively high $E_T(30)$ values (approx. 50–55 kcal mol^{-1}) such as acetic acid and MeOH. Even when the homopolymers of both zwitterionic monomers **P(M1)** and P(SPE) are insoluble in these protic solvents [124, 125], terpolymers **P(SPE$_{90}$-M1$_{10}$)**, **P(SPE$_{70}$-M1$_{30}$)**, and **P(SPE$_{50}$-M1$_{50}$)** show certain solubility in both acetic acid and MeOH (See Table 4.4).

Comparing the solubilities of the terpolymers **P(SPE$_{90}$-M1$_{10}$)**, **P(SPE$_{70}$-M1$_{30}$)**, and **P(SPE$_{50}$-M1$_{50}$)** to the ones of their parent homopolymers P(SPE) and **P(M1)** in water also reveals a rather counterintuitive effect on their solubility. As with an increasing amount of amphiphilic copolymer **M1** in the copolymers, an increase in their solubility in water is observed (See Table 4.4). This could be explained by the dampening of the intra- and intermolecular electrostatic interactions by the irregularities within the polymer chain introduced by the different copolymers.

Table 4.4: Solubility of amphiphilic copolymers **P(SPE-M1)** in selected solvents.

	Polymer		
Solvent	**P(SPE$_{90}$-M1$_{10}$)**	**P(SPE$_{70}$-M1$_{30}$)**	**P(SPE$_{50}$-M1$_{50}$)**
dioxane	–	–	–
tetrahydrofuran	–	–	–
ethyl acetate	–	–	–
chloroform	–	–	–
dichloromethane	–	–	–
acetone	–	–	–
dimethyl formamide	–	–	–
dimethyl sulfoxide	–	–	–
acetic acid	∼	∼	∼
ethanol	–	–	–
formic acid	+	+	+
methanol	∼	∼	∼
formamide	+	+	+
trifluoroacetic acid	+	∼	+
trifluoroethanol	+	+	+
hexafluoroisopropanol	+	+	+
water	–	∼	+
normal saline (0.9% NaCl)	+	+	+
artificial sea water	+	+	+
saturated NaCl	+	+	+

+ = soluble
– = not soluble
∼ = slightly soluble (swollen)

Chapter 5

New Vinyl Amide Monomers

5.1 Synthesis and Characterization of New Vinyl Amide Zwitterionic Monomers

A mentioned in Chapter 1, the introduction of a new family of vinyl amide zwitterionic monomers was done in order to have a positive impact on the hydrolytic stability of the resulting polymers when compared to the methacrylic zwitterionic monomers and polymers. The synthesis of the new vinyl amide zwitterionic monomers was thought to be done through the *N*-acylation of 1-methylpiperazine, followed by the quaternization of the tertiary amine. A vinyl amide would then be produced by the Hoffmann-elimination of the quaternized piperazinium ion.

A first attempt to synthesize the desired vinyl amide was done by the quaternization of the intermediary tertiary amine with methyl iodide, however, the obtained piperazinium iodide resulted insoluble in most solvents appropriate for the Hoffmann-elimination. The poor solubility of the piperazinium iodide in suitable solvents hindered this synthetic path towards the vinyl amide.

In order to overcome this solubility issue, a piperazinium tosylate was synthesized instead in an attempt to improve its solubility in organic solvents compared to the previously synthesized piperazinium iodide. The piperazinium tosylate was soluble in *tert*-butanol (*t*-BuOH) and the Hoffmann-elimination was done using potassium *tert*-butoxide (*t*-BuOK). Through this synthetic path, the vinyl amide *N*-(2-(dimethylamino)ethyl)-*N*-vinylacetamide (**I-5**) was obtained after purification via column chromatography (See Scheme 5.1).

Zwitterionic vinyl amides **M2**, **M3**, and **M4** were synthesized in good yields by quaternization of the tertiary amine in **I-5** with cyclic sulfonates and sulfates (See Scheme 5.2).

After isolation of the products, the analytical data confirmed the successful synthesis of monomers **M2**, **M3**, and **M4**. Characteristic features of the new monomer **M2** are the methylene protons at the α-position to the amide group (signal "e") at 4.16 ppm, the ^{1}H NMR signals of the methyl and the methylene protons at the α-position to the quaternized amine (signals "g" and "f&h")

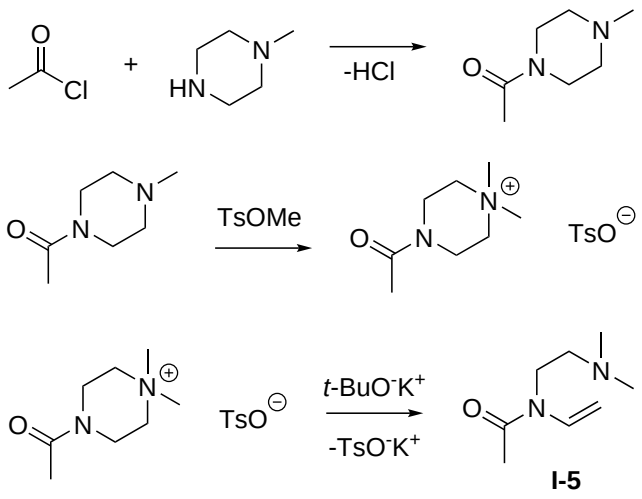

Scheme 5.1: Synthetic path to intermediate vinyl amide **I-5**.

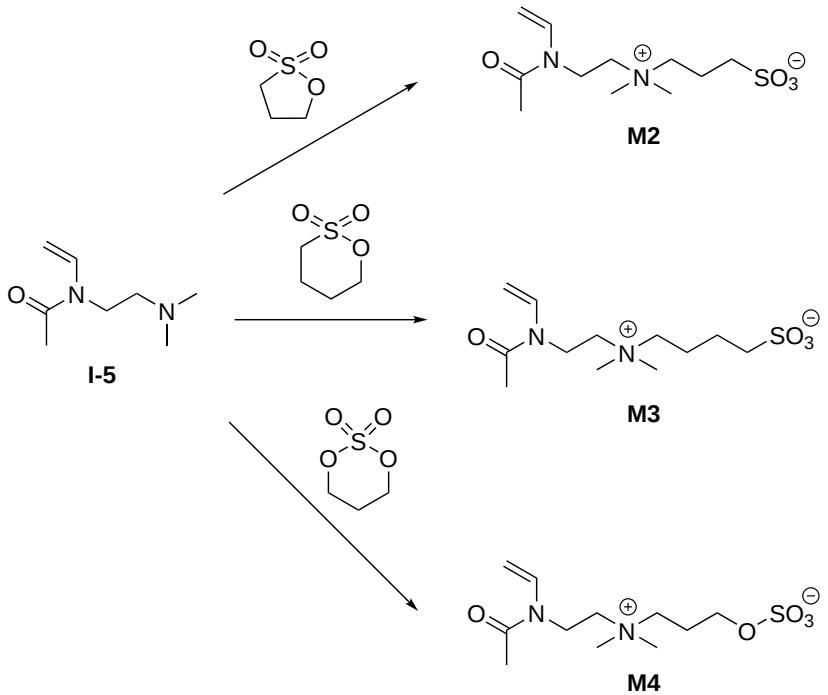

Scheme 5.2: Synthesis of zwitterionic vinyl amides **M2**, **M3**, and **M4**.

at 3.22 ppm and 3.55 ppm, respectively, and the methylene protons at the α-position to the sulfonate moiety characteristic of sulfobetaines (signal "j") at 3.00 ppm. The fully characterized ^{1}H NMR-spectrum is shown in Figure 5.1.

Similar to monomer **M2**, the ^{1}H NMR-spectrum of sulfobetaine vinyl amide **M3** presents analogue signals for the aforementioned protons (signals "g", "f&h", "e", and "k"), although slightly shifted upfield as an effect of the longer aliphatic chain between the sulfonate group and the quaternized amine. The fully characterized ^{1}H NMR-spectrum is shown in Figure 5.2.

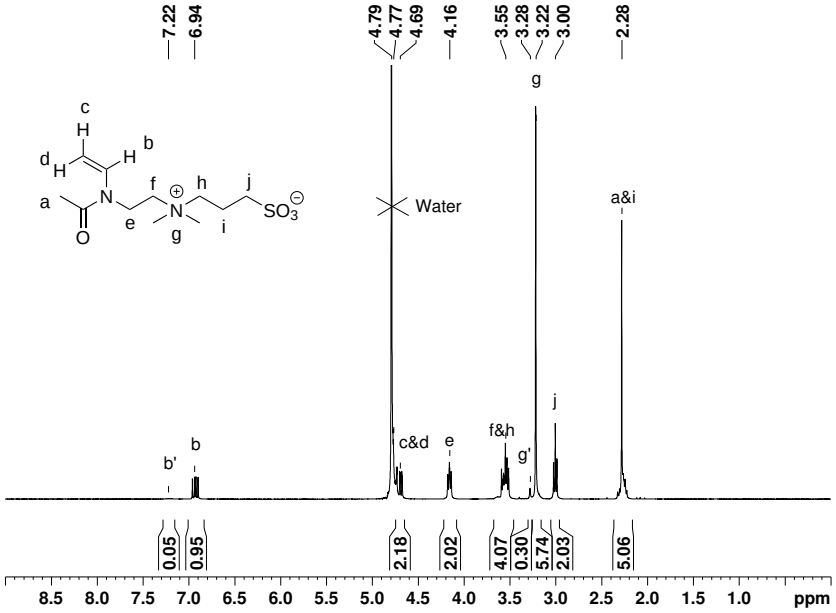

Figure 5.1: ^{1}H NMR spectrum of **M2** in D_2O.

Although monomers **M2** and **M4** share many similar structural characteristics, the main difference between them is the presence of an organosulfate group in vinyl amide sulfabetaine **M4** in contrast to the sulfonate group present in vinyl amide sulfobetaine **M2**. This difference makes most of the previously described ^{1}H NMR-spectrum signals to remain practically constant between the two monomers (signals "g", "f&h", and "e"). However, the methylene protons at the α-position to the organosulfate moiety in monomer **M4** experience a greater chemical shift downfield than their counterpart protons in monomer **M2**. This shift brings the signal of the α-position to the organosulfate moiety (signal "j") in vinyl amide sulfabetaine **M4** to 4.17 ppm, in contrast to the ones in **M2** appearing at 3.00 ppm. A full characterization of the ^{1}H NMR-spectrum is shown in Figure 5.3.

It is also important to notice the evidence of the *cis* and *trans* conformations of the tertiary amide. Particularly for the vinylidene proton (signal "b"), as the rotation about the central C−N bond of amides is hindered, the rotation is slow enough to be observed in the ^{1}H NMR-spectrum. Moreover, the *cis* and *trans* positions are not magnetically equivalent, resulting in different chemical shifts in the ^{1}H NMR-spectrum [126, 127]. Although this difference in chemical

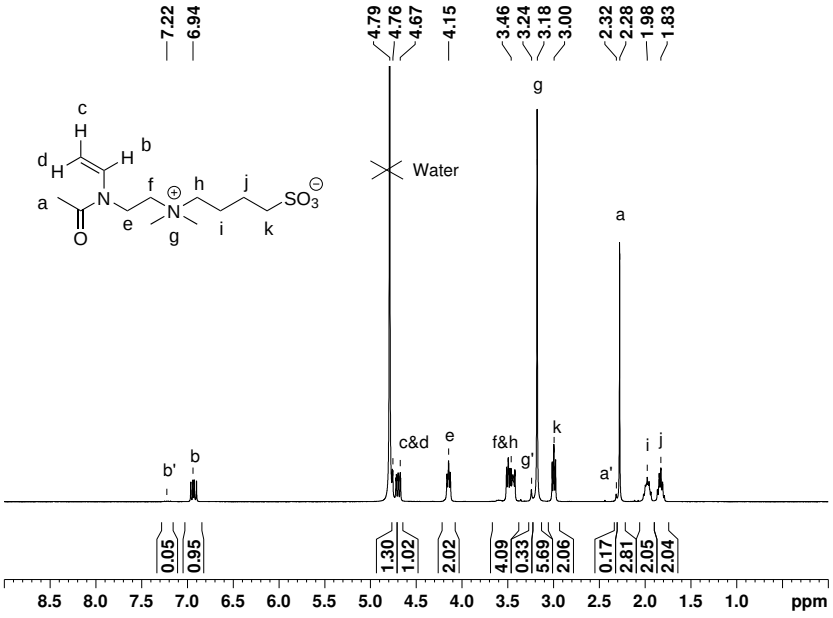

Figure 5.2: ^{1}H NMR spectrum of **M3** in D_2O.

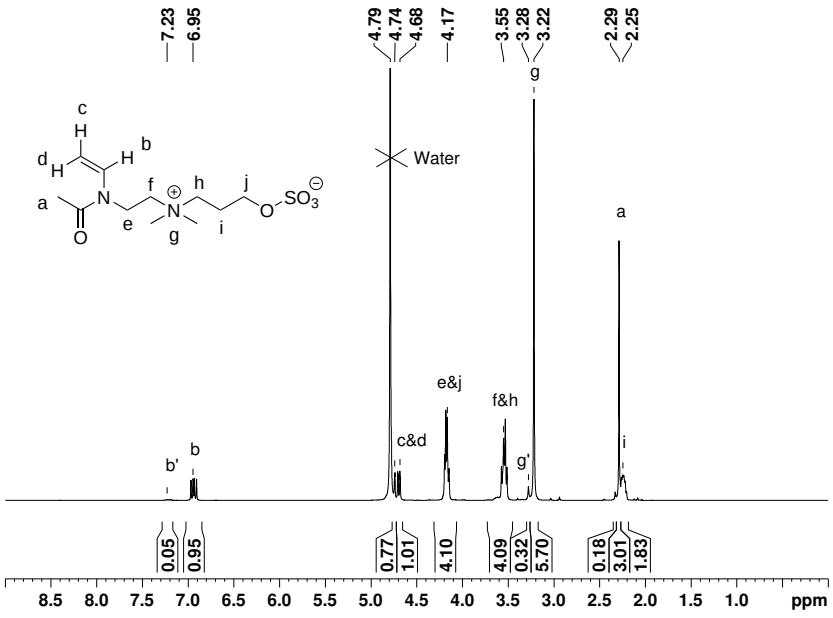

Figure 5.3: ^{1}H NMR spectrum of **M4** in D_2O.

shifts is more readily observed in the vinylidene proton (signal "b"), similar effects of the different conformations are observed for the methyl protons at the α-position to the quaternized amine (signal "g"). The previous is true for the three zwitterionic vinyl amides **M2**, **M3**, and **M4** (See Figures 5.1, 5.2, and 5.3). Furthermore, by analyzing the integrals, it is calculated that the percentage of *cis* and *trans* isomers in the monomers is about 5 % and 95 %, respectively.

Further characterization of the chemical structure of vinyl amide sulfobetaine **M2** was achieved by ^{1}H-^{1}H-COSY NMR, specifically, the overlapping signals of the methylene protons at the α-position to the quaternized amine (See Figure 5.1 signal "f&h"), could be better distinguished, as the coupling to the protons at the directly neighbouring carbons were identified (signals "e/f" and "h/i") (See Figure 5.4). As the overlapping of signals was a common problem in the ^{1}H NMR-spectra of monomers **M2**, **M3**, and **M4**, similar refinement in the characterization of their chemical structures was done by the analysis of the ^{1}H-^{1}H-COSY NMR-spectra. The full ^{1}H-^{1}H-COSY NMR-spectra of **M3** and **M4** are shown in Figures 5.5 and 5.6, respectively.

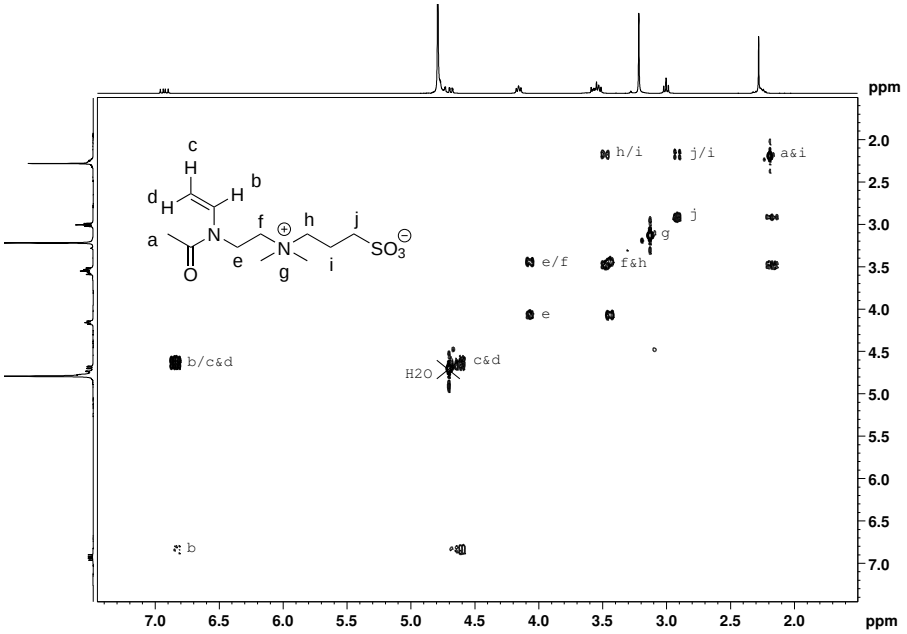

Figure 5.4: ^{1}H-^{1}H-COSY NMR spectrum of **M2** in D_2O.

A more detailed characterization of the chemical structure of monomers **M2**, **M3**, and **M4** was done by ^{13}C (APT) NMR. This characterization method was essential not only to identify the chemical shifts of the different carbon atoms present in the vinyl amides, but also as a confirmation that the desired monomers were synthesized. Important similarities observed throughout the three monomers in the ^{13}C (APT) NMR-spectra are the carbon from the carbonyl group (signal "D") observed at 173.2 ppm, both carbons of the vinyl group (signals "B" and "C") at 132.5 and 97.0 ppm, respectively, and the carbons of the methyl groups at the α-position to the quaternized amine (signal "G") at 51.0 ppm. Full ^{13}C (APT) NMR-spectra are shown in Figures 5.7, 5.8, and 5.9.

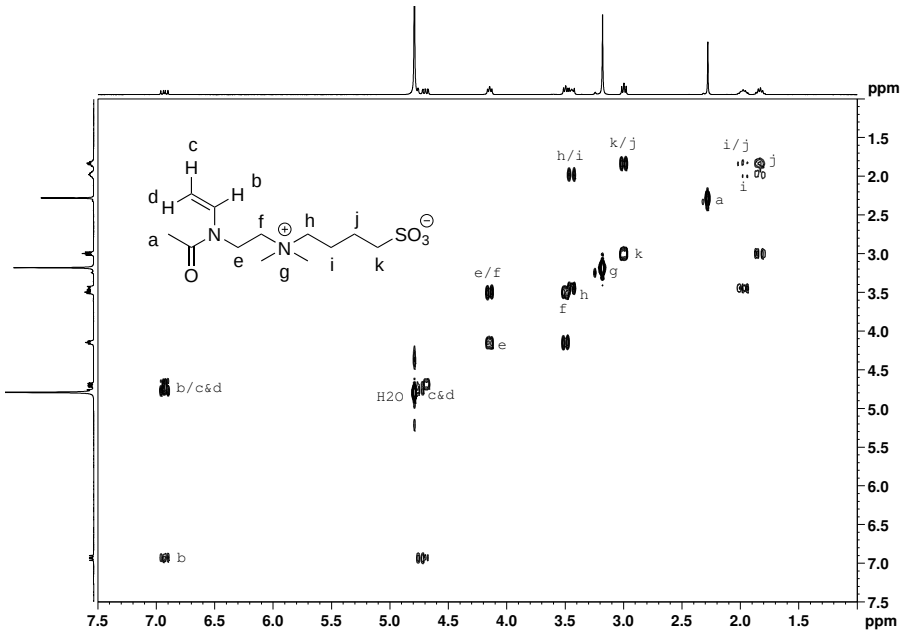

Figure 5.5: ^{1}H-^{1}H-COSY NMR spectrum of **M3** in D_2O.

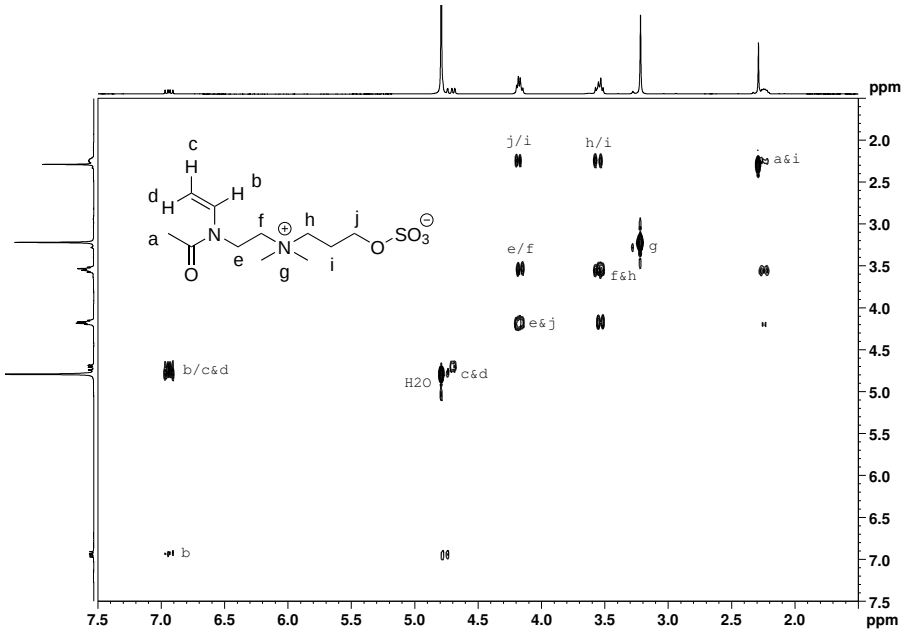

Figure 5.6: ^{1}H-^{1}H-COSY NMR spectrum of **M4** in D_2O.

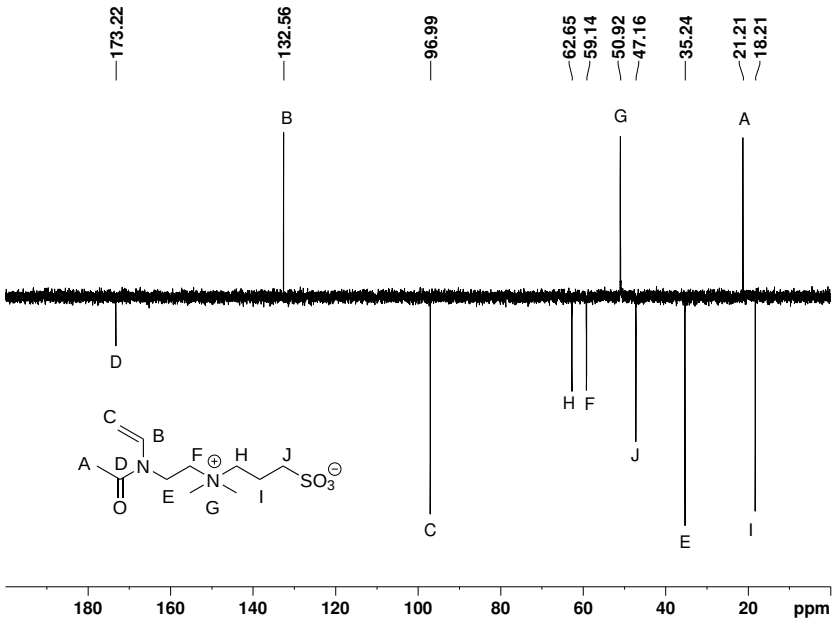

Figure 5.7: ^{13}C (APT) NMR spectrum of **M2** in D_2O.

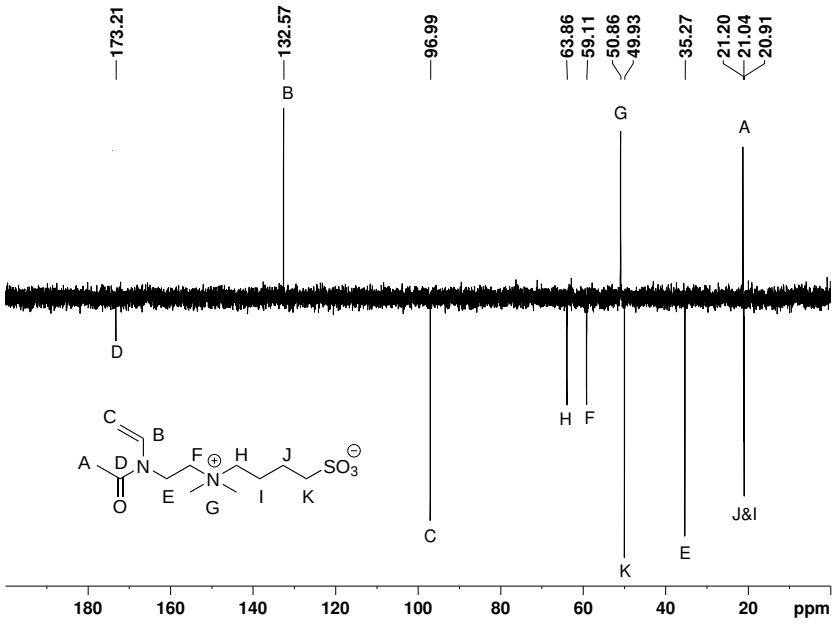

Figure 5.8: ^{13}C (APT) NMR spectrum of **M3** in D_2O.

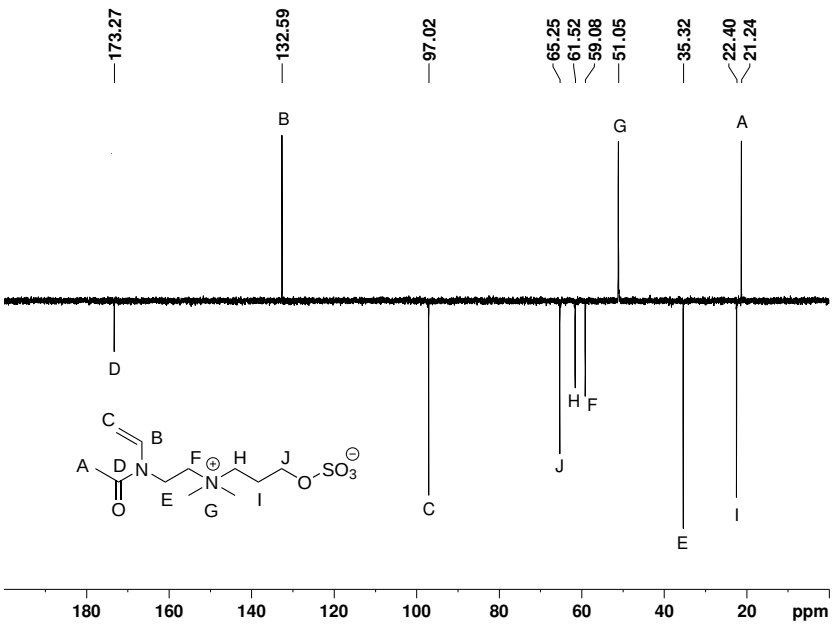

Figure 5.9: ^{13}C (APT) NMR spectrum of **M4** in D_2O.

By ^{1}H-^{13}C-HSQC NMR, it was possible to further confirm the previously assigned signals. This characterization method made possible the better characterization of the otherwise overlapping signals of the methylene protons at the α-position to the quaternized amine (signals "f" and "h"), as with the ^{1}H-^{13}C-HSQC NMR-spectra it was observed that these were two independent sets of protons bonded to two distinct carbons (signals "f/F" and "h/H"). Similarly, overlapping signals of the methyl protons at the α-position to the carbonyl group and the methylene protons at the β-position to the quaternized amine in monomers **M2** and **M4** could also be better characterized by signals "a/A" and "i/I" as two sets of protons bonded to two different carbons (See Figures 5.10 and 5.12). This characterization technique also further improved the characterization of the chemical structure of monomer **M3**, as the ^{13}C (APT) NMR-signals of three carbons were overlapping, i.e., the signal of the methyl carbon at the α-position to the carbonyl group, and the methylene carbons at the β, and γ-position to the quaternized amine (signals "A", "I", and "J", respectively). By ^{1}H-^{13}C-HSQC NMR characterization, it was possible to observe the coupling of these three different carbons to three different sets of protons (signals "a/A", "i/I", and "j/J"), the full ^{1}H-^{13}C-HSQC NMR-spectrum is shown in Figure 5.11.

Thermal properties of monomers **M2**, **M3**, and **M4** were investigated with DSC. Important differences are observed between the sulfa- and sulfobetaines, as vinyl amide sulfobetaines **M2** and **M3** both show a significant amount of water molecules bound to the zwitterionic moieties of the monomers. This is characterized by the endothermic peaks observed in the thermograms of both sulfobetaines (See Figures 5.13 and 5.14). The main reasons to suspect of the endothermic peaks to be caused by the elimination of bound water molecules from the sample rather than from a phase transition of the monomers, are the

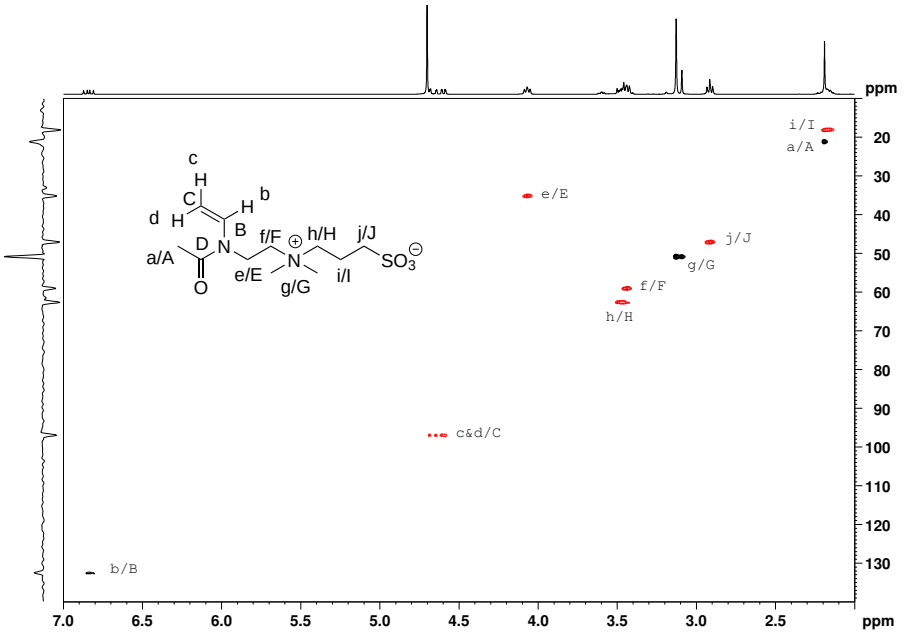

Figure 5.10: ^{1}H-^{13}C-HSQC NMR spectrum of **M2** in D_2O.

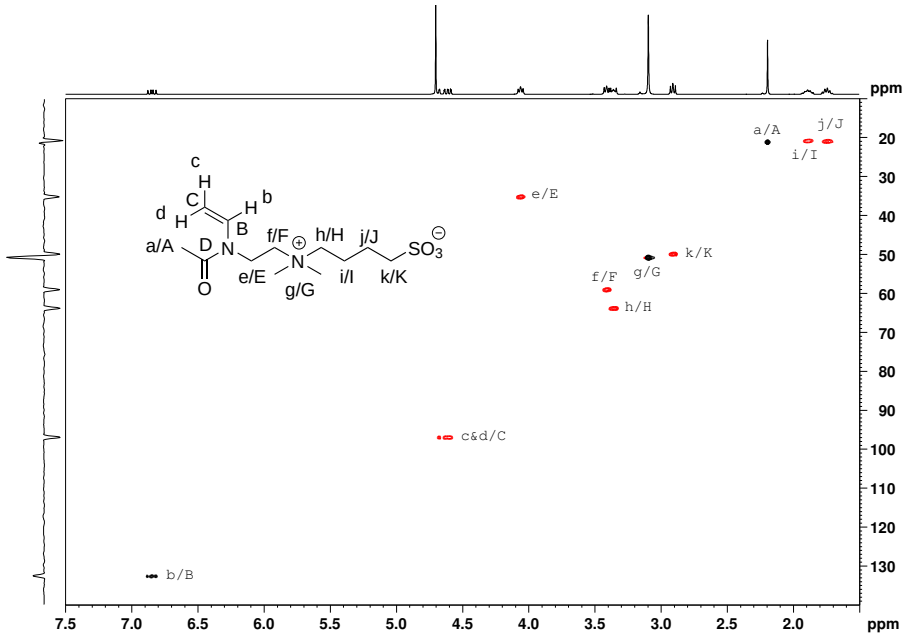

Figure 5.11: ^{1}H-^{13}C-HSQC NMR spectrum of **M3** in D_2O.

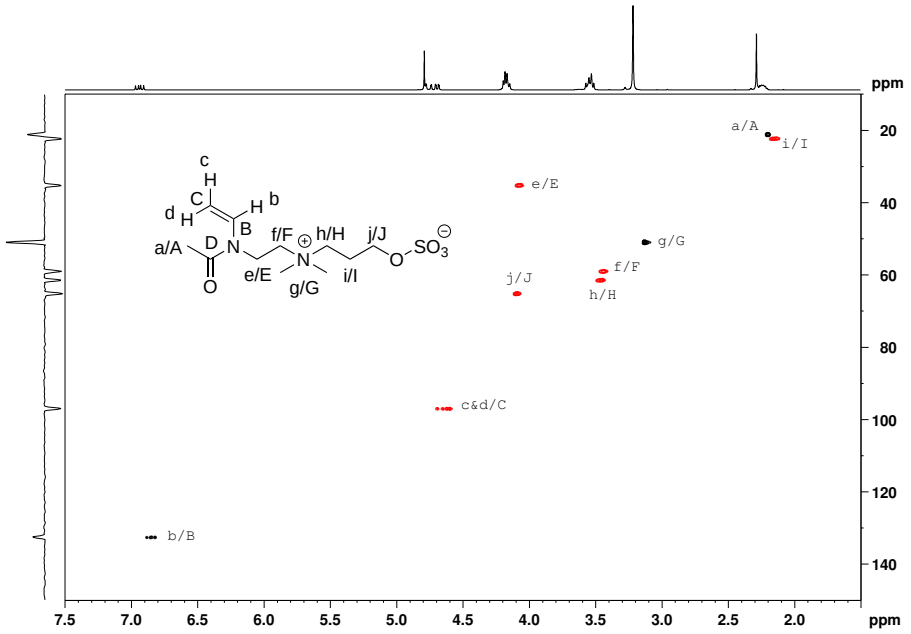

Figure 5.12: ^{1}H-^{13}C-HSQC NMR spectrum of **M4** in D_2O.

temperature at which the endothermic peak takes place (around 100 °C), and the absence of further phase transitions in both the cooling ramp of the 1st cycle and the entirety of the 2nd cycle. These thermograms would then be consistent to water molecules being removed from the sample during the 1st cycle of the calorimetry.

Contrary to the observations made on monomers **M2** and **M3**, the thermogram of vinyl amide sulfabetaine **M4** did not show an endothermic peak during the entirety of the calorimetry (see Figure 5.15). This gives insights on the differences on hygroscopy that the monomers show, i.e., vinyl amide sulfobetaines **M2** and **M3** being more hygroscopic than their sulfabetaine analogue **M4**.

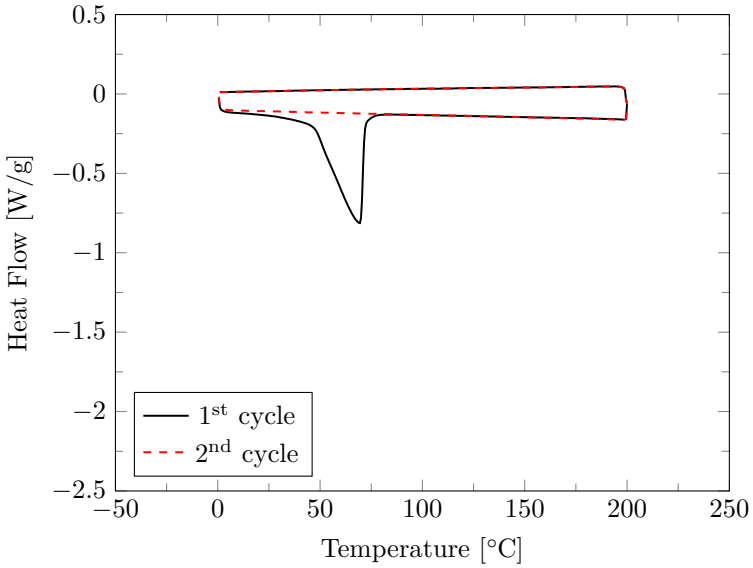

Figure 5.13: DSC thermogram of zwitterionic vinyl amide sulfobetaine **M2**, two cycles 0–200 °C at 5 K min^{-1}.

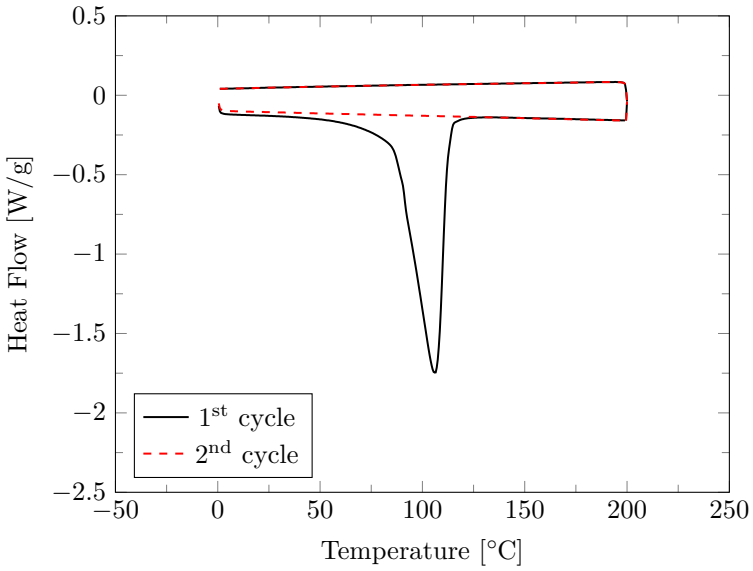

Figure 5.14: DSC thermogram of zwitterionic vinyl amide sulfobetaine **M3**, two cycles 0–200 °C at 5 K min^{-1}.

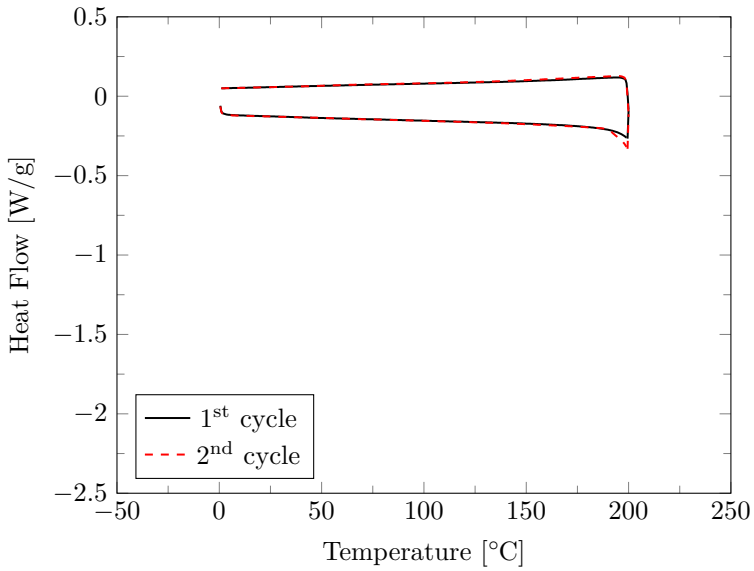

Figure 5.15: DSC thermogram of zwitterionic vinyl amide sulfabetaine **M4**, two cycles 0–200 °C at 5 K min^{-1}.

5.2 Synthesis and Characterization of a New Vinyl Amide Photo-crosslinker

The synthesis of the new vinyl amide benzophenone photo-crosslinker monomer was done by the *N*-acylation of *N*-vinylformamide with the previously synthesized 4-benzoylbenzoyl chloride (**I-6**), and subsequent selective hydrolysis of the formyl group with aqueous NaOH in analogy to a recent procedure for vinylamides [128]. The vinyl amide photo-crosslinker **M5** was purified by crystallization from acetonitrile (MeCN) by dropwise addition of H_2O (See Scheme 5.3).

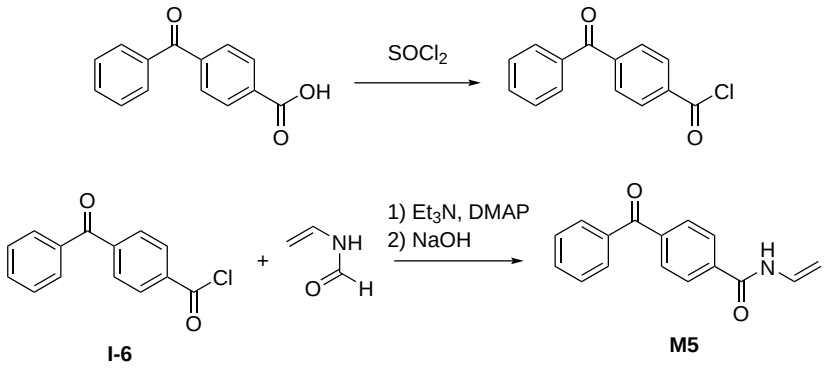

Scheme 5.3: Synthetic path to vinyl amide crosslinker **M5**.

The chemical structure of **M5** was characterized by ^{1}H NMR spectroscopy.

Relevant signals in the ^{1}H NMR-spectrum are the ones of the three distinct vinyl protons (signals "f", "g", and "h") at 7.20, 4.96, and 4.51 ppm, respectively, and the characteristic aromatic protons (signals "a" – "e") at 8.2–7.4 ppm. A full characterization and description of the observed peaks is shown in Figure 5.16.

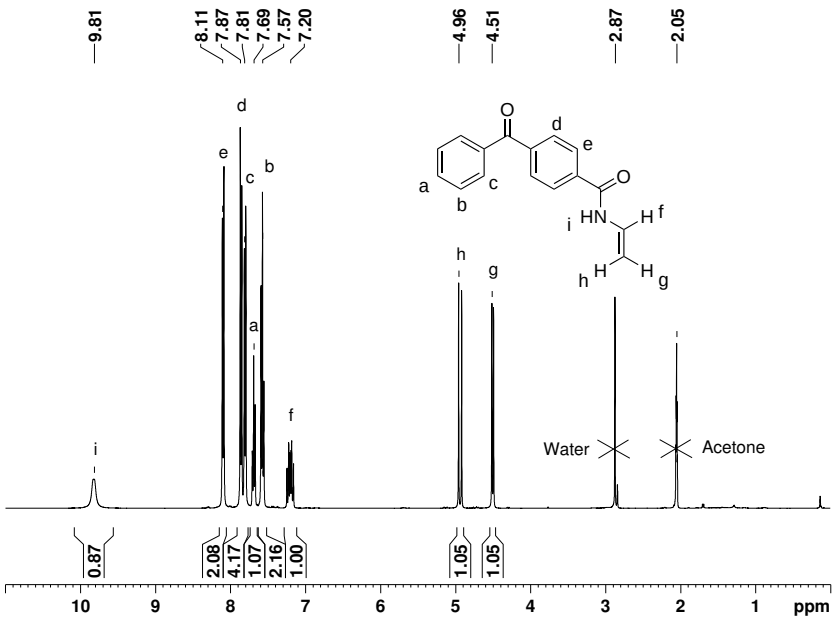

Figure 5.16: ^{1}H NMR spectrum of **M5** in $(CD_3)_2CO$.

Further characterization of the chemical structure of vinyl amide photo-crosslinker **M5** was achieved by ^{1}H-^{1}H-COSY NMR, where the interactions between the vinyl protons "f", "g", and "h" could be observed suggesting that the protons are bonded to directly neighbouring carbons (signals "f/h" and "f/g"). Additionally, a better description of the aromatic protons was possible, by ^{1}H-^{1}H-COSY NMR-spectra of vinyl amide crosslinker **M5** as shown in Figure 5.17.

The chemical structure of **M5** was further characterized with ^{13}C (APT) NMR. This characterization method was important to gain insights on the chemical shifts of the different carbon atoms present in the molecule. Important peaks observed in this spectrum are the carbon at the carbonyl group between the two aromatic rings (signal "I"), and the carbon from the carbonyl group of the amide moiety (signal "L"). As there are no hydrogens bonded to these carbons, this characterization technique was fundamental to the better description of the chemical shifts. The full ^{13}C (APT) NMR-spectrum is shown in Figure 5.18.

The previously assigned chemical shifts were confirmed by ^{1}H-^{13}C-HSQC NMR characterization. In particular, the confirmation that both vinyl protons "g" and "h" were bonded to the same carbon "G" (signals "g/G" and "h/G") was of special importance. The signals for the aromatic carbons and protons were also analyzed to greater detail using this characterization technique. The full ^{1}H-^{13}C-HSQC NMR-spectrum is shown in Figure 5.19.

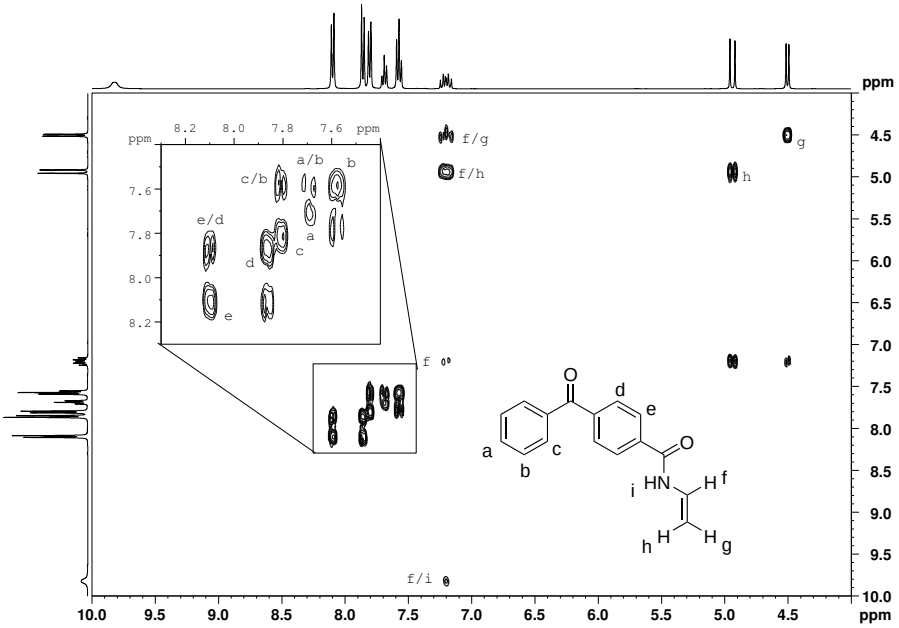

Figure 5.17: ^{1}H-^{1}H-COSY NMR spectrum of **M5** in $(CD_3)_2CO$.

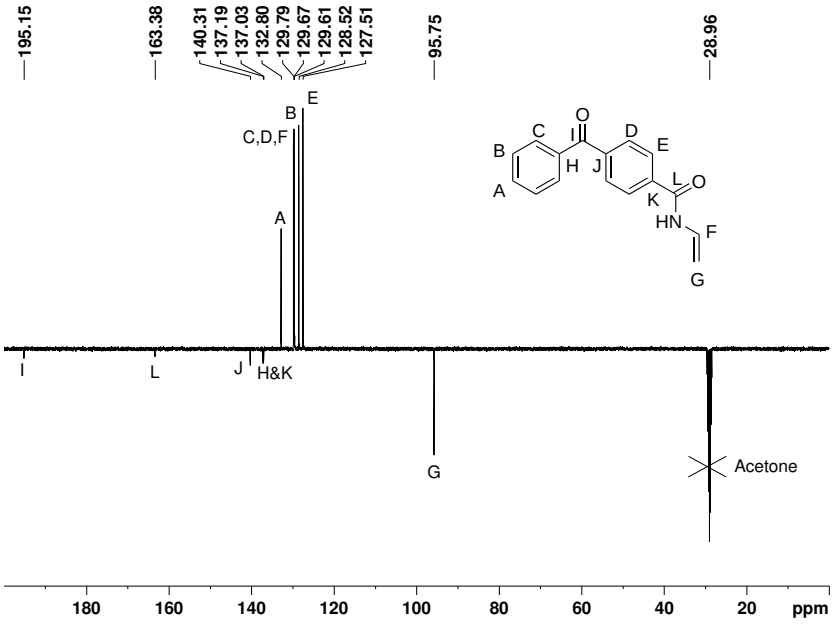

Figure 5.18: ^{13}C (APT) NMR spectrum of **M5** in $(CD_3)_2CO$.

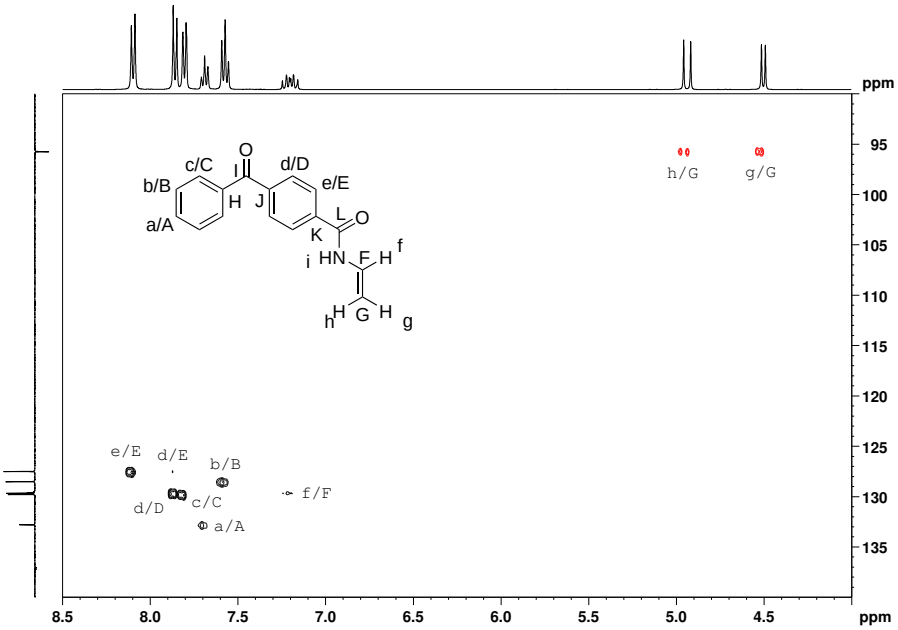

Figure 5.19: ^{1}H-^{13}C-HSQC NMR spectrum of **M5** in $(CD_3)_2CO$.

As monomer **M5** has a photoreactive benzophenone moiety, it was possible to determine its specific ε, which depends on the chemical structure of the molecule. For this, the UV-Vis spectra of samples at different concentrations in TFE were measured (See Figure 5.20). With these measurements, a λ_{max} of 264 nm was determined, value which is in accordance to the Scotts rules for calculation of λ_{max} of aromatic carbonyl compounds [129]. Furthermore, by fitting the absorption measurements at different molar concentrations to a linear regression that intersects at $(0, 0)$, an ε of $20\,087\,\mathrm{L\,cm^{-1}\,mol^{-1}}$ with an estimated error margin of ± 5 rel.% was determined by Equation 3.1 (See Figure 5.21).

The value of ε makes it possible to calculate the concentration of **M5** in a solution of TFE by measuring its absorption at $\lambda = 264$ nm. Moreover, assuming that ε does not change when crosslinker **M5** is incorporated in the copolymers, the amount of **M5** in the copolymers can be determined by UV-Vis spectroscopy.

The thermal properties of **M5** were investigated by DSC (See Figure 5.22). The results of the calorimetry showed an endothermic peak with onset at 160 °C, however, a 2nd peak is also observed in the thermogram which suggests a degradation of the sample. This is further confirmed by the exothermic peak close to 200 °C. Although the endothermic peak with onset at 160 °C is evidence of a phase transition ocurring within the sample, i.e., melting, the presence of more peaks suggest additional processes happening within the sample at the same time. These additional processes are also further confirmed with the 2nd heating cycle of the calorimetry, where these are no longer observed.

As expected, **M5** shows no evidence of hygroscopy, which is in line with the reduced polarity of this molecule.

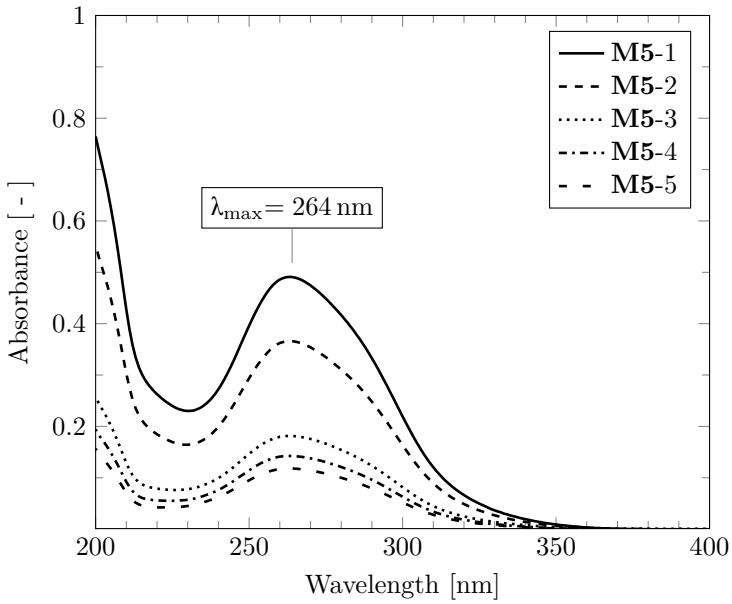

Figure 5.20: UV-Vis spectra of vinyl amide crosslinker **M5** at different concentrations in TFE.

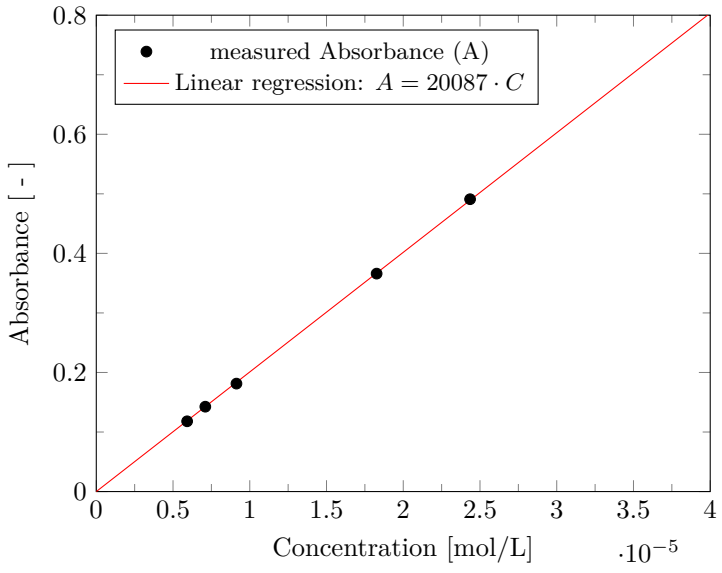

Figure 5.21: Determination of the extinction coefficient of vinyl amide crosslinker **M5** in TFE.

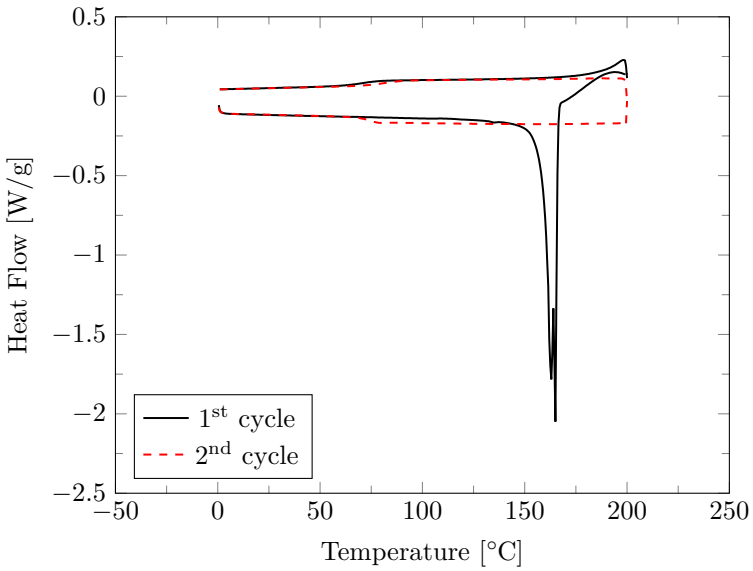

Figure 5.22: DSC thermogram of vinyl amide crosslinker **M5**, two cycles 0–200 °C at 5 K min^{-1}.

5.3 Synthesis and Characterization of Homopolymers of New Vinyl Amide Zwitterionic Monomers

The free-radical solution homopolymerization of the new vinyl amide zwitterionic monomers proved to be challenging. Suitable conditions for the homopolymerization were found only after numerous trials with different azo-initiators, such as AIBN, 4,4'-azobis(4-cyanovaleric acid) (V-501), 2,2'-azobis[2-methyl-*N*-(2-hydroxyethyl)propionamide] (V-086), and 2,2'-azobis(2-methylpropionamidine)-dihydrochloride (V-50); and different solvents as MeOH, H_2O, and mixtures thereof. Finally, homopolymerization was successful with initiator V-086 in H_2O at weakly basic pH (9–10), and with initiator V-50 in a H_2O:MeOH [2:1] (v:v) solution at weakly basic pH (9–10). Homopolymers poly(3-(dimethyl(2-(*N*-vinylacetamido)ethyl)ammonio)propane-1-sulfonate) (**P(M2)**), poly(4-(dimethyl(2-(*N*-vinylacetamido)ethyl)ammonio)butane-1-sulfonate) (**P(M3)**), and poly(3-(dimethyl(2-(*N*-vinylacetamido)ethyl)ammonio)propyl sulfate) (**P(M4)**) were obtained in good yields after dialysis against ultra pure water and lyophilization.

By TGA characterization, upper thermal stabilities were studied, as well as the amount of water attached to the homopolymers **P(M2)**, **P(M3)**, and **P(M4)** was determined. The TGA results of the three homopolymers show a loss of mass in the range of 11.3–12.7 % at temperatures up to 150 °C (See Figures 5.23, 5.24, and 5.25). As this mass loss happens mostly at temperatures below 150 °C, it is attributed to the evaporation of water molecules bound to the zwitterionic moieties of the homopolymers. By calculation, this mass loss would represent about 2 molecules of H_2O per CRU of the polymer, more pre-

cisely, 1.9, 1.8, and 2.1 for **P(M2)**, **P(M3)**, and **P(M4)**, respectively. Further thermolysis of the homopolymers is then observed starting from 250 °C.

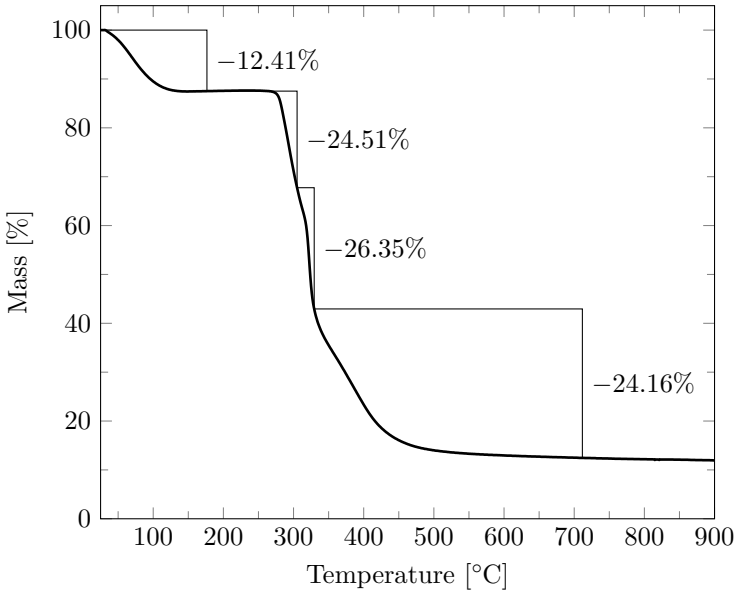

Figure 5.23: TGA thermogram of homopolymer **P(M2)** under N_2 atmosphere with a heating rate of $10\,\mathrm{K\,min^{-1}}$.

As homopolymers **P(M2)**, **P(M3)**, and **P(M4)** are members of a new family of polyzwitterions, an extensive solubility test was done. The results of these solubility tests, together with the $E_T(30)$ values of the solvents [120–122], are listed in Table 5.1.

Homopolymers **P(M2)**, **P(M3)**, and **P(M4)** were insoluble in aprotic solvents, such as dioxane, THF, chloroform, acetone, DMF or DMSO, which is in agreement with the reported solubilities of many polyzwitterions [3, 123, 124]. Similarly to prior research on polyzwitterions, the homopolymers **P(M2)**, **P(M3)**, and **P(M4)** were only soluble in protic solvents with high $E_T(30)$ values ($E_T(30) \gtrapprox 55\,\mathrm{kcal\,mol^{-1}}$) [124], such as formic acid, formamide, and TFE.

From the results of the solubility tests it was surprising that, unlike many zwitterionic polymers, all three homopolymers (**P(M2)**, **P(M3)**, and **P(M4)**) were readily soluble in water at room temperature (See Table 5.1). This is evidence of the high hydrophilicity of the produced homopolymers [123, 130, 131]. Upon addition of salt, the homopolymers **P(M2)**, **P(M3)**, and **P(M4)** showed characteristic polyzwitterionic behaviour and remained in solution (See Table 5.1).

Another remarkable finding was that homopolymers **P(M2)** and **P(M4)** were insoluble in HFIP, which is often an excellent choice for the dissolution of polyzwitterions (See Table 5.1) [3]. However, homopolymer **P(M3)** was indeed soluble in HFIP, in agreement to the general trends seen in previous works on polyzwitterions [3, 124] (See Table 5.1).

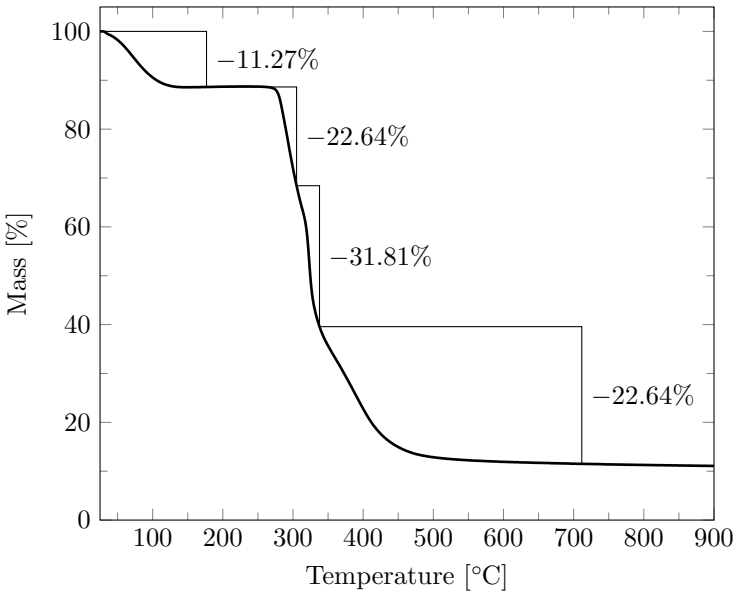

Figure 5.24: TGA thermogram of homopolymer **P(M3)** under N_2 atmosphere with a heating rate of $10\,\mathrm{K\,min^{-1}}$.

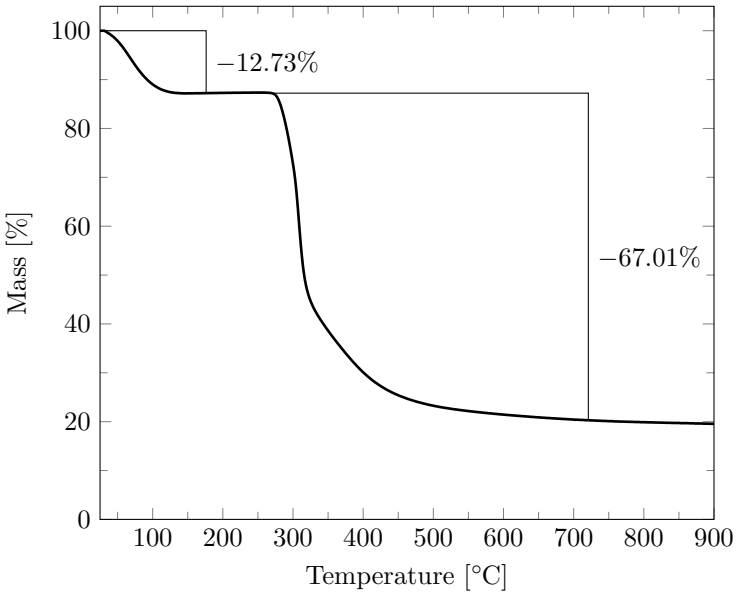

Figure 5.25: TGA thermogram of homopolymer **P(M4)** under N_2 atmosphere with a heating rate of $10\,\mathrm{K\,min^{-1}}$.

Table 5.1: Solubility of the vinyl amide homopolymers **P(M2)**, **P(M3)**, and **P(M4)** in selected solvents.

Solvent	$E_T(30)$[a] [kcal/mol]	Polymer		
		P(M2)	**P(M3)**	**P(M4)**
dioxane	36.0	–	–	–
tetrahydrofuran	37.5	–	–	–
ethyl acetate	38.0	–	–	–
chloroform	39.1	–	–	–
dichloromethane	40.7	–	–	–
acetone	42.3	–	–	–
dimethyl formamide	43.2	–	–	–
dimethyl sulfoxide	45.1	–	–	–
acetic acid	51.7[b]	+	∼	–
ethanol	51.8	–	–	–
formic acid	54.3[b]	+	+	+
methanol	55.4	–	–	–
formamide	55.9	+	+	+
trifluoroacetic acid	−−	+	+	∼
trifluoroethanol	59.8	+	+	+
hexafluoroisopropanol	65.3	–	+	–
water	63.1	+	+	+
normal saline (0.9% NaCl)	−−	+	+	+
artificial sea water	−−	+	+	+
saturated NaCl	−−	+	+	+

[a] Unless otherwise stated, obtained from [120]
[b] Values calculated from Kosower's Z values, see references [121, 122]
+ = soluble
– = not soluble
∼ = slightly soluble (swollen)

5.4 Synthesis and Characterization of Copolymers of Vinyl Amide Zwitterionic Monomers and Vinyl Amide Photo-crosslinker

The copolymerization of vinyl amide zwitterionic monomers **M2**, **M3**, **M4**, and vinyl amide photo-crosslinker **M5**, proved to be non-trivial, as the difference in polarities between the zwitterionic monomers and the vinyl amide crosslinker brought in difficulties to find not only a suitable solvent in which to successfully perform the copolymerization but also an initiator that would perform in the selected solvent. After extensive trials with different solvents, mixtures of solvents, and initiators, copolymerization of each of the zwitterionic vinyl amides **M2**, **M3**, and **M4**, with the vinyl amide photo-crosslinker **M5** was successful with initiator V-50 in a H_2O:MeOH [1:1] (v:v) solution at weakly basic pH (8–9). Copolymers poly((3-(dimethyl(2-(*N*-vinylacetamido)-ethyl)ammonio)propane-1-sulfonate)-*co*-(4-benzoyl-*N*-vinylbenzamide)) (**P(M2-*co*-M5)**), poly((4-(dimethyl(2-(*N*-vinylacetamido)ethyl)ammonio)butane-1-sulfonate)-*co*-(4-benzoyl-*N*-vinylbenzamide)) (**P(M3-*co*-M5)**), and poly((3-(dimethyl(2-(*N*-vinylacetamido)ethyl)ammonio)propyl sulfate)-*co*-(4-benzoyl-*N*-vinylbenzamide)) (**P(M4-*co*-M5)**) were obtained after dialysis against ultra pure water using a membrane with MWCO of 3500 g mol^{-1} and lyophilization for the removal of H_2O.

Due to the broad and poorly resolved signals, the ^{1}H NMR spectra do not enable a precise compositional analysis (See Figures 5.26, 5.27, and 5.28). The evaluation of the data from the elemental analysis for determining the composition of the copolymers allowed a good estimation of the amount of zwitterionic moieties in the copolymers, as the element S occurs only in the zwitterionic units. Therefore, compositions could be calculated from the analytical data using the C/N and C/S ratios. The information obtained from the elemental analysis suggests amounts of crosslinker in the copolymers in the order of: 8.3 mol% for copolymer **P(M2-*co*-M5)**, 6.7 mol% for copolymer **P(M3-*co*-M5)**, and 10.6 mol% for copolymer **P(M4-*co*-M5)**. Still, the precision of the calculated ratios is inevitably limited and the values are only reliable ± 10 rel.%. A rough estimation according to the integrals of the characteristic ^{1}H NMR signals of **M5** support the view of their approximately equivalent incorporation into the copolymers, i.e., the **M5** content is the order of 5 mol% with an estimated error margin of ±50 rel.% (See Figures 5.26, 5.27, and 5.28).

Alternatively, the content of photoreactive **M5** units in the copolymers was quantified by UV-Vis spectroscopy. As previously mentioned, the absorbance band of the **M5** chromofore was determined at λ_{max}=264 nm with an absorption coefficient ε of 20 087 L mol^{-1} cm^{-1} and an estimated error margin of ±5 rel.%. The absorbances at a wavelength of 264 nm for weighed-in masses of the copolymers in TFE were determined. The measured absorptions of the amphiphilic copolymers were 0.343, 0.330, and 0.380 for copolymers **P(M2-*co*-M5)**, **P(M3-*co*-M5)**, and **P(M4-*co*-M5)**, respectively (See Figure 5.29). Under the assumption that the absorption coefficient does not change after incorporation to the copolymers, when compared to the weighed-in mass of the sample, these values represent a 6.6 mol% of photo-crosslinker **M5** in copolymer **P(M2-*co*-M5)**, 4.0 mol% in copolymer **P(M3-*co*-M5)**, and 9.9 mol% in copolymer **P(M4-*co*-M5)**. Given the experimental errors, these results further

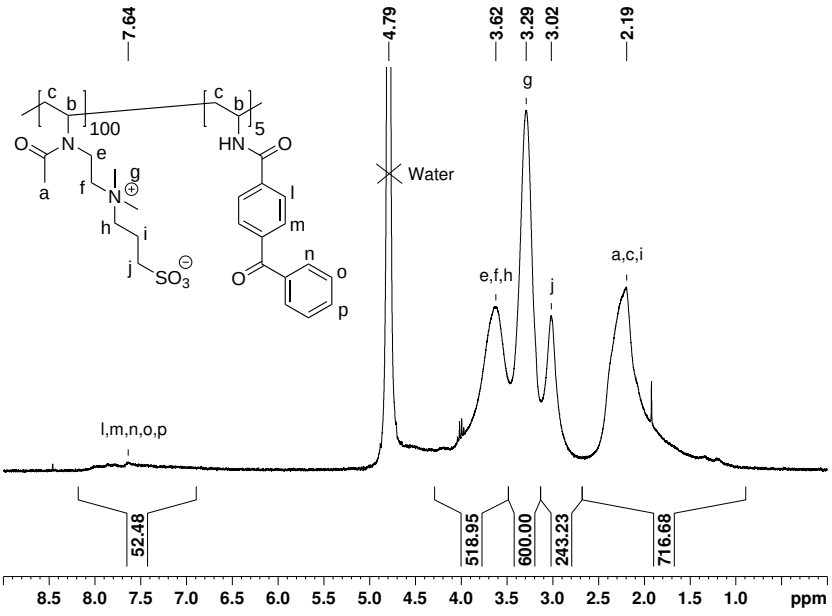

Figure 5.26: ^{1}H NMR spectrum of copolymer **P(M2-*co*-M5)** in a saturated solution of NaCl in D_2O.

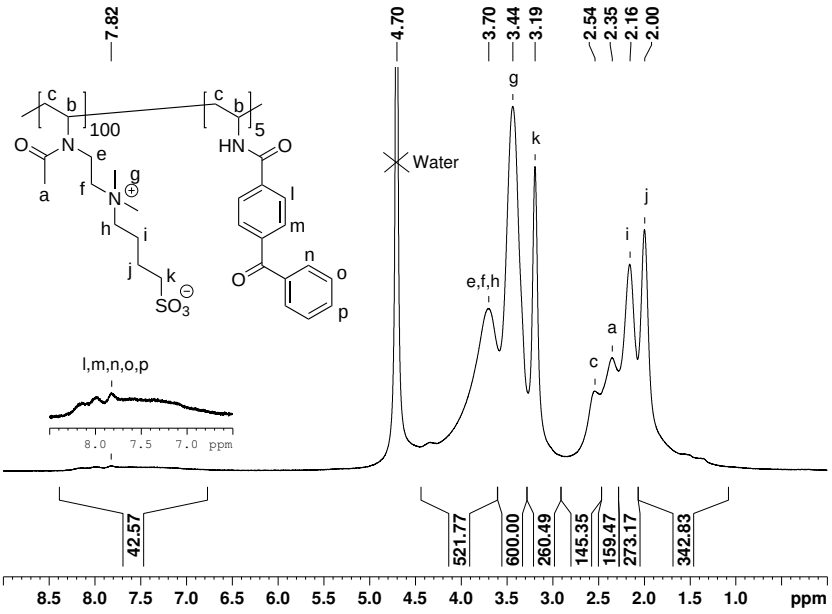

Figure 5.27: ^{1}H NMR spectrum of copolymer **P(M3-*co*-M5)** in a saturated solution of NaCl in D_2O.

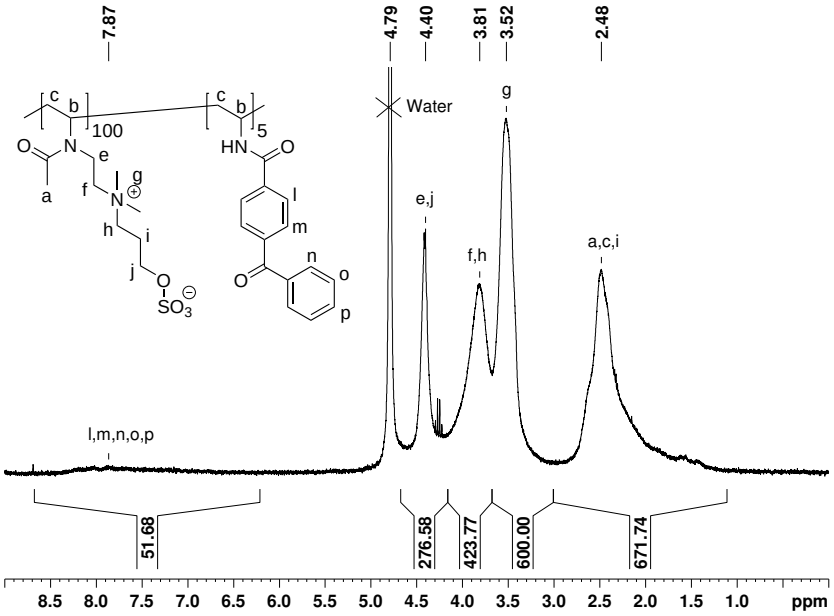

Figure 5.28: ^{1}H NMR spectrum of copolymer **P(M4-*co*-M5)** in a saturated solution of NaCl in D_2O.

support a BPEMA content of about 7 mol% in the final copolymers.

Molar mass distributions of the amphiphilic copolymers were measured by GPC using HFIP with 50 mM of sodium trifluoroacetate as eluent and a calibration by narrowly distributed P(MMA) standards (See Figure 5.30). From the GPC data, values for M_n, M_w, and Đ of each amphiphilic copolymer were determined, these are summarized in Table 5.2.

From the results obtained from the GPC analysis, it was evident that the copolymerization of the vinyl amide zwitterionic monomers (**M2**, **M3**, and **M4**) with the vinyl amide crosslinker (**M5**) proved to be challenging as only low molar mass oligomers with M_n values in the range of 4–7 kg mol^{-1} were produced, despite several trials with different solvents and initiators.

Table 5.2: Apparent molar masses of vinyl amide copolymers according to GPC analysis (See Figure 5.30).

Copolymer	M_n [kg/mol]	M_w [kg/mol]	Đ [–]
P(M2-*co*-M5)	6.6	13.1	2.0
P(M3-*co*-M5)	4.2	8.8	2.1
P(M4-*co*-M5)	5.4	12.5	2.3

With the values of M_n and a weighted average molecular weight of the monomers, X_n values in the range of 15–25 were calculated. As determined by UV-Vis

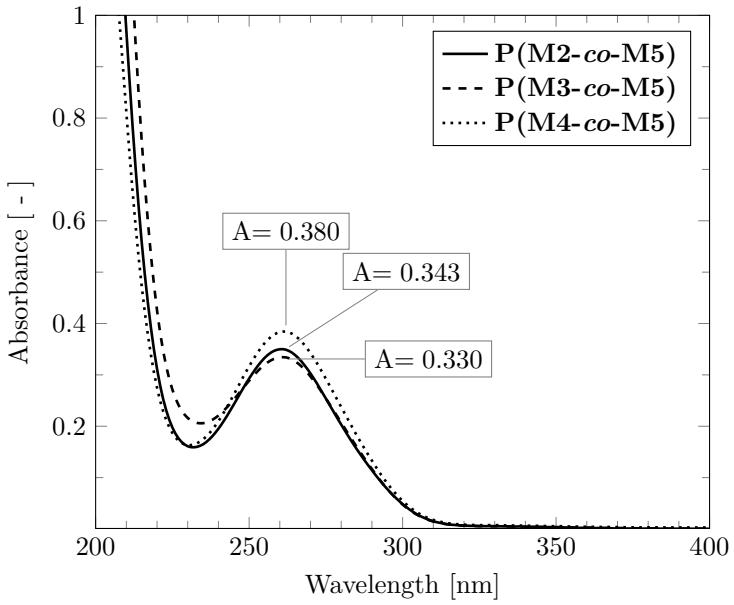

Figure 5.29: UV-Vis spectra of the **M5**-derived absorption maxima of dilute solutions of vinyl amide copolymers **P(M2-*co*-M5)**, **P(M3-*co*-M5)**, and **P(M4-*co*-M5)** in TFE with concentrations of 71, 120, and 56 mg L^{-1}, respectively.

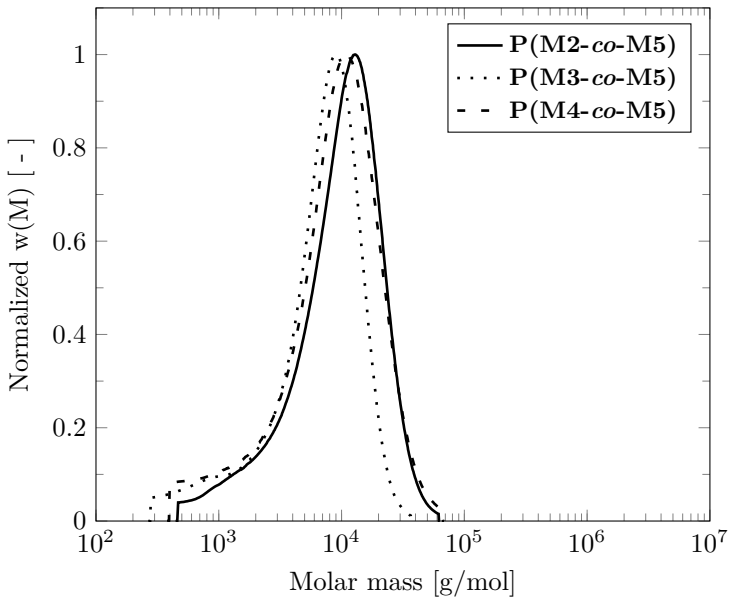

Figure 5.30: Molar mass distributions of vinyl amide copolymers **P(M2-*co*-M5)**, **P(M3-*co*-M5)**, and **P(M4-*co*-M5)** according to GPC-analysis (eluent HFIP with 50 mM of sodium trifluoroacetate, calibration by narrowly distributed P(MMA) standards).

and other characterization techniques, the synthesized amphiphilic copolymers contain, within the experimental error, 7 mol% of vinyl amide photo-crosslinker **M5**. With this information, on average, the number of crosslinker moieties per copolymer chain is expected to be in the range of 0.6–1.8. This value is of importance for the formation of hydrogel networks, as at least >1 crosslinking sites per polymer chain, on average, are needed in order to form a stable hydrogel network. That being said, the obtained values of 0.6–1.8 crosslinker moieties per copolymer chain are relatively low for the desired functionality of the polymers, as the efficiency of the crosslinks can be significantly reduced by the creation of loops or the formation of redundant crosslinks. It is for this reason that the stability of the hydrogels produced with these copolymers might be at risk.

Analogous to the solubility tests done for the parent homopolymers discussed in the previous Section 5.3, the solubilities of the copolymers **P(M2-*co*-M5)**, **P(M3-*co*-M5)**, and **P(M4-*co*-M5)** in selected solvents are shown in Table 5.3. Compared to the solubilities of their parent homopolymers (**P(M2)**, **P(M3)**, and **P(M4)**), the solubilities of the copolymers **P(M2-*co*-M5)**, **P(M3-*co*-M5)**, and **P(M4-*co*-M5)** remained fairly similar.

Main differences are the improved solubilities of copolymers **P(M2-*co*-M5)** and **P(M4-*co*-M5)** in HFIP, in contrast to their parent homopolymers **P(M2)** and **P(M4)** which rendered insoluble in the fluorinated alcohol (See Table 5.3).

The solubilities of copolymer **P(M4-*co*-M5)** in both water and normal saline solution (0.9% NaCl) were another interesting finding, as only swelling of the sample and no full dissolution was observed (See Table 5.3). This observation constrasts with the solubility of its parent homopolymer **P(M4)** where the sample was fully soluble in both water and normal saline solution (0.9% NaCl) (See Table 5.1). A hypothesis of this effect can be that the hydrophobicity added by the crosslinker **M5** was enough to render the produced copolymer insoluble in these solvents, as copolymer **P(M4-*co*-M5)** showed the highest amount of crosslinker **M5** incorporated into the copolymer chains (9.9 mol%).

Table 5.3: Solubility of the vinyl amide copolymers **P(M2-*co*-M5)**, **P(M3-*co*-M5)**, and **P(M4-*co*-M5)** in selected solvents.

	Polymer		
Solvent	**P(M2-*co*-M5)**	**P(M3-*co*-M5)**	**P(M4-*co*-M5)**
dioxane	–	–	–
tetrahydrofuran	–	–	–
ethyl acetate	–	–	–
chloroform	–	–	–
dichloromethane	–	–	–
acetone	–	–	–
dimethyl formamide	–	–	–
dimethyl sulfoxide	–	–	–
acetic acid	+	–	–
ethanol	–	–	–
formic acid	+	+	+
methanol	–	–	–
formamide	+	+	+
trifluoroacetic acid	+	+	+
trifluoroethanol	+	+	+
hexafluoroisopropanol	+	+	+
water	+	+	∼
normal saline (0.9% NaCl)	+	+	∼
artificial sea water	+	+	+
saturated NaCl	+	+	+

+ = soluble
– = not soluble
∼ = slightly soluble (swollen)

Chapter 6

New Quaternized Diallylamine Sulfobetaine Photo-crosslinker

6.1 Synthesis and Characterization of Quaternized Diallylamine Photo-crosslinker Monomer

A new quaternized diallylamine sulfobetaine photo-crosslinker was synthesized by the alkylation of diallylamine with synthesized bromide (4-(2-bromoethoxy)-phenyl)(phenyl)methanone (**I-7**), followed by the quaternization of the obtained tertiary amine (4-(2-(diallylamino)ethoxy)phenyl)(phenyl)methanone (**I-8**) with 1,3-propane sultone. Quaternized diallylamine **M6** was recovered as a precipitate of the reaction mixture (See Scheme 6.1).

The chemical structure of **M6** was characterized by ^{1}H NMR spectroscopy, although the amount of signals is numerous, important information on the chemical structure of **M6** was obtained from the ^{1}H NMR-spectrum, such as the presence of the 6 vinyl protons expected from a diallylamine moiety (signals "i" and "j&j′") at 6.11 and 5.72 ppm, respectively. Another important characteristic found in the ^{1}H NMR-spectrum was the methylene protons at the α-position to the sulfonate moiety characteristic of sulfobetaines (signal "m") at 2.83 ppm and the 8 methylene protons at the α-position to the quaternized amine (signals "h", "a", and "'k") at 4.10, 3.87, and 3.54 ppm, respectively. The fully characterized ^{1}H NMR-spectrum is shown in Figure 6.1.

Further insights on the chemical structure of **M6** were obtained by ^{1}H-^{1}H-COSY NMR spectroscopy. Especially important to the characterization of the quaternized diallylamine was the coupling of the vinyl protons "j" and "i" (signal "i/j"), as well as the coupling of the methylene protons on the zwitterionic side chain "k", "l", and "m" (signals "k'/l" and "m/l"). Additionally, the coupling of the methylene protons at the α and β-position to the aryloxy group "a" and "b" (signal "b/a") was important for further characterization of the quaternized diallylamine **M6**. The fully assigned ^{1}H-^{1}H-COSY NMR-spectrum is shown in Figure 6.2.

In order to better characterize the chemical shifts of the carbons on dially-

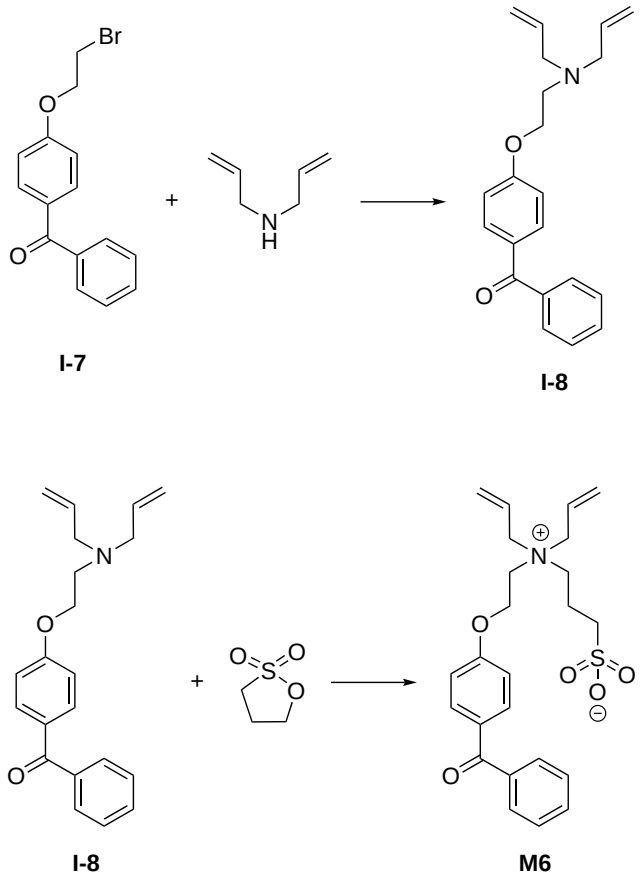

Scheme 6.1: Synthetic path to diallylamine sulfobetaine photo-crosslinker **M6**.

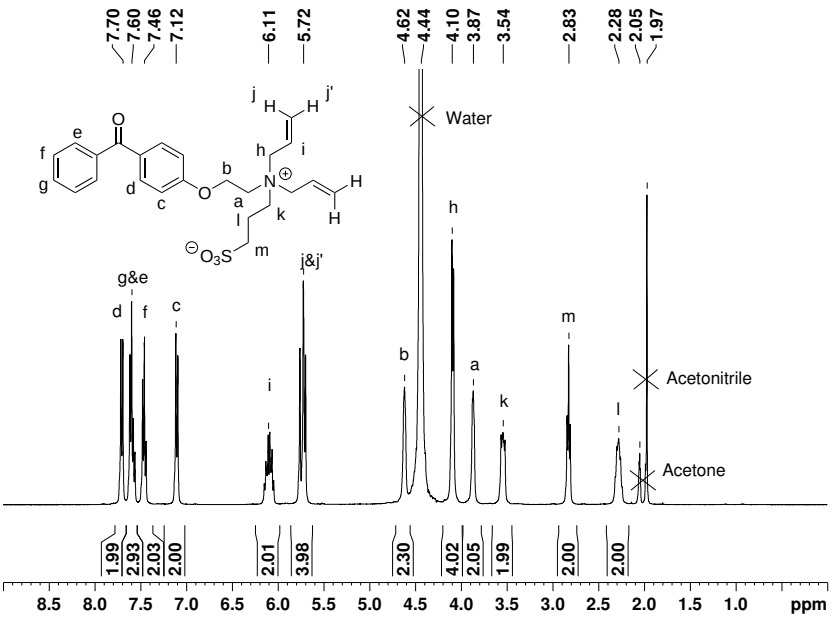

Figure 6.1: ^{1}H NMR spectrum of **M6** in D_2O:$(CD_3)_2CO$ [1:1].

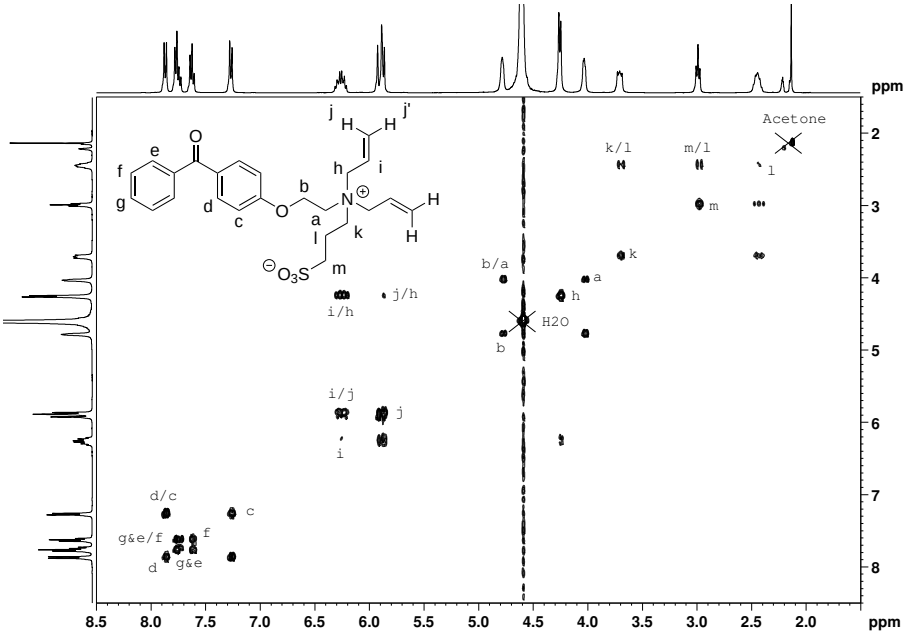

Figure 6.2: ^{1}H-^{1}H-COSY NMR spectrum of **M6** in D_2O:$(CD_3)_2CO$ [1:1].

lamine **M6**, ^{13}C (APT) NMR characterization was performed. This characterization method was specially useful to indicate the presence of carbons with no protons bonded to them, as these signals are overlooked by ^{1}H NMR-spectra. Of particular interest for the characterization of **M6** were, the carbonyl group (signal "P") at 196.7 ppm, and the quaternary aromatic carbons (signals "N", "Q", and "O") at 161.3, 137.4, and 130.4 ppm, respectively. Another characteristic that gave useful insights on the chemical structure of **M6** was the methylidene and the methine carbons having negative and positive values and thus, confirming the expected amount of protons bonded to them (signals "J" and "I") at 129.6 and 124.1 ppm, respectively. A fully characterized ^{13}C NMR-spectrum of diallylamine **M6** is shown in Figure 6.3.

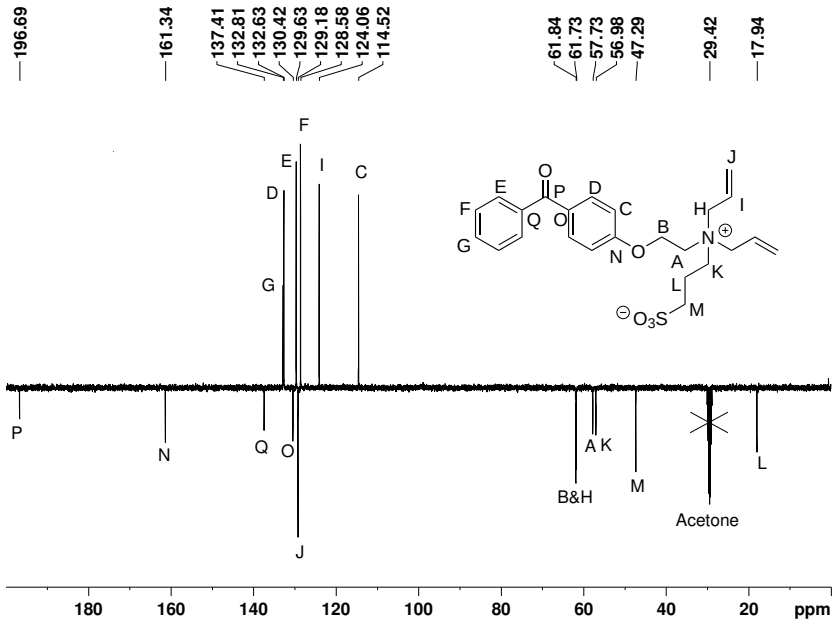

Figure 6.3: ^{13}C (APT) NMR spectrum of **M6** in D_2O:$(CD_3)_2CO$ [1:1].

By ^{1}H-^{13}C-HSQC NMR it was possible to better characterize signals that were otherwise overlapping, specially the ones of the methylene carbons at the α-position to the quaternized amine "A" and "K", with ^{1}H-^{13}C-HSQC NMR it was possible to identify the signals as two different carbons, as two distinct sets of protons are bonded to each one of them (signals "a/A" and "k/K"). Similarly, the otherwise overlapping signals of the methylene carbon at the α position to the aryloxy group and the one of the allylic carbon "B" and "H", were better resolved by ^{1}H-^{13}C-HSQC NMR as two distinct sets of protons were bonded to these carbons. The fully characterized ^{1}H-^{13}C-HSQC NMR-spectrum is shown in Figure 6.4.

As monomer **M6** has a photoreactive benzophenone moiety, its specific ε and λ_{max} were determined, as these values depend on the chemical structure of the molecule. For this, the UV-Vis spectra of samples at different concentrations in TFE were measured (See Figure 6.5). With these measurements a λ_{max} of 284 nm was determined, which is in accordance to the typical absorption pattern

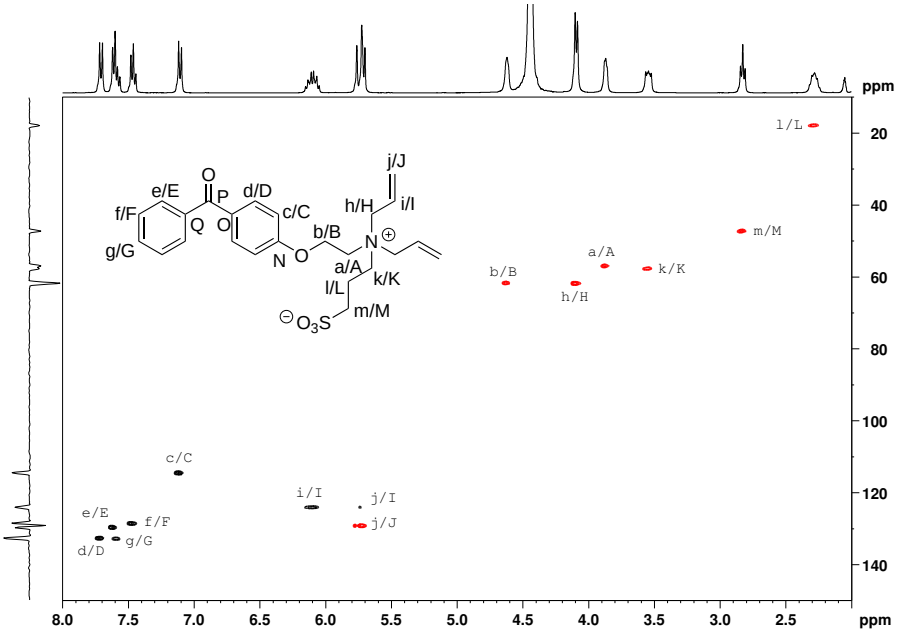

Figure 6.4: ^{1}H-^{13}C-HSQC NMR spectrum of **M6** in D_2O:$(CD_3)_2CO$ [1:1].

of a donor substituted benzophenone [132, 133]. Furthermore, by fitting the absorption measurements at different molar concentrations to a linear regression that intersects at $(0, 0)$, an ε of $19\,635\,\mathrm{L\,cm^{-1}\,mol^{-1}}$ with an estimated error margin of ± 5 rel.% was determined by Equation 3.1 (See Figure 6.6).

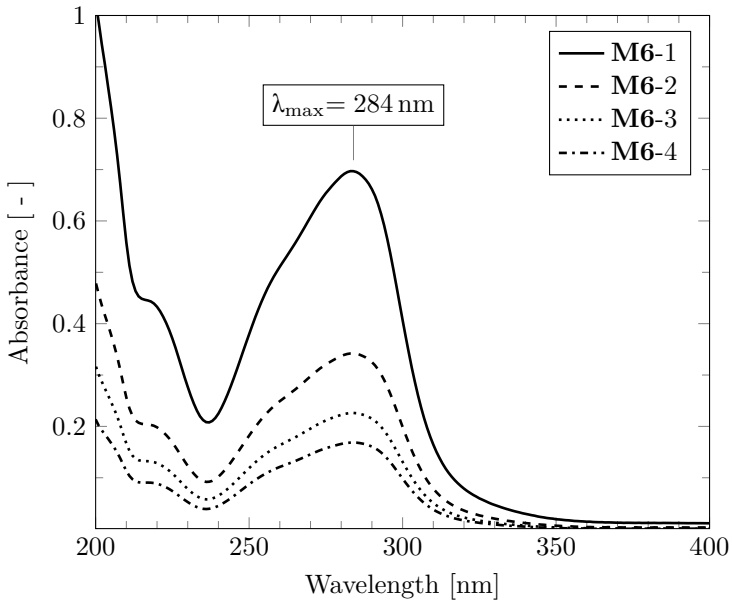

Figure 6.5: UV-Vis spectra of quaternized diallylamine **M6** at different concentrations in TFE.

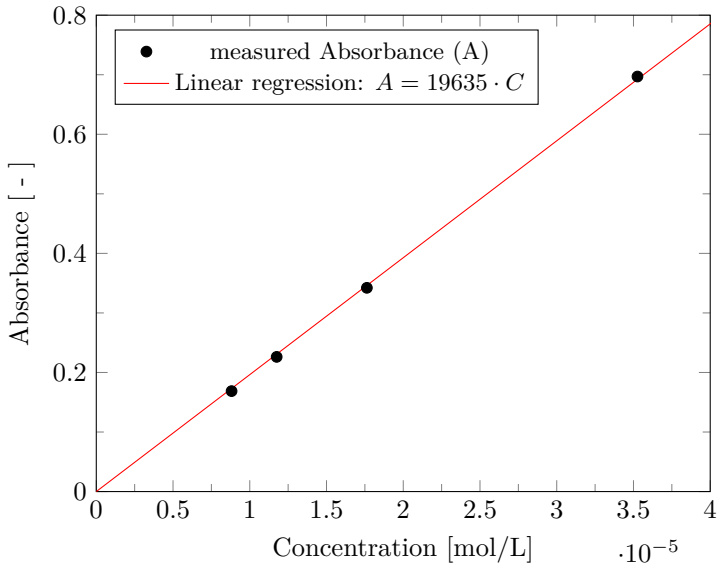

Figure 6.6: Determination of the extinction coefficient of quaternized diallylamine **M6** in TFE.

6.2 Synthesis and Characterization of Copolymers of Diallylamine Sulfobetaine Photo-crosslinker and Vinyl Amide Sulfobetaines

Although diallylammonium compounds are known to readily polymerize [134, 135], neither a homopolymerization nor a copolymerization with the zwitterionic vinyl amides was achieved, despite several trials with different initiators and solvents. This can be due to the steric hinderance produced by the bulky side groups, which might prevent the polymerization of the quaternized diallylamine. Similar challenges with the polymerization of diallylammonium compounds with bulky side groups have been reported in the literature, and successful polymerization was only achieved under very specific conditions, i.e., UV initiation while cooling with ice, which may point to a low ceiling temperature [136–138].

In order to further test the copolymerization of diallylammonium monomer **M6** with vinyl amides, trials with secondary vinyl amides such as *N*-vinylformamide or *N*-vinylacetamide are recommended.

Chapter 7

Summary and Conclusion

In an effort to explore strategies to more stable hydrogels for low fouling coatings, amphiphilic terpolymers of SPE, BMA, and BPEMA suitable for the production of thin hydrogel films were succesfully synthesized by free-radical copolymerization in TFE. The incorporation of hydrophobic comonomer BMA in the terpolymers showed positive results in the protein adsorption and antifouling assessments. Moreover the mechanical stability of the hydrogels also benefited from the presence of hydrophobic comonomer BMA in the copolymers.

In order to further test the impact that hydrophobicity has on both the antifouling properties and the mechanical stability of zwitterionic hydrogels, the new amphiphilic zwitterionic monomer **M1** was synthesized in good yields. The new monomer was thoroughly characterized by a detailed chemical structure analysis by spectroscopic techniques and calorimetry measurements. High molar mass homopolymers of the new amphiphilic zwitterionic monomer **M1** were obtained by free-radical polymerization with AIBN in TFE. The homopolymers showed solubilities similar to the ones characteristic for polysulfobetaines, as it resulted soluble only in protic solvents with high $E_T(30)$ values, and fluorinated alcohols such as TFE and HFIP. Terpolymers of the new amphiphilic zwitterionic monomer **M1**, stablished methacrylic sulfobetaine SPE, and photo-crosslinker BPEMA were obtained by free-radical copolymerization. The successful incorporation of the comonomers in the final copolymers was determined by UV-Vis spectroscopy and EA. Among other interesting effects of the incorporation of amphiphilic sulfobetaine **M1** in the terpolymers, it was surprising that the copolymers showed better solubility in water as the amount of amphiphilic sulfobetaine **M1** increased. Molar masses of the terpolymers seem to decrease with increasing contents of **M1**, this could be caused by a decreasing solvent quality of the eluent due to the difference of polarity between the comonomers. This decrease of molar masses impacts the number of potential crosslinking sites per copolymer chain, which in turn might render the production of stable hydrogel films challenging.

A new family of zwitterionic monomers, i.e., vinyl amide zwitterionic monomers was introduced within the scope of this work. Vinyl amide zwitterionic monomers **M2**, **M3**, and **M4** were synthesized in a multistep synthesis in good yields and thoroughly characterized by different spectroscopic and calorimetric techniques. The DSC thermogram showed that sulfobetaines **M2** and **M3**

are more hygroscopic than their sulfabetaine analogue **M4**. The homopolymers **P(M2)**, **P(M3)**, and **P(M4)**, unlike many zwitterionic polymers, resulted fully soluble in water at room temperature, confirming their high hydrophilicity.

A new vinyl amide photo-crosslinker **M5** was also introduced within the scope of the present work. Characterization of the photo-crosslinker was achieved by different spectroscopic and calorimetric techniques. Although the copolymerization of the new vinyl amide photo-crosslinker **M5** with the vinyl amide zwitterionic monomers **M2**, **M3**, and **M4** proved to be challenging, successful copolymerization was achieved with initiator V-50 in a H_2O:MeOH solution at weakly basic pH. However, due to the low molar mass of the obtained copolymers, the production of stable hydrogel films might be at stake, as the number of potential crosslinking sites per copolymer chain might not be sufficient.

Finally, a new quaternized diallylamine sulfobetaine photo-crosslinker **M6** is also introduced in the present work. The chemical structure of **M6** was thoroughly characterized by spectroscopic techniques. Additionally, its specific λ_{max} and ε in TFE were determined by UV-Vis spectroscopy. Despite several attempts, however, copolymerization with zwitterionic vinyl amides **M2**, **M3**, and **M4** was not successful.

Chapter 8

Experimental

8.1 Materials

Table 8.1: Utilized chemicals.

Chemical	Formula	CAS	Purity	Supplier
acetic acid	$C_2H_4O_2$	64-19-7	$\geq$ 99.5%	Chemsolute
acetone	C_3H_6O	67-64-1	$\geq$ 99%	VWR
acetone - d6	C_3D_6O	666-52-4	99.9%	Merck
acetonitrile	C_2H_3N	75-05-8	$\geq$ 99.5%	Roth
acetyl chloride	C_2H_3ClO	75-36-5	$>$ 99%	Acros Organics
4,4'-azobis(4-cyanovaleric acid) (V-501)	$C_{12}H_{16}N_4O_4$	2638-94-0	$\geq$ 98%	Wako
2,2'-azobis-(isobutyronitrile) (AIBN)	$C_8H_{12}N_4$	78-67-1	98%	Merck
2,2'-azobis[2-methyl-*N*-(2-hydroxy-ethyl)propion-amide] (VA-086)	$C_{12}H_{24}N_4O_4$	61551-69-7	$\geq$ 98%	Wako

Continued on next page

Table 8.1: *(Continued)* Utilized chemicals.

Chemical	Formula	CAS	Purity	Supplier
2,2'-azobis(2-methylpropion-amidine)dihydro-chloride (V-50)	$C_8H_{20}Cl_2N_6$	2997-92-4	97%	Wako
benzene	C_6H_6	71-43-2	$\geq$ 99.5%	Roth
4-benzoylbenzoic acid	$C_{14}H_{10}O_3$	611-95-0	$>$ 99%	Acros Organics
1,4-butane sultone	$C_4H_8O_3S$	1633-83-6	$>$ 99%	Acros Organics
tert-butanol	$C_4H_{10}O$	75-65-0	$\geq$ 99.5%	Sigma-Aldrich
calcium hydride	CaH_2	7789-78-8	$\geq$ 95%	Merck
chloroform	$CHCl_3$	67-66-3	99.5%	Th. Geyer
chloroform - d	$CDCl_3$	865-49-6	99.8%	VWR
deuterium oxide	D_2O	7789-20-0	99.9%	VWR
diallylamine	$C_6H_{11}N$	124-02-7	99%	Sigma-Aldrich
1,2-dibromoethane	$C_2H_4Br_2$	106-93-4	$\geq$ 98%	Sigma-Aldrich
dichloromethane	CH_2Cl_2	75-09-2	$\geq$ 99.5%	Roth
dichloromethane - d2	CD_2Cl_2	1665-00-5	99.8%	VWR
dimethylamine (40 % solution in H_2O)	C_2H_7N	124-02-7	40%	Fluka
4-dimethylamino-pyridine	$C_7H_{10}N_2$	1122-58-3	$\geq$ 98%	Fluka
N-*N*-dimethyl-formamide	C_3H_7NO	68-12-2	$\geq$ 99.5%	Applichem
dimethyl sulfoxide	C_2H_6OS	67-68-5	$\geq$ 99.8%	Roth
1,4-dioxane	$C_4H_8O_2$	123-91-1	$\geq$ 99%	TCI Chemicals

Continued on next page

Table 8.1: *(Continued)* Utilized chemicals.

Chemical	Formula	CAS	Purity	Supplier
1,2-epoxyhexane	$C_6H_{12}O$	1436-34-6	96%	Alfa-Aesar
ethanol	C_2H_6O	64-17-5	$\geq$ 99.9%	Merck
ethyl acetate	$C_4H_8O_2$	141-78-6	99.9%	VWR
1,2-ethylene sulfate	$C_2H_4O_4S$	1072-53-3	$>$ 98%	TCI Chemicals
formamide	CH_3NO	75-12-7	$\geq$ 99.5%	Merck
formic acid	CH_2O_2	64-18-6	$\geq$ 99%	Acros Organics
n-hexane	C_6H_{14}	110-54-3	$\geq$ 96%	Chemsolute
hexafluoro-isopropanol	$C_3H_2F_6O$	920-66-1	99%	Fluorochem
hexafluoro-isopropanol - d2	$C_3D_2F_6O$	38701-74-5	99%	abcr
4-hydroxy-benzophenone	$C_{13}H_{10}O_2$	1137-42-4	98%	abcr
magnesium sulfate	$MgSO_4$	7487-88-9	96%	Applichem
methanol	CH_4O	67-56-1	$\geq$ 98.5%	VWR
methanol - d4	CD_4O	811-98-3	99.8%	VWR
methyl *tert*-butyl ether	$C_5H_{12}O$	1634-04-4	99%	Riedel-de Haën
1-methylpiperazine	$C_5H_{12}N_2$	109-01-3	99%	Acros Organics
methacryloyl chloride	C_4H_5ClO	920-46-7	97%	Alfa-Aesar
methyl *p*-toluenesulfonate	$C_8H_{10}O_3S$	80-48-8	98%	Alfa-Aesar
nitrobenzene	$C_6H_5NO_2$	98-95-3	99%	Acros Organics

Continued on next page

Table 8.1: *(Continued)* Utilized chemicals.

Chemical	Formula	CAS	Purity	Supplier
potassium carbonate	K_2CO_3	584-08-7	$\geq$ 99%	Sigma-Aldrich
potassium *tert*-butoxide	C_4H_9KO	865-47-4	$\geq$ 98%	Merck
1,3-propane sultone	$C_3H_6O_3S$	1120-71-4	$>$ 99%	TCI Chemicals
1,3-propylene sulfate	$C_3H_6O_4S$	1073-05-8	$>$ 98%	TCI Chemicals
sodium carbonate	Na_2CO_3	497-19-8	$\geq$ 99.5%	Sigma-Aldrich
tetrahydrofuran	C_4H_8O	109-99-9	99.5%	Acros Organics
thionyl chloride	$SOCl_2$	7719-09-7	$>$ 99%	Fluka
triethylamine	$C_6H_{15}N$	121-44-8	99%	Acros Organics
trifluoroacetic acid	$C_2HF_3O_2$	76-05-1	$\geq$ 99.9%	Roth
2,2,2-trifluoro-ethanol	$C_2H_3F_3O$	75-89-8	$>$ 99.8%	Roth
N-vinyl formamide	C_3H_5NO	13162-05-5	98%	Sigma-Aldrich

All chemicals were used as received unless otherwise stated. Solvent *t*-BuOH was dried over magnesium sulfate and fractionally distilled. MeCN was dried over potassium carbonate. Dichloromethane (DCM) was refluxed over calcium hydride and distilled. AIBN was crystallized from methanol.

8.2 Methods and Calculations

8.2.1 Nuclear Magnetic Resonance (NMR) Spectroscopy

^{1}H and ^{13}C NMR spectra, ^{1}H-^{1}H-Correlation Spectra (COSY), and ^{1}H-^{13}C-Heteronuclear Multiple Quantum Coherence spectra (HMQC) were recorded with a Bruker Avance™ 300 spectrometer operating at 300 MHz or with a Bruker Avance NEO™ 400 spectrometer operating at 400 MHz at ambient temperature in deuterated solvents. ^{13}C NMR spectra were recorded in Attached Proton Test (APT) mode. Solvent signals were used as internal shift secondary reference.

8.2.2 Elemental Analysis

Elemental analysis was carried out in Fraunhofer IAP (Golm, Germany) using a FlashEA® 1112 CHNS/O Elemental Analyser from Thermo Scientific.

8.2.3 Mass Spectrometry

High resolution mass spectra (HR-MS) were recorded with a Thermo Scientific ESI-Q-TOFmicro (Quadropol - Time of Flight). Electrospray ionization (ESI) and an appropriate polar solvent were used as a method.

8.2.4 Gel Permeation Chromatography (GPC)

Gel permeation chromatography (GPC) was carried out by Dr. Kathrin Geßner in Fraunhofer IAP (Golm, Germany) on a WGE Dr. Bures system with an SEC 3010 pump, a refractive index (RI) detector Dn-2010, and two columns PL HFIPgel (300 mm × 7.5 mm) from Agilent Technologies using HFIP with 50 mmol L^{-1} sodium trifluoracetate as eluent at a flow rate of 0.8 mL min^{-1} at a temperature of 40 °C.

8.2.5 Differential Scanning Calorimetry (DSC)

DSC measurements were performed on a Discovery DSC250 instrument from TA Instruments under N_2 flow (50 mL min^{-1}) in temperatures 0–200 °C, two heating-cooling cycles at 5 K min^{-1} with 2 min isotherm for temperature stabilization before the start of each cycle.

8.2.6 Thermogravimetric Analysis (TGA)

TGA measurements were carried out by Dr. Kathrin Geßner in Fraunhofer IAP (Golm, Germany) on a TGA 2 LF/1100/885 from Mettler Toledo under N_2 flow (50 mL min^{-1}) in temperatures 30–900 °C at 10 K min^{-1}.

8.2.7 Ultraviolet-visible (UV-vis) spectroscopy

Absorption spectra were recorded by a Perkin Elmer UV/Vis spectrometer Lambda 35, using quartz sample cells with 1 cm path length.

8.2.8 Fourier Transform - Infrared (FT-IR) spectroscopy

Fourier transform infrared (FT-IR) spectra were recorded in a N_2 purged atmosphere using a Thermo Nicolet Nexus FT-IR spectrometer from Thermo Scientific equipped with an attenuated total reflection (ATR) element.

8.2.9 Spin Coating

Silicon wafers (2.0 cm × 2.0 cm, 0.725 mm thickness, front polished, Silicon Materials, Kaufering, Germany) and glass substrates (2.5 cm × 2.5 cm, cut from microscope slides, VWR) were washed and hydrophilized for 6 h in a 2.5 mg mL^{-1} solution of potassium permanganate in concentrated sulfuric acid. The substrates were washed three times with ultra pure water, followed by washes with ethanol and toluene lastly. The surface of the substrates was then modified by silanization to enable grafting of the copolymers, samples were immersed in 1 vol% solutions of (3-aminopropyl)dimethylethoxysilane in toluene for 12 h. The samples were washed with toluene and twice with ethanol, and dried under nitrogen flow.

Solutions of the copolymers in TFE were spin-coated onto the modified substrates with a spin-coater (KL-SCV, Schaefer Technologie GmbH, Langen, Germany). One droplet of a 1.3–1.9 wt.% solution was added on the wafer rotating at 2500 RPM for 10 s. Concentrations and rotation speeds were adjusted to produce coatings of 130 ± 10 nm thickness. The coated films were cured under UV-light in a UVACUBE 100 radiation chamber (Hönle, Gräfelfing, Germany) using a 100 W iron doped mercury vapor lamp equipped with sheet glass as a filter (cut-off 310 nm) for 30 min at room temperature (RT) in air. The distance from the light source to the sample was 20 cm.

After photo-curing, the samples were washed three times with ultra pure water baths while agitated and dried with a nitrogen stream.

8.2.10 Ellipsometry

The film thickness of the coated substrates was measured in the dry state by ellipsometry using an apparatus Multiscope from Optrel GbR (Kleinmachnow, Germany). The ellipsometer was equipped with a HeNe Laser (632.8 nm wavelength) with an angle of incidence of 70°. Film thicknesses were calculated by the software "Elli", version 5.2 (Optrel GbR, Kleinmachnow, Germany), using a four-layer model with the following parameters: Layer 1: Air ($n = 1.0000$, $k = 0.0000$), layer 2: Organic layer ($n = 1.4800$, $k = 0.0000$), layer 3: SiO_2 ($d = 1.0$ nm, $n = 1.4580$, $k = 0.0000$), layer 4: Silicon ($n = 3.8858$, $k = -0.0200$).

8.3 Monomer synthesis

8.3.1 Synthesis of Amphiphilic Sulfobetaines

8.3.1.1 Synthesis of 1-(dimethylamino)hexan-2-ol (I-1)

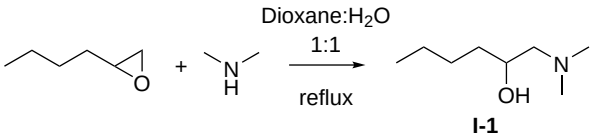

I-1

1,2-epoxyhexane (1.00 eq., 5.02 g, 50 mmol) was diluted in distilled dioxane (17 mL) in a 100 mL 3-neck round-bottom flask. A 40 wt.% solution of dimethylamine in H_2O (5.00 eq., 28.18 g, 250 mmol) was added to the reaction mixture. The reaction vessel was then equipped with a Dimroth reflux condenser and a thermometer, the third neck was sealed with a rubber septum. The top of the Dimroth reflux condenser was closed with a plastic plug.

The reaction was brought to 60 °C by an oil bath. The temperature was then slowly increased to 70 °C until a slow but steady reflux was achieved (1 drop per 10 s). It is important to have a good control of the temperature as the dimethylamine solution has a relatively low boiling point (≈40 °C). The reaction continued at 70 °C for the following 3.5 h at which point the temperature was raised to 75 °C. The reaction then continued at 75 °C for the following 16 h; a final increase of temperature to 80 °C was then made and the reaction continued at 80 °C for the following 5.5 h.

The reaction was stopped by removing the solvents by rotary evaporation at 60 °C and 5 mbar, resulting in a slightly yellow oil. This was dissolved in DCM and extracted with a 1.5 wt.% solution of sodium carbonate in H_2O. The organic phase was dried with magnesium sulfate, and the solvent was removed by rotary evaporation. Pure 1-(dimethylamino)hexan-2-ol (**I-1**) was obtained as a colorless oil (n_D^{20}= 1.4355) (yield 3.0 g, 41%).

^{1}H NMR(400 MHz, $CDCl_3$, 298 K): δ (ppm) = 3.58 (md, J = 3.4, 4.5 Hz, 1H, C$\underline{H}$−OH), 2.30–2.16 (m, 7H,(C$\underline{H}_3$)$_2$−N and C$\underline{H}_2$−N), 2.12 (dd, J = 3.1, 12.1 Hz, 1H, C$\underline{H}_2$−N), 1.54–1.18 (m, 6H, −C$\underline{H}_2$−C$\underline{H}_2$−C$\underline{H}_2$−), 0.87 (t, 3H,C$\underline{H}_3$−CH_2).

^{13}C NMR(101 MHz, $CDCl_3$, 298 K): δ (ppm) = 66.80 (C$\underline{H}$−OH), 65.63 ($\underline{C}H_2$−N), 45.45 ($\underline{C}H_3$−N), 34.65 ($\underline{C}H_2$−CH−OH), 27.80 (CH_2−$\underline{C}H_2$−CH_2), 22.83 ($\underline{C}H_2$−CH_3), 14.00 ($\underline{C}H_3$).

8.3.1.2 Synthesis of 1-(dimethylamino)hexan-2-yl methacrylate (I-2)

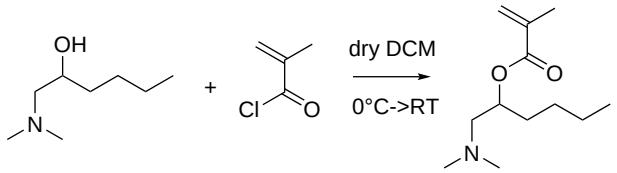

I-1 **I-2**

Finely milled sodium carbonate (1.11 g, 10.5 mmol) was added to dry DCM (6 mL) in a 25 mL round-bottom flask. This was then cooled down to 0 °C in an ice bath. Freshly distilled methacryloyl chloride (1.30 eq., 0.95 g, 9.10 mmol) was subsequently added. A solution of alkanolamine **I-1** (1.00 eq., 1.02 g, 7 mmol) in DCM (7 mL) was added drop-wise to the reaction mixture. The addition of **I-1** was completed within 10 min.

10 min after the end of additions, the reaction vessel was taken out of the ice bath and the reaction was allowed to continue at RT for the following 23 h. The reaction was then stopped by filtering off the solids, which were washed twice with freshly distilled DCM.

The combined filtrates containing **I-2** were subsequently extracted three times with a dilute solution of sodium carbonate in H_2O (20 mL, pH = 12). The organic phase was then dried with magnesium sulfate and the solvent was removed by rotary evaporation.

After column chromatography using a mixture of petrol ether and ethyl acetate (1:1 v/v) as eluent, and removal of the chromatography solvents, pure **I-2** was obtained as a slightly yellow oil (n_D^{20}= 1.4475) (yield 1.03 g, 70%).

^{1}H NMR(400 MHz, $CDCl_3$, 298 K): δ (ppm) = 6.08 (s, 1H, C$\underline{H}_2$=C *cis*), 5.53 (s, 1H, C$\underline{H}_2$=C *trans*), 5.06 (tt, J = 6.9, 7.8 Hz, 1H, C$\underline{H}$−O), 2.52 (dd, J = 6.8, 13.0 Hz, 1H, C$\underline{H}_2$−N), 2.37 (dd, J = 5.0, 13.0 Hz, 1H, C$\underline{H}_2$−N), 2.26 (s, 6H, (C$\underline{H}_3$)$_2$−N), 1.93 (s, 3H, C$\underline{H}_3$−C=), 1.72–1.49 (m, 2H, C$\underline{H}_2$−CH−O), 1.39–1.20 (m, 4H, −C$\underline{H}_2$−C$\underline{H}_2$−CH$_3$), 0.88 (t, J = 6.7 Hz, 3H, C$\underline{H}_3$−CH$_2$).

^{13}C NMR(101 MHz, $CDCl_3$, 298 K): δ (ppm) = 167.11 (C$\underline{}$=O), 136.65 (C$\underline{}$=CH$_2$), 125.19 (C$\underline{}$H$_2$=C), 72.22 (C$\underline{}$H−O), 62.68 (C$\underline{}$H$_2$−N), 45.97 (C$\underline{}$H$_3$−N), 32.45 (C$\underline{}$H$_2$−CH−O), 27.46 (CH$_2$−C$\underline{}$H$_2$−CH$_2$), 22.60 (C$\underline{}$H$_2$−CH$_3$), 18.38 (C$\underline{}$H$_3$−C=), 13.99 (C$\underline{}$H$_3$−CH$_2$).

FT-IR (selected bands, cm^{-1}): 2958 ν(=C−H), 2861 ν(C−H), 1716 ν(C=O), 1639 ν(C=C), 1456 δ(CH$_3$), 1295 ν(C−N), 1164 ν(C−O), 937 δ(C=C), 813 δ(CH$_2$).

ESI-MS: Calculated: 213.17 g/mol $[M]^+$; found: 214.2 g/mol $[M+H]^+$.

8.3.1.3 Synthesis of 3-((2-(methacryloyloxy)hexyl)dimethylammonio)-propane-1-sulfonate (M1)

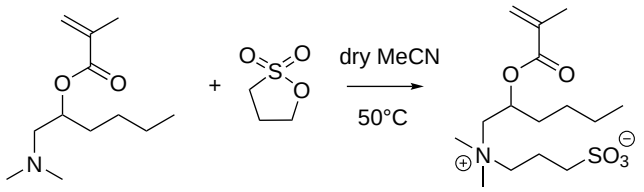

I-2 **M1**

Amine **I-2** (1.00 eq., 6.24 g, 30 mmol) was dissolved in dry MeCN (64 mL) in a 250 mL round-bottom flask. Nitrobenzene (0.08 g, 0.6 mmol) was then added as polymerization inhibitor.

A solution of 1,3-propane sultone (0.9 eq., 3.30 g, 27 mmol) in dry MeCN was subsequently added to the reaction mixture. After purging with N_2 for 45 min, the reaction vessel was sealed with a rubber septum and the temperature was raised to 50 °C by an oil bath. The reaction continued at 50 °C for the following 120 h, it was then stopped by reducing the temperature to RT.

The produced **M1** precipitated from the reaction mixture as a colorless solid. The precipitate was filtered off and washed three times with dry MeCN. The obtained solids were placed in an oven at 30 °C and 50 mbar over night to remove traces of the solvent, colourless powder, m.p. 167 °C (yield 5.7 g, 65%).

^{1}H NMR(400 MHz, D_2O, 298 K): δ (ppm) = 6.24 (s, 1H, C$\underline{H}_2$=C *cis*), 5.83 (s, 1H, C$\underline{H}_2$=C *trans*), 5.52 (td, J = 7.2, 6.2 Hz, 1H, C$\underline{H}$−O), 3.96 (dd, J = 9.0, 14.7 Hz, 1H, C$\underline{H}_2$−N^+), 3.62 (d, J = 14.6 Hz, 1H, C$\underline{H}_2$−N^+), 3.58–3.43 (m, 2H, C$\underline{H}_2$−N^+), 3.17 (s, 6H, (C$\underline{H}_3$)$_2$−N^+), 2.94 (t, J = 7.3 Hz, 2H, C$\underline{H}_2$−SO_3^-), 2.27 (tdd, J = 6.8, 13.6, 23.6 Hz, 2H, C$\underline{H}_2$−CH_2−SO_3^-), 1.96 (s, 3H, CH_3−C=), 1.84–1.67 (m, 2H, C$\underline{H}_2$−CH−O), 1.43–1.25 (m, 4H, −C$\underline{H}_2$−C$\underline{H}_2$−CH_3), 0.88 (t, J = 6.9 Hz, 3H,C$\underline{H}_3$−CH_2).

^{13}C NMR(101 MHz, D_2O, 298 K): δ (ppm) = 168.17 ($\underline{C}$=O), 135.32 ($\underline{C}$=CH_2), 128.20 ($\underline{C}H_2$=C), 68.98 ($\underline{C}$H−O), 65.94 ($\underline{C}H_2$−N^+), 63.49 ($\underline{C}H_2$−N^+), 51.42 ($\underline{C}H_3$−N^+), 47.17 ($\underline{C}H_2$−SO_3^-), 32.19 ($\underline{C}H_2$−CH−O), 25.78 ($\underline{C}H_2$−CH_2−CH), 21.72 ($\underline{C}H_2$−CH_3), 18.28 ($\underline{C}H_2$−CH_2−SO_3^-), 17.18 ($\underline{C}H_3$−C=), 13.04 ($\underline{C}H_3$−CH_2).

FT-IR (selected bands, cm^{-1}): 2958 ν(=C−H), 2872 ν(C−H), 1708 ν(C=O), 1634 ν(C=C), 1458 δ(CH_3), 1317 ν(S=O), 1296 ν(C−N), 1161 ν(C−O), 1037 ν(S−O), 932 δ(C=C), 816 δ(CH_2).

Elemental analysis ($C_{15}H_{29}NO_5S$ M_r = 335.46): Calculated: C = 53.71 %, H = 8.71 %, N = 4.18 %, S = 9.56 %; found: C = 53.54 %, H = 8.82 %, N = 4.19 %, S = 9.18 %.

ESI-MS: Calculated: 335.18 g/mol $[M]^+$; found: 336.0 g/mol $[M+H]^+$.

8.3.2 Synthesis of Vinyl Amide Sulfo- and Sulfabetaines

8.3.2.1 Synthesis of 4-acetyl-1-methylpiperazine (I-3)

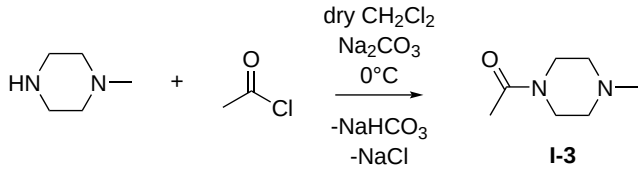

Finely milled sodium carbonate (79.49 g, 750 mmol) was added to dry DCM (330 mL) in a 1 L round-bottom flask. This was then cooled down to 0 °C in an ice bath. Acetyl chloride (1.30 eq., 51.02 g, 650 mmol) was then added and the solution was purged with N_2. The reaction vessel was then equipped with a 250 mL pressure-equalizing dropping funnel followed by a drying tube, and a solution of 1-methylpiperazine (1.00 eq., 50.15 g, 500 mmol) in DCM (340 mL) was subsequently added drop-wise to the reaction mixture. The addition of the 1-methylpiperazine was completed within 50 min. The reaction temperature was kept at 0 °C throughout the addition of 1-methylpiperazine and up to 1 h after the end of additions, at which point the reaction temperature was allowed to rise to 4 °C.

2 h after the end of additions, the reaction vessel was taken out of the ice bath and the reaction was allowed to continue at RT. After 3 h of the reaction being at RT, an extra portion of acetyl chloride (0.14 eq., 5.5 g, 70 mmol) was added. After 30 min, the reaction was stopped by filtering off the solids and washing them twice with freshly distilled DCM.

The filtrate containing 4-acetyl-1-methylpiperazine (**I-3**) was reduced to 400 mL by rotary evaporation and subsequently extracted three times with a concentrated solution of sodium carbonate in H_2O (20 mL).

The organic phase was dried with magnesium sulfate and the solvent was removed by rotary evaporation under reduced pressure. Pure 1-(4-methyl-piperazin-1-yl)-ethan-1-one was isolated as a yellow oil (n_D^{20}= 1.4880) (yield 69.2 g, 97%).

^{1}H NMR(400 MHz, CD_2Cl_2, 298 K): δ (ppm) = 3.52 (t, J = 5.1 Hz, 2H, −C$\underline{H}_2$−NCO), 3.40 (t, J = 5.1 Hz, 2H, −C$\underline{H}_2$−NCO), 2.33 (t, J = 5.1 Hz, 2H, −C$\underline{H}_2$−N−), 2.28 (t, J = 5.1 Hz, 2H, −C$\underline{H}_2$−N−), 2.23 (s, 3H, C$\underline{H}_3$−N−), 2.00 (s, 3H,C$\underline{H}_3$−CO).

^{13}C NMR(101 MHz, D_2O, 298 K): δ (ppm) = 172.39 ($\underline{C}$O−N), 53.56 ($\underline{C}H_2$−N), 53.23 ($\underline{C}H_2$−N), 45.67 ($\underline{C}H_2$−NCO), 44.22 ($\underline{C}H_3$−N), 41.07 ($\underline{C}H_2$−NCO), 20.23 ($\underline{C}H_3$−CO).

8.3.2.2 Synthesis of 4-acetyl-1,1-dimethylpiperazin-1-ium tosylate (I-4)

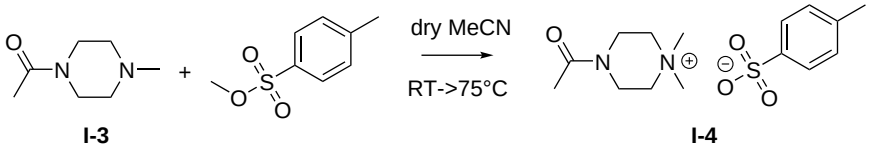

I-3 **I-4**

Amine **I-3** (1.00 eq., 32.57 g, 230 mmol) was dissolved in dry MeCN (66 mL) in a 500 mL round-bottom flask. A solution of methyl *p*-toluenesulfonate (1.50 eq., 64.32 g, 345 mmol) in MeCN (128 mL) was added to the reaction mixture. The reaction vessel was then sealed with a rubber septum and purged with N_2 for 20 min at RT. After purging, the temperature was raised to 75 °C by an oil bath. The reaction continued at 75 °C for the following 2.5 h.

Pure 4-acetyl-1,1-dimethylpiperazin-1-ium tosylate (**I-4**) was isolated by removing 100 mL of the solvent by rotary evaporation. The remaining solution was then poured in a 1 L Erlenmeyer flask. Methyl *tert*-butyl ether (MTBE) was added drop-wise under agitation until the solution was not translucent. The Erlenmeyer flask containing the **I-4** in solution was then brought to the boiling point by a hot plate, MTBE was continued to be added drop-wise until right before the solution turned cloudy at boiling point. At this moment the Erlenmeyer flask was removed from the heat source and allowed to cool to RT. Once the solution reached RT, it was further cooled down to 0 °C by an ice bath. The product precipitated rapidly and the obtained colorless crystals were then washed with a mixture of MeCN and MTBE (1 : 1 v/v) at 4 °C (yield 60.3 g, 80%).

^{1}H NMR(300 MHz, D_2O, 298 K): δ (ppm) = 7.69 (d, J = 8.2 Hz, 2H, =C$\underline{H}$−phenyl), 7.37 (d, J = 7.9 Hz, 2H, =C$\underline{H}$−phenyl), 3.82–3.96 (m, 4H, C$\underline{H}_2$−N^+), 3.51 (t, J = 5.3 Hz, 2H, C$\underline{H}_2$−N−CO), 3.44 (t, J = 5.3 Hz, 2H, C$\underline{H}_2$−N−CO), 3.22 (s, 6H, (C$\underline{H}_3$)$_2$−N^+), 2.39 (s, 3H, C$\underline{H}_3$−aryl), 2.15 (s, 3H, C$\underline{H}_3$−CO).

^{13}C NMR(101 MHz, D_2O, 298 K): δ (ppm) = 172.74 ($\underline{C}$O−N), 142.46 ($\underline{C}$−SO_3^-), 139.44 ($\underline{C}$−CH_3), 129.44 ($\underline{C}$H−C−CH_3), 125.33 ($\underline{C}$H−C−SO_3^-), 60.70 ($\underline{C}H_2$−N^+), 51.26 (($\underline{C}H_3$)$_2$−N^+), 40.26 and 35.64 ($\underline{C}H_2$−N−CO), 20.44 ($\underline{C}H_3$−C=), 20.11 ($\underline{C}H_3$−CO).

8.3.2.3 Synthesis of *N*-(2-(dimethylamino)ethyl)-*N*-vinylacetamide (I-5)

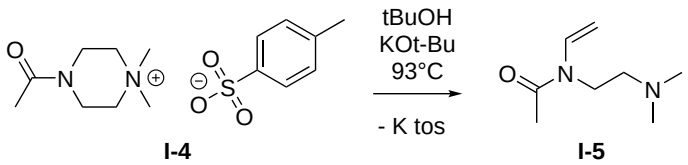

I-4 **I-5**

The ammonium salt **I-4** (1.00 eq., 14.78 g, 45 mmol) was dissolved in dry *t*-BuOH (200 mL) in a 500 mL 3-neck round-bottom flask. Nitrobenzene (0.30 g, 2.5 mmol) was then added to the reaction mixture as polymerization inhibitor, and the reaction flask was equipped with a Dimroth reflux condenser equipped with a drying tube.

After purging with N_2 for 30 min, the reaction mixture was placed in an oil bath at 93 °C. A solution of *t*-BuOK (1.50 eq., 7.57 g, 67.5 mmol) in *t*-BuOH (200 mL) was then added drop-wise. The addition of the *t*-BuOK solution was completed within 16 min.

The reaction was stopped 15 min after the end of additions by filtering off the produced solids and washing them thrice with dry *t*-BuOH. The solvent was then removed by rotary evaporation under reduced pressure. The resulting brown paste was dissolved in benzene and the remaining solids were filtered off. Benzene was then removed by freeze-drying, leaving an orange oil.

I-5 was isolated by column chromatography using a mixture of DCM and MeOH (3 : 1 v/v) as eluent. The solvents were removed by rotary evaporation under reduced pressure to obtain an orange oil (n_D^{20}= 1.4675) (yield 4.6 g, 65%).

^{1}H NMR(400 MHz, CD_3OD, 298 K): δ (ppm) = 7.36 (dd, J = 9.5, 16.3 Hz, 0.2H, $-C\underline{H}=CH_2$ *cis*), 6.93 (dd, J = 9.2, 15.4 Hz, 0.8H, $-C\underline{H}=CH_2$ *trans*), 4.65 (dd, J = 15.3, 1.1 Hz, 1H, $C\underline{H}_2=CH-$ *cis*), 4.48 (dd, J = 9.2, 1.1 Hz, 1H, $C\underline{H}_2=CH-$ *trans*), 3.83 (t, J = 7.4 Hz, 1.6H, $C\underline{H}_2-N-CO$), 3.75 (t, J = 7.7 Hz, 0.4H, $C\underline{H}_2-N-CO$), 2.55 (t, J = 7.8 Hz, 0.4H, $C\underline{H}_2-N<$), 2.50 (t, J = 7.4 Hz, 1.6H, $C\underline{H}_2-N<$), 2.34 (s, 6H, $(C\underline{H}_3)_2-N-$), 2.27 (s, 0.6H, $C\underline{H}_3-CO$), 2.23 (s, 2.4H, $C\underline{H}_3-CO$).

^{13}C NMR(101 MHz, CD_3OD, 298 K): δ (ppm) = 172.07 ($\underline{C}O-N$), 134.49 and 131.80 ($\underline{C}H=CH_2$), 95.28 and 94.87 ($\underline{C}H_2=CH-$), 56.67 and 56.00 ($\underline{C}H_2-N-CO$), 45.80 and 45.64 ($(\underline{C}H_3)_2-N-$), 43.81 and 40.02 ($\underline{C}H_2-N<$), 21.95 ($\underline{C}H_3-CO$).

FT-IR (selected bands, cm^{-1}): 2974 ν(=C−H), 2901 ν(C−H), 1670 ν(C=O), 1620 ν(C=C), 1456 $\delta(-CH_2)$, 1383 $\delta(-CH_3)$, 1342 ν(C−N, 1234 ν(C−N), 1180 ν(C−N), 1036 δ(C=C), 843 $\delta(CH_2)$, 780 $\delta(CH_3)$.

ESI-MS: Calculated: 156.13 g/mol $[M]^+$; found: 157.1 g/mol $[M+H]^+$.

8.3.2.4 Synthesis of 3-(dimethyl(2-(*N*-vinylacetamido)ethyl)ammonio)-propane-1-sulfonate (M2)

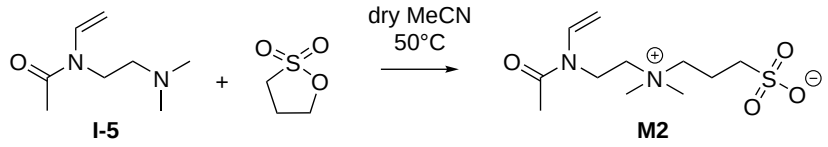

I-5 **M2**

Amidoamine **I-5** (1.00 eq., 3.91 g, 25 mmol) was dissolved in dry MeCN (39 mL) in a 100 mL round-bottom flask. Nitrobenzene (0.08 g, 0.65 mmol) was added as polymerization inhibitor and the reaction mixture was purged with N_2. A solution of 1,3-propane sultone (0.90 eq., 2.75 g, 22.5 mmol) in dry MeCN (28 mL) was then added to the reaction mixture and the reaction vessel was sealed with a rubber septum and purged with N_2 for additional 15 min.

The reaction temperature was then brought to 50 °C by an oil bath, and the reaction was continued at this temperature. After 23 h, an extra addition of 1,3-propane sultone (0.15 eq., 0.3 g, 2.5 mmol) in dry MeCN (3 mL) was done. The reaction was continued for the following 20 h, making a total reaction time of 43 h. Pure **M2** was obtained as a colorless powder precipitate from the reaction. The precipitate was filtered off and washed three times with dry MeCN, and placed in an oven at 30 °C and ≤50 mbar over night to remove traces of the solvent (yield 5.7 g, 90%).

^{1}H NMR(400 MHz, D_2O, 298 K): δ (ppm) = 7.22 (dd, J = 9.7, 16.1 Hz, 0.05H, =C$\underline{H}$−N), 6.93 (dd, J = 9.2, 15.6 Hz, 0.95H, =C$\underline{H}$−N), 4.75 (dd, J = 1.1, 15.6 Hz, 1H, C$\underline{H}_2$=CH− *cis*), 4.69 (dd, J = 2.1, 9.2 Hz, 1H, C$\underline{H}_2$=CH− *trans*), 4.16 (t, J = 7.3 Hz, 2H, C$\underline{H}_2$−N−CO), 3.68–3.47 (m, 4H, C$\underline{H}_2$−N^+−C$\underline{H}_2$), 3.28 (s, 0.3H, (C$\underline{H}_3$)$_2$−N^+), 3.22 (s, 5.7H, (C$\underline{H}_3$)$_2$−N^+), 3.00 (t, J = 7.2 Hz, 2H, C$\underline{H}_2$−SO_3^-), 2.36–2.20 (m, 5H, C$\underline{H}_3$−CO and C$\underline{H}_2$−CH_2−SO_3^-).

^{13}C NMR(101 MHz, D_2O, 298 K): δ (ppm) = 173.22 ($\underline{C}$O−N−), 132.56 ($\underline{C}$H=CH_2), 96.99 ($\underline{C}H_2$=CH−), 62.65 (−$\underline{C}H_2$−N^+), 59.14 (−$\underline{C}H_2$−N^+), 50.92 (($\underline{C}H_3$)$_2$−N^+), 47.16 ($\underline{C}H_2$−SO_3^-), 35.24 ($\underline{C}H_2$−N−CO), 21.21 ($\underline{C}H_3$−CO), 18.21 ($\underline{C}H_2$−CH_2−SO_3^-).

FT-IR (selected bands, cm^{-1}): 3030 ν(=C−H), 2926 ν(C−H), 1664 ν(C=O), 1622 ν(C=C), 1387 δ(CH_3), 1360 ν(S=O), 1200 ν(C−N), 1036 ν(S−O), 920 δ(CH_2), 860 δ(CH_2), 723 δ(CH_3).

Elemental analysis ($C_{11}H_{22}N_2SO_4$ M_r = 278.37): Calculated: C = 47.46 %, H = 7.97 %, N = 10.06 %, S = 11.52 %; found: C = 41.66 %, H = 8.13 %, N = 9.05 %, S = 10.58 %.

ESI-MS: Calculated: 278.13 g/mol $[M]^+$; found: 301.1 g/mol $[M+Na]^+$.

8.3.2.5 Synthesis of 4-(dimethyl(2-(*N*-vinylacetamido)ethyl)ammonio)-butane-1-sulfonate (M3)

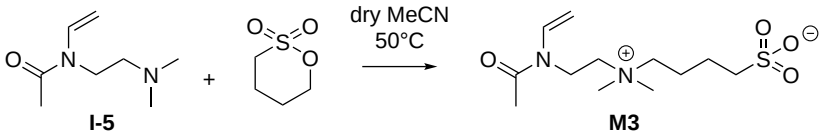

Amidoamine **I-5** (1.00 eq., 3.12 g, 20 mmol) was dissolved in dry MeCN (31.5 mL) in a 100 mL round-bottom flask. Nitrobenzene (0.05 g, 0.4 mmol) was added as polymerization inhibitor and the reaction mixture was purged with N_2. A solution of Butane sultone (0.90 eq., 2.5 g, 18 mmol) in dry MeCN (24 mL) was then added to the reaction mixture and the reaction vessel was sealed with a rubber septum and purged with N_2 for additional 15 min.

The reaction temperature was then brought to 50 °C by an oil bath, and the reaction was continued at this temperature. After 24 h, an extra addition of Butane sultone (0.19 eq., 0.5 g, 3.7 mmol) in dry MeCN (3.5 mL) was done. The reaction was continued for the following 18 h, making a total reaction time of 43 h. Pure **M3** was obtained as a colorless powder precipitate from the reaction. The precipitate was filtered off and washed three times with dry MeCN. It was placed in an oven at 30 °C and 50 mbar over night to remove traces of the solvent (yield 2.5 g, 50%).

^{1}H NMR(400 MHz, D_2O, 298 K): δ (ppm) = 7.22 (dd, J = 9.6, 16.3 Hz, 0.05H, =C$\underline{H}$−N), 6.93 (dd, J = 9.2, 15.4 Hz, 0.95H, =C$\underline{H}$−N), 4.74 (dd, J = 1.9, 15.5 Hz, 1H, C$\underline{H}_2$=CH− *cis*), 4.68 (dd, J = 2.0, 9.1 Hz, 1H, C$\underline{H}_2$=CH− *trans*), 4.15 (t, J = 7.3 Hz, 2H, C$\underline{H}_2$−N−CO), 3.65–3.38 (m, 4H, C$\underline{H}_2$−N^+−C$\underline{H}_2$), 3.24 (s, 0.3H, (C$\underline{H}_3$)$_2$−N^+), 3.18 (s, 5.7H, (C$\underline{H}_3$)$_2$−N^+), 3.00 (t, J = 7.6 Hz, 2H, C$\underline{H}_2$−SO_3^-), 2.31 (s, 0.15H, C$\underline{H}_3$−CO), 2.28 (s, 2.85H, C$\underline{H}_3$−CO), 1.98 (m, J = 5.3 Hz, 2H, C$\underline{H}_2$−CH_2−N^+), 1.83 (m, J = 7.5 Hz, 2H, C$\underline{H}_2$−CH_2−SO_3^-).

^{13}C NMR(101 MHz, D_2O, 298 K): δ (ppm) = 173.21 (C$\underline{O}$−N−), 132.57 (C$\underline{H}$=CH_2), 96.99 (C$\underline{H}_2$=CH−), 63.86 (−C$\underline{H}_2$−N^+), 59.11 (−C$\underline{H}_2$−N^+), 50.86 ((C$\underline{H}_3$)$_2$−N^+), 49.93 (C$\underline{H}_2$−SO_3^-), 35.27 (C$\underline{H}_2$−N−CO), 21.20 (C$\underline{H}_3$−CO−), 21.04 (C$\underline{H}_2$−CH_2−SO_3^-), 20.91 (C$\underline{H}_2$−CH_2−N^+).

FT-IR (selected bands, cm^{-1}): 3498, 3027 ν(=C−H), 1656 ν(C=O), 1611 ν(C=C), 1387 δ(CH_3), 1341 ν(S=O), 1234 ν(C−N), 1180 ν(C−N), 1033 δ(C=C), 920 δ(CH_2), 878 δ(CH_2), 800 δ(CH_2), 798 δ(CH_3).

Elemental analysis ($C_{12}H_{24}N_2O_4S$ M_r = 292.39): Calculated: C = 49.29 %, H = 8.27 %, N = 9.58 %, S = 10.96 %; found: C = 43.60 %, H = 8.83 %, N = 8.98 %, S = 9.59 %.

ESI-MS: Calculated: 292.15 g/mol $[M]^+$; found: 315.1 g/mol $[M+Na]^+$.

8.3.2.6 Synthesis of 3-(dimethyl(2-(*N*-vinylacetamido)ethyl)ammonio)-propyl sulfate (M4)

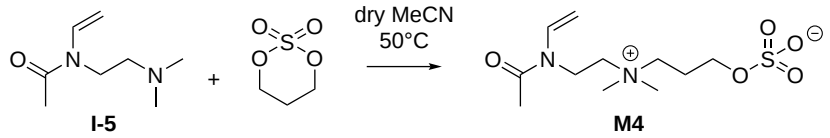

I-5 **M4**

Amidoamine **I-5** (1.00 eq., 3.12 g, 20 mmol) was dissolved in dry MeCN (31.5 mL) in a 100 mL round-bottom flask. Nitrobenzene (0.05 g, 0.4 mmol) was added as polymerization inhibitor and the reaction mixture was purged with N_2. A solution of 1,3-propylene sulfate (0.90 eq., 2.5 g, 18 mmol) in dry MeCN (24 mL) was then added to the reaction mixture and the reaction vessel was sealed with a rubber septum and purged with N_2 for additional 15 min.

The reaction temperature was then brought to 50 °C by an oil bath, and the reaction was continued at this temperature. After 24 h, an extra addition of 1,3-propylene sulfate (0.13 eq., 0.35 g, 2.5 mmol) in dry MeCN (3.5 mL) was done. The reaction was continued for the following 18 h, making a total reaction time of 42 h. Pure **M4** was obtained as a colorless powder precipitate from the reaction. The precipitate was filtered off and washed three times with dry MeCN. It was placed in an oven at 30 °C and 50 mbar over night to remove traces of the solvent (yield 5.4 g, 96%).

^{1}H NMR(400 MHz, D_2O, 298 K): δ (ppm) = 7.22 (dd, J = 9.6, 16.2 Hz, 0.05H, =C$\underline{H}$−N), 6.94 (dd, J = 9.2, 15.5 Hz, 0.95H, =C$\underline{H}$−N), 4.74 (dd, J = 1.9, 9.2 Hz, 1H, C$\underline{H}_2$=CH− *cis*), 4.69 (dd, J = 1.9, 9.2 Hz, 1H, C$\underline{H}_2$=CH− *trans*), 4.29–4.05 (m, 4H, C$\underline{H}_2$−N−CO and C$\underline{H}_2$−O), 3.68–3.43 (m, 4H, C$\underline{H}_2$−N^+−C$\underline{H}_2$), 3.28 (s, 0.3H, (C$\underline{H}_3$)$_2$−N^+), 3.22 (s, 5.7H, (C$\underline{H}_3$)$_2$−N^+), 2.36–2.18 (m, 5H, C$\underline{H}_3$−CO and C$\underline{H}_2$−CH_2−OSO_3^-).

^{13}C NMR(101 MHz, D_2O, 298 K): δ (ppm) = 173.27 ($\underline{C}$O−N−), 132.59 ($\underline{C}$H=CH_2), 97.02 ($\underline{C}H_2$=CH−), 65.25 (−$\underline{C}H_2$−O), 61.52 (−$\underline{C}H_2$−N^+), 59.08 (−$\underline{C}H_2$−N^+), 51.05 (($\underline{C}H_3$)$_2$−N^+), 35.32 ($\underline{C}H_2$−N−CO), 22.40 ($\underline{C}H_2$−CH_2−O), 21.24 ($\underline{C}H_3$−CO).

FT-IR (selected bands, cm^{-1}): 3029 ν(=C−H), 1662 ν(C=O), 1621 ν(C=C), 1384 δ(CH_3), 1322 ν(S=O), 1247 ν(C−N), 1209 ν(C−N), 1165 ν(C−O), 1026 δ(C=C), 923 δ(CH_2), 860 δ(CH_2), 813 δ(CH_2), 774 δ(CH_2), 747 δ(CH_3).

Elemental analysis ($C_{11}H_{22}N_2O_5S$ M_r = 294.37): Calculated: C = 44.88 %, H = 7.53 %, N = 9.52 %, S = 10.89 %; found: C = 44.26 %, H = 7.72 %, N = 9.89 %, S = 10.70 %.

ESI-MS: Calculated: 294.12 g/mol $[M]^+$; found: 295.12 g/mol $[M+H]^+$.

8.3.3 Synthesis of Vinyl Amide Crosslinker

8.3.3.1 Synthesis of 4-benzoylbenzoyl chloride (I-6)

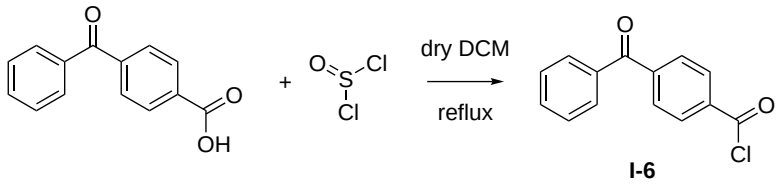

I-6

4-Benzylbenzoic acid (1.00 eq., 10.18 g, 45 mmol) was added to dry DCM (100 mL) in a 250 mL 3-neck round-bottom flask. Thionyl chloride (9.30 eq., 49.98 g, 418.5 mmol) was added to the reaction mixture, and the 3-neck round-bottom flask was equipped with a Dimroth reflux condenser followed by a gas bubbler. The reaction mixture was subsequently purged with N_2 for 35 min.

The reaction was then brought to reflux by an oil bath at 55 °C. After 17.5 h, the reaction was stopped by cooling to RT. The solvent and excess thionyl chloride were removed by rotary evaporation. Residual thionyl chloride was further removed by azeotropic distillation with toluene. Pure **I-6** was obtained quantitatively as a white powder (yield 11 g, 100%).

^{1}H NMR(400 MHz, $CDCl_3$, 298 K): δ (ppm) = 8.24 (d, J = 8.4 Hz, 2H, C$\underline{H}$=C−COCl), 7.89 (d, J = 8.3 Hz, 2H, C$\underline{H}$=C−CO), 7.81 (d, J = 7.3 Hz, 2H, C$\underline{H}$=C−CO), 7.65 (dd, J = 7.4, 7.4 Hz, 1H, C$\underline{H}$=CH−CH), 7.52 (dd, J = 7.6, 7.6 Hz, 2H, C$\underline{H}$−CH=C).

^{13}C NMR(101 MHz, $CDCl_3$, 298 K): δ (ppm) = 195.38 (C$\underline{O}$), 167.95 (C$\underline{O}$Cl), 143.34 (C$\underline{}$−CO), 136.43 (C$\underline{}$−CO), 135.83 (C$\underline{}$−COCl), 133.38 (C$\underline{H}$=CH−CH), 131.21 (C$\underline{H}$=C−COCl), 130.14 (C$\underline{H}$=C−CO), 130.06 (C$\underline{H}$=C−CO), 128.64 (C$\underline{H}$=CH−C).

8.3.3.2 Synthesis of 4-benzoyl-N-vinylbenzamide (M5)

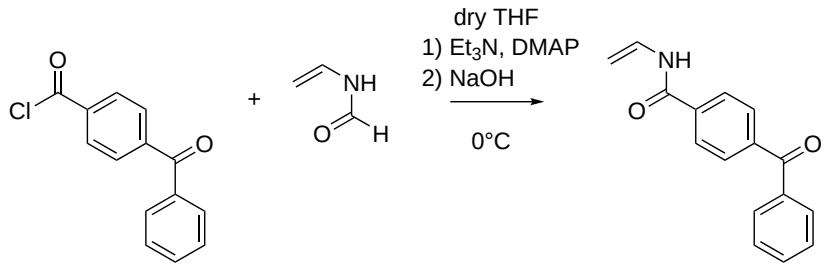

N-vinyl formamide (1.00 eq., 1.08 g, 15 mmol), triethylamine (1.20 eq., 1.84 g, 18 mmol) and 4-dimethylamino-pyridine (DMAP) (5 mol%, 0.09 g, 0.75 mmol) were dissolved in THF (60 mL) in a 250 mL 3-neck round-bottom flask equipped with a thermometer and a 50 mL pressure-equalizing dropping funnel followed by a gas bubbler. This was then cooled down to 0 °C in an ice bath and purged with N_2 for 40 min.

A solution of acyl chloride **I-6** (1.15 eq., 4.22 g, 17.25 mmol) in THF (30 mL) was then added drop-wise within 22 min, controlling that the temperature was always maintained below 5 °C. The reaction was then allowed to reach RT during the following 19 h.

Subsequently, the mixture was cooled down to 5 °C. A solution of 5 M NaOH (9 mL) was added drop-wise within 1 h, controlling that the temperature was always maintained below 5 °C. The reaction was stopped 2 h after the addition of NaOH and the reaction mixture was repeatedly washed against distilled DCM. The organic phase was then recovered, dried over $MgSO_4$, and the solvents removed by rotary evaporation under reduced pressure. The crude product was dissolved in MeCN, pure **M5** was obtained as colorless crystals by adding H_2O to the solution in MeCN, colourless powder, m.p. 160 °C (yield 0.8 g, 23%).

^{1}H NMR(400 MHz, acetone-d6, 298 K): δ (ppm) = 9.81 (br, 1H, N$\underline{\text{H}}$), 8.10 (d, J = 8.2 Hz, 2H, C$\underline{\text{H}}$−C−CO−N), 7.86 (d, J = 8.2 Hz, 2H, C$\underline{\text{H}}$=C−CO), 7.80 (d, J = 7.4 Hz, 2H, C$\underline{\text{H}}$=C−CO), 7.69 (dd, J = 7.4, 7.4 Hz, 1H, C$\underline{\text{H}}$=CH−CH), 7.57 (dd, J = 7.6, 7.6 Hz, 2H, C$\underline{\text{H}}$−CH=C), 7.20 (ddd, J = 9.5, 9.5, 16.0 Hz, 1H, C$\underline{\text{H}}$=CH_2), 4.94 (d, J = 16.0 Hz, 1H, C$\underline{\text{H}}_2$=CH *trans*), 4.50 (d, J = 9.0 Hz, 1H, C$\underline{\text{H}}_2$=CH *cis*).

^{13}C NMR(101 MHz, acetone-d6, 298 K): δ (ppm) = 195.15 ($\underline{\text{C}}$=O), 163.38 (−NH−$\underline{\text{C}}$=O), 140.31 ($\underline{\text{C}}$−CO), 137.19 ($\underline{\text{C}}$−CO), 137.03 ($\underline{\text{C}}$−CO−N), 132.80 ($\underline{\text{C}}$H=CH−CH), 129.79 ($\underline{\text{C}}$H=C−CO), 129.67 ($\underline{\text{C}}$H=C−CO), 129.61 (N−$\underline{\text{C}}$H=CH_2), 128.52 ($\underline{\text{C}}$H=CH−C), 127.51 ($\underline{\text{C}}$H=C−CO), 95.75 ($\underline{\text{C}}H_2$=CH).

FT-IR (selected bands, cm^{-1}): 3345 ν(N−H), 3062 ν(=C−H), 1654 ν(C=O), 1633 ν(C=O), 1595 ν(C=C), 1275 ν(C−N), 974 δ(C=C).

Elemental analysis ($C_{16}H_{13}NO_2$ M_r = 251.29): Calculated: C = 76.48 %, H = 5.21 %, N = 5.57 %, S = 0.00 %; found: C = 75.78 %, H = 5.26 %, N = 5.71 %, S = 0.00 %.

ESI-MS: Calculated: 251.09 g/mol $[M]^+$; found: 252.1 g/mol $[M+H]^+$.

8.3.4 Synthesis of Zwitterionic Crosslinkers

8.3.4.1 Synthesis of (4-(2-bromoethoxy)phenyl)(phenyl)methanone (I-7)

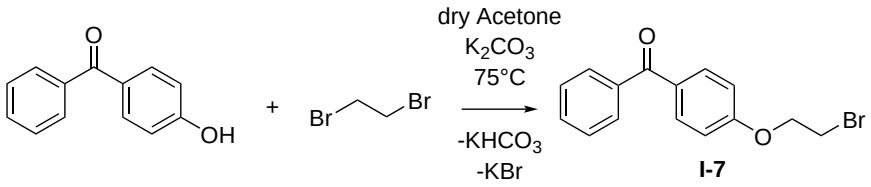

I-7

4-Hydroxybenzophenone (1.00 eq., 6.94 g, 35 mmol) was dissolved in dry acetone (150 mL) in a 250 mL round-bottom flask, finely milled potassium carbonate (10.37 g, 75 mmol) was then added to the reaction mixture, followed by 1,2-dibromoethane (3.00 eq., 19.78 g, 105 mmol).

The reaction mixture was purged with N_2 for 10 min and sealed with a rubber septum. This was subsequently brought to 75 °C by an oil bath. The reaction continued at 75 °C for the following 91.5 h and then stopped by cooling the reaction mixture to 0 °C by an ice bath. The solids were then filtered off while cold, and the filtrate was removed by rotary evaporation.

After removing the acetone, the product was dissolved in freshly distilled DCM (100 mL) and extracted with a half concentrated aqueous solution of sodium carbonate (15 mL) several times in order to remove unreacted 4-hydroxybenzophenone. The organic phase was recovered and dried with magnesium sulfate. After filtering off the magnesium sulfate, *n*-hexane (100 mL) was added to the organic phase.

Pure **I-7** was crystallized by removing a portion of the DCM by rotary evaporation. Once the solution was not translucent anymore, this was let to cool to room temperature and subsequently brought to 4 °C in a refrigerator. The crystals of **I-7** were then filtered off and washed with *n*-hexane. This process was repeated four times by adding small amounts of DCM to the filtrate and collecting the resulting crystals (yield 3.5 g, 33%).

^{1}H NMR(400 MHz, CD_2Cl_2, 298 K): δ (ppm) = 7.81 (dd, J = 2.1, 6.8 Hz, 2H, C$\underline{H}$=C−CO), 7.74 (m, J = 2.3 Hz, 2H, C$\underline{H}$−C−CO), 7.59 (m, J = 2.2 Hz, 1H, C$\underline{H}$=CH−CH), 7.49 (m, J = 3.7 Hz, 2H, C$\underline{H}$=CH−C), 6.99 (dd, J = 2.1, 6.8 Hz, 2H, C$\underline{H}$−C−O−), 4.39 (t, J = 6.0 Hz, 2H, O−C$\underline{H}_2$), 3.71 (t, J = 6.0 Hz, 2H, C$\underline{H}_2$−Br).

^{13}C NMR(101 MHz, CD_2Cl_2, 298 K): δ (ppm) = 195.01 (C$\underline{}$=O), 161.68 (C$\underline{}$−O−), 138.18 (C$\underline{}$−CO), 132.43 (C$\underline{H}$=C−CO), 131.91 (C$\underline{H}$=CH−CH), 130.77 (C$\underline{}$−CO), 129.62 (C$\underline{H}$=C−CO), 128.18 (C$\underline{H}$=CH−C), 114.11 (C$\underline{H}$=C−O), 68.05 (C$\underline{H}_2$−CH_2), 29.18 (C$\underline{H}_2$−Br).

8.3.4.2 Synthesis of (4-(2-(diallylamino)ethoxy)phenyl)(phenyl)methanone (I-8)

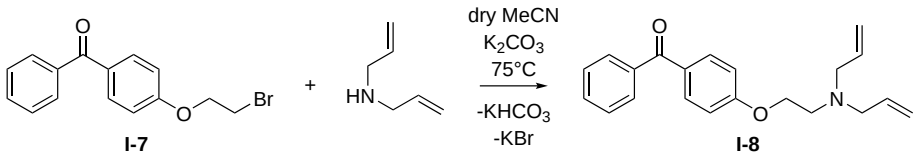

Finely milled potassium carbonate (6.91 g, 50 mmol) was added to dry MeCN (25 mL) in a 50 mL round-bottom flask. Bromide **I-7** (1.00 eq., 3.05 g, 10 mmol) and diallylamine (3.00 eq., 2.93 g, 30 mmol) were then added to the reaction mixture. After purging with N_2 for 20 min, the reaction mixture was sealed with a rubber septum and brought to 75 °C by an oil bath.

The reaction continued at 75 °C for 27 h, at which point it was stopped by cooling to RT. The solids were then filtered off and washed with dry MeCN repeatedly. The solvent was subsequently removed from the filtrate by rotary evaporation under reduced pressure. Pure **I-8** was isolated as a yellowish oil (n_D^{20}= 1.5805), the remaining diallylamine was successfully removed by rotary evaporation at 50 °C and 50 mbar (yield 3.13 g, 97%).

^{1}H NMR(400 MHz, acetone-d6, 298 K): δ (ppm) = 7.82–7.76 (m, 2H, C$\underline{H}$=C−CO), 7.76–7.71 (m, 2H, C$\underline{H}$−C−CO), 7.65–7.59 (m, 1H, C$\underline{H}$=CH−CH), 7.56–7.50 (m, 2H, C$\underline{H}$=CH−C), 7.10–7.04 (m, 2H, C$\underline{H}$=C−O−), 5.88 (tdd, J = 6.3, 10.3, 17.2 Hz, 2H, C$\underline{H}$=CH_2), 5.23 (ddd, J = 3.6, 1.6, 17.2 Hz, 2H, C$\underline{H_2}$=CH *cis*), 5.12 (tdd, J = 1.1, 2.3, 10.2 Hz, 2H, C$\underline{H_2}$=CH *trans*), 4.20 (t, J = 6.1 Hz, 2H, C$\underline{H_2}$−O), 3.22 (ddd, J = 1.3, 1.3, 6.3 Hz, 4H, C$\underline{H_2}$−CH=CH_2), 2.91 (t, J = 6.1 Hz, 2H, CH_2−N).

^{13}C NMR(101 MHz, acetone-d6, 298 K): δ (ppm) = 194.28 (C$\underline{}$=O), 162.69 (C$\underline{}$−O−), 138.47 (C$\underline{}$−CO), 136.27 (C$\underline{}$H=CH_2), 132.19 (C$\underline{}$H=C−CO), 131.78 (C$\underline{}$H=CH−CH), 130.01 (C$\underline{}$−CO), 129.36 (C$\underline{}$H=C−CO), 128.25 (C$\underline{}$H=CH−C), 116.55 (C$\underline{H_2}$=CH), 114.17 (C$\underline{}$H=C−O), 66.93 (C$\underline{H_2}$−CH_2), 57.26 (C$\underline{H_2}$−CH=CH_2), 51.72 (C$\underline{H_2}$−N).

8.3.4.3 Synthesis of 3-(diallyl(2-(4-benzoylphenoxy)ethyl)ammonio)-propane-1-sulfonate (M6)

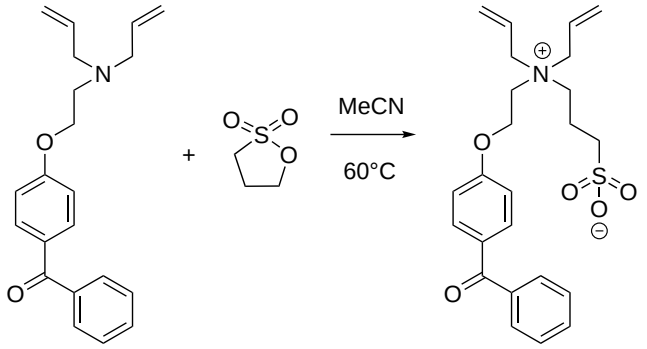

I-8 **M6**

Diallylamine **I-8** (1.00 eq, 2.90 g, 9 mmol) and nitrobenzene (0.06 g, 0.47 mmol) as polymerization inhibitor were dissolved in dry MeCN (10 mL) in a 50 mL round-bottom flask. A solution of 1,3-propane sultone (1.00 eq, 1.15 g, 10 mmol) in dry MeCN (10 mL) was then added to the reaction mixture.

After purging with N_2 for 35 min, the reaction mixture was sealed with a rubber septum and brought to 60 °C by an oil bath. The reaction continued at 60 °C for 72 h. Pure **M6** was obtained as a precipitate from the reaction. The precipitate was filtered off, washed three times with cold dry MeCN, and placed in an oven at 30 °C and 50 mbar over night to remove traces of the solvent (yield 2.1 g, 54%).

^{1}H NMR(400 MHz, acetone-d6, 298 K): δ (ppm) = 7.71 (d, J = 8.7 Hz, 2H, C$\underline{\text{H}}$=C−CO), 7.65–7.54 (m, 3H, C$\underline{\text{H}}$=C−CO and C$\underline{\text{H}}$=CH−CH), 7.51–7.42 (m, 2H, C$\underline{\text{H}}$=CH−C), 7.11 (d, J = 8.7 Hz, 2H, C$\underline{\text{H}}$=C−O−), 6.10 (tdd, J = 7.3, 9.5, 16.6 Hz, 2H, C$\underline{\text{H}}$=CH_2), 5.82–5.66 (m, 4H, C$\underline{\text{H}}_2$=CH), 4.70–4.57 (br, 2H, C$\underline{\text{H}}_2$−O), 4.09 (d, J = 7.1 Hz, 4H, C$\underline{\text{H}}_2$−CH=CH_2), 3.94–3.81 (m, 2H, C$\underline{\text{H}}_2$−CH_2−O−), 3.63–3.47 (m, J = 4.2 Hz, 2H, C$\underline{\text{H}}_2$−N^+), 2.83 (t, J = 6.9 Hz, 2H, C$\underline{\text{H}}_2$−SO_3^-), 2.37–2.21 (m, J = 7.5 Hz, 2H, C$\underline{\text{H}}_2$−CH_2−SO_3^-).

^{13}C NMR(101 MHz, acetone-d6, 298 K): δ (ppm) = 196.69 (C$\underline{\text{C}}$=O), 161.34 (C$\underline{\text{C}}$−O−), 137.41 (C$\underline{\text{C}}$−CO), 132.81 (C$\underline{\text{C}}$H=CH−CH), 132.63 (C$\underline{\text{C}}$H=C−CO), 130.42 (C$\underline{\text{C}}$−CO), 129.63 (C$\underline{\text{C}}$H−C−CO), 129.18 (C$\underline{\text{C}}_2$=CH), 128.58 (C$\underline{\text{C}}$H=CH−C), 124.06 (C$\underline{\text{C}}$H=CH_2), 114.52 (C$\underline{\text{C}}$H=C−O), 61.84 (C$\underline{\text{C}}_2$−O), 61.73 (C$\underline{\text{C}}_2$−CH=CH_2), 57.73 (C$\underline{\text{C}}_2$−CH_2−O), 56.98 (C$\underline{\text{C}}_2$−N^+), 47.29 (C$\underline{\text{C}}_2$−SO_3^-), 17.94 (C$\underline{\text{C}}_2$−CH_2−SO_3^-).

FT-IR (selected bands, cm^{-1}): 3016 ν(=C−H), 1643 ν(C=O), 1596 ν(C=C), 1323 ν(S=O), 1245 ν(C−N), 1211 ν(C−O), 1184 ν(C−N), 1145 ν(C−O), 1033 ν(S−O), 1002 δ(CH_2), 863 δ(CH_2), 790 δ(CH_2), 740 δ(CH_2).

Elemental analysis ($C_{24}H_{29}NO_5S$ M_r = 443.56): Calculated: C = 64.99 %, H = 6.59 %, N = 3.16 %, S = 7.23 %; found: C = 64.83 %, H = 6.72 %, N = 3.45 %, S = 7.14 %.

ESI-MS: Calculated: 443.18 g/mol $[M]^+$; found: 444.1 g/mol $[M+H]^+$.

8.4 Polymer Synthesis

8.4.1 Synthesis of Homopolymers

8.4.1.1 Synthesis of poly(3-((2-(methacryloyloxy)hexyl)dimethylammonio)-propane-1-sulfonate) (P(M1))

Amphiphilic zwitterion **M1** (508.16 mg, 1.5 mmol) and initiator AIBN (1.0 mg, 0.01 mmol, 0.6 mol%) were dissolved in TFE (3 mL).

After deoxygenation by purging with nitrogen for 30 min, the reaction mixture was polymerized at 63 °C for 22 h. After conversion check, a solution of AIBN in TFE (1 mg/mL, 0.4 mL) was added to the reaction mixture, the reaction continued at 63 °C for the following 75 h.

The product was dialyzed against ultra pure water for 4 d using a membrane type ZelluTrans (Roth, Germany) with a MWCO of 3500 g mol^{-1}. The homopolymer was isolated by lyophilization as colorless hygroscopic solids (yield 200 mg, 40%).

Isolated polymers were characterized by ^{1}H NMR, EA, GPC, and FT-IR.

8.4.1.2 Synthesis of poly(3-(dimethyl(2-(*N*-vinylacetamido)ethyl)ammonio)-propane-1-sulfonate) (P(M2))

Zwitterionic vinyl amide **M2** (513.0 mg, 1.8 mmol) was dissolved in ultra pure water (0.33 mL) in a 5 mL round-bottom flask. A solution of initiator V-50 in H_2O (36.21 mg/mL) (0.673 mL, 2 mol%) followed by pyridine (0.75 mL) and MeOH (1.25 mL) was then added to the reaction mixture (pH = 9).

After deoxygenation by purging with nitrogen for 30 min, polymerization started at 60 °C for 22 h.

The product was dialyzed against ultra pure water for 4 d using a membrane type ZelluTrans (Roth, Germany) with a MWCO of 3500 g mol^{-1}. The homopolymer was isolated by lyophilization as a colorless hygroscopic solid (yield 300 mg, 60%).

Isolated polymers were characterized by ^{1}H NMR, EA, and FT-IR.

8.4.1.3 Synthesis of poly(4-(dimethyl(2-(*N*-vinylacetamido)ethyl)ammonio)-butane-1-sulfonate) (P(M3))

Zwitterionic vinyl amide **M3** (503.4 mg, 1.7 mmol) was dissolved in ultra pure water (1.0 mL) in a 5 mL round-bottom flask. A solution of initiator V-50 in H_2O (25.38 mg/mL) (0.365 mL, 2 mol%) followed by pyridine (0.54 mL) and MeOH (0.5 mL) was then added to the reaction mixture (pH = 8).

After deoxygenation by purging with nitrogen for 20 min, polymerization started at 60 °C for 20 h.

The product was diluted with TFE and dialyzed against ultra pure water for 4 d using a membrane type ZelluTrans (Roth, Germany) with a MWCO of 3500 g mol^{-1}. The homopolymer was isolated by lyophilization as a colorless hygroscopic solid (yield 70 mg, 14%).

Isolated polymers were characterized by ^{1}H NMR, EA, and FT-IR.

8.4.1.4 Synthesis of poly(3-(dimethyl(2-(*N*-vinylacetamido)ethyl)ammonio)-propyl sulfate) (P(M4))

Zwitterionic vinyl amide **M4** (504.8 mg, 1.7 mmol) was dissolved in ultra pure water (1.0 mL) in a 5 mL round-bottom flask. A solution of initiator V-50 in H_2O (25.38 mg/mL) (0.363 mL, 2 mol%) followed by pyridine (0.42 mL) and MeOH (0.5 mL) was then added to the reaction mixture (pH = 8).

After deoxygenation by purging with nitrogen for 20 min, polymerization started at 60 °C for 20 h.

The product was diluted with TFE and dialyzed against ultra pure water for 4 d using a membrane type ZelluTrans (Roth, Germany) with a MWCO of 3500 g mol^{-1}. The homopolymer was isolated by lyophilization as a colorless hygroscopic solid (yield 200 mg, 40%).

Isolated polymers were characterized by ^{1}H NMR, EA, and FT-IR.

8.4.2 Synthesis of SPE-BMA-BPEMA Copolymers

The predefined amounts of zwitterionic SPE, hydrophobic BMA, photo-crosslinker BPEMA, and initiator AIBN, 0.5 mol% were dissolved in TFE. After deoxygenation by purging with nitrogen for 30 min, the reaction mixtures were polymerized at 63 °C for 20 h. The products were dialyzed against ultra pure water for 4 d using a membrane type ZelluTrans (Roth, Germany) with a MWCO of 3500 g mol^{-1}. The copolymers were isolated by lyophilization as colorless hygroscopic solids.

Isolated polymers were characterized by ^{1}H NMR, TGA, EA, DSC, GPC, UV-Vis spectroscopy, and FT-IR.

8.4.2.1 Synthesis of poly($\mathbf{SPE_{90}}$-*co*-$\mathbf{BMA_{10}}$-*co*-$\mathbf{BPEMA_1}$) (P($\mathbf{SPE_{90}}$-$\mathbf{BMA_{10}}$))

Amounts engaged of SPE (5.028 g, 18 mmol), BMA (285 mg, 2 mmol), BPEMA (62.3 mg, 0.2 mmol), AIBN (16.6 mg, 0.1 mmol, 0.5 mol%), TFE (21.5 g). Yield 3.39 g (63%).

FT-IR (selected bands in cm^{-1}): 2979, 2902 ν(CH_3, CH_2), 1722 ν(C=O), 1402 δ(CH_3), 1047 ν_s(SO_3^-).

Elemental analysis: Calculated C = 48.69 %, H = 7.63 %, N = 4.69 %, S = 10.73 %; ratio C/N = 10.4; ratio C/S = 4.54 (for dry copolymer assuming no compositional drift). Found: C = 42.62 %, H = 7.58 %, N = 3.96 %, S = 9.40 %; ratio C/N = 10.8; ratio C/S = 4.53 (for dry copolymer assuming no compositional drift). Under the assumption that the molar ratio of hydrophobic monomers BMA/BPEMA of 10:1 in the feed is preserved in the copolymers, a composition of 88 mol% of SPE, 10.9 mol% of BMA, and 1.1 mol% of BPEMA is calculated, with a water content of 1.6 H_2O molecules per SPE repeat unit.

8.4.2.2 Synthesis of poly($\mathbf{SPE_{70}}$-*co*-$\mathbf{BMA_{30}}$-*co*-$\mathbf{BPEMA_1}$) (P($\mathbf{SPE_{70}}$-$\mathbf{BMA_{30}}$))

Amounts engaged of SPE (3.909 g, 14 mmol), BMA (850 mg, 6 mmol), BPEMA (62.6 mg, 0.2 mmol), AIBN (16.5 mg, 0.1 mmol, 0.5 mol%), TFE (19.45 g). Yield 3.56 g (74%).

FT-IR (selected bands in cm^{-1}): 2979, 2902 $\nu(CH_3, CH_2)$, 1722 $\nu(C{=}O)$, 1402 $\delta(CH_3)$, 1039 $\nu_s(SO_3^-)$.

Elemental analysis: Calculated C = 51.24 %, H = 7.92 %, N = 4.07 %, S = 9.29 %; ratio C/N = 12.6; ratio C/S = 5.52 (for dry copolymer assuming no compositional drift). Found: C = 45.81 %, H = 7.85 %, N = 3.49 %, S = 8.22 %; ratio C/N = 13.1; ratio C/S = 5.53 (for dry copolymer assuming no compositional drift). Under the assumption that the molar ratio of hydrophobic monomers BMA/BPEMA of 30:1 in the feed is preserved in the copolymers, a composition of 72 mol% of SPE, 27.1 mol% of BMA, and 0.9 mol% of BPEMA is calculated, with a water content of 1.4 H_2O molecules per SPE repeat unit.

8.4.2.3 Synthesis of poly(SPE$_{50}$-*co*-BMA$_{50}$-*co*-BPEMA$_1$) (P(SPE$_{50}$-BMA$_{50}$))

Amounts engaged of SPE (2.794 g, 10 mmol), BMA (1.424 g, 10 mmol), BPEMA (62.3 mg, 0.2 mmol), AIBN (16.3 mg, 0.1 mmol, 0.5 mol%), TFE (17.24 g). Yield 3.61 g (84%).

FT-IR (selected bands in cm^{-1}): 2979, 2904 $\nu(CH_3, CH_2)$, 1722 $\nu(C{=}O)$, 1400 $\delta(CH_3)$, 1039 $\nu_s(SO_3^-)$.

Elemental analysis: Calculated C = 54.44 %, H = 8.28 %, N = 3.28 %, S = 7.49 %; ratio C/N = 16.6; ratio C/S = 7.27 (for dry copolymer assuming no compositional drift). Found: C = 50.23 %, H = 8.19 %, N = 2.81 %, S = 6.59 %; ratio C/N = 17.9; ratio C/S = 7.62. Under the assumption that the molar ratio of hydrophobic monomers BMA/BPEMA of 50:1 in the feed is preserved in the copolymers, a composition of 53 mol% of SPE, 46.1 mol% of BMA, and 0.9 mol% of BPEMA is calculated, with a water content of 1.2 H_2O molecules per SPE repeat unit.

8.4.3 Synthesis of SPE-M1-BPEMA Copolymers

The predefined amounts of zwitterionic SPE, amphiphilic zwitterion **M1**, photocrosslinker BPEMA, and initiator AIBN, 1 mol% were dissolved in TFE. After deoxygenation by purging with nitrogen for 30 min, the reaction mixtures were polymerized at 65 °C for 20 h. The products were dialyzed against a solution (MeOH:H_2O) [1:1] (v:v) for 4 d using a membrane type ZelluTrans (Roth, Germany) with a MWCO of 3500 g mol^{-1}. The copolymers were isolated by lyophilization as colorless hygroscopic solids.

Isolated polymers were characterized by ^{1}H NMR, EA, GPC, UV-Vis spectroscopy, and FT-IR.

8.4.3.1 Synthesis of poly(SPE$_{90}$-*co*-M1$_{10}$-*co*-BPEMA$_1$) (P(SPE$_{90}$-M1$_{10}$))

Amounts engaged of SPE (2.543 g, 9 mmol), **M1** (343.62 mg, 1 mmol), BPEMA (31.0 mg, 0.1 mmol), AIBN (8.3 mg, 0.1 mmol, 1 mol%), TFE (5.49 mL). Yield 1.33 g (46%).

FT-IR (selected bands in cm^{-1}): 2960, 1722 $\nu(C{=}O)$, 1477 $\delta(CH_3)$, 1168 $\nu(C{-}O)$, 1037 $\nu_s(SO_3^-)$.

Elemental analysis: Calculated C = 48.34 %, H = 7.64 %, N = 4.87 %, S = 11.12 %; ratio C/N = 9.93; ratio C/S = 4.35 (for dry copolymer assuming

no compositional drift). Found: C = 43.50 %, H = 7.75 %, N = 4.31 %, S = 9.97 %; ratio C/N = 10.09; ratio C/S = 4.36 (for dry copolymer assuming no compositional drift). Under the assumption that the molar ratio of hydrophobic monomers **M1**/BPEMA of 10:1 in the feed is preserved in the copolymers, a composition of 87.5 mol% of SPE, 11.7 mol% of BMA, and 0.8 mol% of BPEMA is calculated, with a water content of 1.4 H_2O molecules per zwitterionic repeat unit.

8.4.3.2 Synthesis of poly(SPE_{70}-*co*-$M1_{30}$-*co*-$BPEMA_1$) (P(SPE_{70}-$M1_{30}$))

Amounts engaged of SPE (1.961 g, 7 mmol), **M1** (1.009 g, 3 mmol), BPEMA (31.0 mg, 0.1 mmol), AIBN (8.3 mg, 0.1 mmol, 1 mol%), TFE (5.83 mL). Yield 0.730 g (25%).

FT-IR (selected bands in cm^{-1}): 2964, 1720 ν(C=O), 1479 $\delta(CH_3)$, 1169 ν(C−O), 1036 $\nu_s(SO_3^-)$.

Elemental analysis: Calculated C = 49.74 %, H = 7.89 %, N = 4.68 %, S = 10.71 %; ratio C/N = 10.62; ratio C/S = 4.65 (for dry copolymer assuming no compositional drift). Found: C = 44.49 %, H = 7.92 %, N = 4.96 %, S = 9.57 %; ratio C/N = 8.97; ratio C/S = 4.65 (for dry copolymer assuming no compositional drift). Under the assumption that the molar ratio of hydrophobic monomers **M1**/BPEMA of 30:1 in the feed is preserved in the copolymers, a composition of 68.2 mol% of SPE, 31.0 mol% of BMA, and 0.8 mol% of BPEMA is calculated, with a water content of 1.4 H_2O molecules per zwitterionic repeat unit.

8.4.3.3 Synthesis of poly(SPE_{50}-*co*-$M1_{50}$-*co*-$BPEMA_1$) (P(SPE_{50}-$M1_{50}$))

Amounts engaged of SPE (1.405 g, 5 mmol), **M1** (1.679 g, 5 mmol), BPEMA (31.0 mg, 0.1 mmol), AIBN (8.3 mg, 0.1 mmol, 1 mol%), TFE (6.16 mL). Yield 0.430 g (15%).

FT-IR (selected bands in cm^{-1}): 2962, 1720 ν(C=O), 1477 $\delta(CH_3)$, 1168 ν(C−O), 1036 $\nu_s(SO_3^-)$.

Elemental analysis: Calculated C = 51.04 %, H = 8.12 %, N = 4.51 %, S = 10.32 %; ratio C/N = 11.31; ratio C/S = 4.95 (for dry copolymer assuming no compositional drift). Found: C = 41.43 %, H = 7.42 %, N = 4.47 %, S = 8.49 %; ratio C/N = 9.27; ratio C/S = 4.88 (for dry copolymer assuming no compositional drift). Under the assumption that the molar ratio of hydrophobic monomers **M1**/BPEMA of 50:1 in the feed is preserved in the copolymers, a composition of 52.8 mol% of SPE, 46.4 mol% of BMA, and 0.8 mol% of BPEMA is calculated, with a water content of 1.5 H_2O molecules per zwitterionic repeat unit.

8.4.4 Synthesis of Vinyl Amide Copolymers

8.4.4.1 Synthesis of P(M2-*co*-M5)

Zwitterionic vinyl amide **M2** (1.67 g, 6 mmol) was dissolved in ultra pure water (3.06 mL) in a 10 mL round-bottom flask. A solution of vinyl amide crosslinker **M5** in a mixture of (MeOH:H_2O) [9:2] (v:v) (21.08 mg/mL) (3.4 mL) was then

added. A solution of initiator V-50 in H_2O (144.23 mg/mL) (0.237 mL, 2 mol%) followed by pyridine (0.9 mL) and extra MeOH (1.0 mL) was then added to the reaction mixture (pH = 8).

After deoxygenation by purging with nitrogen for 20 min, polymerization started at 60 °C for 22 h. After conversion check, additional initiator V-50 (52.56 mg, 0.2 mmol, 3 mol%) was added and the polymerization continued at 60 °C for 24 h.

The product was dialyzed against ultra pure water for 4 d using a membrane type ZelluTrans (Roth, Germany) with a MWCO of 3500 g mol^{-1}. The copolymer was isolated by lyophilization as a colorless hygroscopic solid (yield 880 mg, 50%).

Isolated polymers were characterized by ^{1}H NMR, EA, GPC, UV-Vis spectroscopy, and FT-IR.

8.4.4.2 Synthesis of P(M3-*co*-M5)

Zwitterionic vinyl amide **M3** (1.68 g, 5.7 mmol) was dissolved in ultra pure water (3.08 mL) in a 10 mL round-bottom flask. A solution of vinyl amide crosslinker **M5** in a mixture of (MeOH:H_2O) [9:2] (v:v) (21.08 mg/mL) (3.4 mL) was then added. A solution of initiator V-50 in H_2O (144.23 mg/mL) (0.225 mL, 2 mol%) followed by pyridine (0.9 mL) and extra MeOH (1.5 mL) was then added to the reaction mixture (pH = 8).

After deoxygenation by purging with nitrogen for 20 min, polymerization started at 60 °C for 22 h. After conversion check, additional initiator V-50 (52.56 mg, 0.2 mmol, 3 mol%) was added and the polymerization continued at 60 °C for 24 h.

The reaction solvents were removed by rotary evaporation and the product was dissolved in TFE. The polymer was then precipitated by dropwise addition of the solution in TFE into MeOH. After collecting the precipitate by centrifugation, the product was dissolved in TFE and dialyzed against ultra pure water for 4 d using a membrane type ZelluTrans (Roth, Germany) with a MWCO of 3500 g mol^{-1}. The copolymer was isolated by lyophilization as a colorless hygroscopic solid (yield 250 mg, 14%).

Isolated polymers were characterized by ^{1}H NMR, EA, GPC, UV-Vis spectroscopy, and FT-IR.

8.4.4.3 Synthesis of P(M4-*co*-M5)

Zwitterionic vinyl amide **M4** (1.69 g, 5.8 mmol) was dissolved in ultra pure water (3.08 mL) in a 10 mL round-bottom flask. A solution of vinyl amide crosslinker **M5** in a mixture of (MeOH:H_2O) [9:2] (v:v) (21.08 mg/mL) (3.43 mL) was then added. A solution of initiator V-50 in H_2O (144.23 mg/mL) (0.227 mL, 2 mol%) followed by pyridine (0.9 mL) and extra MeOH (0.5 mL) was then added to the reaction mixture (pH = 8).

After deoxygenation by purging with nitrogen for 20 min, polymerization started at 60 °C for 22 h. After conversion check, additional initiator V-50 (52.56 mg, 0.2 mmol, 3 mol%) was added and the polymerization continued at 60 °C for 24 h.

The reaction solvents were removed by rotary evaporation and the product was dissolved in TFE. The polymer was then precipitated by dropwise addition

of the solution in TFE into MeOH. After collecting the precipitate by centrifugation, the product was dissolved in TFE and dialyzed against ultra pure water for 4 d using a membrane type ZelluTrans (Roth, Germany) with a MWCO of 3500 g mol^{-1}. The copolymer was isolated by lyophilization as a colorless hygroscopic solid (yield 800 mg, 45%).

Isolated polymers were characterized by ^{1}H NMR, EA, GPC, UV-Vis spectroscopy, and FT-IR.

Appendix A

Supporting Information

A.1 ^{1}H NMR-Spectra

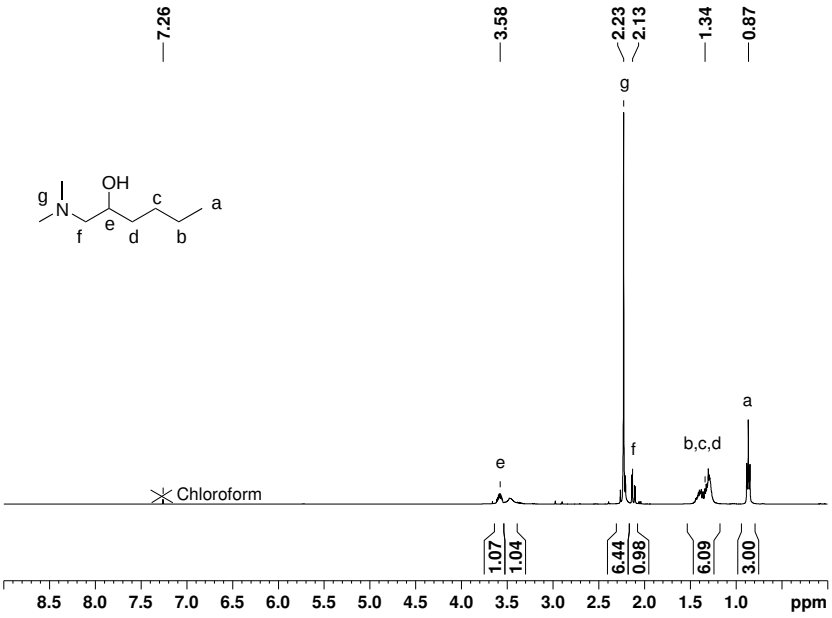

Figure A.1: ^{1}H NMR spectrum of intermediate **I-1** in $CDCl_3$.

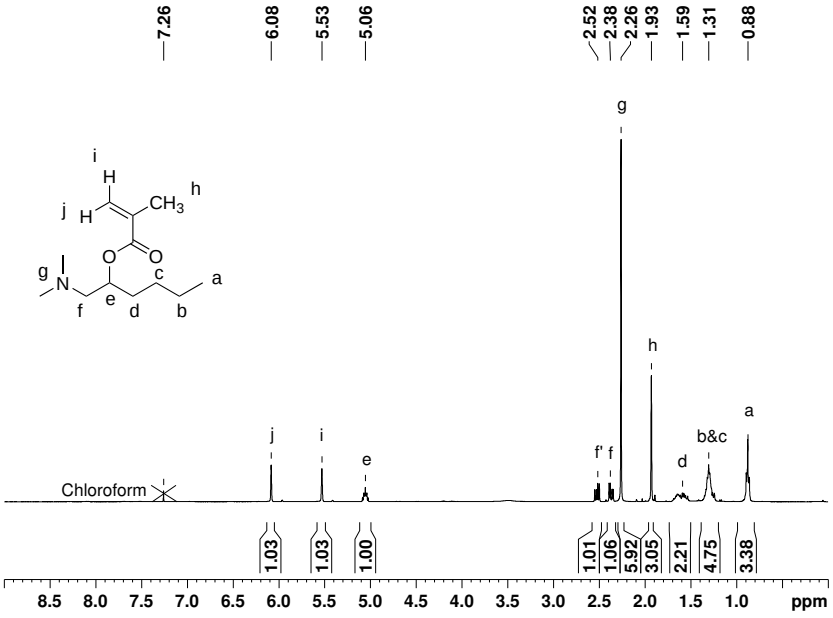

Figure A.2: ^{1}H NMR spectrum of intermediate **I-2** in $CDCl_3$.

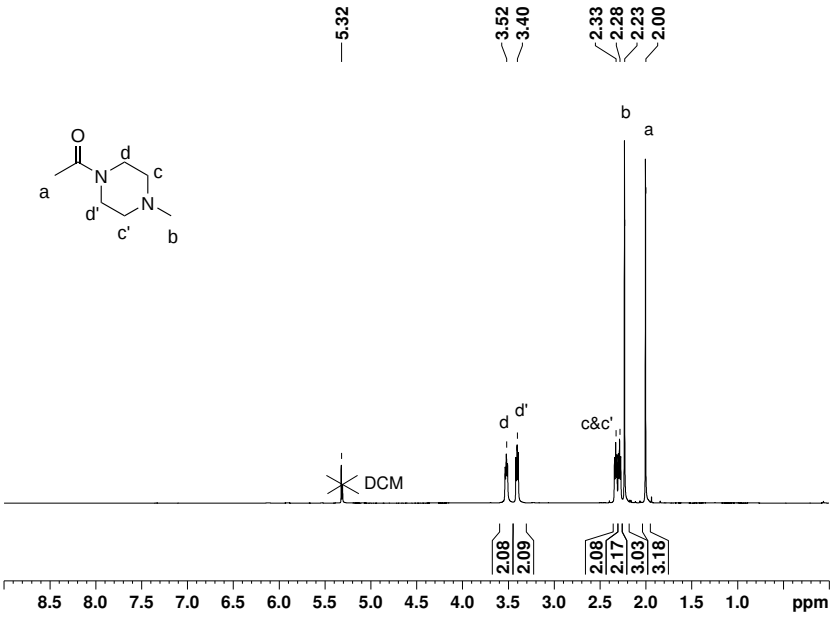

Figure A.3: ^{1}H NMR spectrum of intermediate **I-3** in CD_2Cl_2.

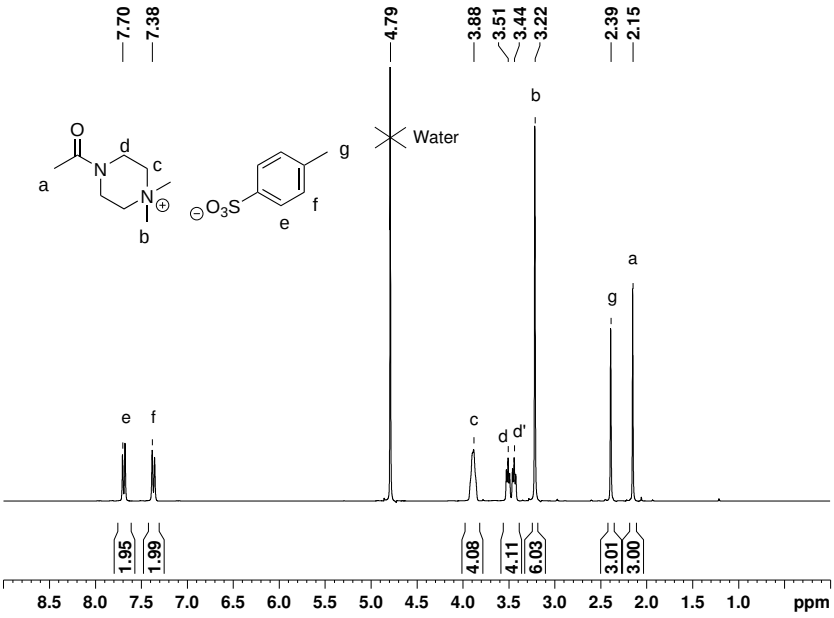

Figure A.4: ^{1}H NMR spectrum of intermediate **I-4** in D_2O.

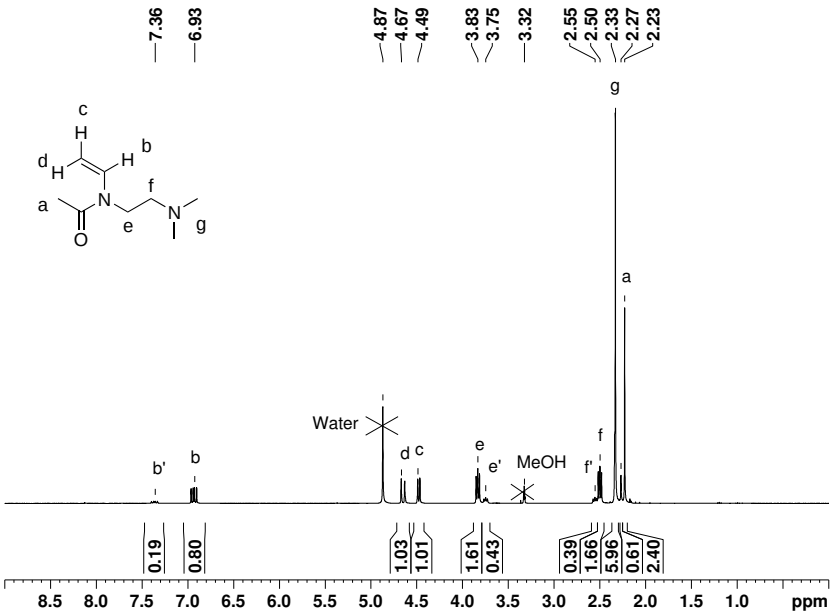

Figure A.5: ^{1}H NMR spectrum of vinyl amide **I-5** in CD_3OD.

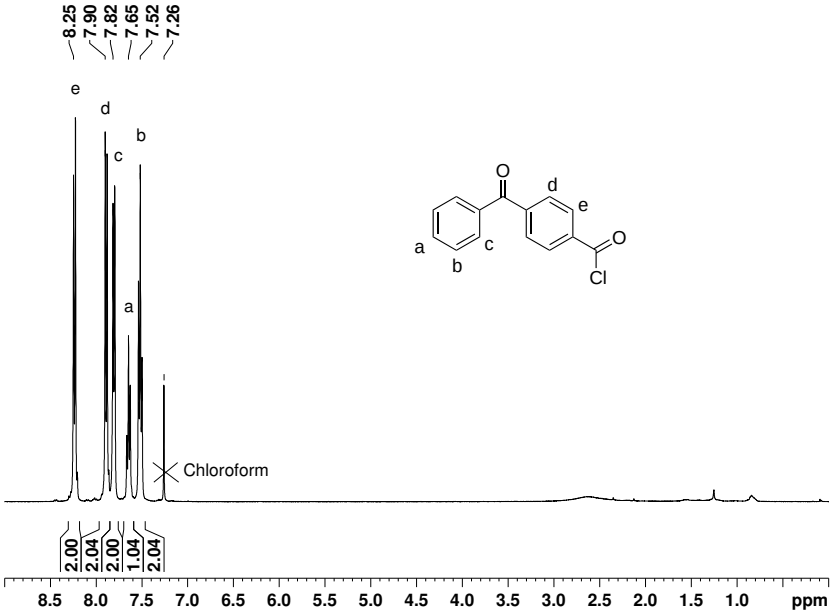

Figure A.6: ^{1}H NMR spectrum of intermediate **I-6** in $CDCl_3$.

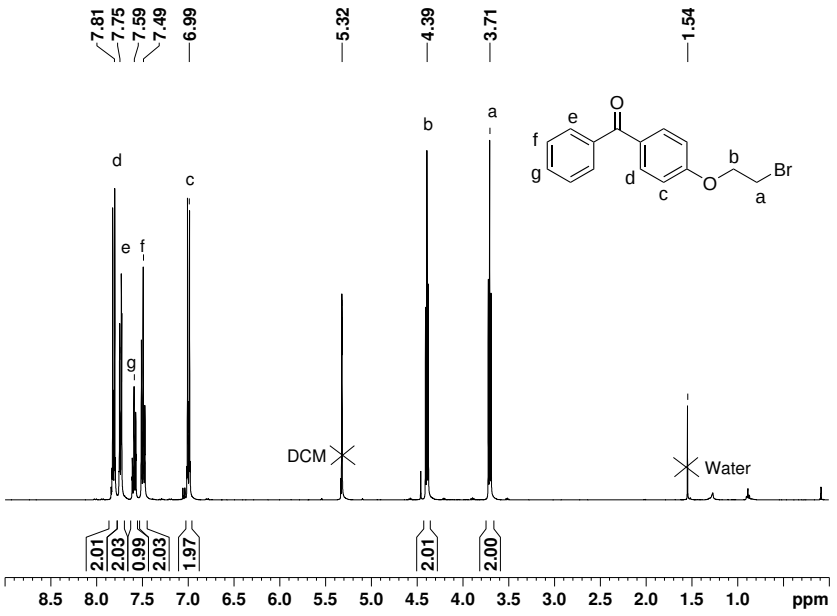

Figure A.7: ^{1}H NMR spectrum of intermediate **I-7** in CD_2Cl_2.

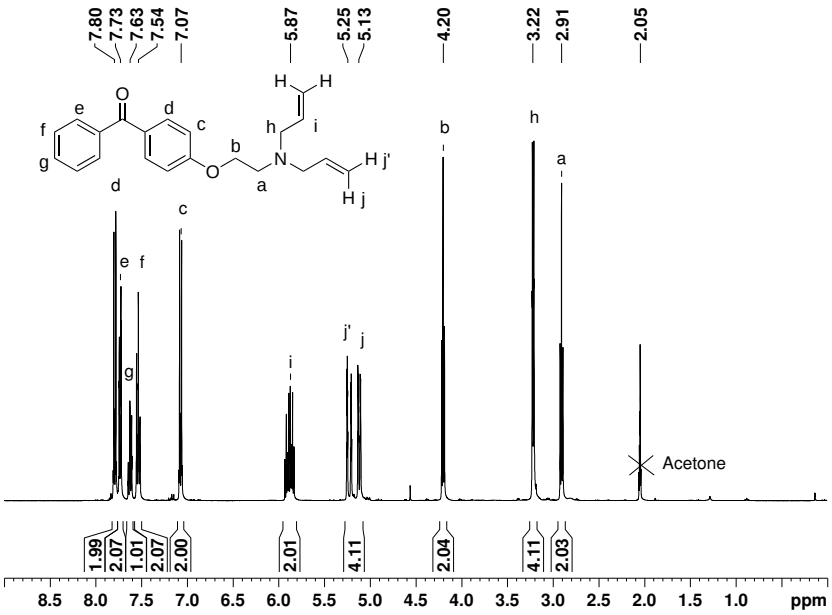

Figure A.8: ^{1}H NMR spectrum of intermediate **I-8** in $(CD_3)_2CO$.

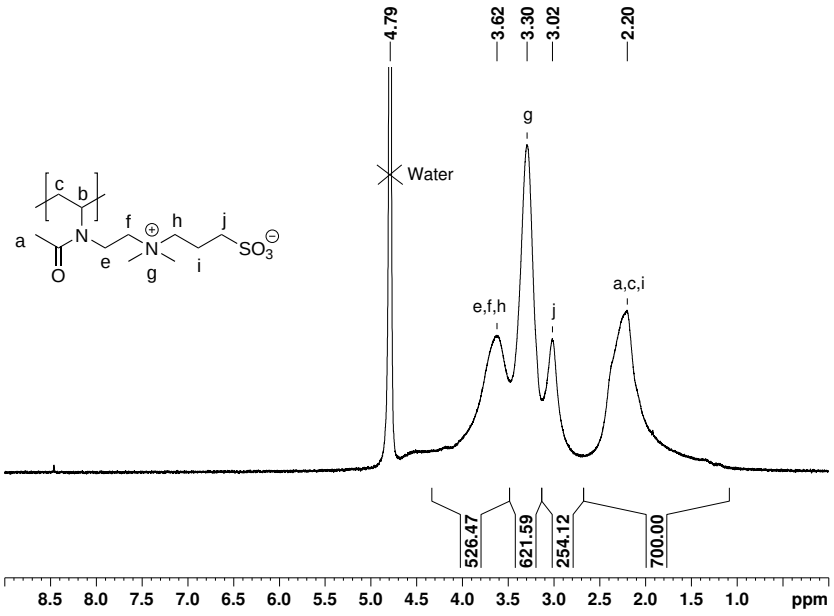

Figure A.9: ^{1}H NMR spectrum of homopolymer **P(M2)** in D_2O.

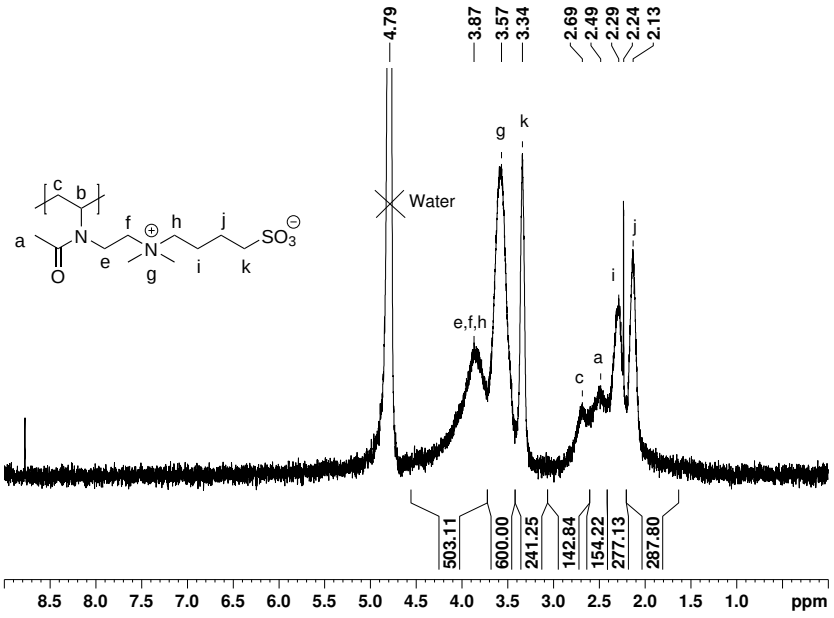

Figure A.10: ^{1}H NMR spectrum of homopolymer **P(M3)** in a saturated solution of NaCl in D_2O.

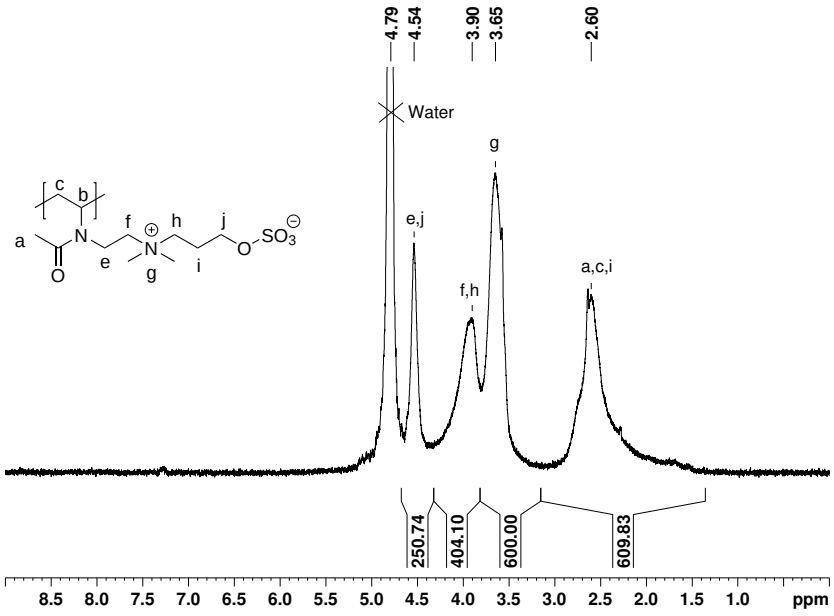

Figure A.11: ^{1}H NMR spectrum of homopolymer **P(M4)** in a saturated solution of NaCl in D_2O.

A.2 ^{1}H-^{1}H-COSY NMR-Spectra

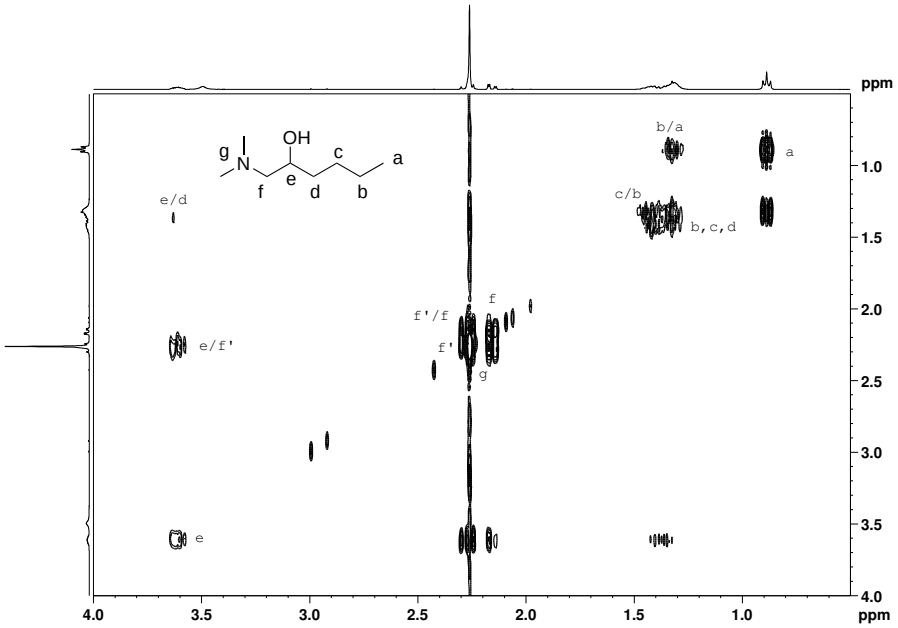

Figure A.12: ^{1}H-^{1}H-COSY NMR spectrum of intermediate **I-1** in $CDCl_3$.

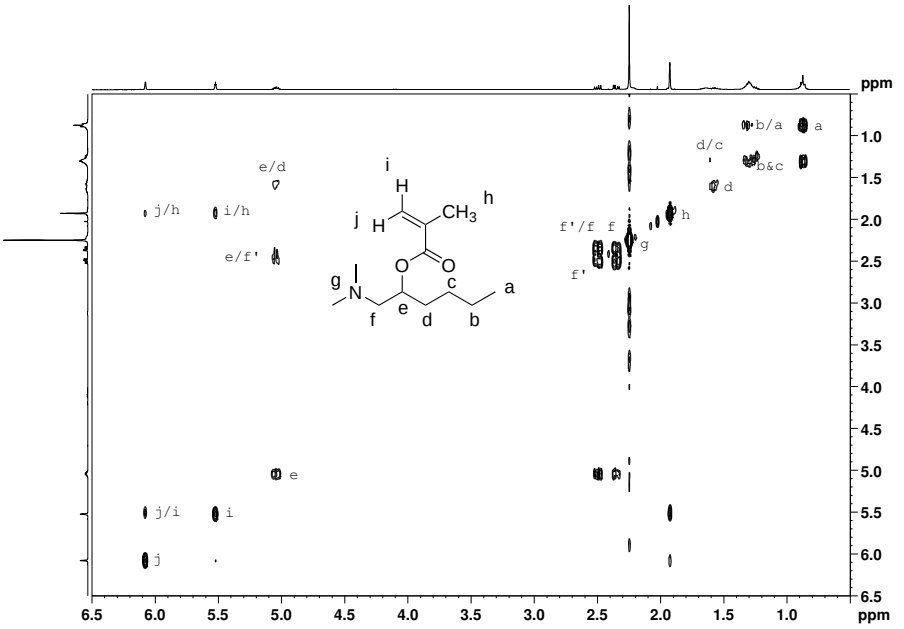

Figure A.13: ^{1}H-^{1}H-COSY NMR spectrum of intermediate **I-2** in $CDCl_3$.

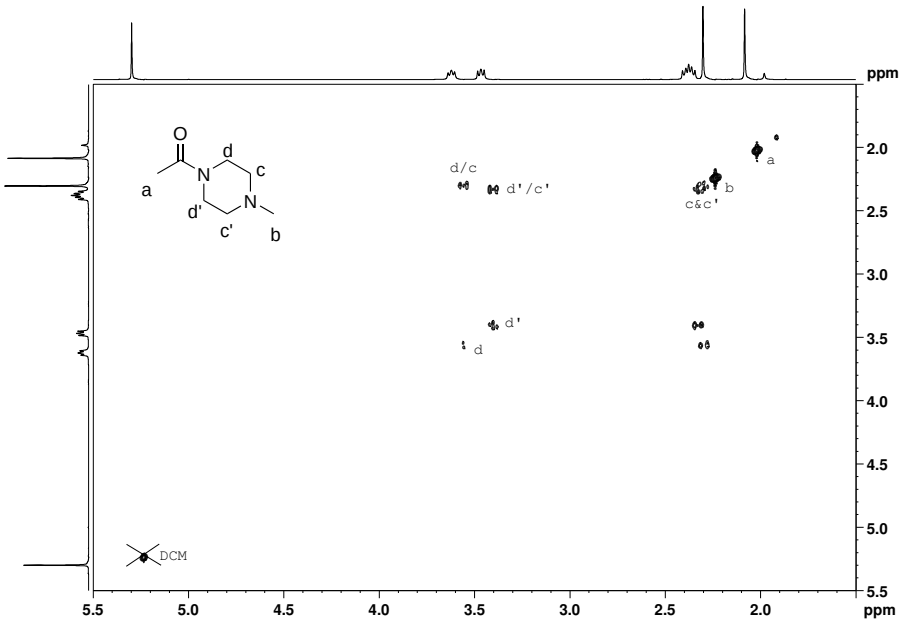

Figure A.14: ^{1}H-^{1}H-COSY NMR spectrum of intermediate **I-3** in CD_2Cl_2.

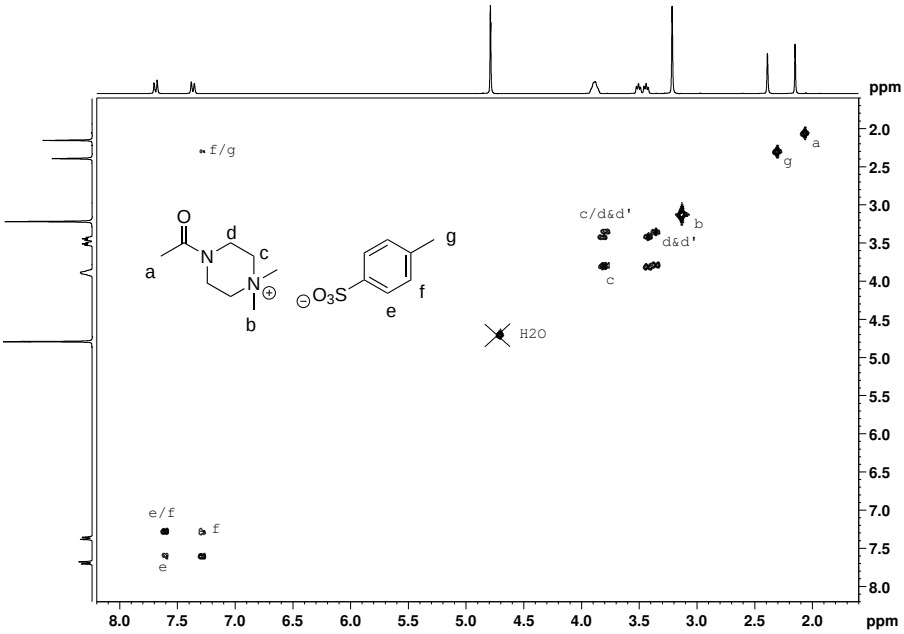

Figure A.15: ^{1}H-^{1}H-COSY NMR spectrum of intermediate **I-4** in D_2O.

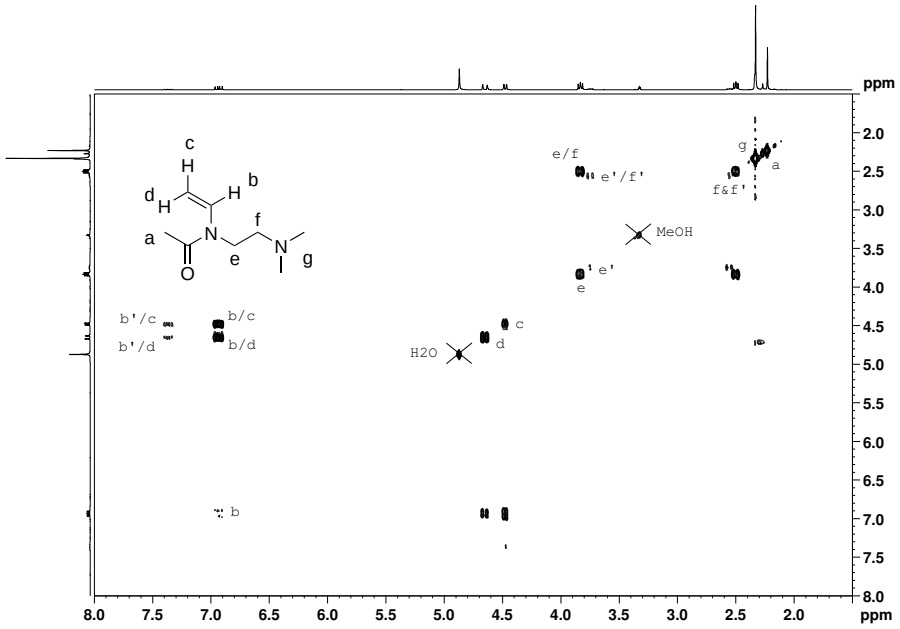

Figure A.16: ^{1}H-^{1}H-COSY NMR spectrum of vinyl amide **I-5** in CD_3OD.

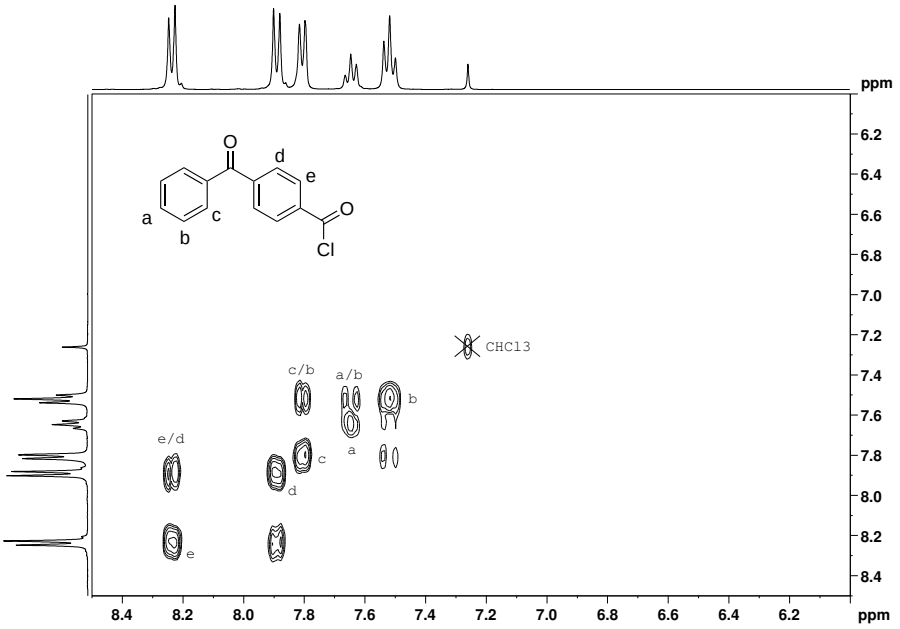

Figure A.17: ^{1}H-^{1}H-COSY NMR spectrum of intermediate **I-6** in $CDCl_3$.

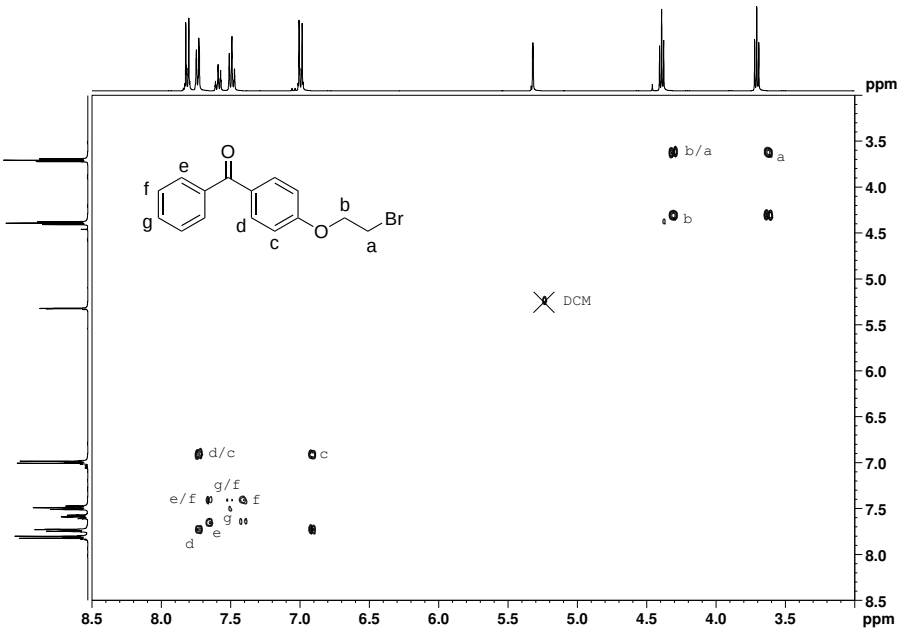

Figure A.18: ^{1}H-^{1}H-COSY NMR spectrum of intermediate **I-7** in CD_2Cl_2.

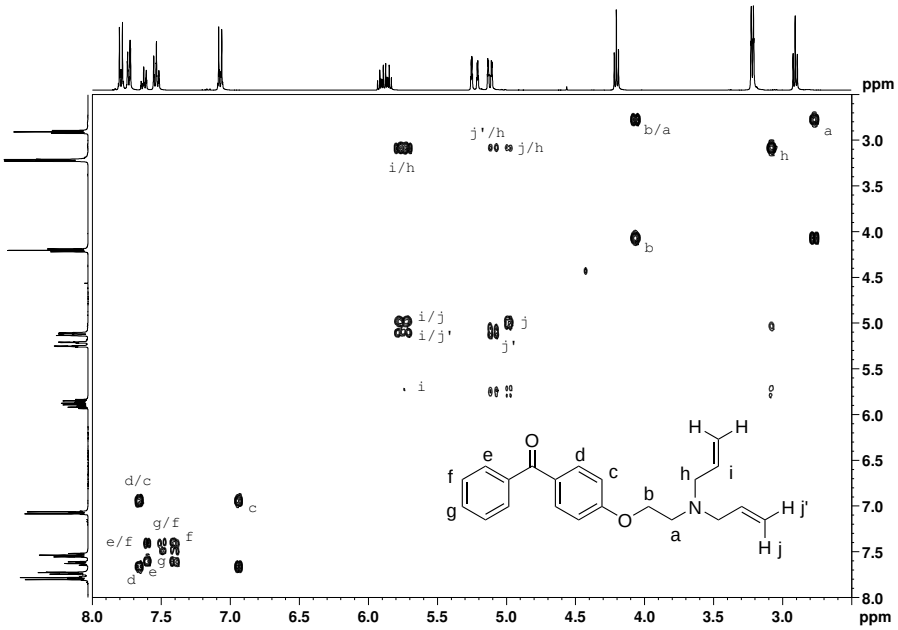

Figure A.19: ^{1}H-^{1}H-COSY NMR spectrum of intermediate **I-8** in $(CD_3)_2CO$.

A.3 ^{13}C NMR-Spectra

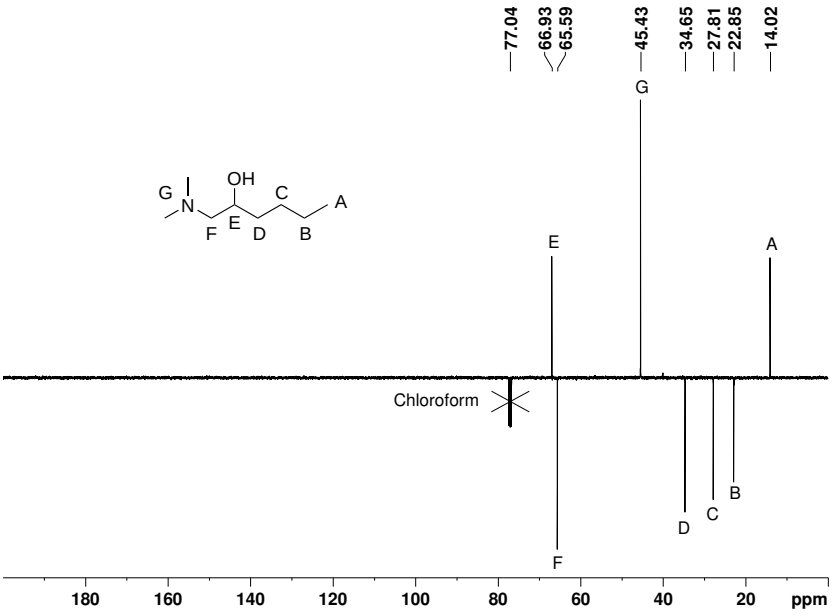

Figure A.20: ^{13}C (APT) NMR spectrum of intermediate **I-1** in $CDCl_3$.

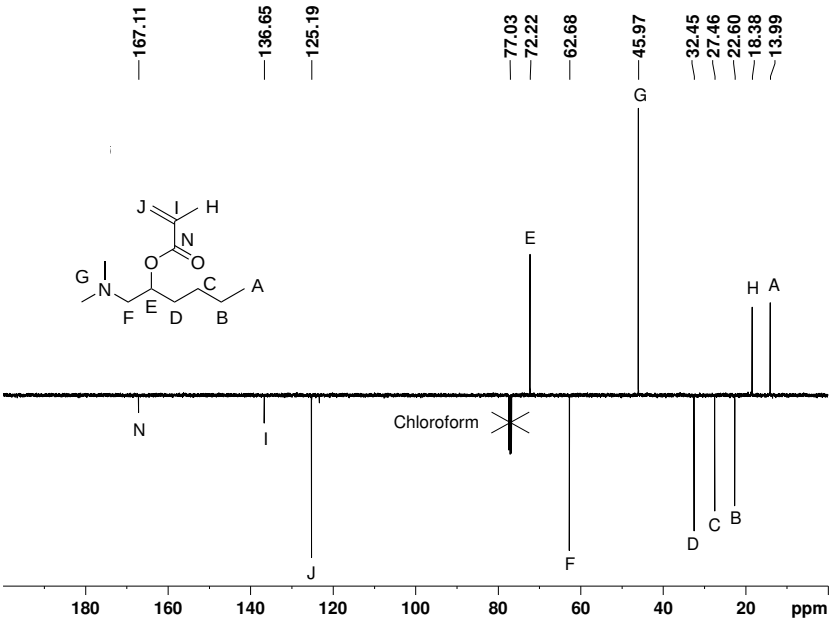

Figure A.21: ^{13}C (APT) NMR spectrum of intermediate **I-2** in $CDCl_3$.

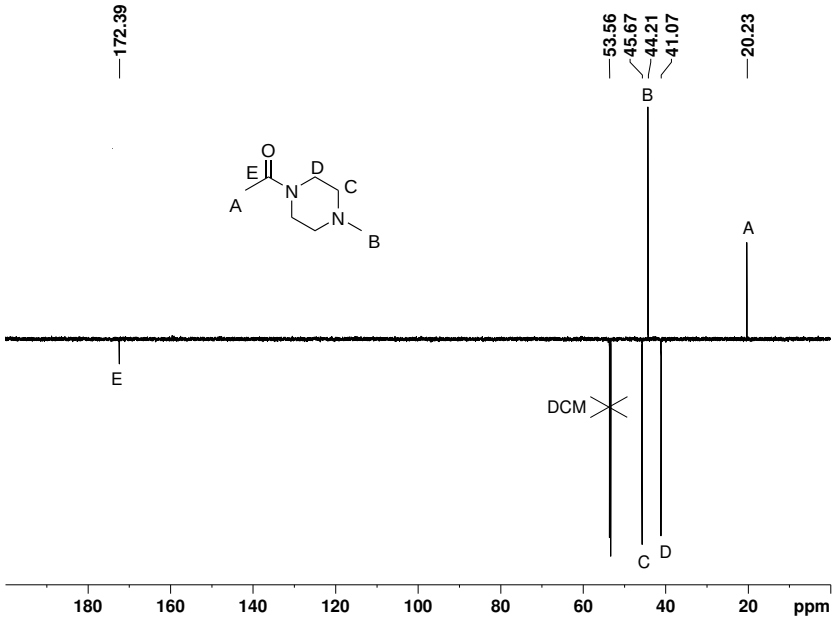

Figure A.22: ^{13}C (APT) NMR spectrum of intermediate **I-3** in D_2O.

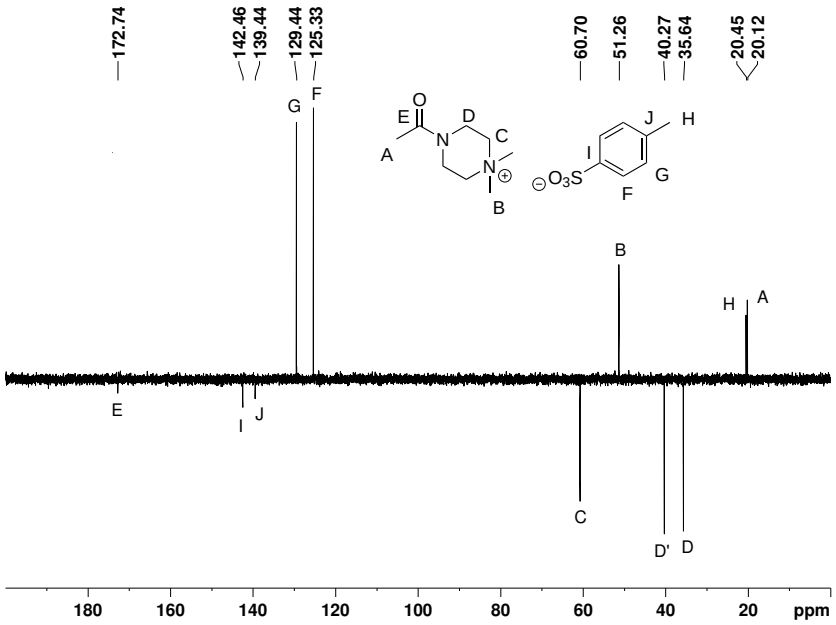

Figure A.23: ^{13}C (APT) NMR spectrum of intermediate **I-4** in D_2O.

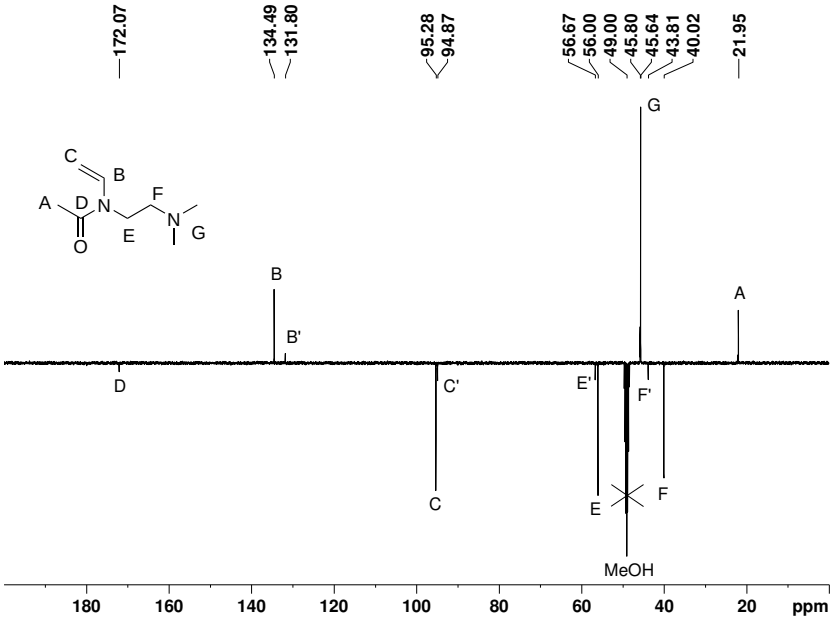

Figure A.24: ^{13}C (APT) NMR spectrum of vinyl amide **I-5** in CD_3OD.

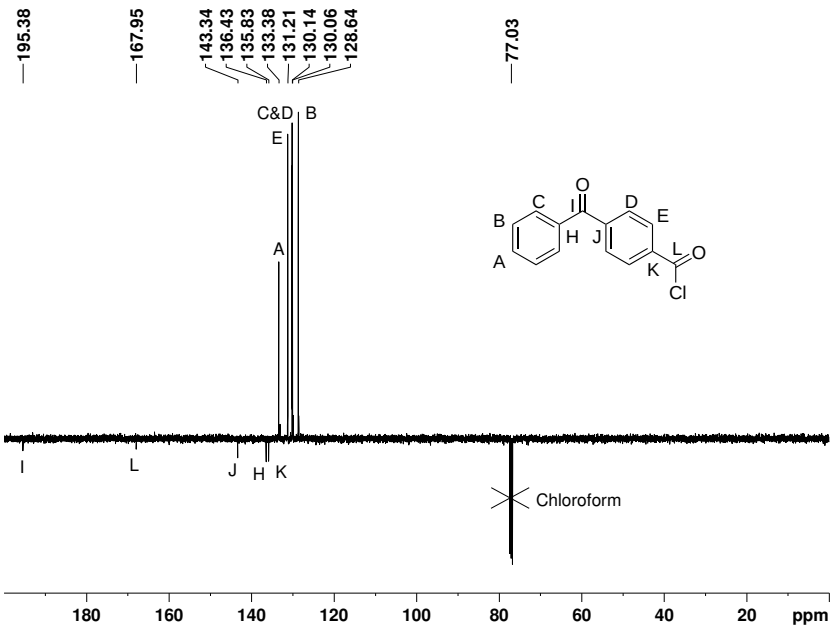

Figure A.25: ^{13}C (APT) NMR spectrum of intermediate **I-6** in $CDCl_3$.

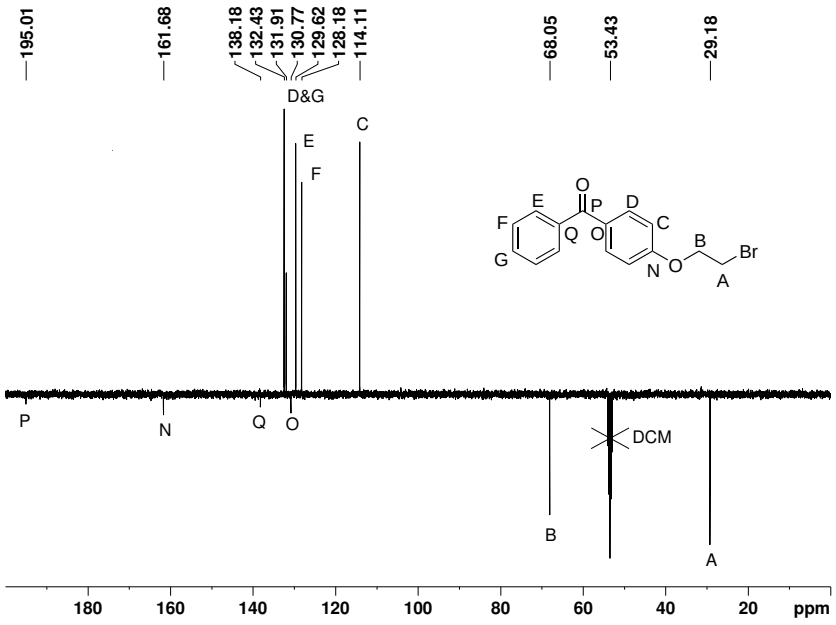

Figure A.26: ^{13}C (APT) NMR spectrum of intermediate **I-7** in CD_2Cl_2.

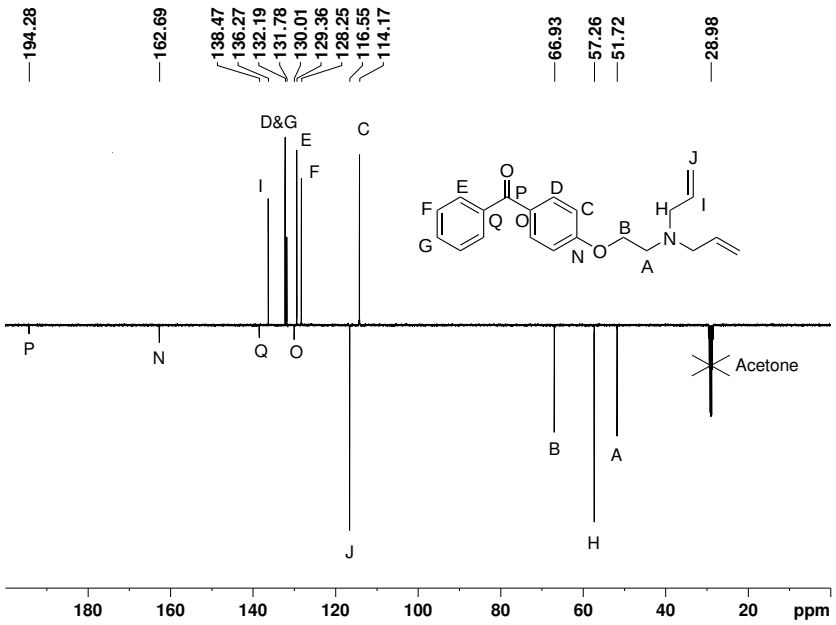

Figure A.27: ^{13}C (APT) NMR spectrum of intermediate **I-8** in $(CD_3)_2CO$.

A.4 ATR-FTIR-Spectra

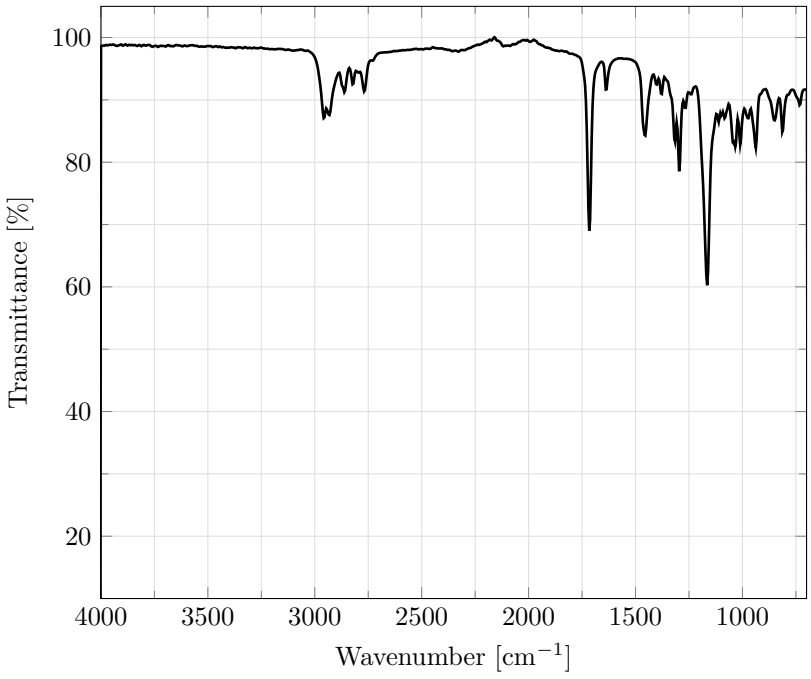

Figure A.28: FT-IR spectrum of intermediate **I-2**.

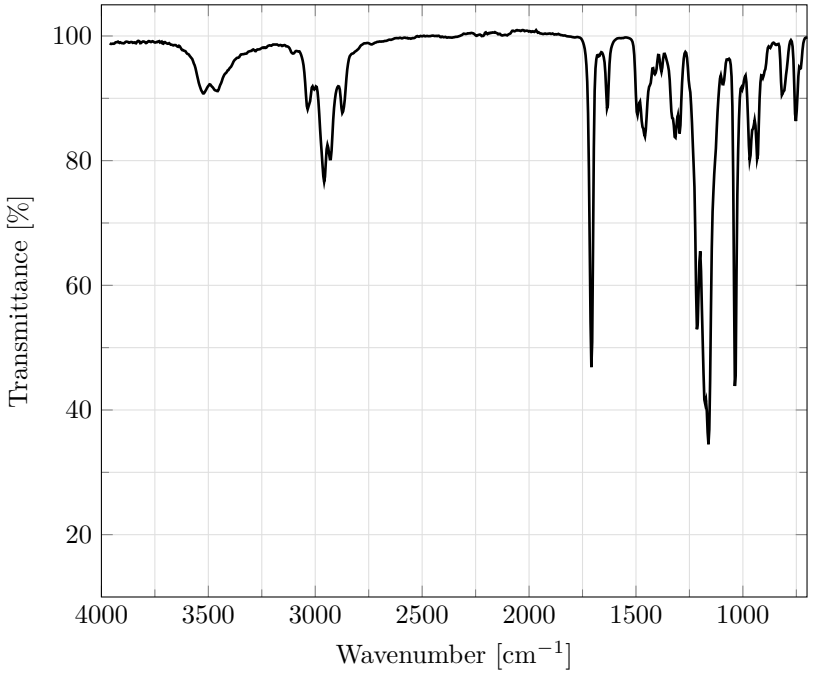

Figure A.29: FT-IR spectrum of amphiphilic monomer **M1**.

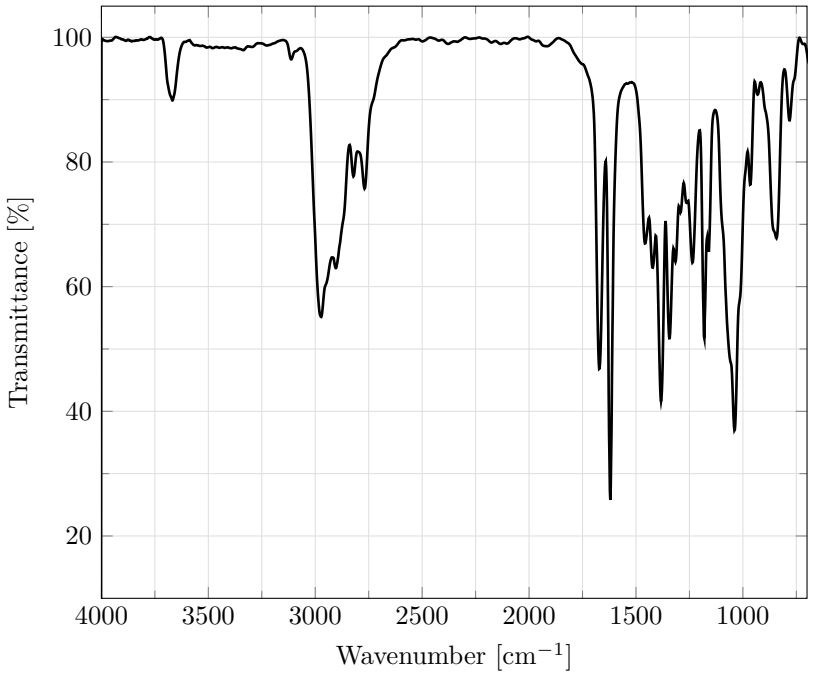

Figure A.30: FT-IR spectrum of vinyl amide **I-5**.

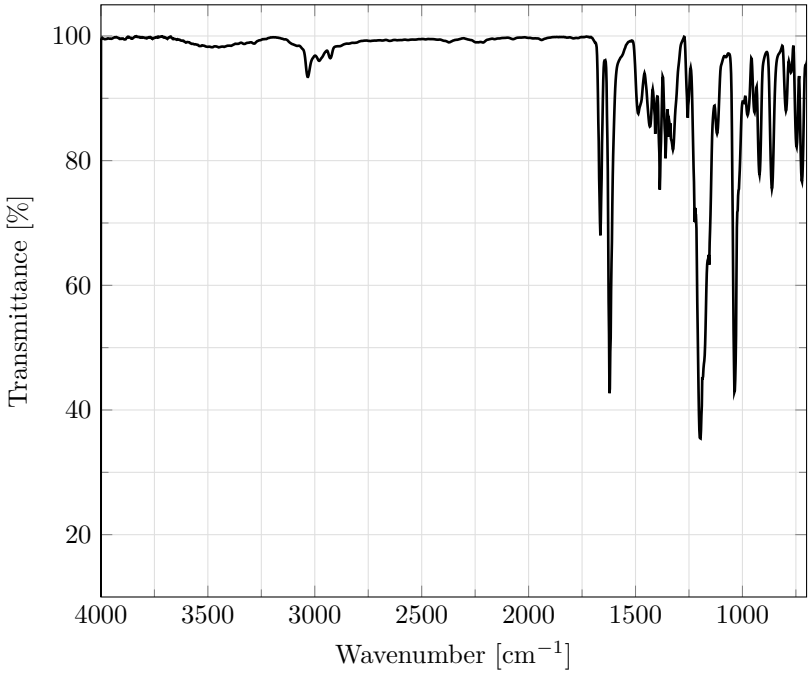

Figure A.31: FT-IR spectrum of monomer **M2**.

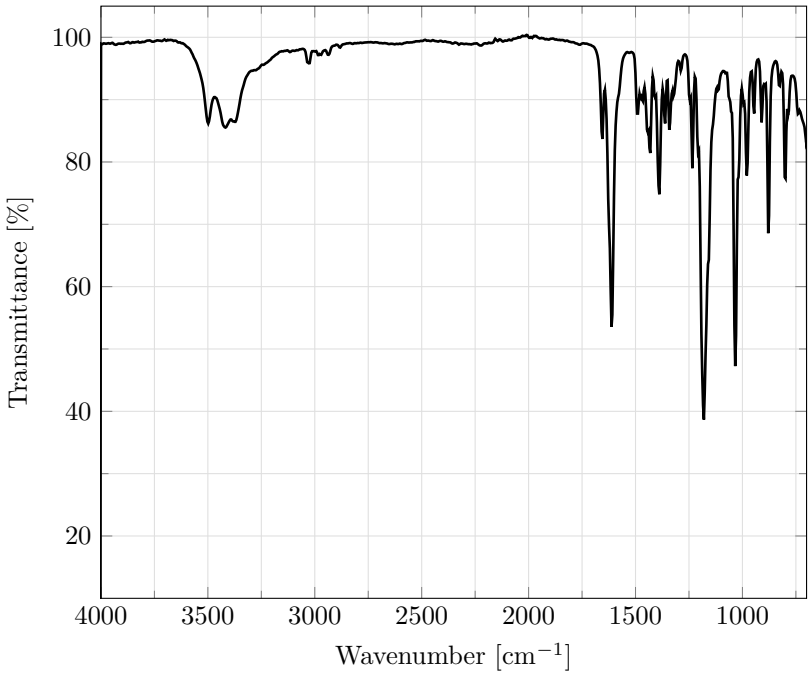

Figure A.32: FT-IR spectrum of monomer **M3**.

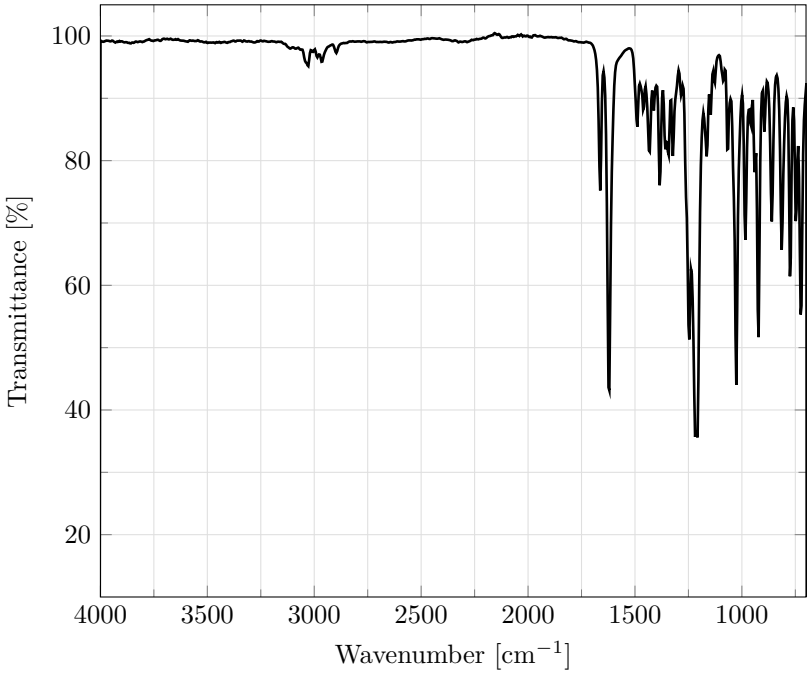

Figure A.33: FT-IR spectrum of monomer **M4**.

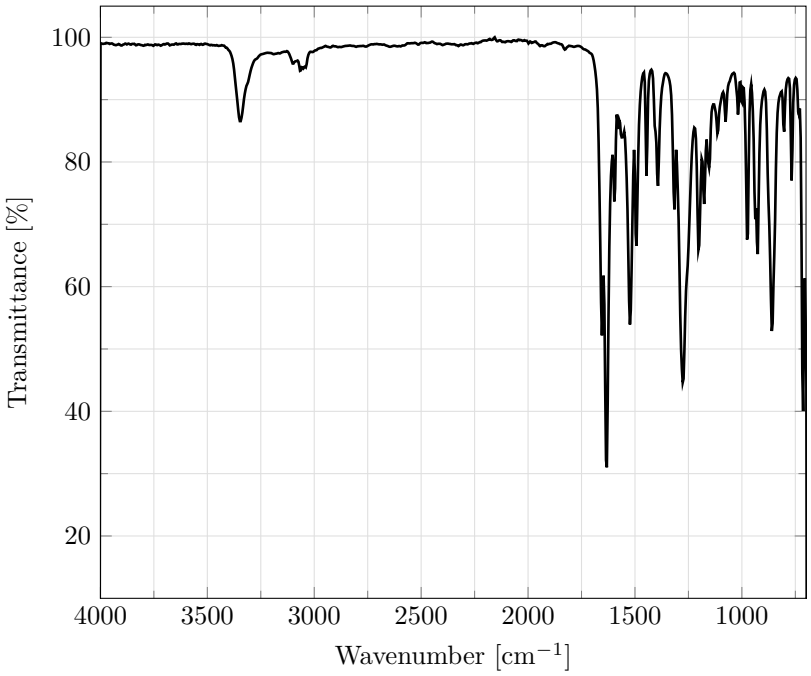

Figure A.34: FT-IR spectrum of photo-crosslinker **M5**.

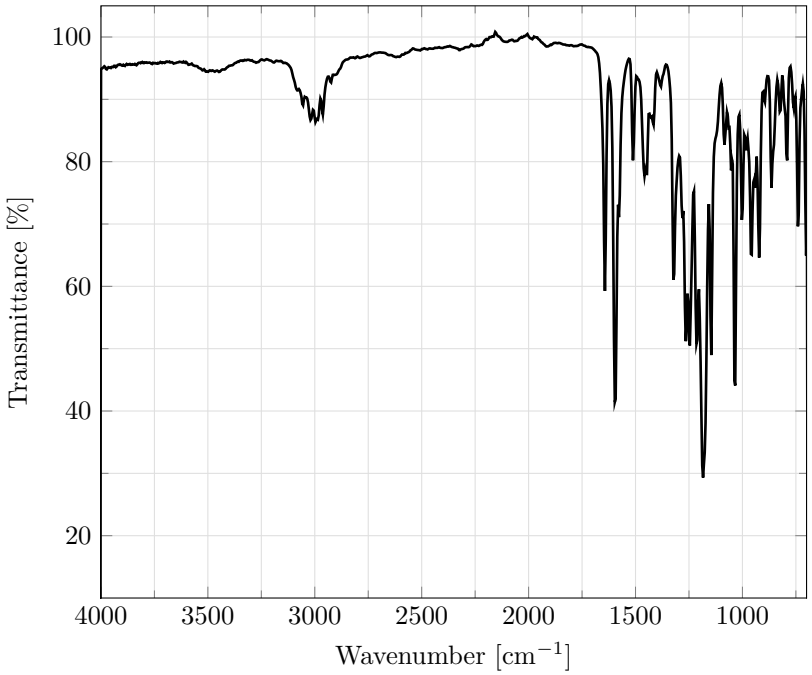

Figure A.35: FT-IR spectrum of quaternized diallylamine photo-crosslinker monomer **M6**.

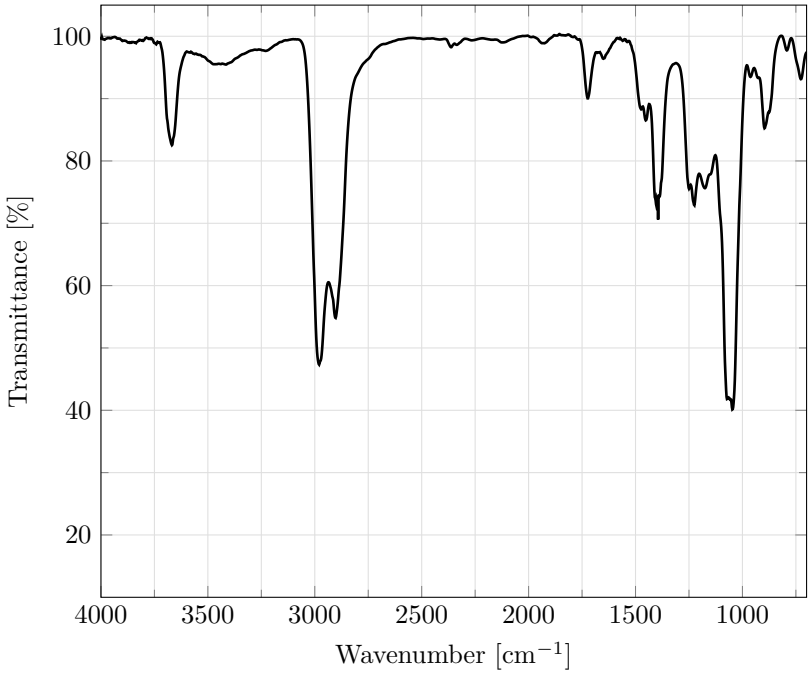

Figure A.36: FT-IR spectrum of copolymer **P(SPE$_{90}$-BMA$_{10}$)**.

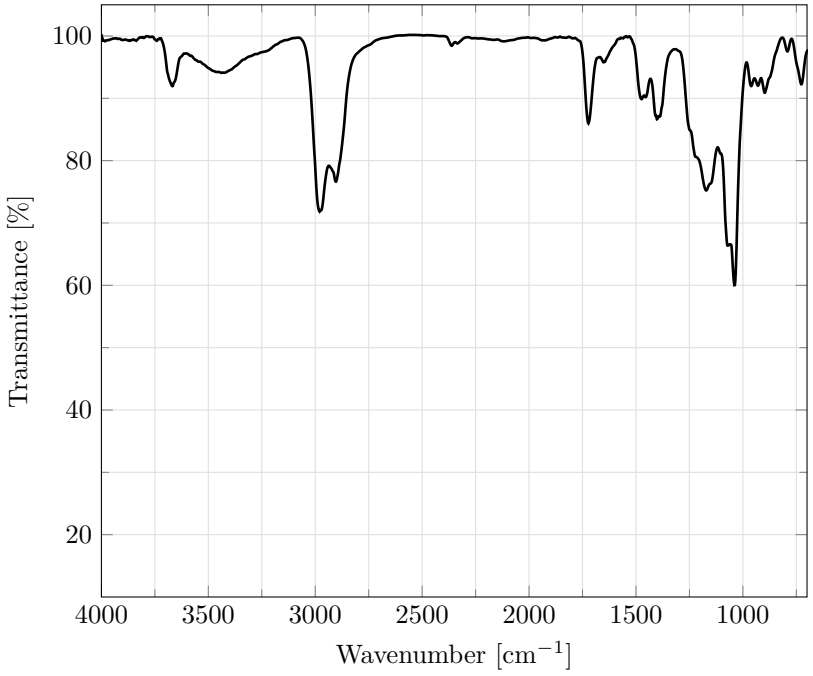

Figure A.37: FT-IR spectrum of copolymer **P(SPE$_{70}$-BMA$_{30}$)**.

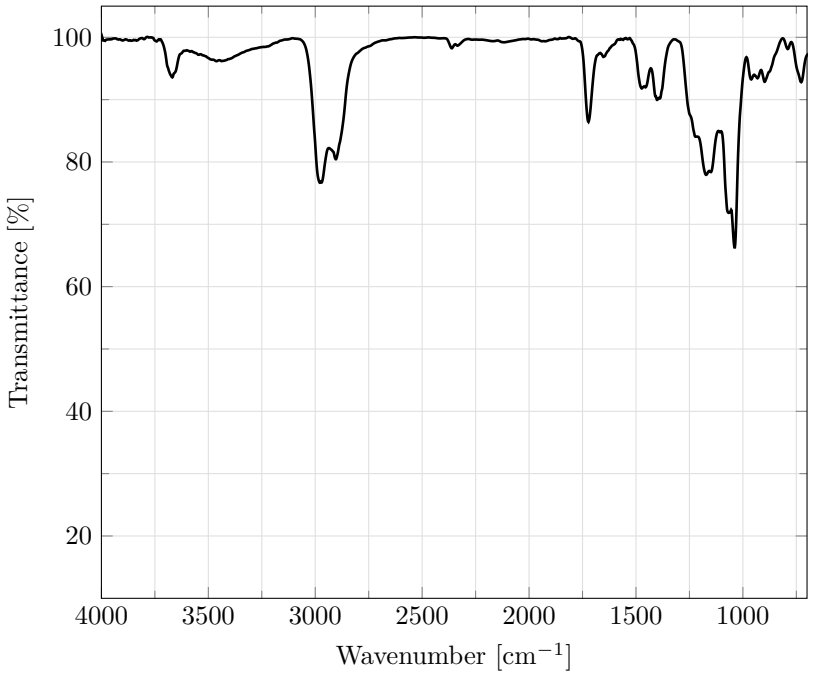

Figure A.38: FT-IR spectrum of copolymer **P(SPE$_{50}$-BMA$_{50}$)**.

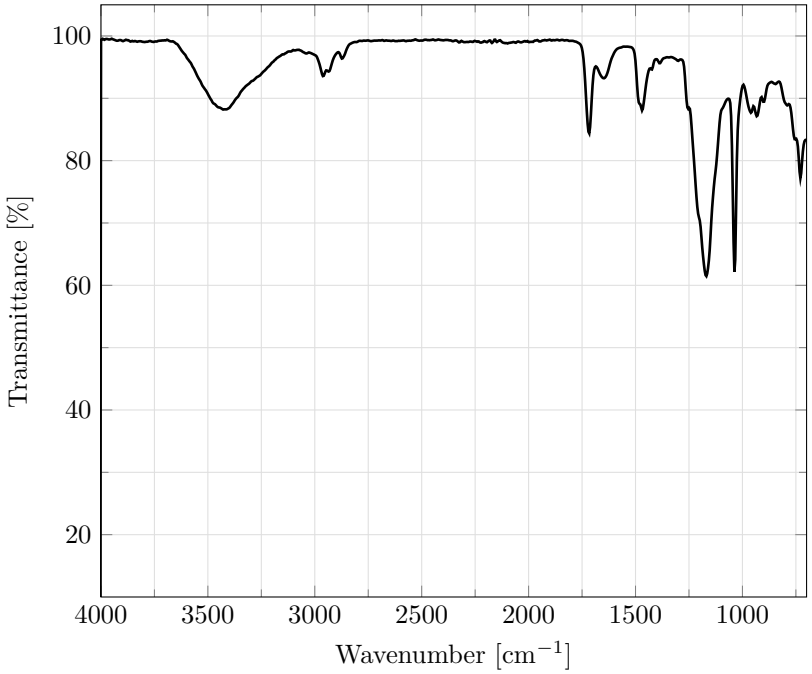

Figure A.39: FT-IR spectrum of homopolymer **P(M1)**.

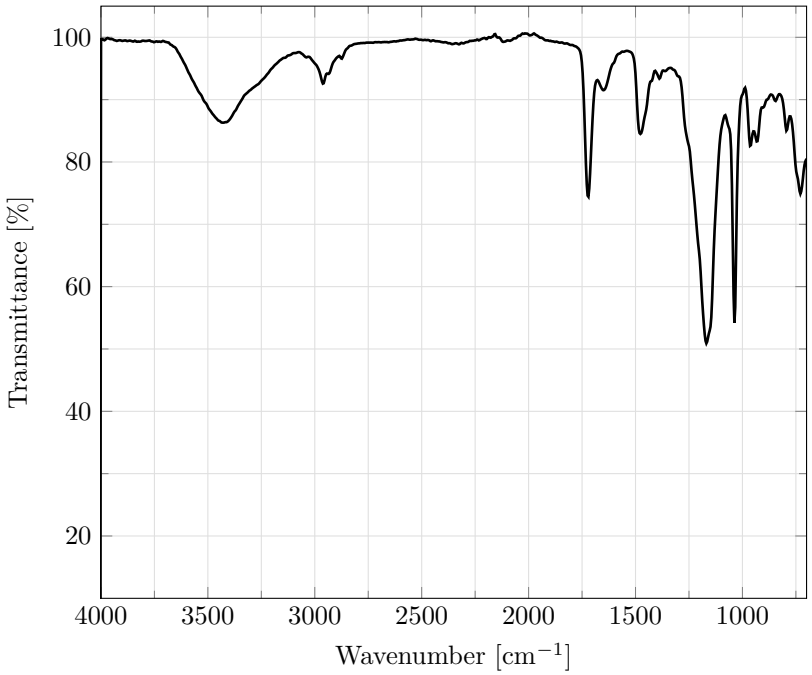

Figure A.40: FT-IR spectrum of copolymer **P(SPE$_{90}$-M1$_{10}$)**.

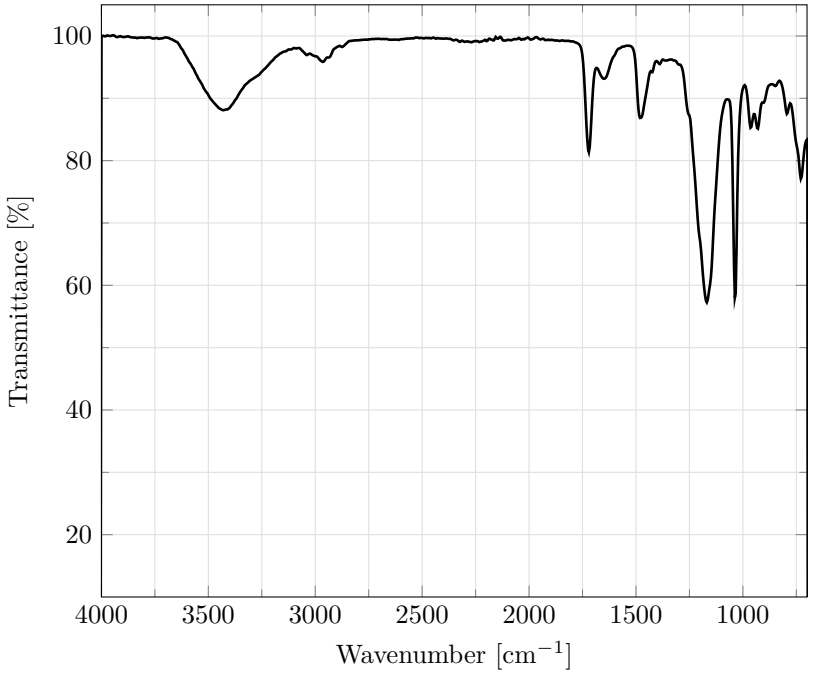

Figure A.41: FT-IR spectrum of copolymer **P(SPE$_{70}$-M1$_{30}$)**.

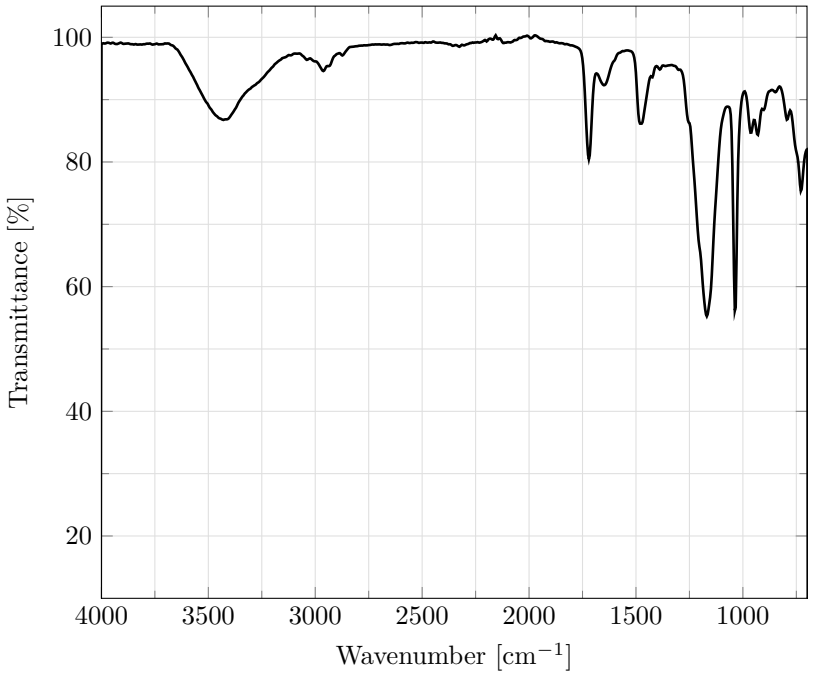

Figure A.42: FT-IR spectrum of copolymer **P(SPE$_{50}$-M1$_{50}$)**.

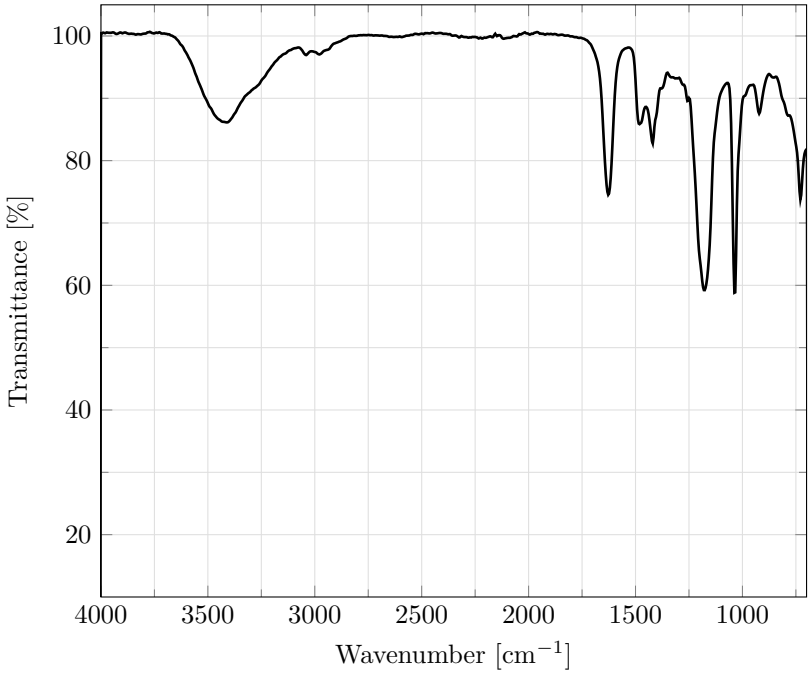

Figure A.43: FT-IR spectrum of homopolymer **P(M2)**.

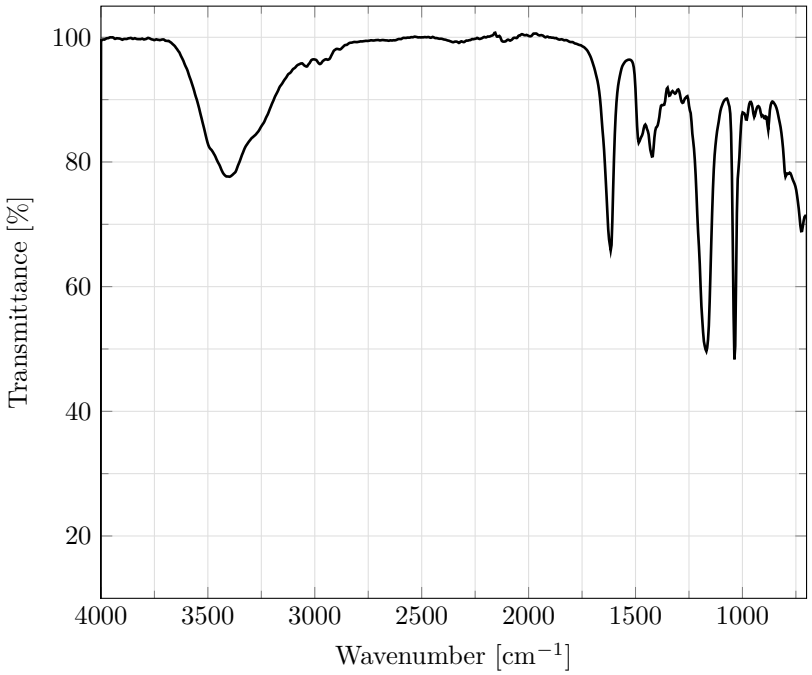

Figure A.44: FT-IR spectrum of homopolymer **P(M3)**.

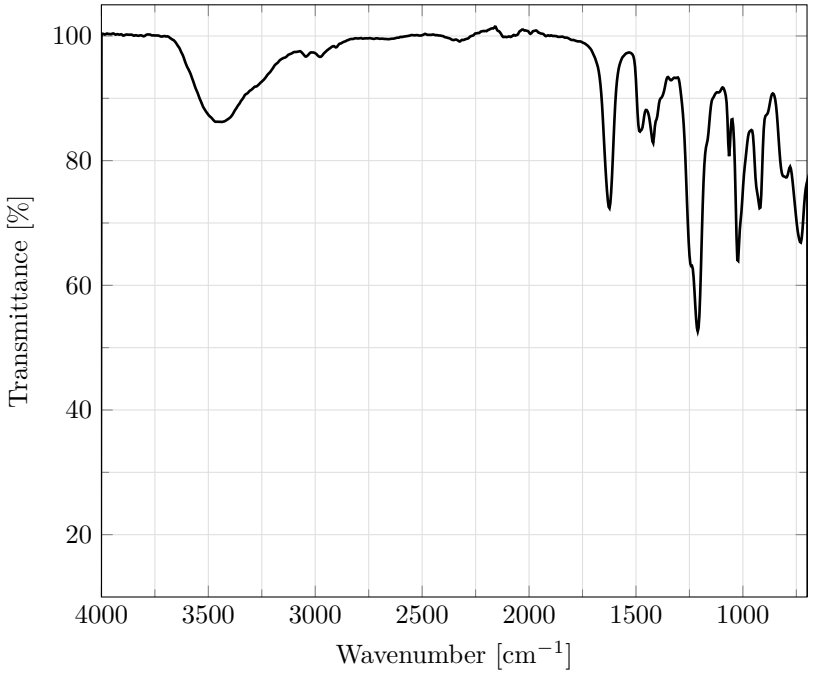

Figure A.45: FT-IR spectrum of homopolymer **P(M4)**.

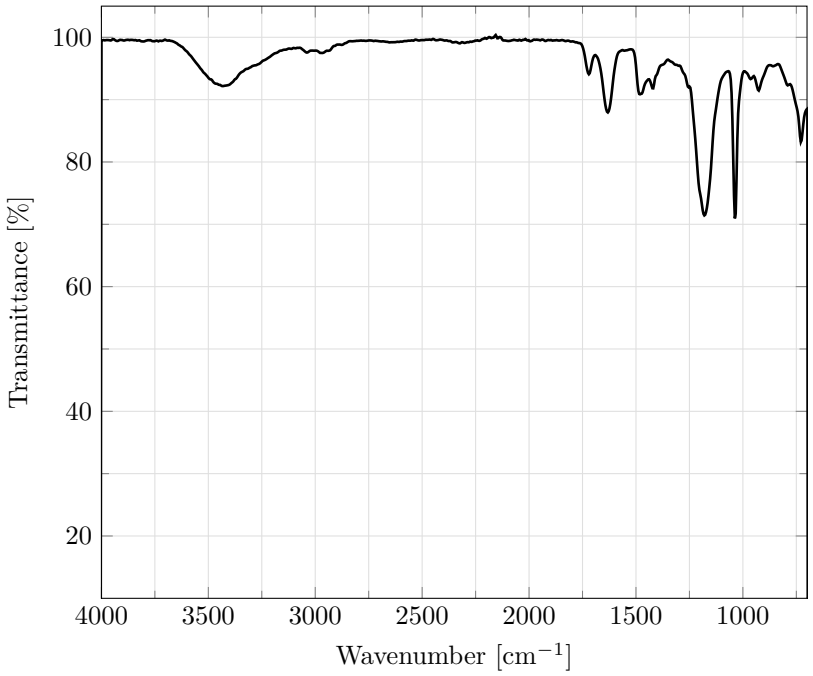

Figure A.46: FT-IR spectrum of copolymer **P(M2-*co*-M5)**.

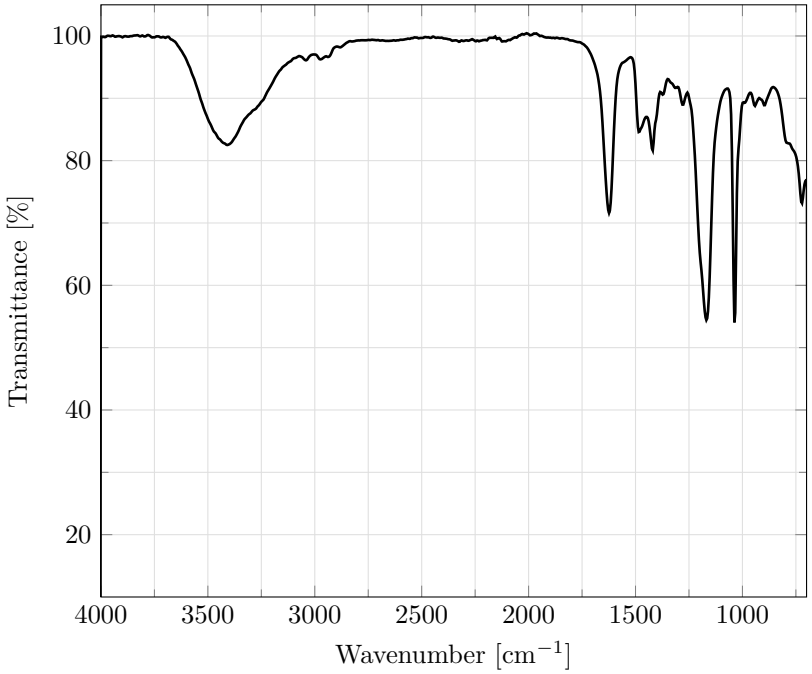

Figure A.47: FT-IR spectrum of copolymer **P(M3-*co*-M5)**.

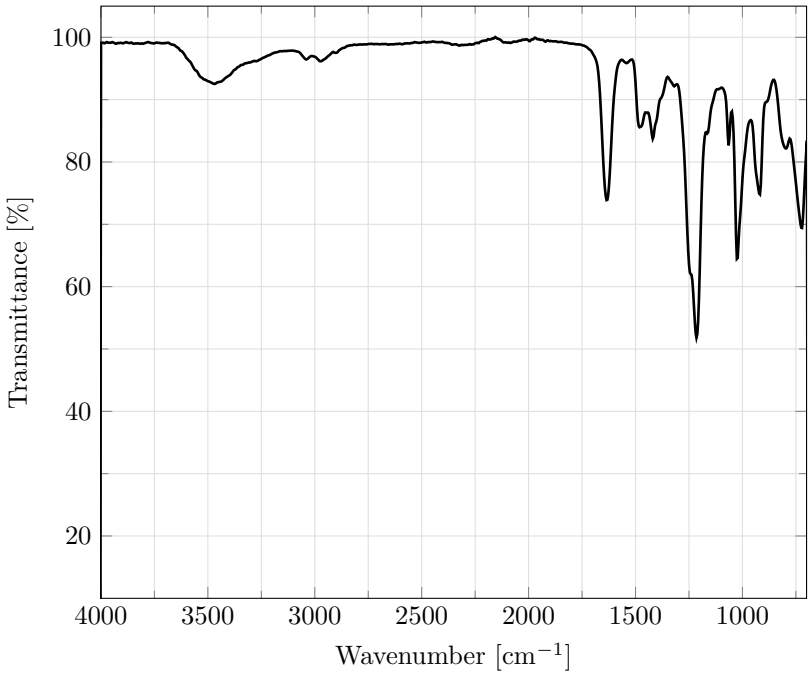

Figure A.48: FT-IR spectrum of copolymer **P(M4-*co*-M5)**.

Bibliography

[1] K. Ishihara, H. Nomura, T. Mihara, K. Kurita, Y. Iwasaki, and N. Nakabayashi, "Why do phospholipid polymers reduce protein adsorption?," *Journal of Biomedical Material Research*, vol. 39, pp. 323–330, February 1998.

[2] Z. Chen, "Surface hydration and antifouling activity of zwitterionic polymers," *Langmuir*, vol. 38, pp. 4483–4489, April 2022.

[3] A. Laschewsky, "Structures and synthesis of zwitterionic polymers," *Polymers*, vol. 6, no. 5, pp. 1544–1601, 2014.

[4] E. Schönemann, A. Laschewsky, and A. Rosenhahn, "Exploring the long-term hydrolytic behavior of zwitterionic polymethacrylates and polymethacrylamides," *Polymers*, vol. 10, no. 6, p. 639, 2018.

[5] J. Koc, T. Simovich, E. Schönemann, A. Chilkoti, H. Gardner, G. W. Swain, K. Z. Hunsucker, A. Laschewsky, and A. Rosenhahn, "Sediment challenge to promising ultra-low fouling hydrophilic surfaces in the marine environment," *Biofouling*, vol. 35, no. 4, pp. 454–462, 2019.

[6] D. Ruppelt, J. Kötz, W. Jaeger, S. E. Friberg, and R. A. Mackay, "Influence of cationic polyelectrolytes on structure formation in lamellar liquid crystalline systems," *Langmuir*, vol. 13, no. 13, pp. 3316–3319, 1997.

[7] K. Glinel, A. Moussa, A. M. Jonas, and A. Laschewsky, "Influence of polyelectrolyte charge density on the formation of multilayers of strong polyelectrolytes at low ionic strength," *Langmuir*, vol. 18, no. 4, pp. 1408–1412, 2002.

[8] A. K. Leonardi and C. K. Ober, "Polymer-based marine antifouling and fouling release surfaces: Strategies for synthesis and modification," *Annual Review of Chemical and Biomolecular Engineering*, vol. 10, pp. 241–264, 2019.

[9] J. A. Callow and M. E. Callow, "Trends in the development of environmentally friendly fouling-resistant marine coatings," *Nature Communications*, vol. 2, no. 244, 2011.

[10] L. D. Chambers, K. R. Stokes, F. C. Walsh, and R. Wood, "Modern approaches to marine antifouling coatings," *Surface & Coatings Technology*, vol. 201, no. 6, pp. 3642–3652, 2006.

[11] M. P. Schultz, J. A. Bendick, E. R. Holm, and W. M. Hertel, "Economic impact of biofouling on a naval surface ship," *Biofouling*, vol. 27, no. 1, pp. 87–98, 2011.

[12] P. J. Molino and R. Wetherbee, "The biology of biofouling diatoms and their role in the development of microbial slimes," *Biofouling*, vol. 24, no. 5, pp. 365–379, 2008.

[13] J. J. Corbett and P. Fischbeck, "Emissions from ships," *Science*, vol. 278, no. 5339, pp. 823–824, 1997.

[14] C. L. Hewitt, S. Gollasch, and D. Minchin, "The vessel as a vector – biofouling, ballast water and sediments," in *Biological Invasions in Marine Ecosystems* (M. M. Caldwell, G. Heldmaier, R. B. Jackson, O. L. Lange, H. A. Mooney, E.-D. Schulze, U. Sommer, G. Rilov, and J. A. Crooks, eds.), vol. 204 of *Ecological Studies*, pp. 117–131, Berlin, Heidelberg: Springer Berlin Heidelberg, 2009.

[15] J. Drake, "Hull fouling is a risk factor for intercontinental species exchange in aquatic ecosystems," *Aquatic Invasions*, vol. 2, no. 2, pp. 121–131, 2007.

[16] S. Liu, D. Brunel, G. Noirbent, A. Mau, H. Chen, F. Morlet-Savary, B. Graff, D. Gigmes, P. Xiao, F. Dumur, and J. Lalevée, "New multifunctional benzophenone-based photoinitiators with high migration stability and their applications in 3D printing," *Materials Chemistry Frontiers*, vol. 5, no. 4, pp. 1982–1994, 2021.

[17] D. M. Yebra, S. Kiil, and K. Dam-Johansen, "Antifouling technology—past, present and future steps towards efficient and environmentally friendly antifouling coatings," *Progress in Organic Coatings*, vol. 50, no. 2, pp. 75–104, 2004.

[18] W. J. Yang, K.-G. Neoh, E.-T. Kang, S. L.-M. Teo, and D. Rittschof, "Polymer brush coatings for combating marine biofouling," *Progress in Polymer Science*, vol. 39, no. 5, pp. 1017–1042, 2014.

[19] M. Lejars, A. Margaillan, and C. Bressy, "Fouling release coatings: A nontoxic alternative to biocidal antifouling coatings," *Chemical Reviews*, vol. 112, no. 8, pp. 4347–4390, 2012.

[20] W. Appeltans, S. T. Ahyong, G. Anderson, M. V. Angel, T. Artois, N. Bailly, R. Bamber, A. Barber, I. Bartsch, A. Berta, M. Błażewicz-Paszkowycz, P. Bock, G. Boxshall, C. B. Boyko, S. N. Brandão, R. A. Bray, N. L. Bruce, S. D. Cairns, T.-Y. Chan, L. Cheng, *et al.*, "The magnitude of global marine species diversity," *Current Biology*, vol. 22, no. 23, pp. 2189–2202, 2012.

[21] P. Bouchet, "The magnitude of marine biodiversity," in *The Exploration of Marine Biodiversity* (C. M. Duarte, ed.), pp. 31–64, Fundación BBVA, 2006.

[22] M. E. Callow and R. L. Fletcher, "The influence of low surface energy materials on bioadhesion — a review," *International Biodeterioration & Biodegradation*, vol. 34, no. 3-4, pp. 333–348, 1994.

[23] S. Abarzua and S. Jakubowski, "Biotechnological investigation for the prevention of biofouling. I. Biological and biochemical principles for the prevention of biofouling," *Marine Ecology Progress Series*, vol. 123, pp. 301–312, 1995.

[24] A. S. Clare, D. Rittschof, D. J. Gerhart, and J. S. Maki, "Molecular approaches to nontoxic antifouling," *Invertebrate Reproduction & Development*, vol. 22, no. 1-3, pp. 67–76, 1992.

[25] M. Wahl, "Marine epibiosis. I. Fouling and antifouling: Some basic aspects," *Marine Ecology Progress Series*, vol. 58, pp. 175–189, 1989.

[26] A. Rosenhahn, S. Schilp, H. J. Kreuzer, and M. Grunze, "The role of "inert" surface chemistry in marine biofouling prevention," *Physical Chemistry Chemical Physics*, vol. 12, no. 17, pp. 4275–4286, 2010.

[27] Woods Hole Oceanographic Institution and United States Navy Dept. Bureau of Ships, *Marine Fouling and its Prevention*. Menasha, WI: George Banta Publishing Co., 1952.

[28] G. C. V. Holmes, *Ancient and Modern Ships: Part I. Wooden Sailing-Ships*. London: Wyman and Sons Ltd., 1906.

[29] C. St. Baddeley, "Caligula's galleys in the Lake of Nemi," *Scientific American Supplement*, vol. 67, no. 1737supp, pp. 249–251, 1909.

[30] S. Kiil, C. E. Weinell, M. S. Pedersen, and K. Dam-Johansen, "Analysis of self-polishing antifouling paints using rotary experiments and mathematical modeling," *Industrial & Engineering Chemistry Research*, vol. 40, no. 18, pp. 3906–3920, 2001.

[31] K. N. Somasekharan and R. V. Subramanian, "Structure, mechanism, and reactivity of organotin carboxylate polymers," in *Modification of polymers* (C. E. Carraher and M. Tsuda, eds.), vol. 121 of *ACS Symposium Series*, pp. 165–181, Washington, DC: American Chemical Society, 1980.

[32] M. A. Champ, "A review of organotin regulatory strategies, pending actions, related costs and benefits," *The Science of the Total Environment*, vol. 258, no. 1-2, pp. 21–71, 2000.

[33] A. Abbott, P. D. Abel, D. W. Arnold, and A. Milne, "Cost-benefit analysis of the use of TBT: The case for a treatment approach," *The Science of the Total Environment*, vol. 258, no. 1-2, pp. 5–19, 2000.

[34] J. W. Readman, "Development, occurrence and regulation of antifouling paint biocides: Historical review and future trends," in *Antifouling Paint Biocides* (I. K. Konstantinou, ed.), The Handbook of Environmental Chemistry, pp. 1–15, Springer Berlin Heidelberg, 2006.

[35] T. Horiguchi, "Mechanism of imposex induced by organotins in gastropods," in *Ecotoxicology of Antifouling Biocides* (T. Arai, H. Harino, M. Ohji, and W. J. Langston, eds.), pp. 111–123, Tokyo, Japan: Springer Japan, 2009.

[36] G. W. Swain, "Biofouling control - A critical component of drag reduction," in *Proceedings of the International Symposium on Seawater Drag Reduction* (C. S. J. Meng, ed.), pp. 155–161, 1998.

[37] J. Bellas, "Comparative toxicity of alternative antifouling biocides on embryos and larvae of marine invertebrates," *The Science of the Total Environment*, vol. 367, no. 2-3, pp. 573–585, 2006.

[38] N. Voulvoulis, M. D. Scrimshaw, and J. N. Lester, "Alternative antifouling biocides," *Applied Organometallic Chemistry*, vol. 13, no. 3, pp. 135–143, 1999.

[39] P. Matthiessen, J. Reed, and M. Johnson, "Sources and potential effects of copper and zinc concentrations in the estuarine waters of Essex and Suffolk, United Kingdom," *Marine Pollution Bulletin*, vol. 38, no. 10, pp. 908–920, 1999.

[40] E. Ytreberg, J. Karlsson, and B. Eklund, "Comparison of toxicity and release rates of Cu and Zn from anti-fouling paints leached in natural and artificial brackish seawater," *The Science of the Total Environment*, vol. 408, no. 12, pp. 2459–2466, 2010.

[41] K. Martínez, I. Ferrer, M. D. Hernando, A. R. Fernández-Alba, R. M. Marcé, F. Borrull, and D. Barceló, "Occurrence of antifouling biocides in the spanish mediterranean marine environment," *Environmental Technology*, vol. 22, no. 5, pp. 543–552, 2001.

[42] N. Voulvoulis, M. D. Scrimshaw, and J. N. Lester, "Occurrence of four biocides utilized in antifouling paints, as alternatives to organotin compounds, in waters and sediments of a commercial estuary in the UK," *Marine Pollution Bulletin*, vol. 40, no. 11, pp. 938–946, 2000.

[43] M. Liu, S. Li, H. Wang, R. Jiang, and X. Zhou, "Research progress of environmentally friendly marine antifouling coatings," *Polymer Chemistry*, vol. 12, no. 26, pp. 3702–3720, 2021.

[44] S. Liu, J. Tang, F. Ji, W. Lin, and S. Chen, "Recent advances in zwitterionic hydrogels: Preparation, property, and biomedical application," *Gels*, vol. 8, no. 1, 2022.

[45] J. H. Kardela, I. S. Millichamp, J. Ferguson, A. L. Parry, K. J. Reynolds, N. Aldred, and A. S. Clare, "Nonfreezable water and polymer swelling control the marine antifouling performance of polymers with limited hydrophilic content," *ACS Applied Materials & Interfaces*, vol. 11, no. 33, pp. 29477–29489, 2019.

[46] A. Rakovsky, D. Marbach, N. Lotan, and Y. Lanir, "Poly(ethylene glycol)-based hydrogels as cartilage substitutes: Synthesis and mechanical characteristics," *Journal of Applied Polymer Science*, vol. 112, no. 1, pp. 390–401, 2009.

[47] J. M. Harris, *Poly(Ethylene Glycol) Chemistry: Biotechnical and Biomedical Applications*. Boston, MA: Springer US, 1992.

[48] R. A. Hartvig, M. van de Weert, J. Østergaard, L. Jorgensen, and H. Jensen, "Protein adsorption at charged surfaces: The role of electrostatic interactions and interfacial charge regulation," *Langmuir*, vol. 27, no. 6, pp. 2634–2643, 2011.

[49] A. Gessner, A. Lieske, B. Paulke, and R. Müller, "Influence of surface charge density on protein adsorption on polymeric nanoparticles: Analysis by two-dimensional electrophoresis," *European Journal of Pharmaceutics and Biopharmaceutics*, vol. 54, no. 2, pp. 165–170, 2002.

[50] E. Ostuni, R. G. Chapman, R. E. Holmlin, S. Takayama, and G. M. Whitesides, "A survey of structure−property relationships of surfaces that resist the adsorption of protein," *Langmuir*, vol. 17, no. 18, pp. 5605–5620, 2001.

[51] Q. Shao and S. Jiang, "Molecular understanding and design of zwitterionic materials," *Advanced Materials*, vol. 27, no. 1, pp. 15–26, 2015.

[52] M. Li, B. Zhuang, and J. Yu, "Functional zwitterionic polymers on surface: Structures and applications," *Chemistry, an Asian Journal*, vol. 15, no. 14, pp. 2060–2075, 2020.

[53] J. C. Galin, "Polyzwitterions (overview)," in *Polymeric Materials Encyclopedia* (J. C. Salamone, ed.), vol. 9, pp. 7189–7201, Boca Raton, FL: Taylor & Francis Group, 1996.

[54] M. Hess, R. G. Jones, J. Kahovec, T. Kitayama, P. Kratochvíl, P. Kubisa, W. Mormann, R. F. T. Stepto, D. Tabak, J. Vohlídal, and E. S. Wilks, "Terminology of polymers containing ionizable or ionic groups and of polymers containing ions: (IUPAC recommendations 2006)," *Pure and Applied Chemistry*, vol. 78, no. 11, pp. 2067–2074, 2006.

[55] A. Laschewsky and A. Rosenhahn, "Molecular design of zwitterionic polymer interfaces: Searching for the difference," *Langmuir*, vol. 35, no. 5, pp. 1056–1071, 2019.

[56] A. B. Lowe and C. L. McCormick, "Synthesis and solution properties of zwitterionic polymers," *Chemical Reviews*, vol. 102, no. 11, pp. 4177–4190, 2002.

[57] H. Ohno, M. Yoshizawa-Fujita, and Y. Kohno, "Design and properties of functional zwitterions derived from ionic liquids," *Physical Chemistry Chemical Physics*, vol. 20, no. 16, pp. 10978–10991, 2018.

[58] E. Schönemann, A. Laschewsky, E. Wischerhoff, J. Koc, and A. Rosenhahn, "Surface modification by polyzwitterions of the sulfabetaine-type, and their resistance to biofouling," *Polymers*, vol. 11, no. 6, 2019.

[59] K. Glasmästar, C. Larsson, F. Höök, and B. Kasemo, "Protein adsorption on supported phospholipid bilayers," *Journal of Colloid and Interface Science*, vol. 246, no. 1, pp. 40–47, 2002.

[60] D. Chapman, "Biomembranes and new hemocompatible materials," *Langmuir*, vol. 9, no. 1, pp. 39–45, 1993.

[61] J. B. Schlenoff, "Zwitteration: Coating surfaces with zwitterionic functionality to reduce nonspecific adsorption," *Langmuir*, vol. 30, no. 32, pp. 9625–9636, 2014.

[62] M. Chen, W. H. Briscoe, S. P. Armes, and J. Klein, "Lubrication at physiological pressures by polyzwitterionic brushes," *Science*, vol. 323, no. 5922, pp. 1698–1701, 2009.

[63] M. He, K. Gao, L. Zhou, Z. Jiao, M. Wu, J. Cao, X. You, Z. Cai, Y. Su, and Z. Jiang, "Zwitterionic materials for antifouling membrane surface construction," *Acta Biomaterialia*, vol. 40, pp. 142–152, 2016.

[64] K. Ishihara, "Blood-compatible surfaces with phosphorylcholine-based polymers for cardiovascular medical devices," *Langmuir*, vol. 35, no. 5, pp. 1778–1787, 2019.

[65] L. Schardt, A. Martínez Guajardo, J. Koc, J. L. Clarke, J. A. Finlay, A. S. Clare, H. Gardner, G. W. Swain, K. Z. Hunsucker, A. Laschewsky, and A. Rosenhahn, "Low fouling polysulfobetaines with variable hydrophobic content," *Macromolecular Rapid Communications*, vol. 43, no. 12, 2022.

[66] J. Koc, E. Schönemann, A. Amuthalingam, J. L. Clarke, J. A. Finlay, A. S. Clare, A. Laschewsky, and A. Rosenhahn, "Low-fouling thin hydrogel coatings made of photo-cross-linked polyzwitterions," *Langmuir*, vol. 35, no. 5, pp. 1552–1562, 2019.

[67] E. Schönemann, J. Koc, N. Aldred, A. S. Clare, A. Laschewsky, A. Rosenhahn, and E. Wischerhoff, "Synthesis of novel sulfobetaine polymers with differing dipole orientations in their side chains, and their effects on the antifouling properties," *Macromolecular Rapid Communications*, vol. 41, no. 1, 2020.

[68] J. Lee, S. Yi, K. D. Hong, and J.-H. Seo, "Copolymerization of zwitterionic carboxybetaine and various hydrophobic groups to optimize antifouling and biocompatible properties," *Journal of Industrial and Engineering Chemistry*, vol. 96, no. 25, pp. 284–293, 2021.

[69] S. Jiang and Z. Cao, "Ultralow-fouling, functionalizable, and hydrolyzable zwitterionic materials and their derivatives for biological applications," *Advanced Materials*, vol. 22, no. 9, pp. 920–932, 2010.

[70] J. Baggerman, M. M. J. Smulders, and H. Zuilhof, "Romantic surfaces: A systematic overview of stable, biospecific, and antifouling zwitterionic surfaces," *Langmuir*, vol. 35, no. 5, pp. 1072–1084, 2019.

[71] H. Kitano, T. Mori, Y. Takeuchi, S. Tada, M. Gemmei-Ide, Y. Yokoyama, and M. Tanaka, "Structure of water incorporated in sulfobetaine polymer films as studied by ATR-FTIR," *Macromolecular Bioscience*, vol. 5, no. 4, pp. 314–321, 2005.

[72] E. Schönemann, J. Koc, J. F. Karthäuser, O. Özcan, D. Schanzenbach, L. Schardt, A. Rosenhahn, and A. Laschewsky, "Sulfobetaine methacrylate polymers of unconventional polyzwitterion architecture and their antifouling properties," *Biomacromolecules*, vol. 22, no. 4, pp. 1494–1508, 2021.

[73] Y. Liu, F. Wang, and J. Liu, "Headgroup-inversed liposomes: Biointerfaces, supported bilayers and applications," *Langmuir*, vol. 34, no. 32, pp. 9337–9348, 2018.

[74] S. Morozova, G. Hu, T. Emrick, and M. Muthukumar, "Influence of dipole orientation on solution properties of polyzwitterions," *ACS Macro Letters*, vol. 5, no. 1, pp. 118–122, 2016.

[75] G. Hu and T. Emrick, "Functional choline phosphate polymers," *Journal of the American Chemical Society*, vol. 138, no. 6, pp. 1828–1831, 2016.

[76] S. Monge, B. Canniccioni, A. Graillot, and J.-J. Robin, "Phosphorus-containing polymers: A great opportunity for the biomedical field," *Biomacromolecules*, vol. 12, no. 6, pp. 1973–1982, 2011.

[77] M. A. Hillmyer, "Polymer synthesis," in *Polymer science: A comprehensive reference* (K. Matyjaszewski and M. Möller, eds.), pp. 31–45, Amsterdam, Netherlands: Elseiver, 2012.

[78] G. Moad, *The Chemistry of Radical Polymerization*. Boston, MA: Elsevier, 2nd ed., 2006.

[79] D. Braun, "Origins and development of initiation of free radical polymerization processes," *International Journal of Polymer Science*, vol. 2009, 2009.

[80] G. Moad, "Radical polymerization," in *Polymer science: A comprehensive reference* (K. Matyjaszewski and M. Möller, eds.), pp. 59–118, Amsterdam, Netherlands: Elseiver, 2012.

[81] P. J. Flory, *Principles of polymer chemistry*. Ithaca, NY: Cornell Univ. Press, 1st ed., 1953.

[82] C. Walling, *Free Radicals in Solution*. New York, NY: Wiley, 1957.

[83] G. Moad, E. Rizzardo, and D. H. Solomon, "Selectivity of the reaction of free radicals with styrene," *Macromolecules*, vol. 15, no. 3, pp. 909–914, 1982.

[84] G. Moad, E. Rizzardo, and D. H. Solomon, "Evaluation of end groups in poly(methyl methacrylate-co-styrene) by ^{13}C NMR," *Polymer Bulletin*, vol. 12, no. 5, pp. 471–474, 1984.

[85] G. G. Odian, *Principles of Polymerization*. Hoboken, N.J: John Wiley & Sons, Inc, 4th ed., 2004.

[86] F. A. Bovey, *Chain Structure and Conformation of Macromolecules*. New York, NY: Acad. Press, 1982.

[87] J. L. Koenig, *Spectroscopy of Polymers*. ACS professional reference book, Washington, DC: American Chemical Society, 1st ed., 1993.

[88] K. Hatada and T. Kitayama, *NMR Spectroscopy of Polymers*. Springer Laboratory, New York, NY: Springer Berlin Heidelberg, 2004.

[89] T. Nakamura, W. K. Busfield, I. D. Jenkins, E. Rizzardo, S. H. Thang, and S. Suyama, "Initiation mechanisms for radical polymerization of methyl methacrylate with *tert*-butyl peroxypivalate," *Journal of the American Chemical Society*, vol. 118, no. 44, pp. 10824–10828, 1996.

[90] D. Bednarek, G. Moad, E. Rizzardo, and D. H. Solomon, "End groups of poly(methyl methacrylate-co-styrene) prepared with *tert*-butoxy, methyl, and/or phenyl radical initiation: Effects of solvent, monomer composition, and conversion," *Macromolecules*, vol. 21, no. 5, pp. 1522–1528, 1988.

[91] G. B. Butler, "Cyclopolymerization and cyclocopolymerization," *Accounts of Chemical Research*, vol. 15, no. 11, pp. 370–378, 1982.

[92] H.-G. Elias, *Macromolecules: Synthesis, Materials, and Technology*, vol. 2 of *Macromolecules*. New York, NY: Springer, 2nd ed., 1984.

[93] M. L. Coote and T. P. Davis, "Copolymerization kinetics," in *Handbook of Radical Polymerization* (K. Matyjaszewski and T. P. Davis, eds.), New York, NY: Wiley-Interscience, 2002.

[94] F. R. Mayo and F. M. Lewis, "Copolymerization. I. A basis for comparing the behavior of monomers in copolymerization; The copolymerization of styrene and methyl methacrylate," *Journal of the American Chemical Society*, vol. 66, no. 9, pp. 1594–1601, 1944.

[95] E. Merz, T. Alfrey, and G. Goldfinger, "Intramolecular reactions in vinyl polymers as a means of investigation of the propagation step," *Journal of Polymer Science*, vol. 1, no. 2, pp. 75–82, 1946.

[96] A. Pross, *Theoretical and Physical Principles of Organic Reactivity*. New York, NY: John Wiley & Sons, Inc, 1st ed., 1995.

[97] M. Kamachi, "Influence of solvent on free radical polymerization of vinyl compounds," in *Polymerization Processes* (H.-J. Cantow, G. Dall'Asta, K. Dušek, J. D. Ferry, H. Fujita, M. Gordon, J. P. Kennedy, W. Kern, S. Okamura, C. G. Overberger, T. Saegusa, G. V. Schulz, W. P. Slichter, and J. K. Stille, eds.), vol. 38 of *Advances in Polymer Science*, pp. 55–87, Springer Berlin Heidelberg, 1981.

[98] P. D. Bartlett and K. Nozaki, "The polymerization of allyl compounds. III. The peroxide-induced copolymerization of allyl acetate with maleic anhydride," *Journal of the American Chemical Society*, vol. 68, no. 8, pp. 1495–1504, 1946.

[99] U. S. K. Madduma-Bandarage and S. V. Madihally, "Synthetic hydrogels: Synthesis, novel trends, and applications," *Journal of Applied Polymer Science*, vol. 138, no. 19, 2021.

[100] F. Ullah, M. B. H. Othman, F. Javed, Z. Ahmad, and H. Md Akil, "Classification, processing and application of hydrogels: A review," *Materials Science & Engineering C*, vol. 57, pp. 414–433, 2015.

[101] M. J. Zohourian Mehr and K. Kabiri, "Superabsorbent polymer materials: A review," *Iranian Polymer Journal*, vol. 17, no. 6, pp. 451–477, 2008.

[102] M. A. Zwieniecki, P. J. Melcher, and N. M. Michele Holbrook, "Hydrogel control of xylem hydraulic resistance in plants," *Science*, vol. 291, no. 5506, pp. 1059–1062, 2001.

[103] P. Sánchez-Cid, M. Jiménez-Rosado, A. Romero, and V. Pérez-Puyana, "Novel trends in hydrogel development for biomedical applications: A review," *Polymers*, vol. 14, no. 15, 2022.

[104] O. Wichterle and D. Lím, "Hydrophilic gels for biological use," *Nature*, vol. 185, no. 4706, pp. 117–118, 1960.

[105] J. Kopeček, "Hydrogels: From soft contact lenses and implants to self-assembled nanomaterials," *Journal of Polymer Science Part A: Polymer Chemistry*, vol. 47, no. 22, pp. 5929–5946, 2009.

[106] S. Li, F. Wang, X. Li, J. Chen, X. Zhang, Y. Wang, and J. Liu, "Dipole orientation matters: Longer-circulating choline phosphate than phosphocholine liposomes for enhanced tumor targeting," *ACS Applied Materials & Interfaces*, vol. 9, no. 21, pp. 17736–17744, 2017.

[107] J. Li and D. J. Mooney, "Designing hydrogels for controlled drug delivery," *Nature Reviews Materials*, vol. 1, no. 12, 2016.

[108] J. Koc, L. Schardt, K. Nolte, C. Beyer, T. Eckhard, P. Schwiderowski, J. L. Clarke, J. A. Finlay, A. S. Clare, M. Muhler, A. Laschewsky, and A. Rosenhahn, "Effect of dipole orientation in mixed, charge-equilibrated self-assembled monolayers on protein adsorption and marine biofouling," *ACS Applied Materials & Interfaces*, vol. 12, no. 45, pp. 50953–50961, 2020.

[109] G. Dormán, H. Nakamura, A. Pulsipher, and G. D. Prestwich, "The life of pi star: Exploring the exciting and forbidden worlds of the benzophenone photophore," *Chemical Reviews*, vol. 116, no. 24, pp. 15284–15398, 2016.

[110] G. Dormán and G. D. Prestwich, "Benzophenone photophores in biochemistry," *Biochemistry*, vol. 33, no. 19, pp. 5661–5673, 1994.

[111] R. E. Galardy, L. C. Craig, J. D. Jamieson, and M. P. Printz, "Photoaffinity labeling of peptide hormone binding sites," *Journal of Biological Chemistry*, vol. 249, no. 11, pp. 3510–3518, 1974.

[112] M. Marazzi, S. Mai, D. Roca-Sanjuán, M. G. Delcey, R. Lindh, L. González, and A. Monari, "Benzophenone ultrafast triplet population: Revisiting the kinetic model by surface-hopping dynamics," *The Journal of Physical Chemistry Letters*, vol. 7, no. 4, pp. 622–626, 2016.

[113] S. K. Christensen, M. C. Chiappelli, and R. C. Hayward, "Gelation of copolymers with pendent benzophenone photo-cross-linkers," *Macromolecules*, vol. 45, no. 12, pp. 5237–5246, 2012.

[114] O. Prucker, C. A. Naumann, J. Rühe, W. Knoll, and C. W. Frank, "Photochemical attachment of polymer films to solid surfaces via monolayers of benzophenone derivatives," *Journal of the American Chemical Society*, vol. 121, no. 38, pp. 8766–8770, 1999.

[115] N. J. Turro, V. Ramamurthy, and J. C. Scaiano, *Principles of Molecular Photochemistry: An Introduction*. Sausalito, CA: University Science Books, 2009.

[116] M. A. El-Sayed, "The triplet state: Its radiative and nonradiative properties," *Accounts of Chemical Research*, vol. 1, no. 1, pp. 8–16, 1968.

[117] M. Wakasa, "The magnetic field effects on photochemical reactions in ionic liquids," *The Journal of Physical Chemistry B*, vol. 111, no. 32, pp. 9434–9436, 2007.

[118] A. A. Lin, V. R. Sastri, G. Tesoro, A. Reiser, and R. Eachus, "On the crosslinking mechanism of benzophenone-containing polyimides," *Macromolecules*, vol. 21, no. 4, pp. 1165–1169, 1988.

[119] G. Eisele, J. P. Fouassier, and R. Reeb, "Kinetics of photocrosslinking reactions of a DCPA/EA matrix in the presence of thiols and acrylates," *Journal of Polymer Science Part A: Polymer Chemistry*, vol. 35, no. 12, pp. 2333–2345, 1997.

[120] J. P. Cerón-Carrasco, D. Jacquemin, C. Laurence, A. Planchat, C. Reichardt, and K. Sraïdi, "Solvent polarity scales: Determination of new $E_T(30)$ values for 84 organic solvents," *Journal of Physical Organic Chemistry*, vol. 27, no. 6, pp. 512–518, 2014.

[121] C. Reichardt and T. Welton, *Solvents and solvent effects in organic chemistry*. Weinheim, Germany: Wiley-VCH, 4$^{\text{th}}$ ed., 2011.

[122] T. R. Griffiths and D. C. Pugh, "Solvent polarity studies. Part I. New Z values and relationships with other solvent polarity scales," *Journal of Solution Chemistry*, vol. 8, no. 3, pp. 247–258, 1979.

[123] P. Anton, P. Köberle, and A. Laschewsky, "Recent developments in the field of micellar polymers," *Die Makromolekulare Chemie*, vol. 194, no. 1, pp. 1–27, 1993.

[124] V. M. Monroy Soto and J. C. Galin, "Poly(sulphopropylbetaines): 1. Synthesis and characterization," *Polymer*, vol. 25, no. 1, pp. 121–128, 1984.

[125] A. Laschewsky and I. Zerbe, "Polymerizable and polymeric zwitterionic surfactants: 1. Synthesis and bulk properties," *Polymer*, vol. 32, no. 11, pp. 2070–2080, 1991.

[126] L. A. LaPlanche and M. T. Rogers, "*cis* and *trans* configurations of the peptide bond in *N*-monosubstituted amides by nuclear magnetic resonance," *Journal of the American Chemical Society*, vol. 86, no. 3, pp. 337–341, 1964.

[127] W. D. Phillips, "Restricted rotation in amides as evidenced by nuclear magnetic resonance," *The Journal of Chemical Physics*, vol. 23, no. 7, pp. 1363–1364, 1955.

[128] S. Tu and C. Zhang, "Facile preparation of *N*-vinylisobutyramide and *N*-vinyl-2-pyrrolidinone," *Organic Process Research & Development*, vol. 19, no. 12, pp. 2045–2049, 2015.

[129] B. D. Mistry, *A Handbook of Spectroscopic Data Chemistry: (UV, IR, PMR, ^{13}CNMR and Mass Spectroscopy)*. Jaipur, India: Oxford Book Co., 1st ed., 2009.

[130] J. C. Salamone, W. Volksen, A. P. Olson, and S. C. Israel, "Aqueous solution properties of a poly(vinyl imidazolium sulphobetaine)," *Polymer*, vol. 19, no. 10, pp. 1157–1162, 1978.

[131] V. M. Monroy Soto and J. C. Galin, "Poly(sulphopropylbetaines): 2. Dilute solution properties," *Polymer*, vol. 25, no. 2, pp. 254–262, 1984.

[132] J. Buller, A. Laschewsky, and E. Wischerhoff, "Photoreactive oligoethylene glycol polymers – versatile compounds for surface modification by thin hydrogel films," *Soft Matter*, vol. 9, no. 3, pp. 929–937, 2013.

[133] N. J. Turro, V. Ramamurthy, and J. C. Scaiano, *Modern Molecular Photochemistry of Organic Molecules*. Sausalito, CA: University Science Books, 2010.

[134] J. E. Lancaster, L. Baccei, and H. P. Panzer, "The structure of poly(diallyldimethyl-ammonium) chloride by ^{13}C NMR spectroscopy," *Journal of Polymer Science: Polymer Letters Edition*, vol. 14, no. 9, pp. 549–554, 1976.

[135] G. B. Butler and R. J. Angelo, "Preparation and polymerization of unsaturated quaternary ammonium compounds. VIII. A proposed alternating intramolecular-intermolecular chain propagation," *Journal of the American Chemical Society*, vol. 79, no. 12, pp. 3128–3131, 1957.

[136] P. Favresse and A. Laschewsky, "Synthesis and investigation of new amphiphilic poly(carbobetaine)s made from diallylammonium monomers," *Polymer*, vol. 42, no. 7, pp. 2755–2766, 2001.

[137] P. Anton and A. Laschewsky, "Zwitterionic polysoaps with reduced density of surfactant side groups," *Die Makromolekulare Chemie*, vol. 194, pp. 601–624, 1993.

[138] M. Ali, H. Perzanowski, and S. Ali, "Polymerization of functionalized diallyl quaternary ammonium salt to poly(ampholyte–electrolyte)," *Polymer*, vol. 41, no. 15, pp. 5591–5600, 2000.